An Examination of Subsidence in North-East England due to the Dissolution of Sub-Surface Gypsum using the Shallow Seismic Reflection Technique

Sargent, Colin

An Examination of Subsidence in North-East England due to the Dissolution of Sub-Surface Gypsum using the Shallow Seismic Reflection Technique

By

Colin Sargent

A thesis submitted in partial fulfilment of the requirements for the degree of Doctor of Philosophy

Department of Earth Sciences

Durham University
2009

Volume Two

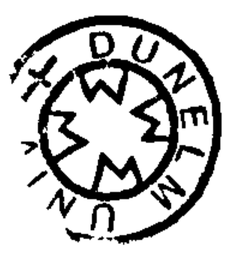

Declaration

The content of this thesis are the original work of the author and has not previously been submitted for a degree at this or any other university. The work of other people is acknowledged by reference.

Colin Sargent
Durham University

Abstract

Along a narrow swath from Nottingham through to Hartlepool, broad shallow depressions up to 100m in diameter and, more rarely, scarp-edged subsidence hollows are observed. These topographical features coincide with the sub-crop of the Permian strata beneath the Quaternary deposits and are attributed to the dissolution of sub-surface gypsum. Boreholes (<150 m deep) prove the existence of several layers of gypsum within the Permian geological succession.

The objective of the work reported here is to image the shallow sub-surface geology at several locations in north-east England, and to detect any structures related to gypsum dissolution, such as faulting, foundering and voids. The purpose is to promote the use of the seismic reflection technique for site investigation to assess the subsidence hazard for new industrial and residential development.

A total of thirty-two 2D seismic profiles were acquired over a period of three years at seven different sites near to Darlington, Church Fenton and Ripon in County Durham and North Yorkshire. Based on the results of the 2D surveys and additional geological information, 3D seismic volumes were collected at three of the sites. The seismic source was a buffalo gun with the signal recorded by vertical geophones of 30 Hz resonant frequency. Raw data were collected in SEG-2 format on a 16-bit, 24-channel Geometrics SmartSeis recording system. Standard digital seismic data processing techniques were employed to transform the raw field data into interpretable seismic sections and volumes.

Gypsum beds between 5 m and 25 m thick are imaged at depths ranging from 30 m to 70 m below the reference datum, the water table. The processed seismic data show metre-scale detail of foundering features in shallow limestone beds overlying the gypsum beds. These features are interpreted as the consequence of gypsum dissolution, and many of them do not have a surface expression. Two mechanisms of gypsum dissolution are inferred from the relationships between the local geology, sub-surface foundering and the difference in seismic character of the gypsum surfaces: firstly, karstifaction of the upper gypsum surface by water percolating down through the overlying strata, and secondly, dissolution of the base of the gypsum bed by water flowing through an underlying artesian aquifer. However, no rectilinear maze cave systems within the gypsum beds were imaged.

3D seismic technology can delineate small areas different geological character that can be missed by a network of 2D seismic profiles, even when supplemented by boreholes.

Acknowledgements

Firstly, I would like to thank my supervisor Professor Neil Goulty for devising this interesting project, for helping out in the entire three seasons of field work and research guidance, and also for securing some monies for this project under the NERC Knowledge Transfer Programme, contract reference NE/D000955/1.

I am grateful to all the landowners, who granted permission for us to conduct seismic surveys on their land: Mr. Alan Fell at Hell Kettles, Mr. Nigel Swinbank at Neasham Fen, The Darlington Cattle Mart at Parkside, Mr. David Metcalffe at Hutton Hill, Mr. Dominic Dale at Sharow, Harrogate Borough Council at Ure Bank, and Mr. Carl Clayton at Ulleskelf Mires. Natural England also granted permission to acquire data at Hell Kettles and Neasham Fen, both designated Sites of Special Scientific Interest.

The keen interest in this research by Jim Gallagher and Stuart Muckle of Darlington Borough Council and the access to confidential borehole information granted by British Gypsum Limited were also very welcome.

I must thank Dr. Richard Hobbs for configuring the computing facilities to enable the processing of the raw 2D and 3D seismic data into geologically interpretable images. I am also grateful to Dave Stevenson and Gary Wilkinson for maintaining all of the Earth Sciences IT services, and to Alan Burchell who helped with maintenance of the SmartSeis seismograph.

The assistance of undergraduates in some of the field work, sometimes in rather inclement conditions, is very much appreciated. In particular I thank Will Kemp, Ahmed Al-

Contents

List of Figures

List of Tables

5.0 Hell Kettles

5.1 Site description

Hell Kettles [NZ 2815 1085] are a couple of ponds approximately 4km south-west of the urban centre of Darlington, County Durham. They are set in agricultural land located on the alluvial floodplain deposits of the nearby River Tees and its tributary, the River Skerne (Figure 5.1), with the Triassic Sherwood Sandstone group forming the bedrock (Figure 5.2).

The southern pond is approximately 20 m in diameter and the waters of this pond are often seen with a bluish tinge which shows up particularly well from the air (Figure 5.3). The blue colour is a result of the pond being fed from below by water rich in carbonate and sulphate (Lamont-Black et al., 2005), which is thought to come from the Seaham Limestone artesian aquifer. The perimeter of the northern pond has the shape of two overlapping circles, and the pond is fed by a pipe leading from the southern pond. The two ponds are separated by an area of very boggy ground. Ecologically, the southern spring-fed pond is much richer and is the only site in County Durham with stands of saw-sedge, which is why the Hell Kettles site has been designated at as Site of Special Scientific Interest (SSSI) by Natural England. To protect the site, the Hell Kettles ponds are completely enclosed by a 200 m by 200 m pasture field which is only used for grazing.

Topographically the survey area can be broadly divided into two areas. Around the southern blue pond the near surface soils comprise light-brown sandy silt of fluvial origin. The quantity of pebbles in the uppermost 1 m of soil increases on north side of the field. The adjoining field to the north stands on slightly higher ground, with an increase in elevation of approximately 1 m. Here the soils are drier and more gravelly, and recent ploughing has given the soil a lighter, less compact texture compared to the adjacent SSSI field. Beyond the fence line on the eastern side of the survey area is a broad shallow curving depression. This is the physical expression of an ancient meander of the River Tees.

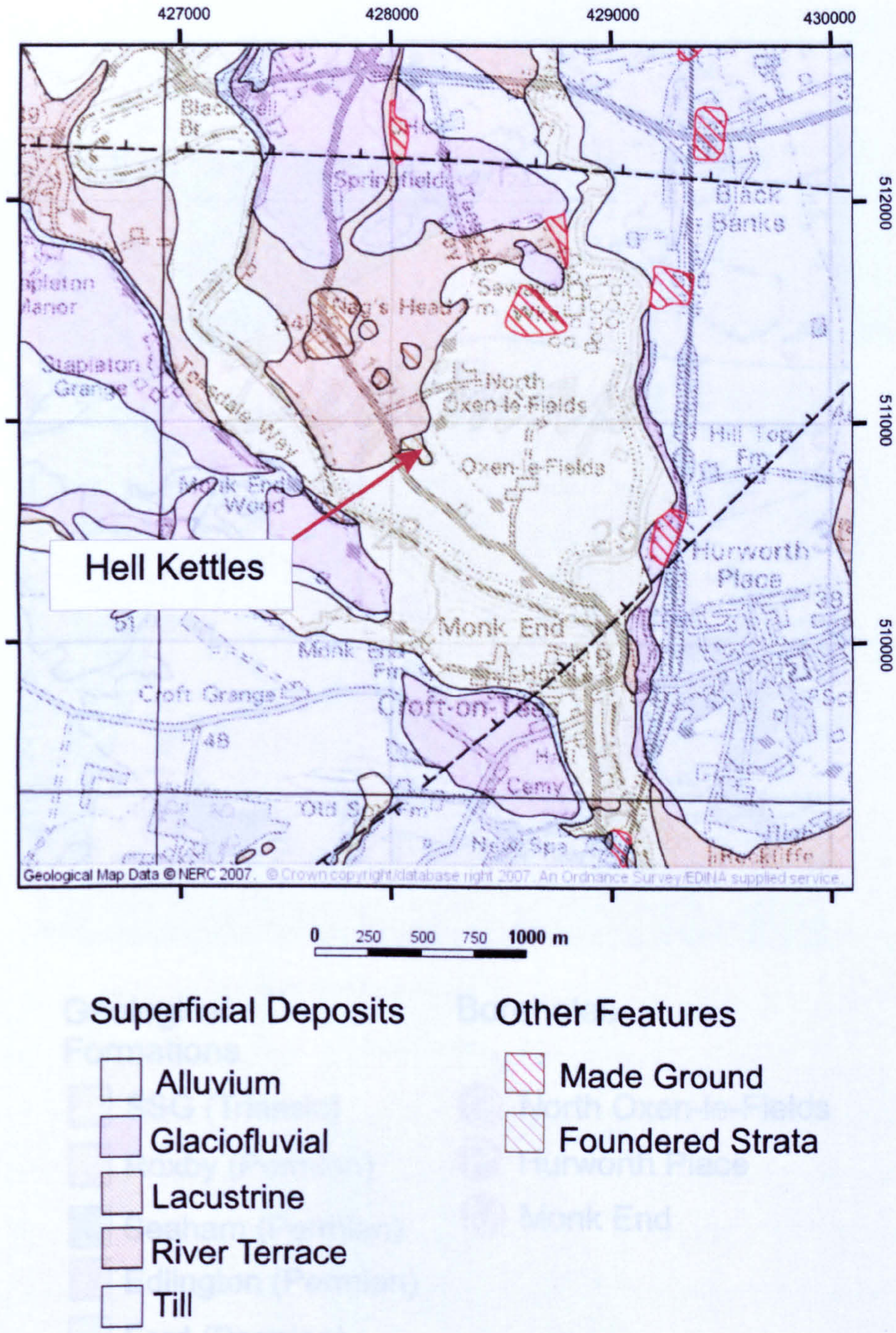

Figure 5.1: Superficial geology at the Hell Kettles survey site.
Data supplied by Ordnance Survey/EDINA service © Crown Copyright Database 2007.

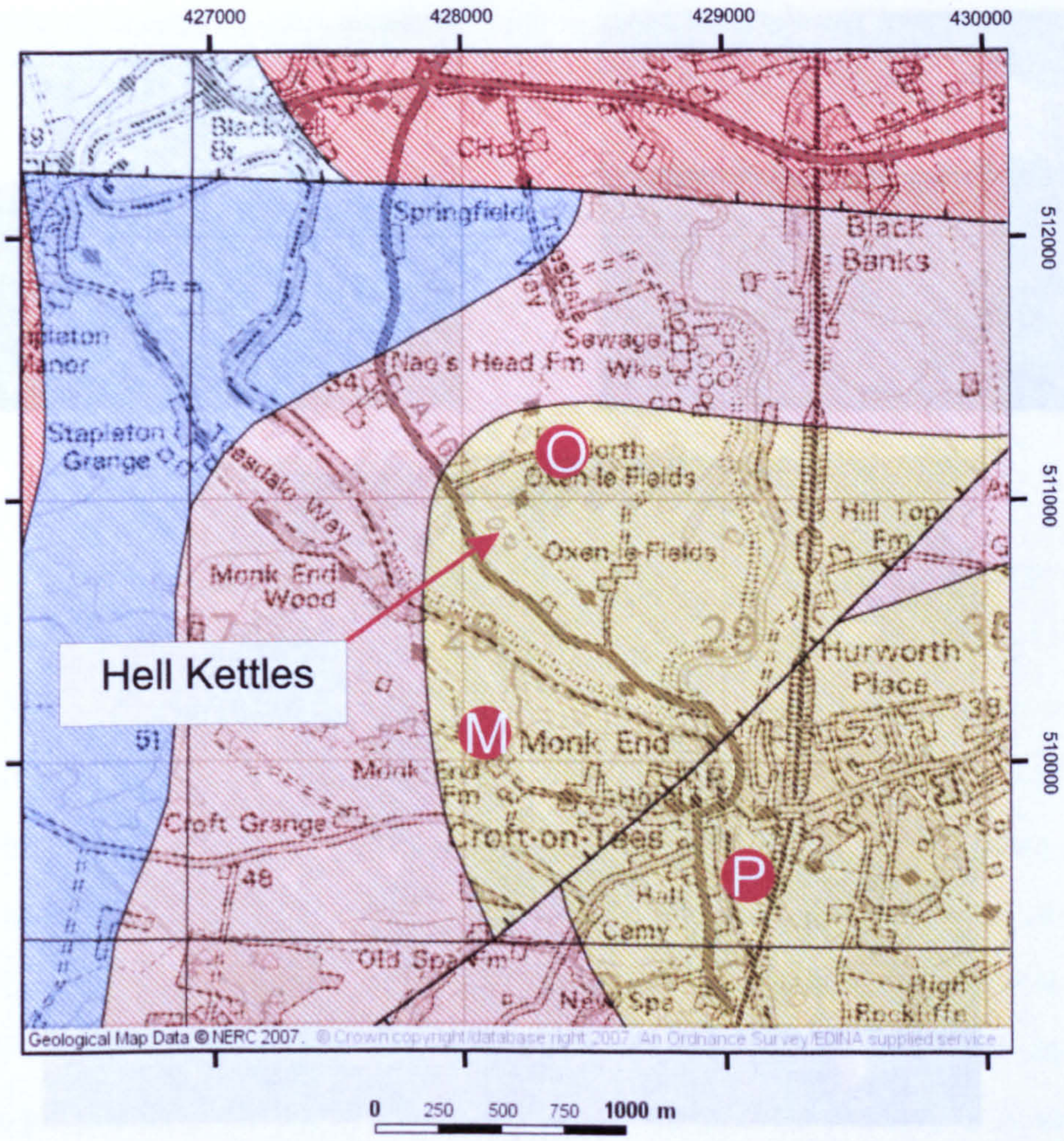

Figure 5.2: Solid geology beneath the Hell Kettles survey site.
Data supplied by Ordnance Survey/EDINA service © Crown Copyright Database 2007.

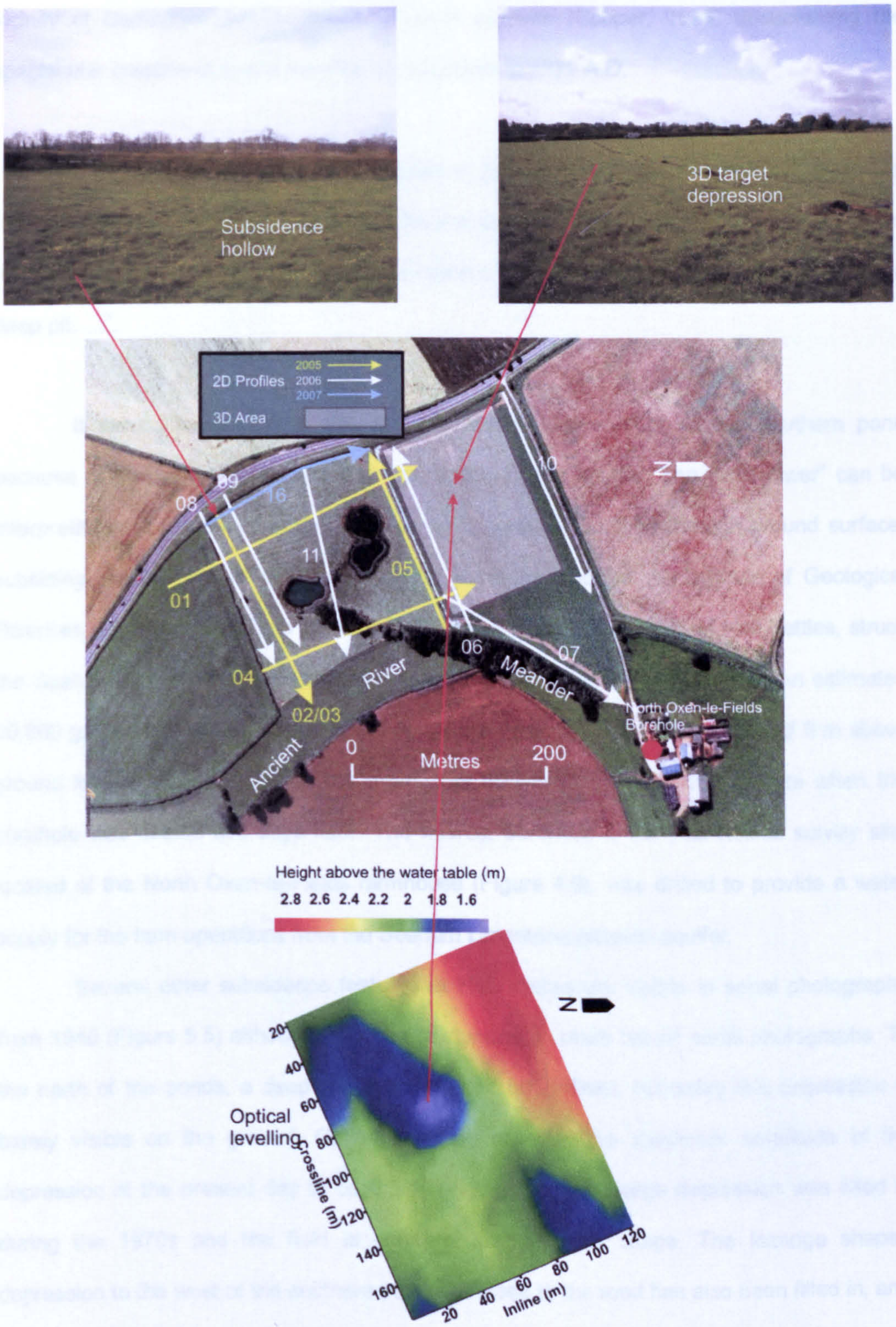

Figure 5.3: Spatial distribution of 2D profiles and 3D volume at Hell Kettles.
The optical levelling contour plot is illuminated at an inclination of 45° from the south-east.

The Hell Kettles ponds are the only example of sudden collapse sinkholes in the vicinity of Darlington. An eyewitness account survives (Cooper, 1995) documenting the spectacular creation of one of the Hell Kettles ponds in 1179 A.D.

"... the earth rose on high in Oxendale, in the district of Darlington, in the likeness of a lofty tower, and so remained from nine in the morning until evening, when it sank down with a terrible noise, to the terror of all those that heard it, and being swallowed up it left behind it a deep pit.....".

It seems probable that this account records the creation of the southern pond because of its depth and its hydraulic connection to the aquifer. The "lofty tower" can be interpreted as a column of water under artesian pressure bursting through ground surface, subsiding towards the evening as the water pressure dropped. An Institute of Geological Sciences exploration borehole at Monk End (Figure 5.4), 800 m south of Hell Kettles, struck the Seaham Limestone artesian aquifer at 50 m depth below ground surface. An estimated 30,000 gallons per hour of water flowed out of the borehole, with a static head of 6 m above ground level. It is reported that the water was flowing at an undiminished rate when the borehole was sealed five days later. The nearest borehole to the Hell Kettles survey site, located at the North Oxen-le-Fields farmhouse (Figure 4.6), was drilled to provide a water supply for the farm operations from the Seaham Limestone artesian aquifer.

Several other subsidence features at Hell Kettles are visible in aerial photography from 1940 (Figure 5.5) although they do not standout in more recent aerial photographs. To the north of the ponds, a deep depression is sharply defined, but today this depression is barely visible on the ground. Optical levelling revealed the maximum amplitude of the depression at the present day to be 0.5 m (Figure 5.3). The large depression was filled in during the 1970s and the field is currently cultivated for silage. The lozenge shaped depression to the west of the southern pond and close to the road has also been filled in, and 20 m south-west of the southern pond is a shallow circular feature that is now also barely visible on the ground. In the south-west corner of the field containing the ponds, there is at the

present day a 15 m diameter, 1 m deep, circular depression that is not picked out on either old or recent aerial photographs.

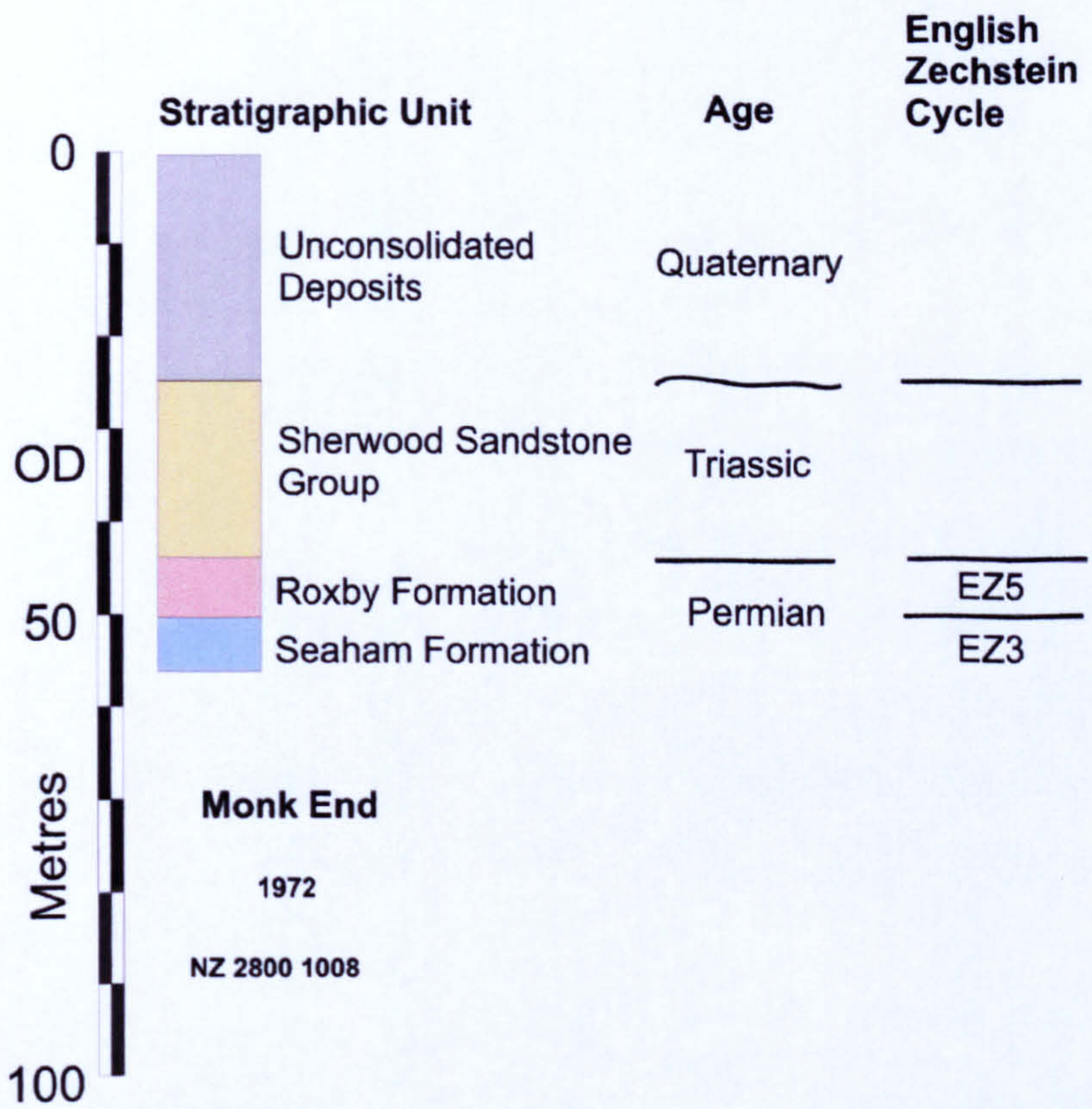

Figure 5.4: Monk End borehole geological succession.

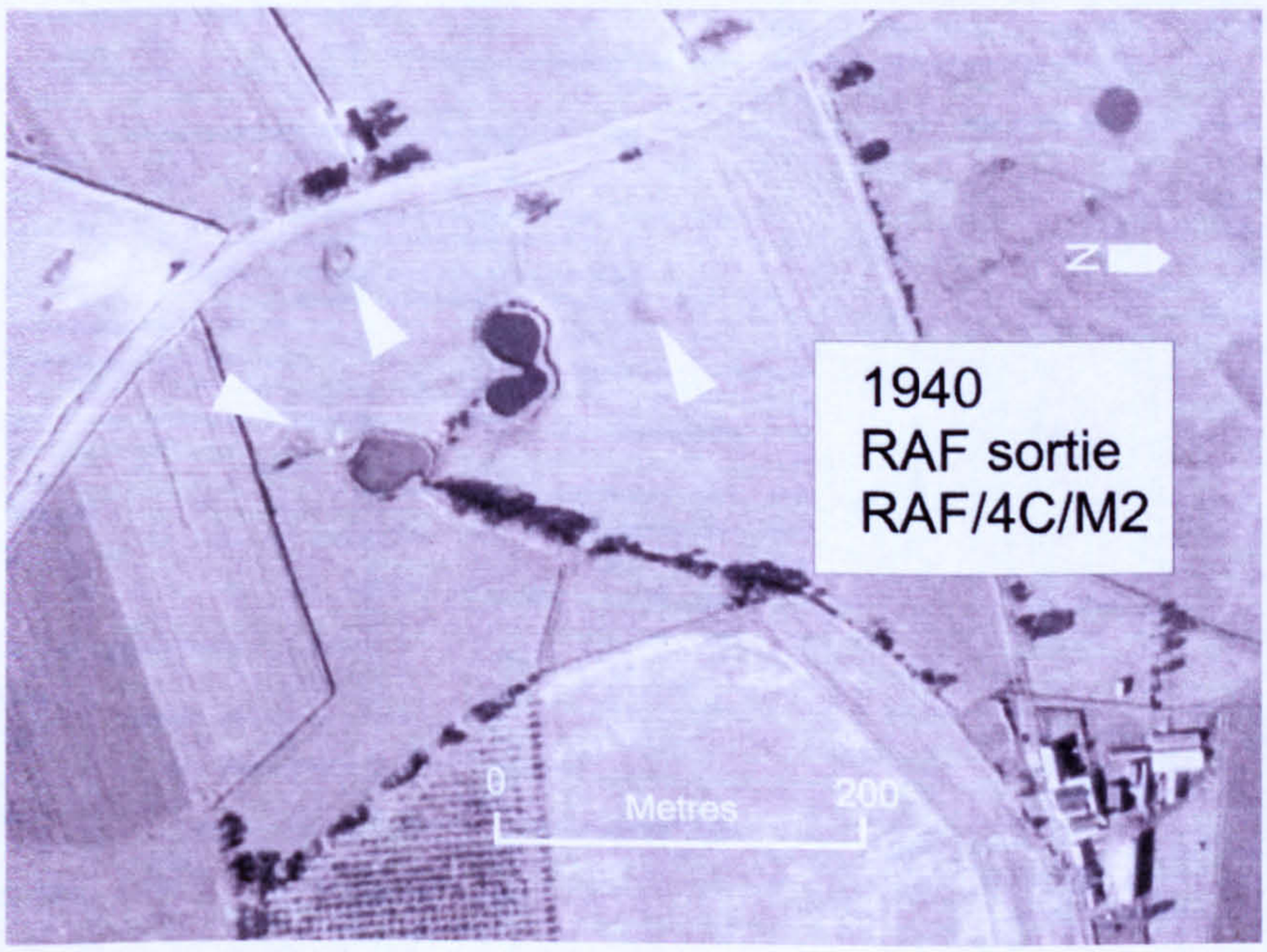

Figure 5.5: Surface depressions identified at Hell Kettles.

5.2 Acquisition

An initial grid of four profiles circumnavigating the Hell Kettles ponds (Figure 5.3) was acquired during the summer months of 2005. The acquisition parameters for these profiles (Figure 5.6, upper panel, Table 5.1) were based on the seismic data collected in a trial 2D profile at Hell Kettles conducted in November 2004. Profile 02, aligned SW-NE past the edge of the southern pond, was reacquired as profile 03 using groups of six geophones in linear arrays (Figure 5.6, middle panel) instead of single geophones.

For the 2D profiles acquired in 2006, it was decided that shot point interval should be increased to 4 m reducing the fold of coverage to twelve. Post-processing of the 2005 2D profiles showed that this alteration to the acquisition parameter would not adversely affect the quality of the final product. Comparison of the datasets from profiles 02 and 03 also led to the decision to compact the soil at shot depth by firing a dummy shot in the drilled shot hole before recording the seismic signal from firing a second blank cartridge. This technique, traditionally known as 'springing the shot hole', to improve the seismic signal quality in unconsolidated ground was described by Sharp (1940).

The final 2D profile acquired at Hell Kettles, profile 16, was located to cross the in-filled depression identified close to the roadside in the 1940 aerial photograph. The orientation of the boundary hedge meant that profile 16 assumed a dog-leg shape. For this profile, the shot interval was 4 m with a maximum shot depth of 2.6 m within the in-filled subsidence feature. The majority of the shot holes were 1.5 m deep; the hand drilling was stymied at this depth by a gravel bed. Slightly larger charges of 7 g of black powder were used in the data collection of profile 16 compared to the previous 2D profiles. Profile 16 was also designed to compare the difference in data quality between single point geophones and groups of six geophones deployed as tight clusters around each peg (Figure 5.6, lower panel).

The 3D survey was acquired in the autumn of 2006 and centred over the depression in the silage field to the north of the ponds (Figure 5.3). The basic shooting template was a linear symmetric split-spread with a geophone spacing of 4 m and a near offset of 26 m (Figure 4.33) with the acquisition parameters specified in Table 5.2. The shot stations were placed on an 8 m by 8 m grid offset by 2 m in both in-line and cross-line directions from the

rectangular 4 m by 4 m grid of receiver stations (Figure 4.34). The shot station grid was modified to build up the fold of coverage both ends in the in-line direction of the 3D survey.

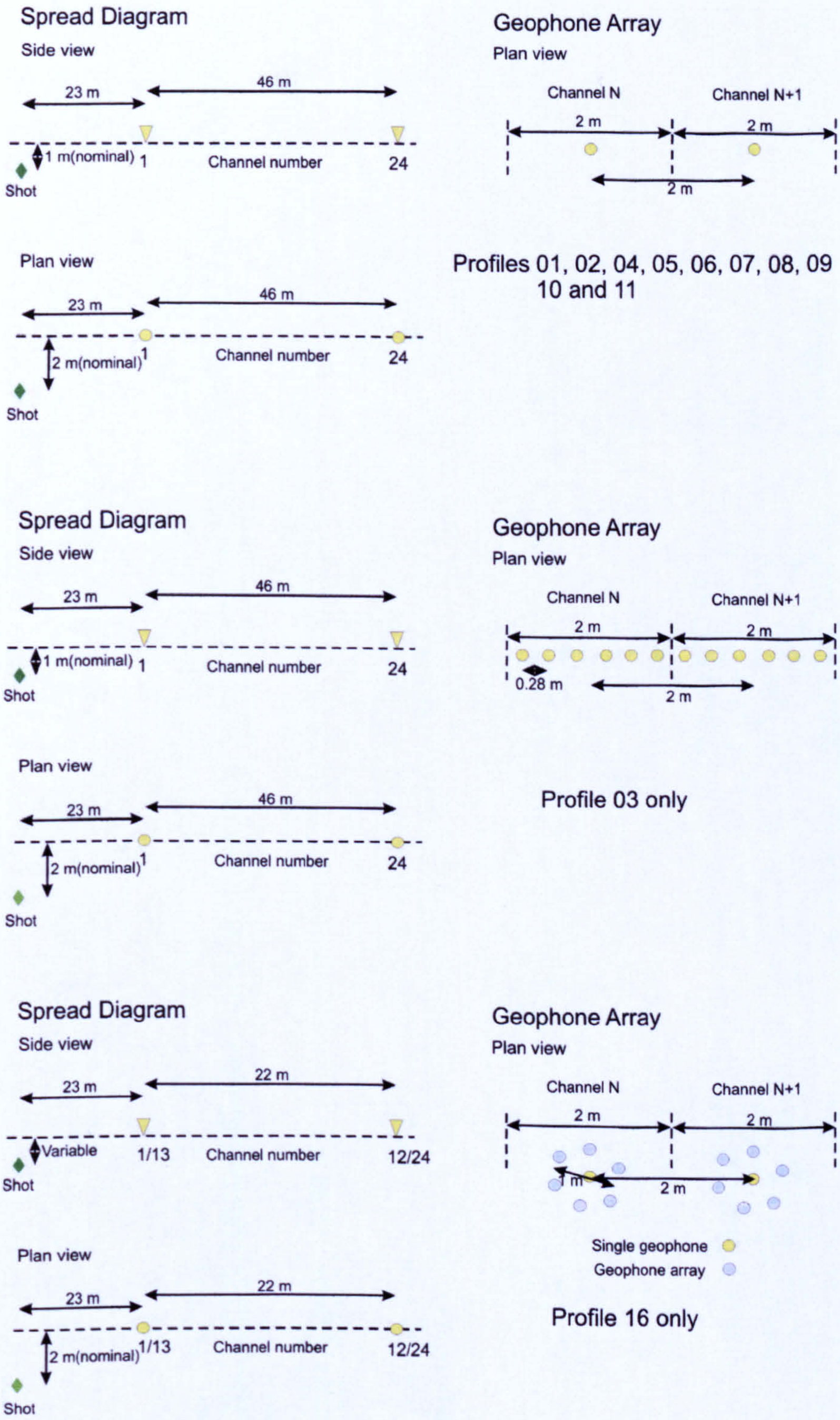

Figure 5.6: Variations in the geophone spreads used in the Hell Kettles 2D profiles.

Instrument Parameters	
Recording instrument	Geometrics SmartSeis S12
Format	SEG-2
Data channels	24
Pre A/D converter low cut filter	10 Hz
Pre A/D converter high cut filter	500 Hz
Sample interval	0.5 ms
Record length	512 ms
Delay	0 ms

Source Parameters	
Source type	Buffalo gun, 5 g black powder blanks
Shot interval	2 m
Shot depth	1 m
Shot in-line skid relative to geophones	1 m
Shot cross-line offset relative to geophones	2 m

Off-end shooting arrangement, forward and reverse shots to simulate symmetric split-spread.
All shot holes tamped with water before firing.

Receiver Parameters	
Geophone type	SM-7/30 Hz
Group interval	2 m
Geophones per group	1
Near-offset	23 m
Far-offset	69 m

Table 5.1: Hell Kettles 2D profiles initial acquisition parameters.

Two lines with shot points at intervals of 4 m were built into the survey design so that a comparison between the results of 2D and 3D data processing could be made. The 2D profile in the middle of the 3D survey passes directly through the small depression. A mobile drilling rig was hired to drill shot holes to fire charges well below the water table. However, this exercise was abandoned because the shot holes collapsed below the water table due to the instability of beds of rounded pebbles and cobbles.

The basic shooting template was rolled along each in-line of receiver stations, building up a dense net of 63 in-line and 83 cross-line sections. This set-up yielded a sub-

surface coverage over an area of 128 m × 168 m with a CMP bin size of 2 m × 2 m and 6-fold CMP gathers with a very narrow azimuth. Yachting blanks of 7 g of black powder were used for the 1512 shots required to complete the Hell Kettles 3D survey.

Instrument Parameters	
Recording instrument	Geometrics SmartSeis S12
Format	SEG-2
Data channels	24
Pre A/D converter low cut filter	10 Hz
Pre A/D converter high cut filter	500 Hz
Sample interval	0.5 ms
Record length	512 ms
Delay	0 ms
Source Parameters	
Source type	Buffalo gun, 7 g black powder blanks
Shot in-line interval	8 m
Shot cross-line interval	8 m
Shot depth	1 m
Shot in-line skid relative to geophones	2 m
Shot cross-line offset relative to geophones	2 m or 6 m
Symmetrical split-spread shooting arrangement.	
All shot holes sprung with a dummy shot tamped with water before firing.	
Receiver Parameters	
Geophone type	SM-7/30 Hz
Group in-line interval	4 m
Group cross-line interval	4 m
Geophones per group	1
Near-offset	±26 m
Far-offset	±70 m

Table 5.2: Hell Kettles 3D seismic volume acquisition parameters.

5.2.1 Tests of seismic acquisition parameters

5.2.1.1 Comparison of single geophones and groups

Large-scale land surveys for hydrocarbon exploration have employed various array designs to suppress unwanted surface wave noise, although experiments for the National Coal Board favoured the use of single point receivers in seismic profiling in coal exploration (Ziolkowski and Lerwill, 1979). Presently, even in hydrocarbon exploration, there is a trend towards the use of point receivers to improve the signal bandwidth (Baeten and van der Heijden, 2008). Unless it is proved that deploying arrays in a shallow seismic project produces a significant benefit to the final product, the extra workload in deploying geophone arrays cannot be justified because of the increase in operational costs.

Profile 02 (Figure 5.7) was acquired with single point geophones and then replicated using a linear array of six geophones as profile 03 (Figure 5.8). The processing flow applied to both datasets was exactly the same and time migrated sections of both profiles imaged foundering of the Seaham Limestone clearly. The quality of profile 03 is marginally better than profile 02. The reflection package of the Roxby-Seaham interface in the foundered zone is more continuous, and the reflection signal interpreted as the top of the Hartlepool Anhydrite Formation is slightly clearer.

The differences may have been caused by collecting each profile on different days under different weather conditions. Also it was thought that the source coupling was improved for profile 03, because the shot holes were sprung by the shots fired in acquiring profile 02. Therefore, this first comparison trial was deemed not to be definitive, and the acquisition parameters for profile 16 were planned to provide an unequivocal test.

To ensure that the environmental conditions, such as wind and traffic noise, and the shot coupling conditions were exactly the same, a blank yachting cartridge was fired into a spread of twelve single geophones and twelve geophone groups deployed simultaneously at the same twelve stations. For this experiment, each group of six geophones was placed in a 1 m diameter circle around the single geophone at the same peg, which was recorded on a separate channel (Figure 5.6, lower panel). All the geophones had identical characteristics. The single geophones had damping resistors of 3300 Ω. The groups were wired in parallel

with a single damping resistor of 560 Ω. These parameters were used to acquire the dog-leg profile 16.

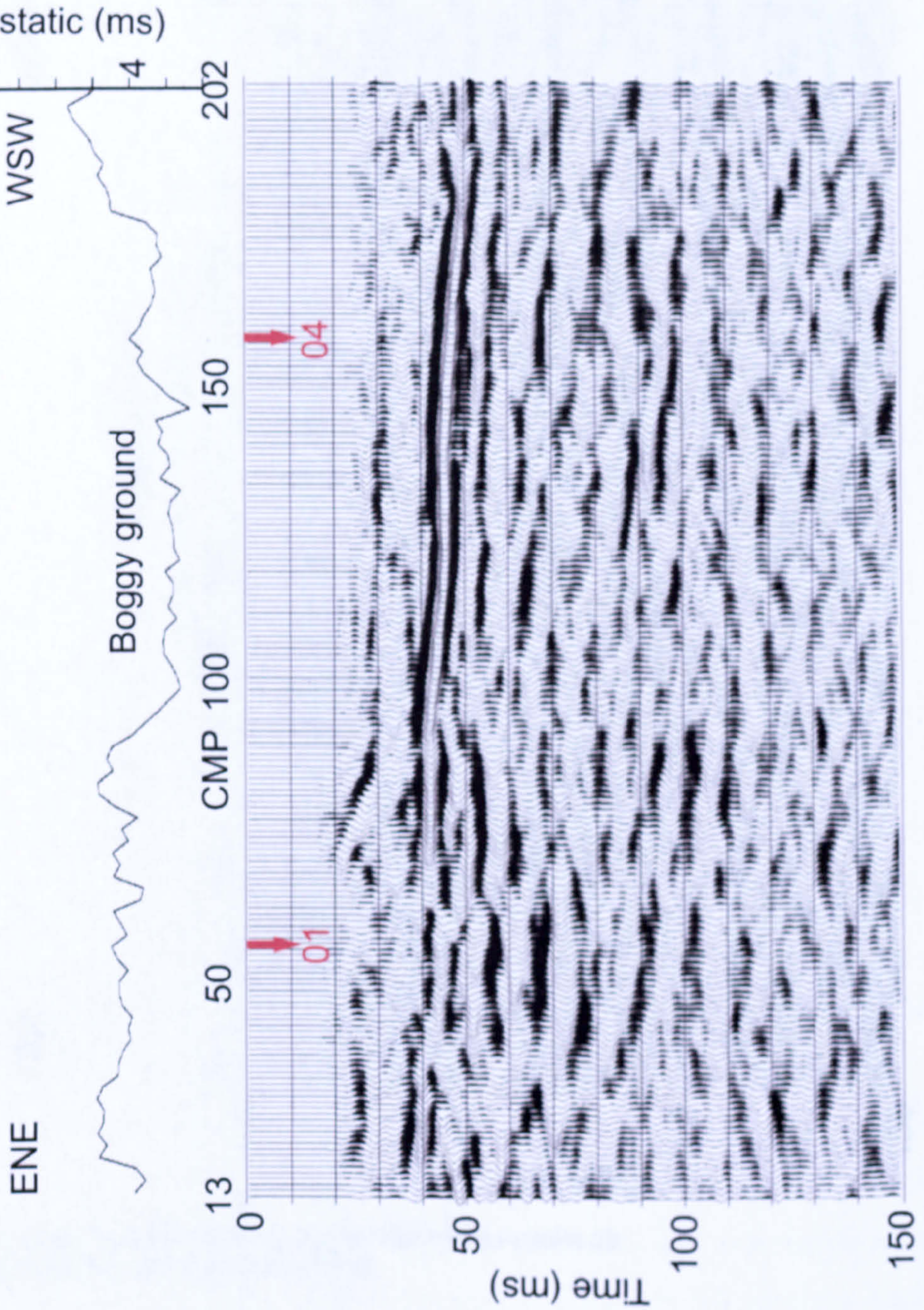

Figure 5.7: Final migrated stack section for Hell Kettles profile 02.
Section is displayed with a scalar multiplier.

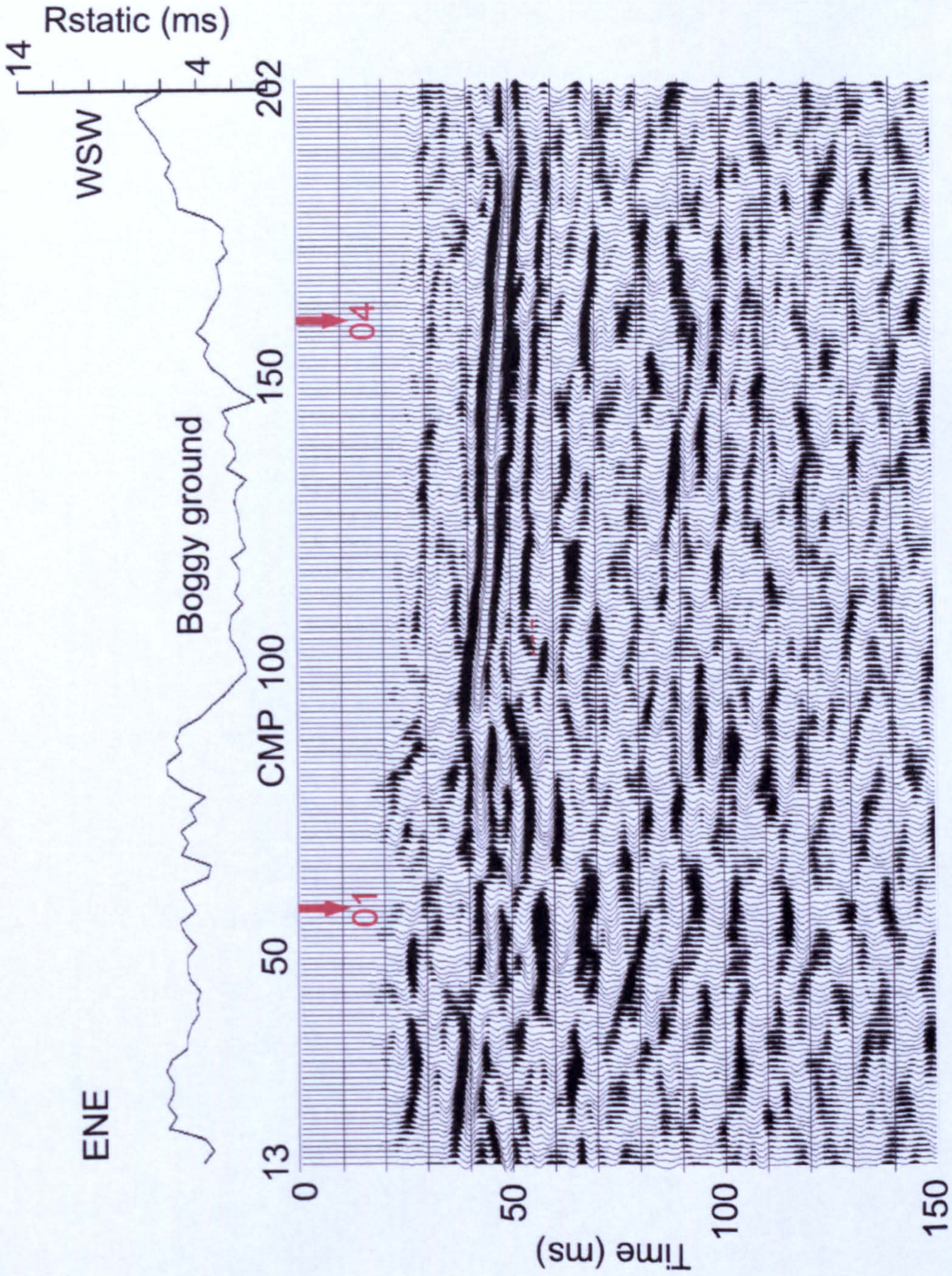

Figure 5.8: Final migrated stack section for Hell Kettles profile 03.
Section is displayed with a scalar multiplier.

At the shot gather level, the frequency content of the single geophones and the groups is comparable (Figure 5.9). However, the coherent reflection event at around 60 ms on the single geophones is not as smooth as on the geophone groups, a difference also reported by Meekes et al. (1990). The millisecond-scale jitter is interpreted as being due to

very local changes in the path of the upcoming wave due to variations in the constitution of the dry near-surface material close to each geophone. The variations in amplitude between the signals recorded on individual geophones are attributed to very local variations in the soil properties and geophone coupling. The small travel path deviations and differences in geophone coupling are to some extent averaged out by the geophone groups. The low-amplitude channels 3, 4, 5 and 6 shift to different channels as the profile rolls along implying that the low-signal is due to the local conditions.

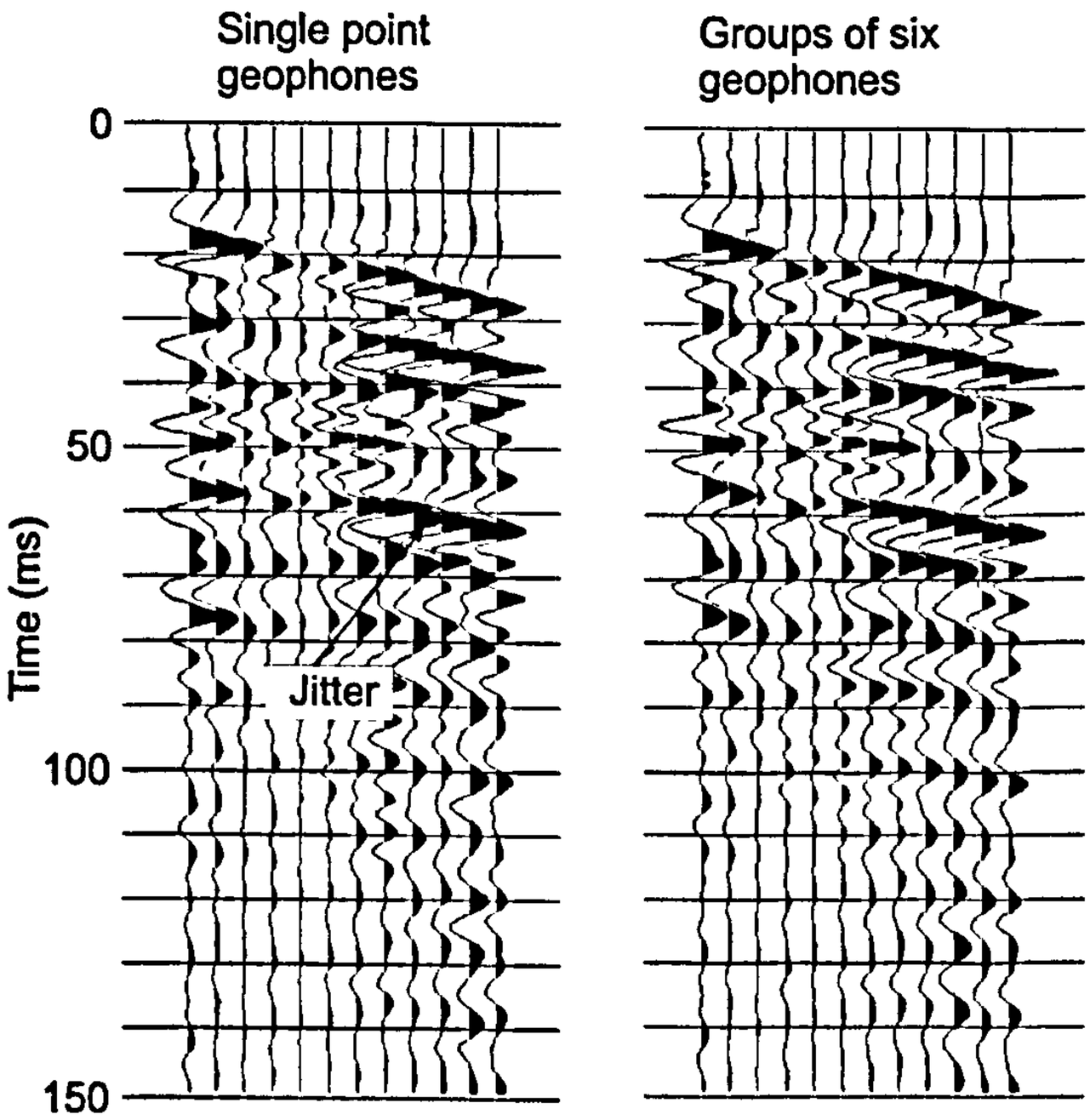

Figure 5.9: Geophone array comparison: shot records from single and array geophone. Comparison shots have field statics and simple bandpass filtering applied. The data are scaled with a scalar multiplier.

A clear difference and improvement in the data collected using the circular groups of geophones is apparent at an early stage in the processing sequence (Figure 5.10). The stacked section using the single geophone data is contaminated with high-frequency background jitter. The superiority of the shot records acquired using the geophone groups propagates through the processing sequence to the final stacked section, where the strong reflection at 48 ms is more continuous (Figure 5.11).

After time migration, the images of the shallow sub-surface geology (Figure 5.12) between each of the different geophone arrangements do have some minor differences.

However, the interpretation of the structure at the top of the Seaham Limestone is not significantly different between the two sections.

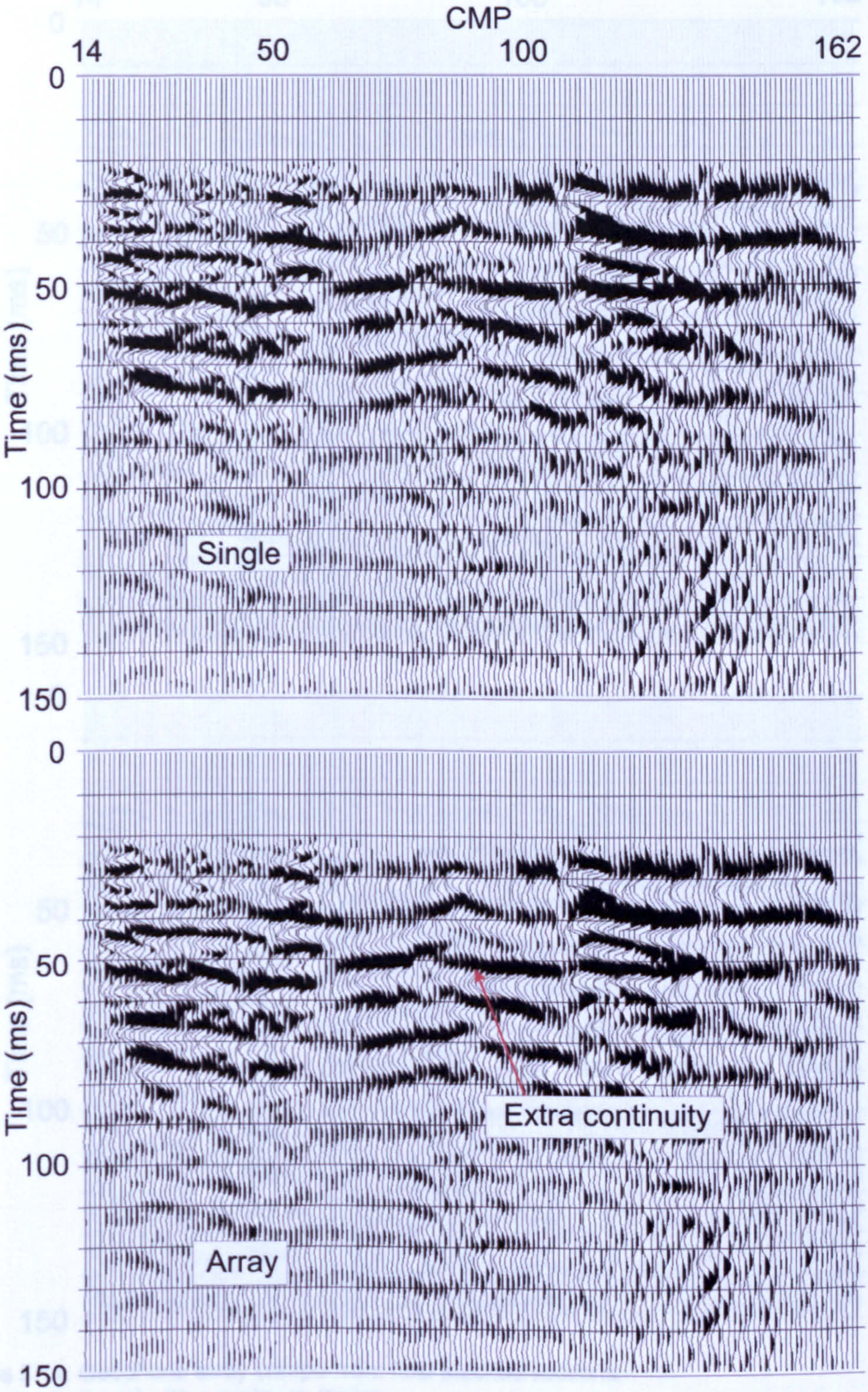

Figure 5.10: Geophone array comparison: sections post field static corrections. Sections are displayed with a scalar multiplier.

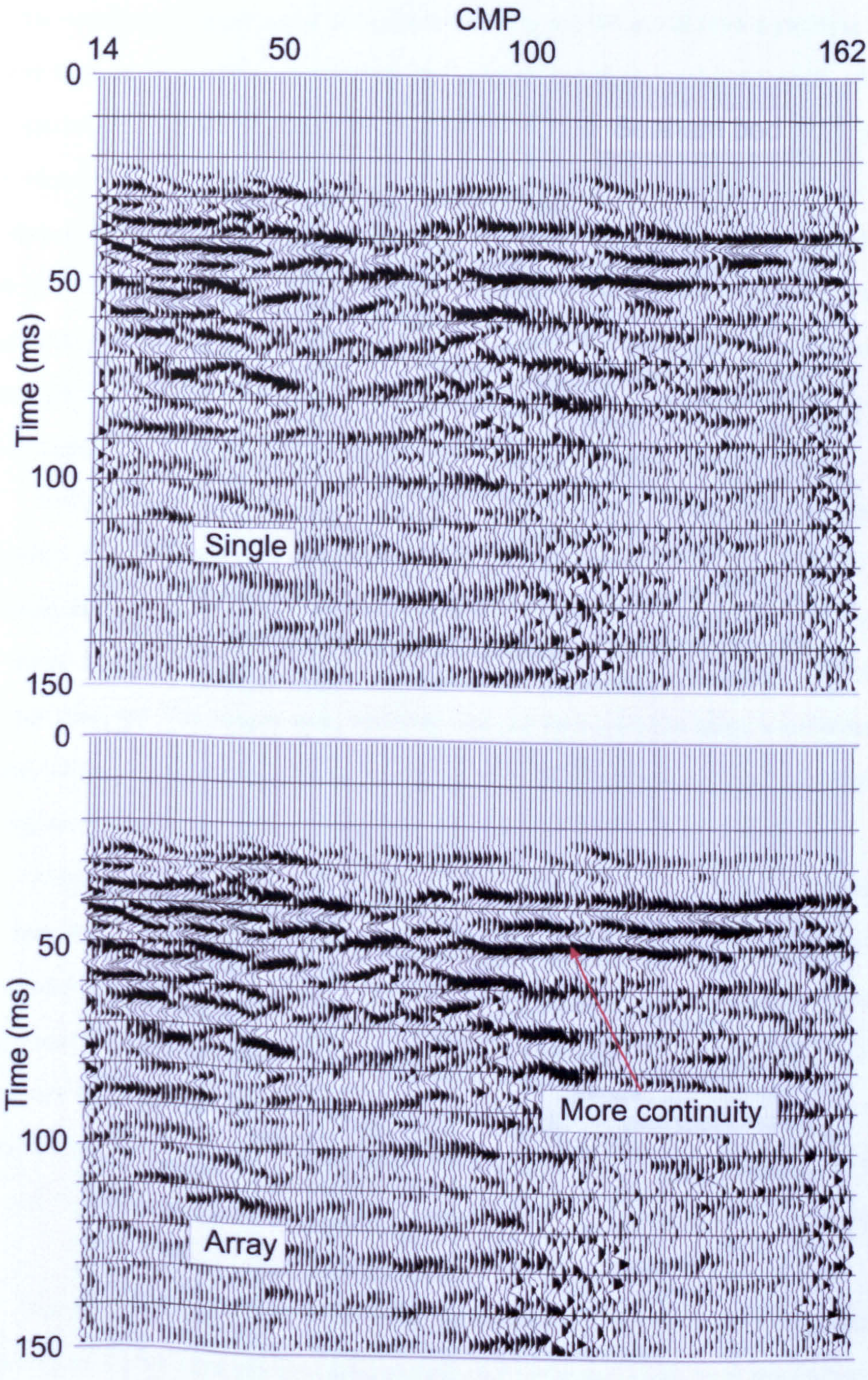

Figure 5.11: Geophone array comparison: final stacked sections.
Data are displayed with a scalar multiplier.

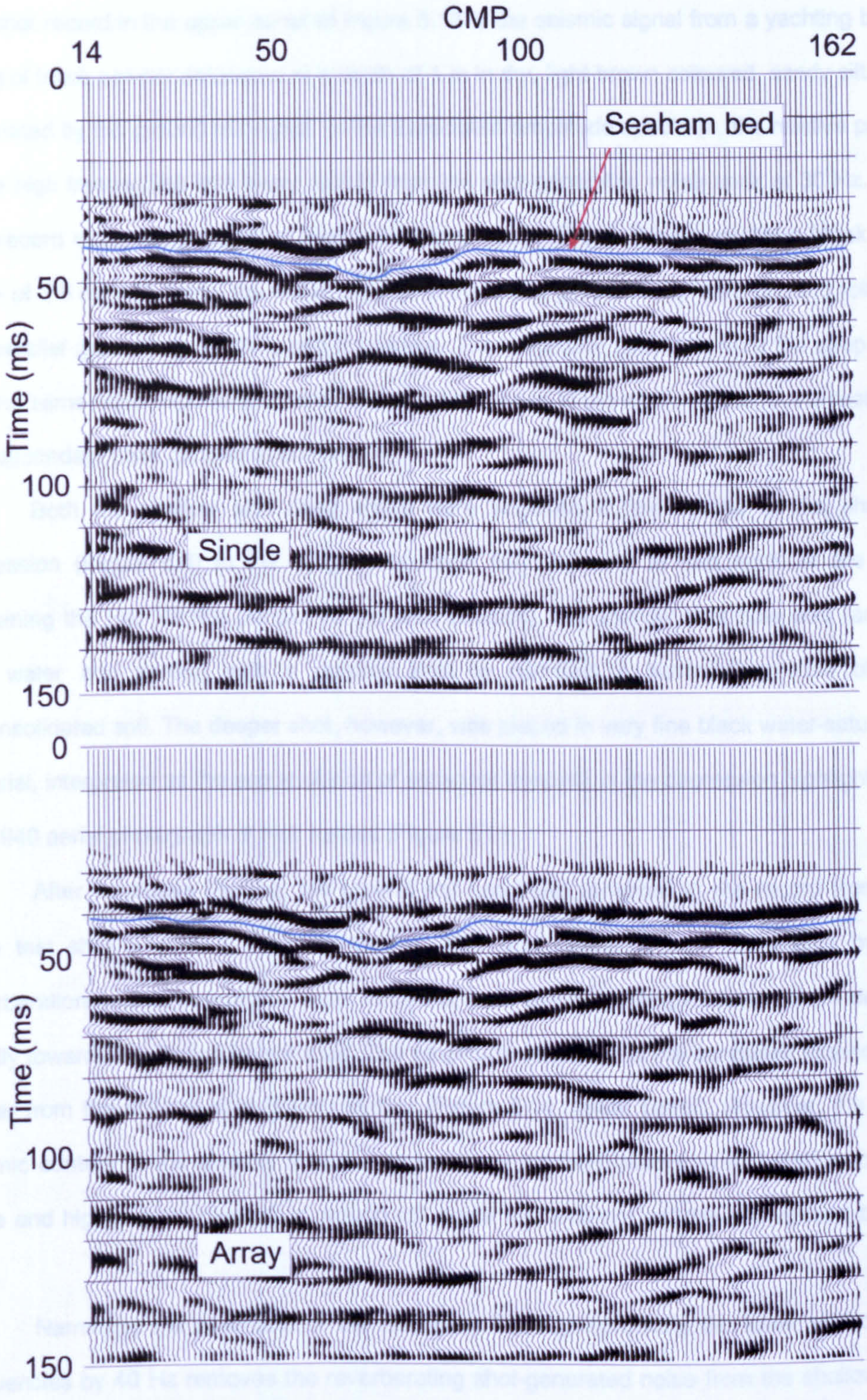

Figure 5.12: Geophone array comparison: trial time migrated sections.
Data are displayed with a scalar multiplier.

5.2.1.2 Comparison of shallow and deep shots

The shot record in the upper panel of Figure 5.13 is the seismic signal from a yachting blank of 7 g of black powder detonated at a depth of 1 m in dry, light brown coloured, sandy silt. It is dominated by the ground roll signal. In the associated amplitude spectrum, the relative power of the high frequencies falls away rapidly from the shot-generated noise peak at 30 Hz. The shot record in the lower panel of Figure 5.13 was generated by firing a yachting blank at a depth of 3.5 m, well below the water table, into the same geophone spread. Ground roll and sub-parallel guided waves are again prominent. The amplitude spectrum from the deep shot has the same rapid exponential decay shape as that seen in the shallow data, but is modified by a secondary peak centred at 80 Hz.

Both the shallow and deep shots were acquired in the middle of the shallow depression (Figure 5.3) in the silage production field adjacent to and north of the field containing the Hell Kettles ponds. To aid shot coupling, the shallow shot hole was tamped with water and sprung with a dummy shot to compact a surrounding shell of dry unconsolidated soil. The deeper shot, however, was placed in very fine black water-saturated material, interpreted as the accumulation of seasonal deposits in the depression highlighted in the 1940 aerial photograph of Hell Kettles (Figure 5.5).

After bandpass filtering, the ground roll has been removed in the record from the deep test shot (Figure 5.14, lower panel). The shot gather is now dominated by the reverberations with an amplitude peak at 80 Hz, from which the amplitude spectrum decays rapidly towards the higher frequencies. The amplitude spectrum of the bandpass filtered shot gather from the shallow shot is very similar (Figure 5.14, upper panel). However, the ringy seismic content of the shallow shot record is further contaminated with high-frequency air-wave and higher order dispersive ground roll noise that was not entirely suppressed by the filter.

Narrowing the passband of the bandpass filter by increasing the lower end corner frequencies by 40 Hz removes the reverberating shot-generated noise from the shallow test shot record (Figure 5.15, upper panel) to reveal a reflection event on the near to mid offsets of the geophone spread. The temporal resolution of the reflection event is poor due to restricted bandwidth. On the deep test shot record (Figure 5.15, lower panel), the reflection event signal

has a comparable temporal resolution, but is more continuous across the shot gather and is not contaminated by any air-wave noise.

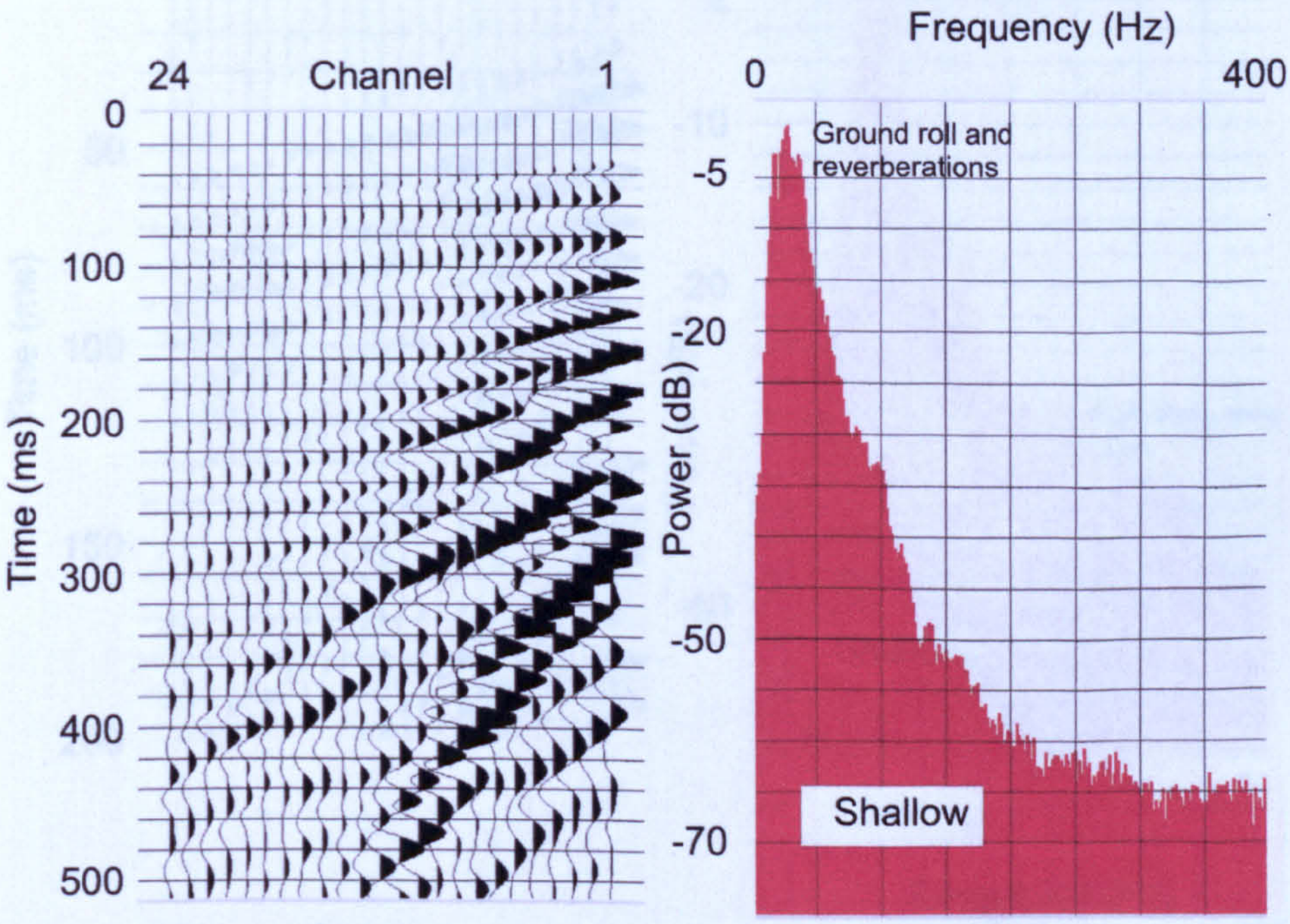

Figure 5.13: Shallow and deep shot comparison.
The data have been pre-conditioned with field statics, gain recovery to account for spherical divergence and the amplitudes normalised within the shot record to lie between -1 and +1. Spectral analysis taken on the whole shot record.

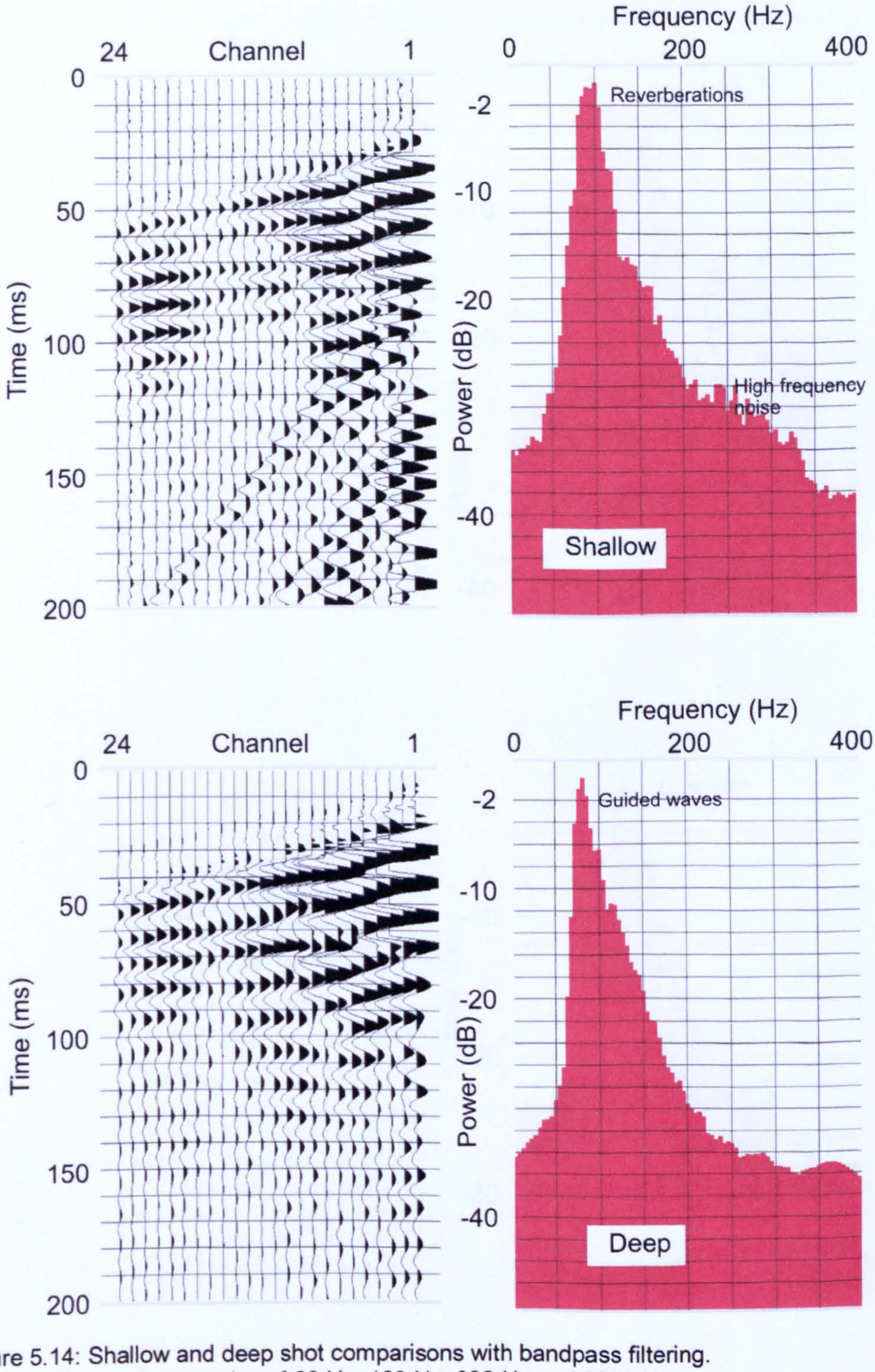

Figure 5.14: Shallow and deep shot comparisons with bandpass filtering.
Bandpass corner frequencies of 60 Hz, 100 Hz, 330 Hz and 350 Hz.

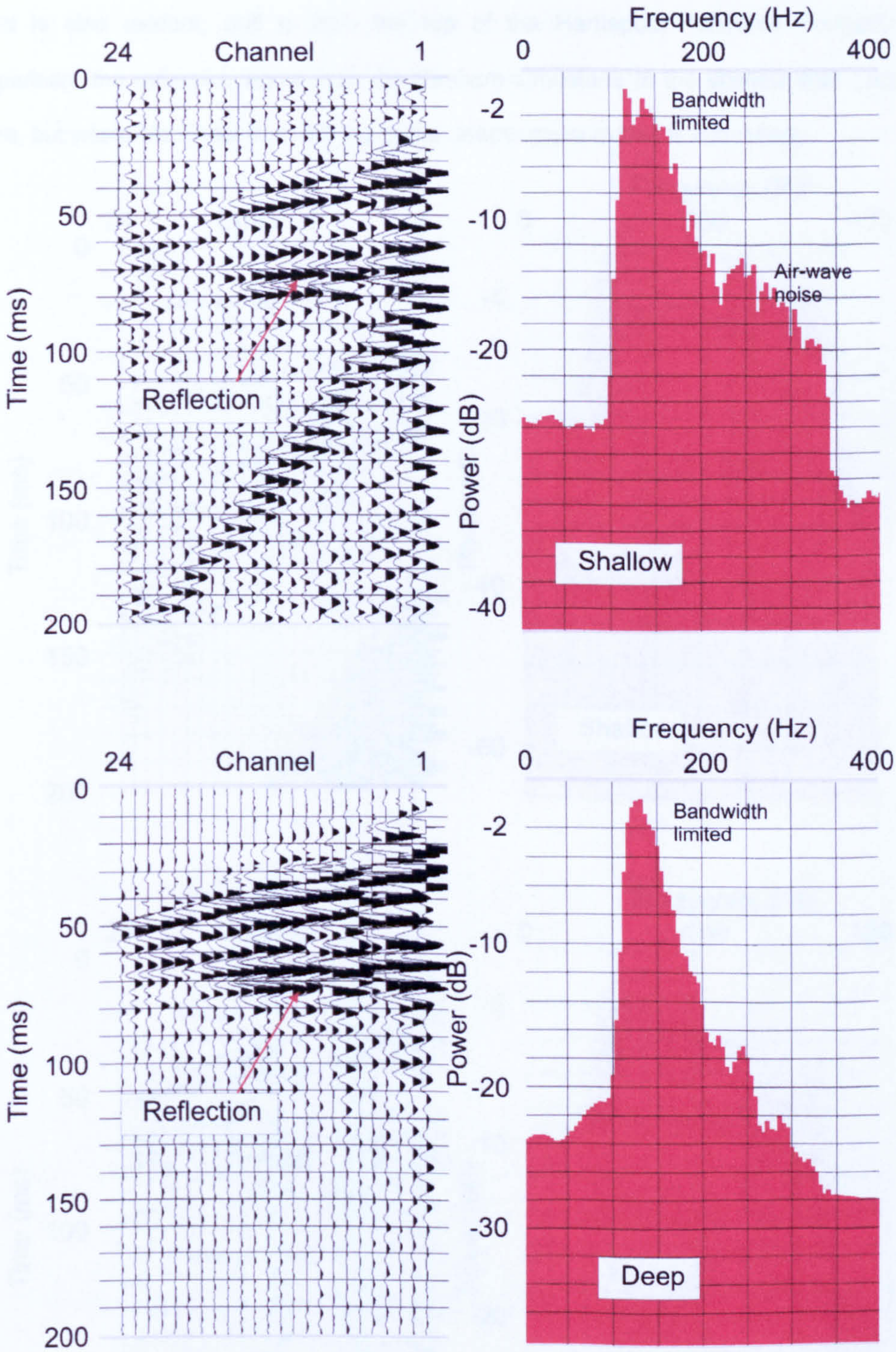

Figure 5.15: Shallow and deep shot comparisons with bandpass filtering.
Bandpass corner frequencies of 100 Hz, 140 Hz, 330 Hz and 350 Hz.

Zero-phase spiking deconvolution efficiently flattens the amplitude spectrum over the target bandwidth of 100 Hz to 330 Hz (Figure 5.16). For the deep shot gather, a hyperbolic reflection event starting at 55 ms on the near-channel is prominent across the whole of the

record, and is interpreted as the Seaham Limestone. A deeper reflection event of limited extent is also evident, and is from the top of the Hartlepool Anhydrite Formation. In comparison, the reflection signal from the Seaham Limestone in the shallow shot gather is visible, but weak. No signal from the top of the deeper gypsum bed is noticeable.

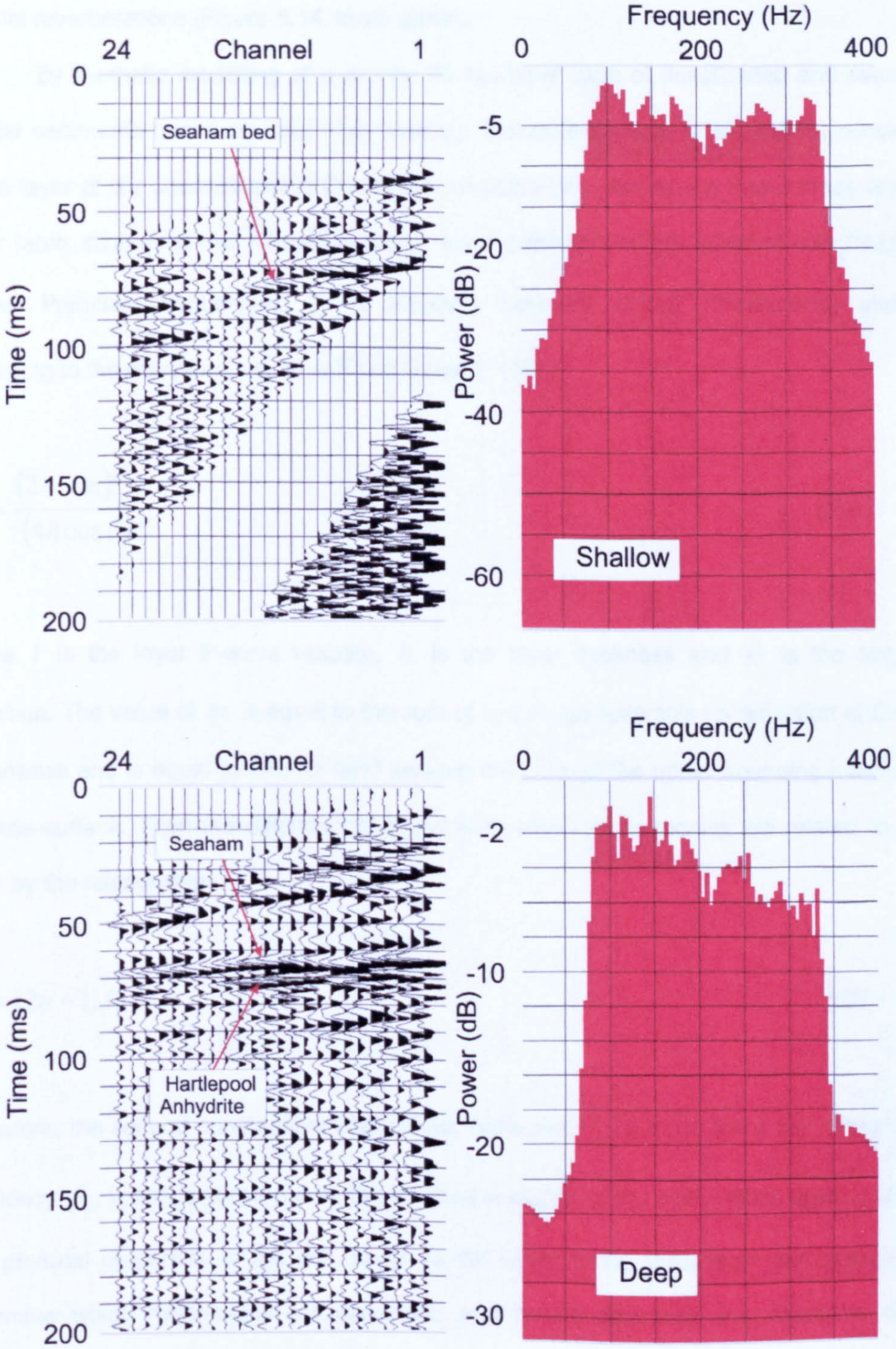

Figure 5.16: Shallow and deep shot comparison with zero-phase spiking deconvolution. Shots have had a bandpass filter applied with corner frequencies of 60 Hz, 100 Hz, 330Hz and 350 Hz before and after deconvolution.

5.2.1.3 Near-surface guided waves

Removing the ground roll and refraction arrivals signal from the raw deep test shot by muting proves that the sub-parallel reverberations have a frequency content of around 25 Hz (Figure 5.17). Bandpass filtering proves that the secondary peak at 80 Hz is another set of sub-parallel reverberations (Figure 5.14, lower panel).

By synthetic modelling of a simple 1D two-layer case of unsaturated and saturated alluvial sediments based on data from northern Switzerland, Roth et al., (1998) concluded that a layer of dry unconsolidated Quaternary deposits bounded by the free-surface and the water table, such as at Hell Kettles, acts as a wave guide for multiply reflected compressional waves. Particular frequencies f_n of internally reflected waves constructively interfere according to the equation (e.g. Sheriff and Geldart, 1995):

$$f_n = \frac{(2n-m)V}{(4h\cos\theta)} \qquad (5.2)$$

where V is the layer P-wave velocity, h is the layer thickness and θ is the angle of reflection. The value of m is equal to the sum of the phase reversals on reflection at the two boundaries and is equal to one for land seismic data where the upper bounding interface is the free-surface. Then the different constructive interference harmonics are related to each other by the relationship:

$$f_n = (2n-1)f_1 \qquad (5.3)$$

Therefore, the second constructive interference harmonic f_2 is three times the fundamental frequency f_1, which is borne out by the spectral analyses of the Hell Kettles deep shot trial. The physical properties of the soil, depth to the water table, shot depth and charge size determine which frequencies are dominant, and hence determine the character of the reverberations.

Figure 5.18 shows the picked first break times to the near-offset geophones for all reverse shots along profile 02. The first break on the near channel on a shot record is the time taken for a wave to travel from the shot to the nearest geophone. At Hell Kettles a large component of the travel time is the time taken for the wave to propagate along the layer immediately below the refracting water table. The remaining component of the travel time is a function of the nature and thickness of the dry near-surface materials in the vicinity of the shot and receiver.

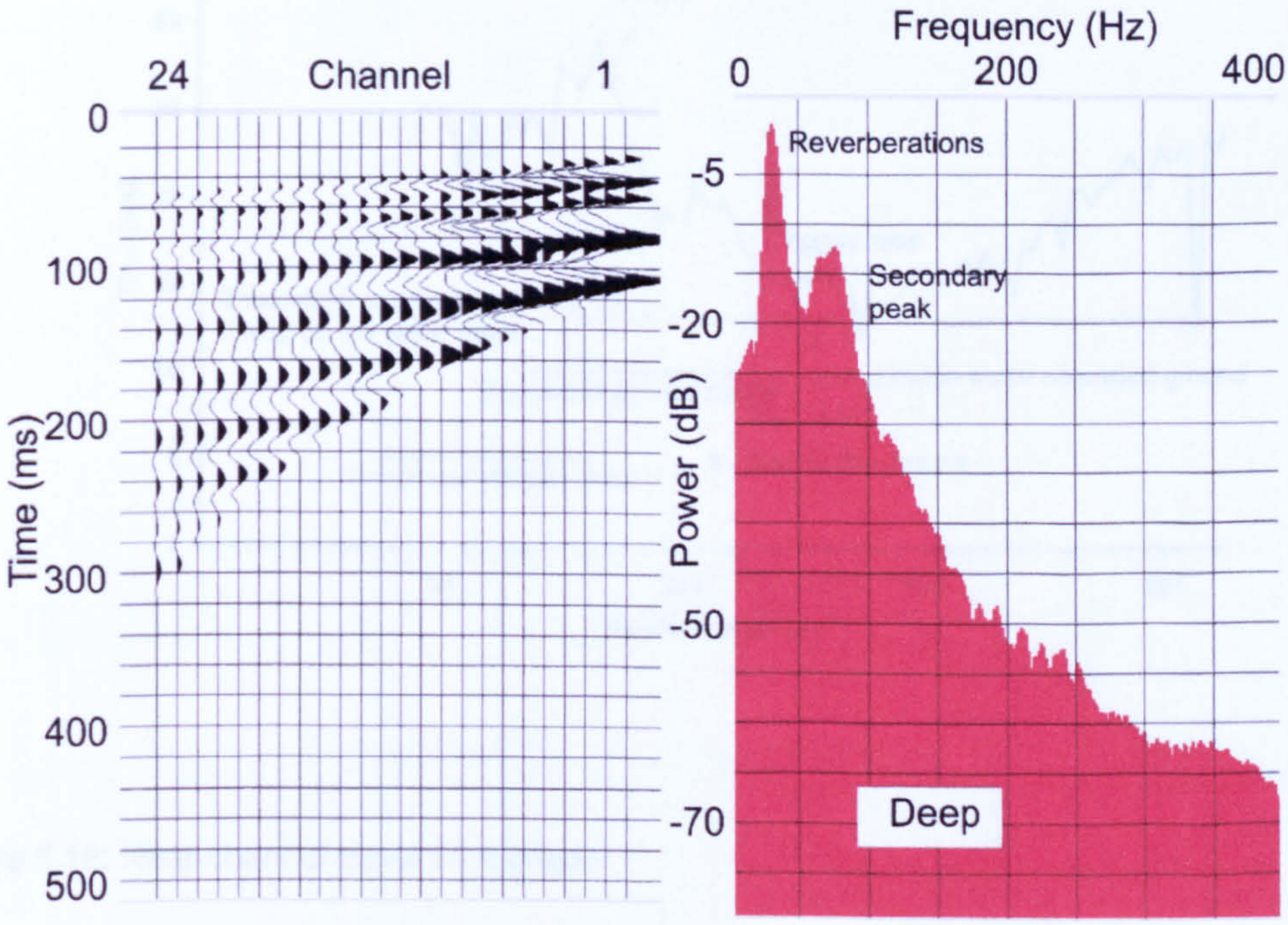

Figure 5.17: Ground roll muted raw deep trial shot.

The near-offset is 23 m and the refractor velocity is 1768 m s^{-1}. If all the shots and receivers were placed on the water table refracting interface, the near-offset travel times would all be 13 ms. The jitter in the first break times may be attributed to errors in the time breaks from the buffalo gun, whereas the broad peak centred at source station distance 70 m is probably an indication of disturbed ground or a localised increase in the gravel content of the near-surface materials. A combination of a wet winter and localised poor drainage created a sub-circular area of water saturated ground between 130 m and 144 m along profile 02 and the minimum on the shot travel time graph is coincident with the boggy ground.

The left panel in Figure 5.19 shows the signal of a blank saluting cartridge detonated at depth of 1 m below ground surface in dry soil conditions. First arrivals and low-frequency

reverberations sub-parallel to the first breaks are the dominant waveforms on the record. This shot gather is typical of the raw data acquired at Hell Kettles dominated by the constructive interference of the guide- waves and refraction arrivals which can be removed efficiently by bandpass filtering.

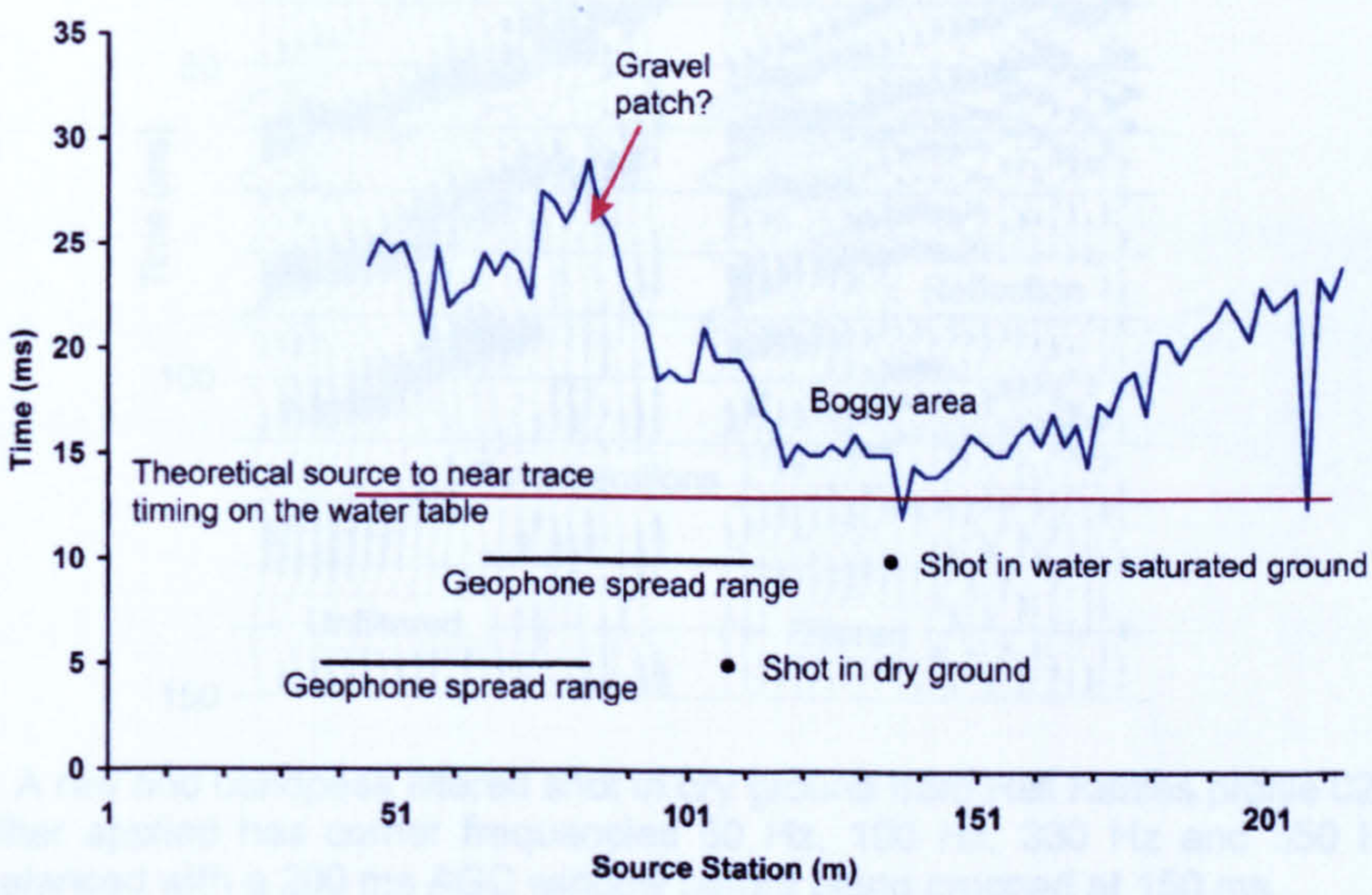

Figure 5.18: Near-channel travel time graph.

Figure 5.20 shows a shot gather from a saluting blank detonated in a shot hole drilled at station 138 m in the middle of the water saturated ground. A clear hyperbolic reflection event interpreted as the signal from the Seaham Limestone is easily traced across the first twelve channels before being overwhelmed by low-frequency reverberations. Along profile 02 at the southern end of the Hell Kettles site, the water table is between 1.5 m and 1 m below the ground surface. Therefore, the surface water in the area of saturated ground may be in direct contact with the water table. If this is case, the water table will effectively be at the free surface. For the near channels, the upcoming P-wave reflection off the Seaham Limestone travels through completely water-saturated ground. At this location no masking reverberations are possible since the presence of a low-velocity near-surface layer is required for guided waves to propagate. For the geophones planted further away from the shot point, the

upcoming reflection will pass through a bounded layer of low P-wave velocity dry unconsolidated material.

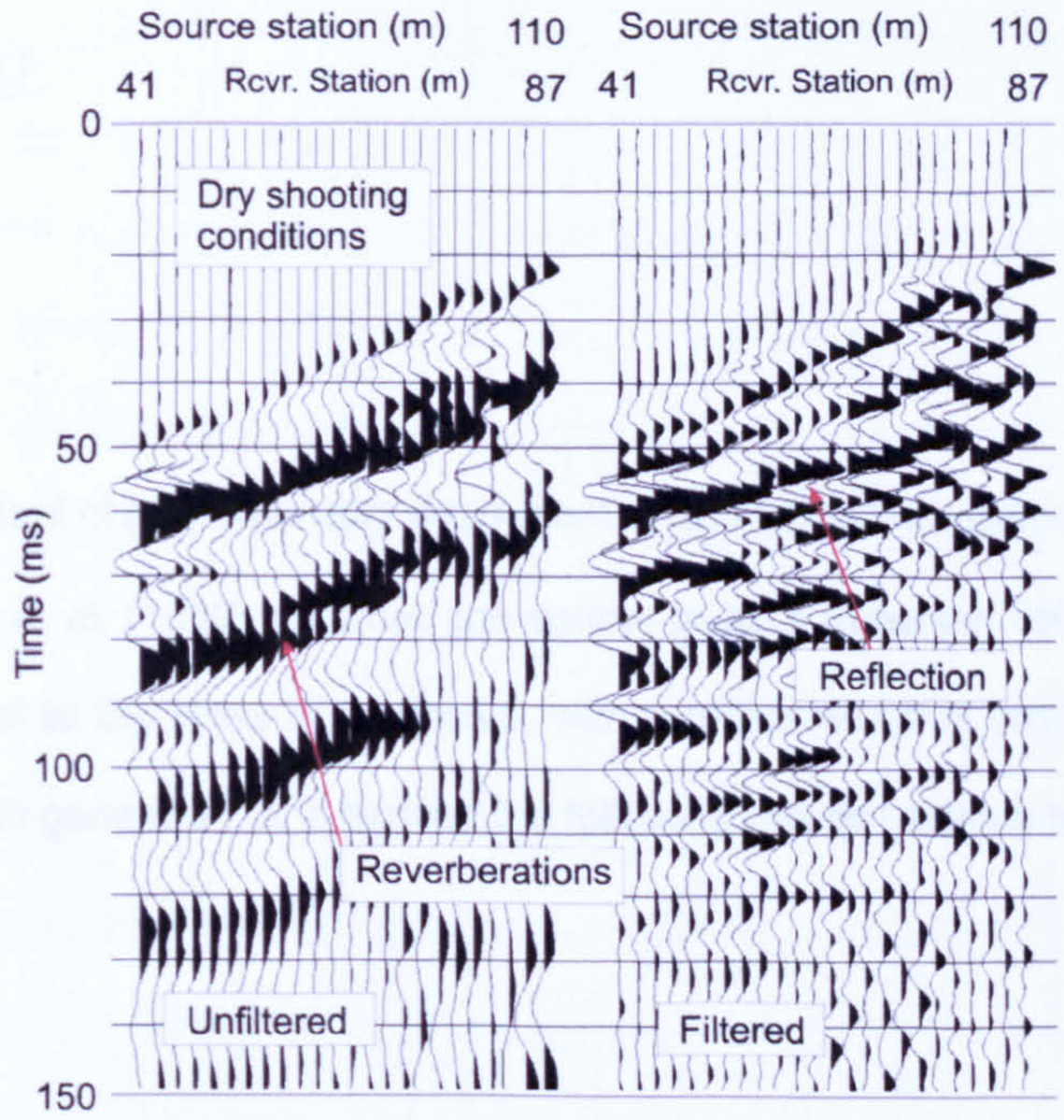

Figure 5.19: A raw and bandpass filtered shot in dry ground from Hell Kettles profile 02. Bandpass filter applied has corner frequencies 60 Hz, 100 Hz, 330 Hz and 350 Hz. The traces are balanced with a 200 ms AGC window before being cropped at 150 ms.

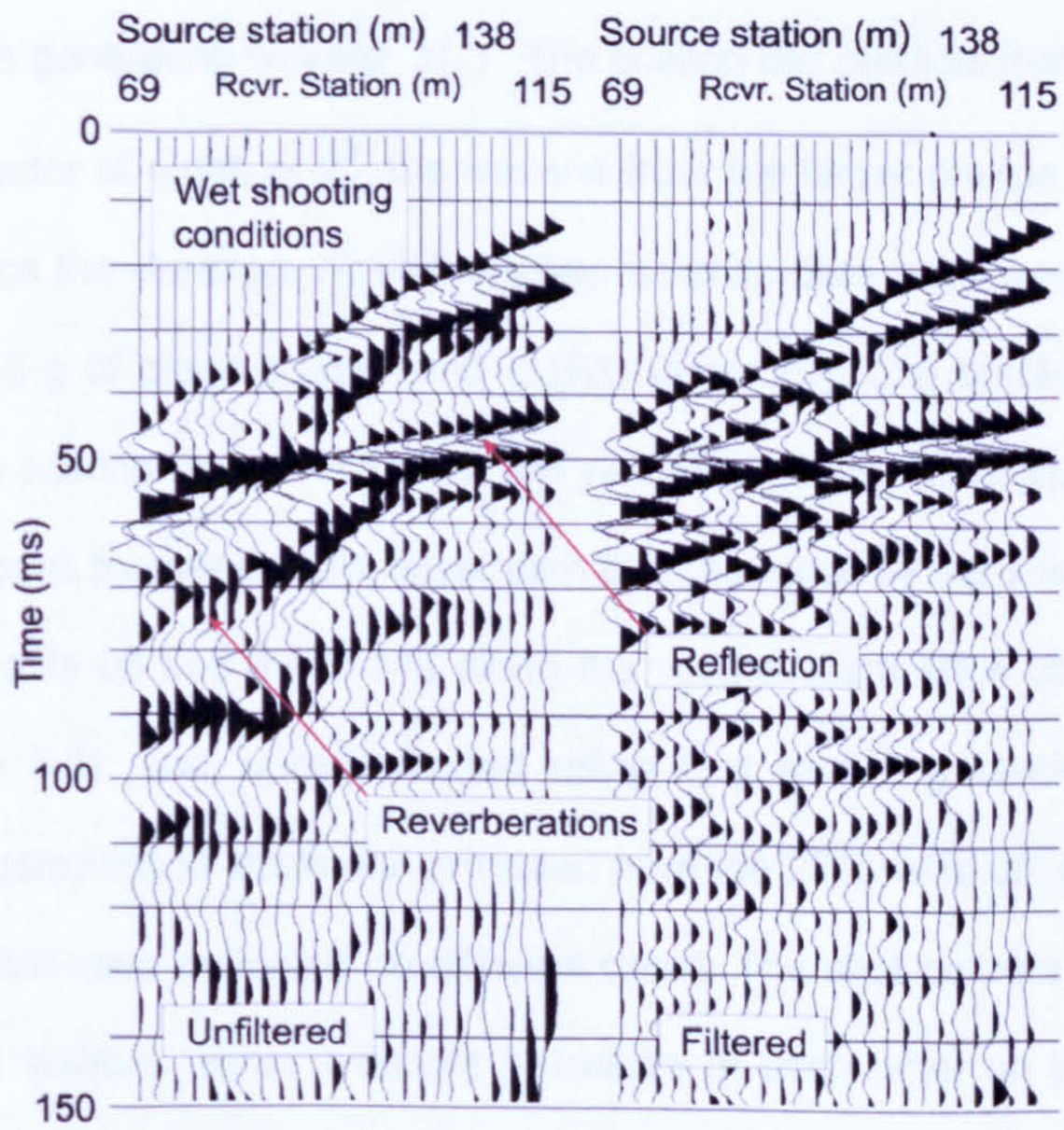

Figure 5.20: A raw and bandpass filtered shot in wet ground from Hell Kettles profile 02. Bandpass filter applied has corner frequencies 60 Hz, 100 Hz, 330 Hz and 350 Hz. The traces are balanced with a 200 ms AGC window before being cropped at 150 ms.

5.2.1.4 Comparison of different size charges

According to Peet (1960), the peak seismic frequency f_m radiated from a shot is proportional to the charge size Q:

$$f_m = cQ^{1/3} \tag{5.4}$$

where c is a constant of proportionality dependent on the type of explosive.

Ziolkowski et al. (1980) assumed the source to be a spherical volume whose size is directly proportional to the mass of explosive, with a radius which is small compared to the shortest wavelength generated, and derived the following wavelet scaling law:

$$s'(t) = \alpha s(t/\alpha) \tag{5.5}$$

where $\alpha = \sqrt[3]{\frac{M'}{M}}$, M' is the mass of the charge generating wavelet $s'(t)$, and M is the mass of the charge generating wavelet $s(t)$. The scaling law predicts that if the difference in charge size is a factor of eight, or 2^3, the wavelet from the larger charge will have twice the amplitude and twice the duration. At Hell Kettles, seismic data were acquired with saluting blanks containing 5 g of black powder and slightly larger yachting blanks containing 7 g of black powder. The scaling law predicts that the yachting blanks will produce a wavelet 12% longer and with a peak frequency 12% lower than that produced by the smaller charge.

The 2D profile 06 and the in-line along the southeastern edge of the 3D survey are coincident (Figure 5.3), and were collected using 5 g and 7 g black powder charges, respectively. The comparison shots are extracted from the 2D profile 06 and the 3D volume, seismic datasets that were collected on different dates. The shot gathers analysed are from shots fired at shot stations within a couple of metres of each other on the ground surface. Additionally, the 3D survey was acquired with a symmetrical split-spread shooting arrangement, as opposed to the end-on shooting pattern for 2D profile 06. In the acquisition design of profile 06, each shot point was used twice with geophone spreads of 24 channels

deployed separately in the forward and reverse directions, with a geophone station spacing of 2 m. To simulate the 3D shooting pattern, the two shot gathers from each shot point were combined and every other trace dropped. Therefore, the comparisons are not exact because both shot and receiver positions are slightly different.

The raw shot records (Figure 5.21) between the two different size charges are very similar in seismic character. Any reflection energy is masked by a central cone of high-amplitude ground roll noise and guided-wave reverberations which form the large peak at 40 Hz in the amplitude spectrum. For the smaller charge size, the signal contribution of higher frequency decays rapidly, whereas frequencies centred around 150 Hz makes a significant input to the signal from the larger charge.

Applying mutes to remove the refraction arrivals and ground roll noise cone plus simple bandpass filtering (Figure 5.22) reveals a reflection event interpreted as originating from the Roxby-Seaham geological boundary. This event is visible in the positive offset arm of both test shot gathers, but clearer in the seismic data recorded from the larger charge. In the associated amplitude spectra from the 7 g yachting blank consists of two peaks. The first centred at 90 Hz represents the remaining guided-wave noise in the left hand side of the shot gather, whilst the second peak centred at 150 Hz is the reflection signal. For the 5 g black powder charge the strength of the reflection signal is small relative to the guided-wave noise, hence the single dominant peak in the amplitude spectra.

Narrowing the passband of the bandpass filter by increasing the lower end corner frequencies by 40 Hz removes the reverberating guided-waves centred at 90 Hz improving the reflection signal in both sizes of charge tested (Figure 5.23). The amplitudes are normalised to range between +1 and -1 over the total length of 512 ms of each shot record after which the same a very low-frequency dummy trace is appended. The dummy trace is designed so that the spectral analysis normalises the amplitude spectra relative to this high peak.

The reflection signal is cleaner in the shot record from the 7g black powder charge size represented in the amplitude spectrum as a smooth curve peaking at 150 Hz. A peak at 150 Hz is also present in the amplitude spectrum of the smaller saluting blank charge. But the signal is contaminated by high-frequency noise and residual guided-waves of frequency of

about 120 Hz. A difference of 4 dB in the reflection signal power is between the two charge sizes of the larger charge this would be expected from the scaling law; however, no shift in the peak frequency is noted.

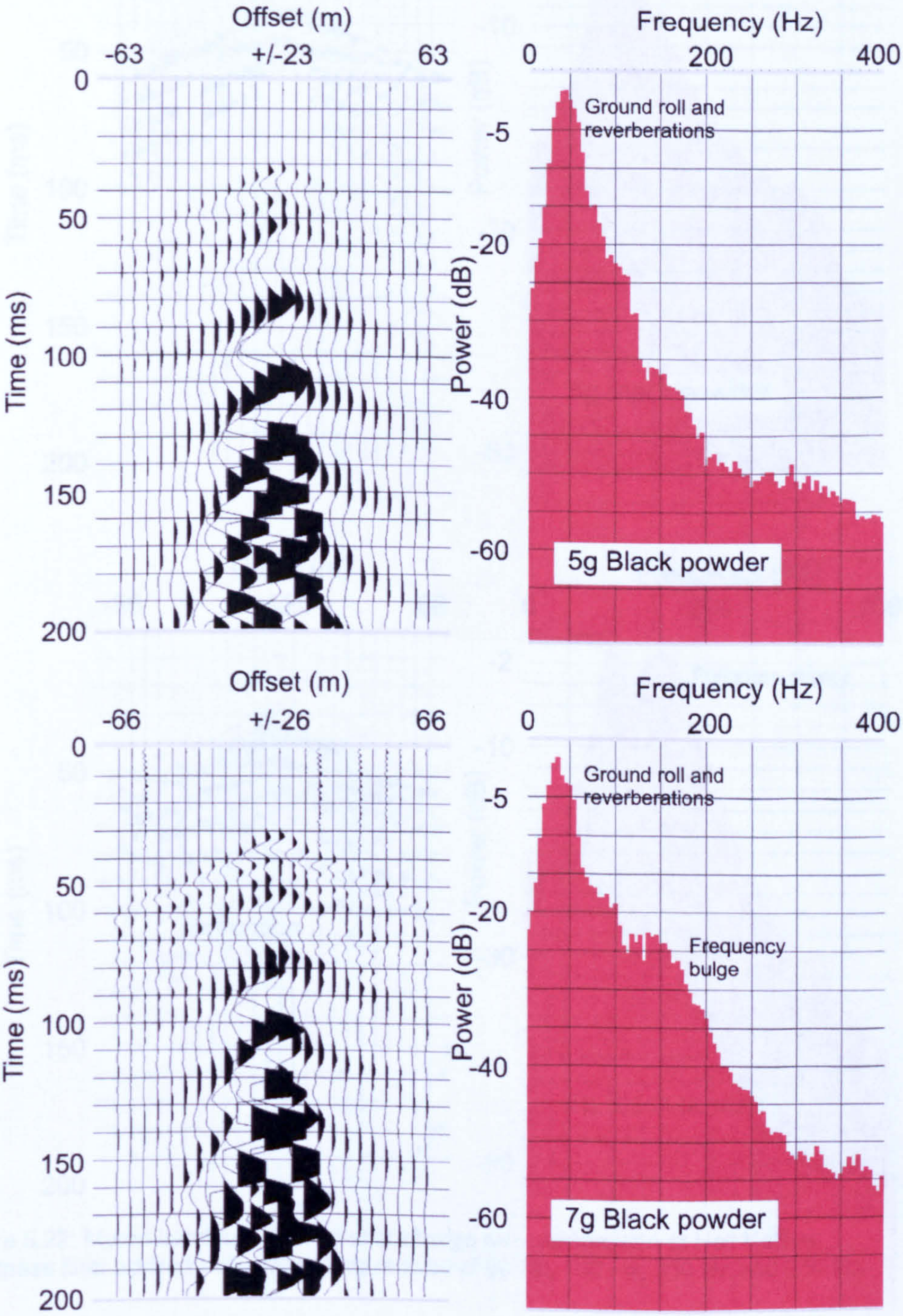

Figure 5.21: Raw shot charge size comparison at Hell Kettles.
The data have had field statics applied and the amplitudes normalised within the shot record to lie between -1 and +1. Spectral analysis is taken on the 200 ms window displayed.

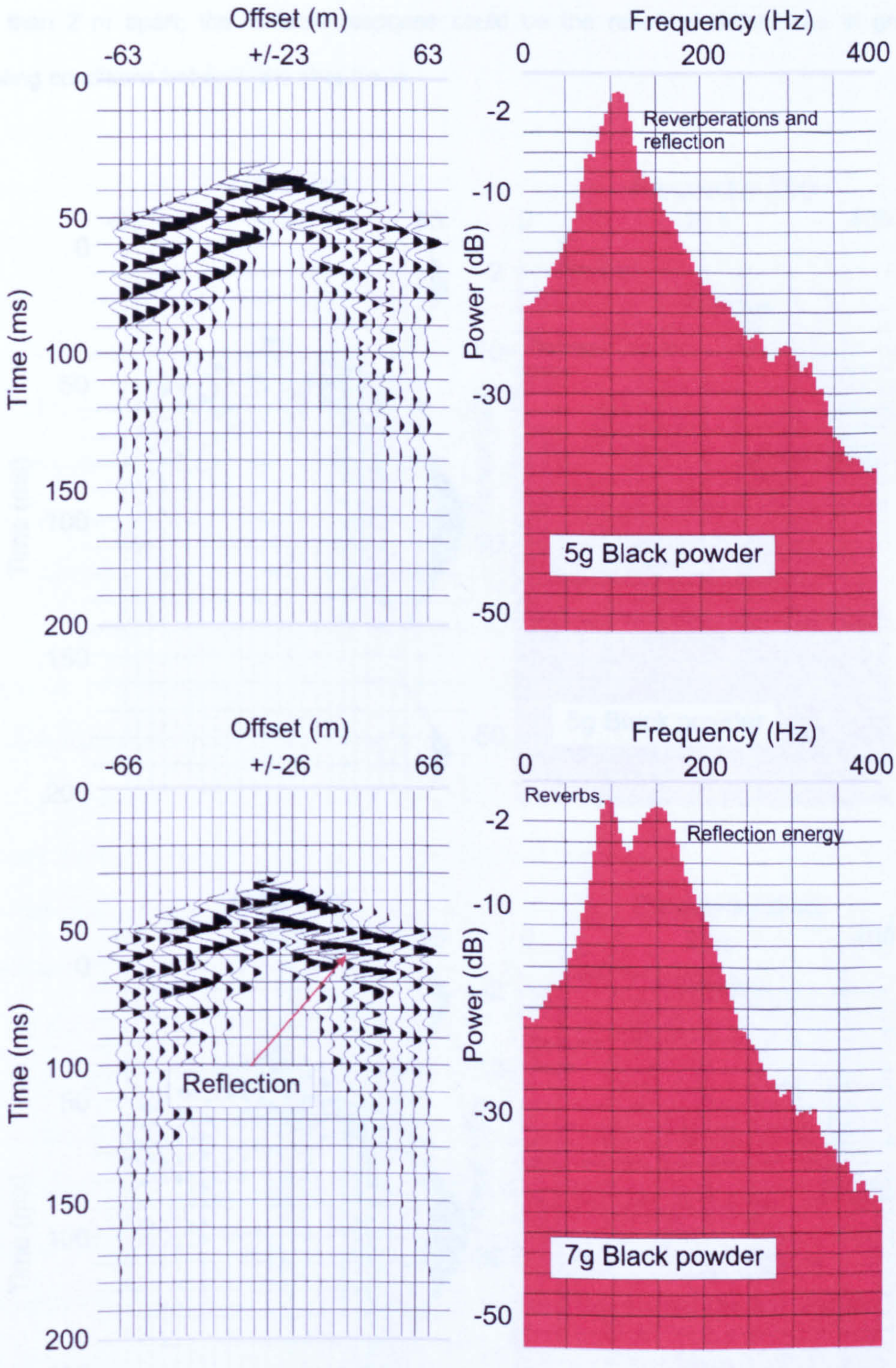

Figure 5.22: Muted bandpass filtered shot charge size comparison at Hell Kettles.
Bandpass filter applied with corner frequencies of 60 Hz, 100 Hz, 330 Hz and 350 Hz.

Shot comparisons at other intersection points between 2D profile 06 and the 3D dataset show a variety of results. No conclusions can be drawn on the comparison trials. The ground conditions were dry unconsolidated soils with localised patches of gravelly material

that have been ploughed in the recently past. Even though the comparison shot holes are less than 2 m apart, the variable response could be the result of differences in ground coupling conditions between the shot holes.

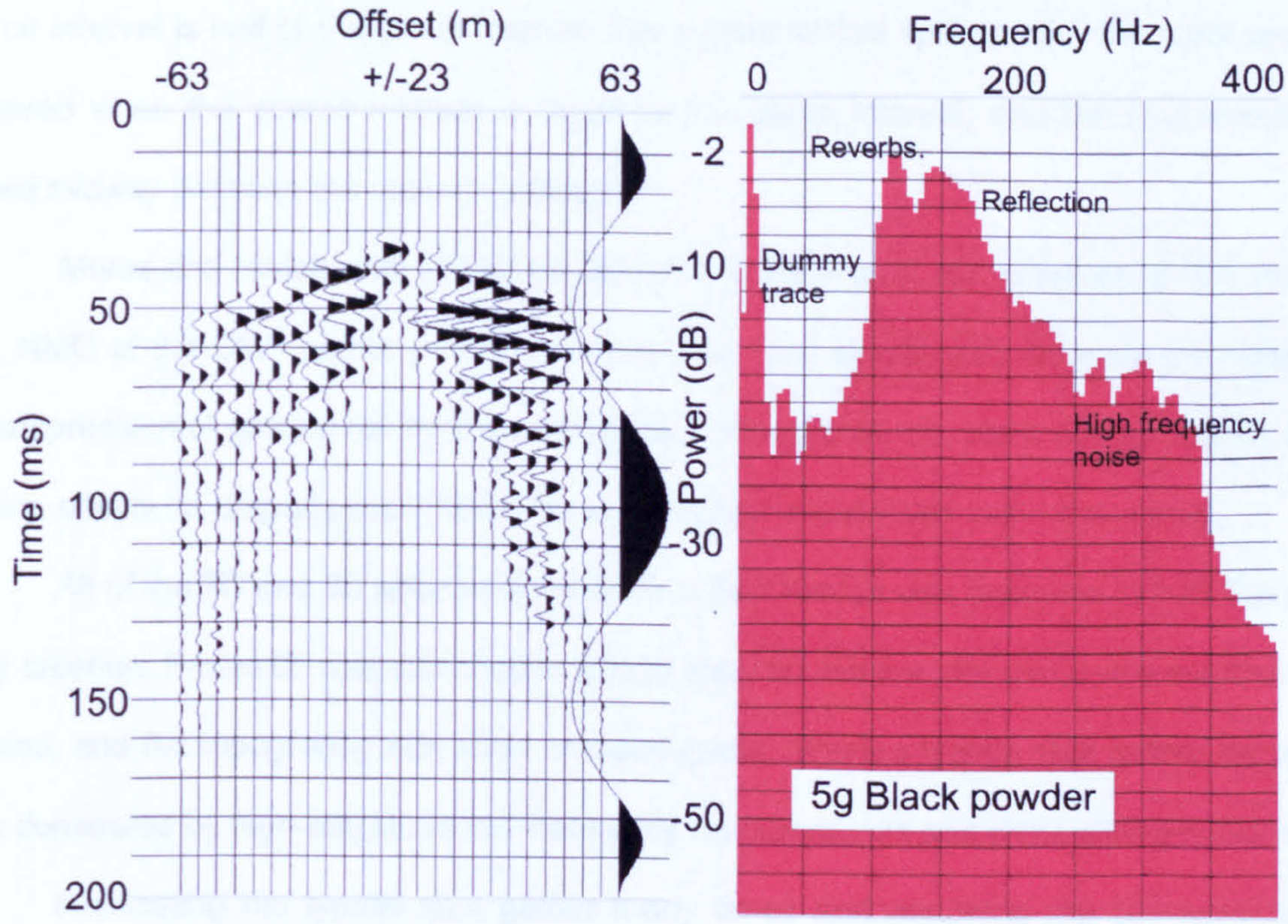

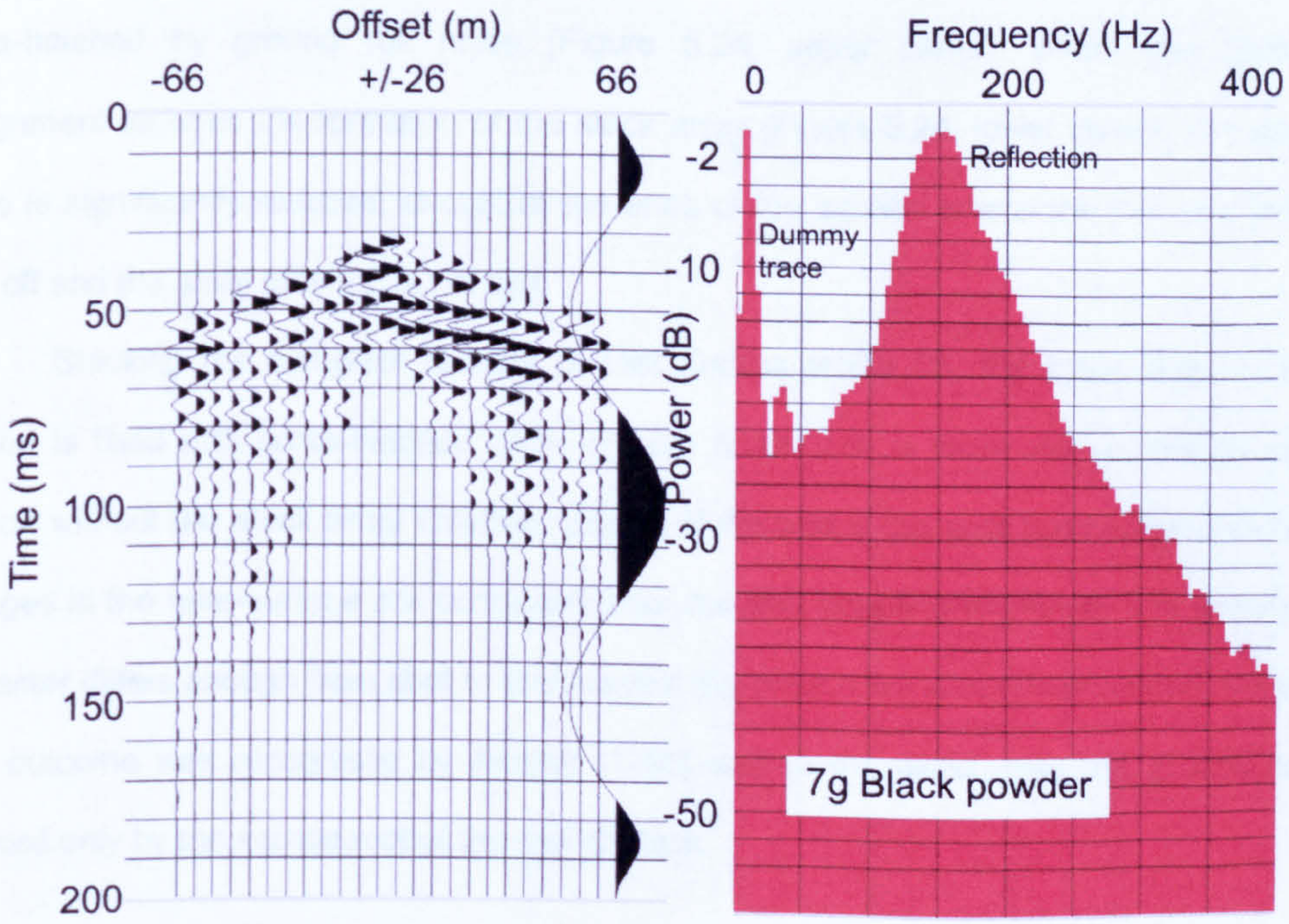

Figure 5.23: Muted bandpass filtered shot charge size comparison at Hell Kettles. Bandpass filter applied with corner frequencies of 100 Hz, 140 Hz, 330 Hz and 350 Hz.

5.2.1.5 Ground roll elimination by the stack array

One approach to the suppression of ground roll is the stack array (Anstey, 1986). The criterion for a stack array is that there must be an even, continuous, uniform succession of geophones across the CMP gather. This can be accomplished for off-end shooting when the source interval is half of the group interval. For a symmetrical split-spread, the stack array is achieved when the source interval is equal to the group interval, and the shot points are placed midway between the receiver stations.

Morse and Hildebrandt (1989) concluded that for ground roll velocities of 300 m s^{-1} or less, NMO of the CMP gather prior to stacking would not significantly degrade the impact of the suppression of ground roll by the stack array. In their analysis, static corrections for near-surface effects do degrade the stack array suppression capabilities, but not severely.

All of the 2D and 3D seismic acquisition at Hell Kettles was designed to fulfil the stack array criterion. Profile 05 was collected in almost ideal conditions: dry and sunny weather with no wind, and flat topography with short cropped grass. where a typical shot gather for profile 05 is dominated by high-amplitude low-frequency reverberations and dispersive ground roll.

Replicating the typical shot gather many times and assigning the geometry to the repeated data so that the stack array criterion is not fulfilled produces a stacked section cross-hatched by ground roll noise (Figure 5.24, upper panel). When the geometry assignment satisfies the formation of the stack array (Figure 5.24, lower panel), the seismic noise is significantly reduced, except at the ends of the section where the fold of coverage rolls off and the array criterion is not met.

Stacking the complete dataset of Hell Kettles profile 05, the lower portion of the section is filled with cross-hatched noise (Figure 5.25), and is more akin to the simulated section without the stack array criterion fulfilled. Even where the shot point interval is small, changes in the near-surface soil conditions alter the shot coupling response. The ground roll character differs enough from shot to shot so that the ground roll is not destructively removed. This outcome was recognised by Anstey (1986) and in the worst case the ground roll is reduced only by the square root of the fold of stack.

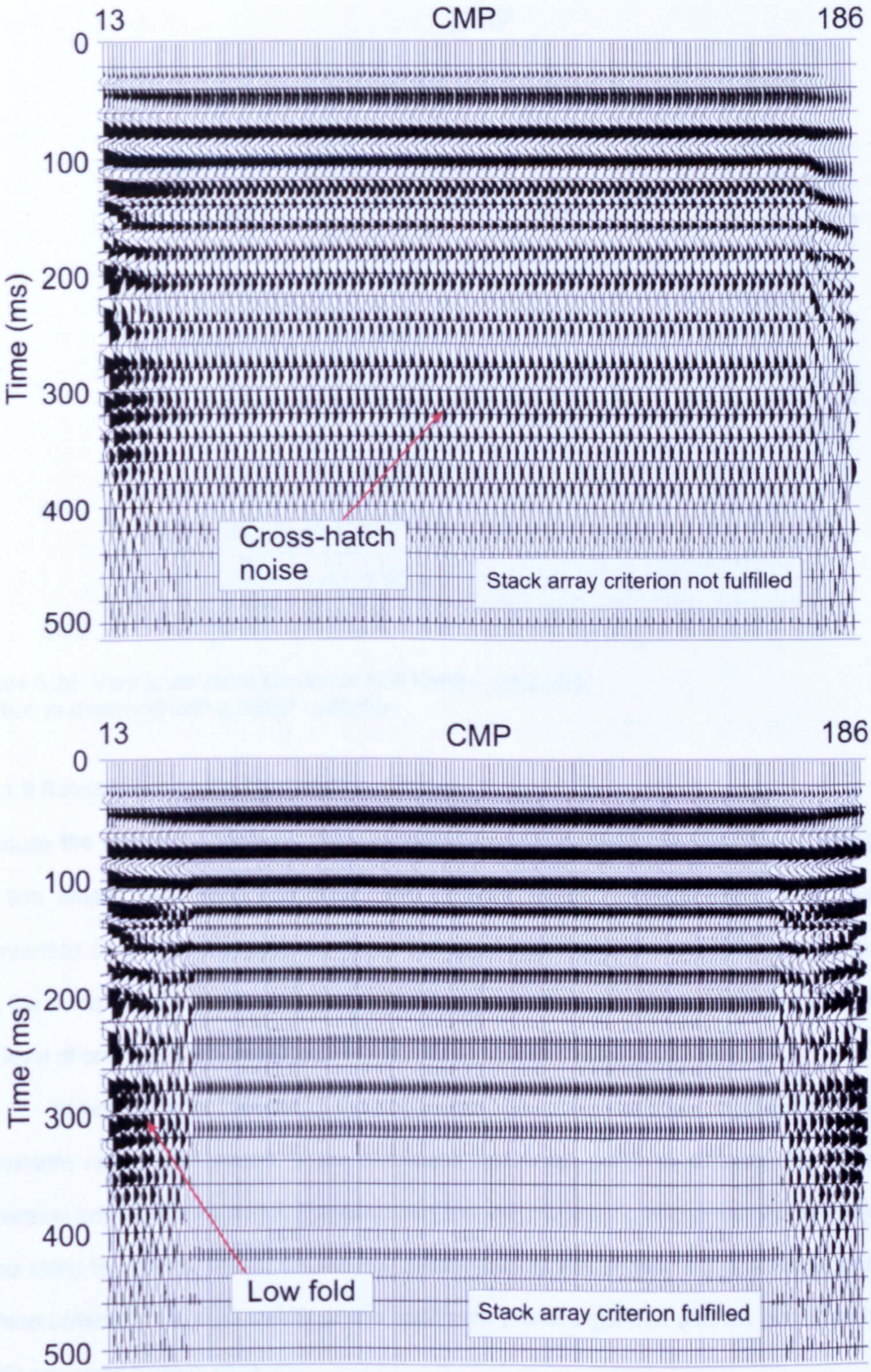

Figure 5.24: Simulated stack array sections
Sections are displayed with a scalar multiplier.

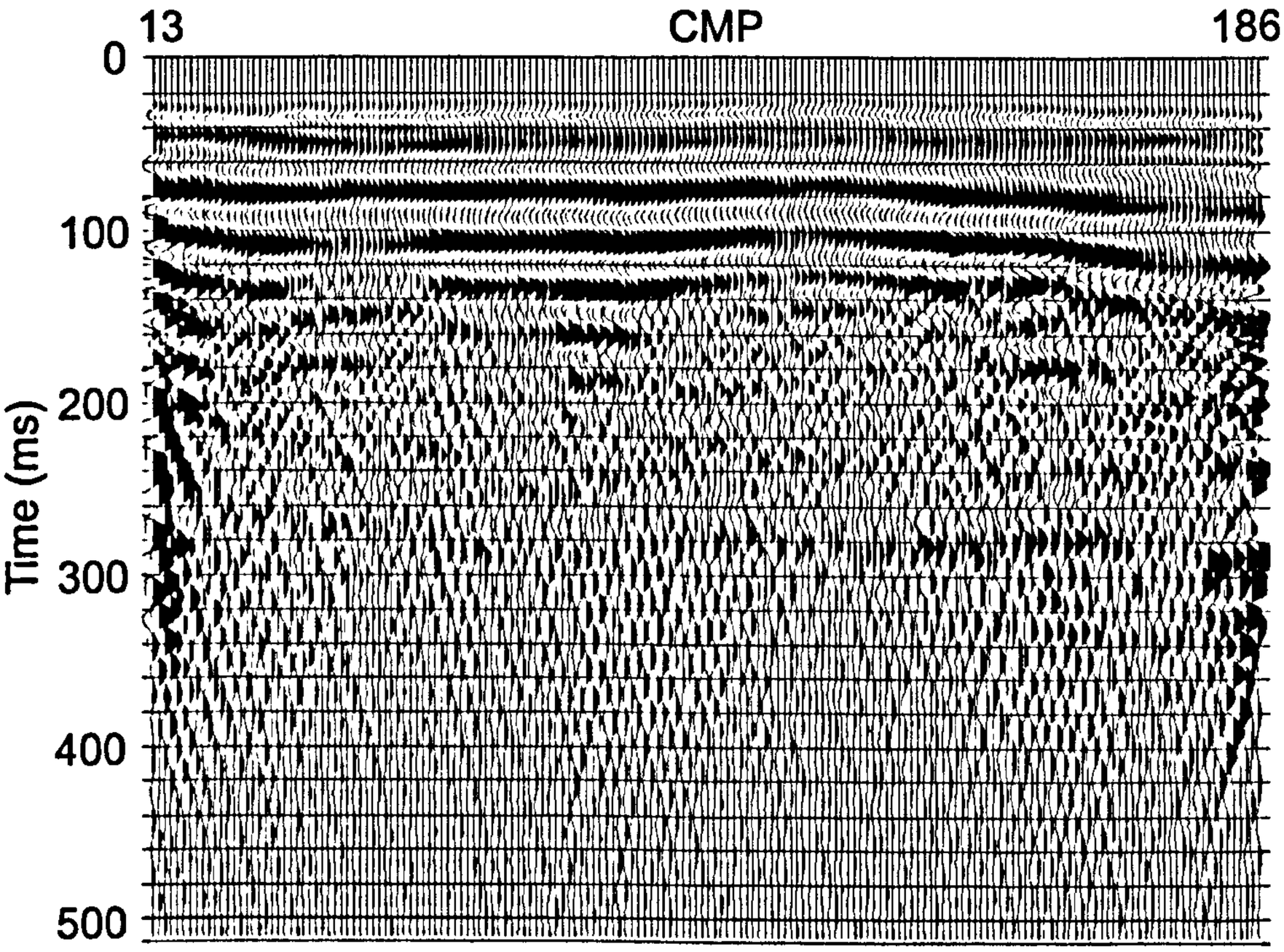

Figure 5.25: Very brute stack section of Hell Kettles profile 05.
Section is displayed with a scalar multiplier.

5.2.1.6 Robustness of the field statics solution

Because the shooting conditions were excellent when Hell Kettles profile 05 was acquired, the first breaks were crisp and clear, and so were picked automatically without manual intervention on all the shot records. Since the acquisition digital sample rate was set at 0.5 ms, the accuracy of the automatically picked first break picks is estimated to be ±0.25 ms at the level of one standard deviation.

To test the effectiveness of the plus-minus field statics solution, increasing amounts of random noise were added to the automatic first break picks to simulate the effect of increasing environmental noise. For each test run the processing sequence was exactly the same using the flow designed for the Hell Kettles survey site (Figure 4.31). A single pass of surface-consistent residual statics of the maximum power algorithm (Ronen and Claerbout, 1985) was used in each case.

The baseline comparison stacked section without any additional noise (Figure 5.26, upper panel) exhibits a strong gently dipping reflector with some associated hyperbolic diffraction energy. For the baseline trial a RMS convergence criterion of 0.5 ms was set in the

maximum power algorithm and was met on the first iteration where each trace was adjusted by less than ±1 ms.

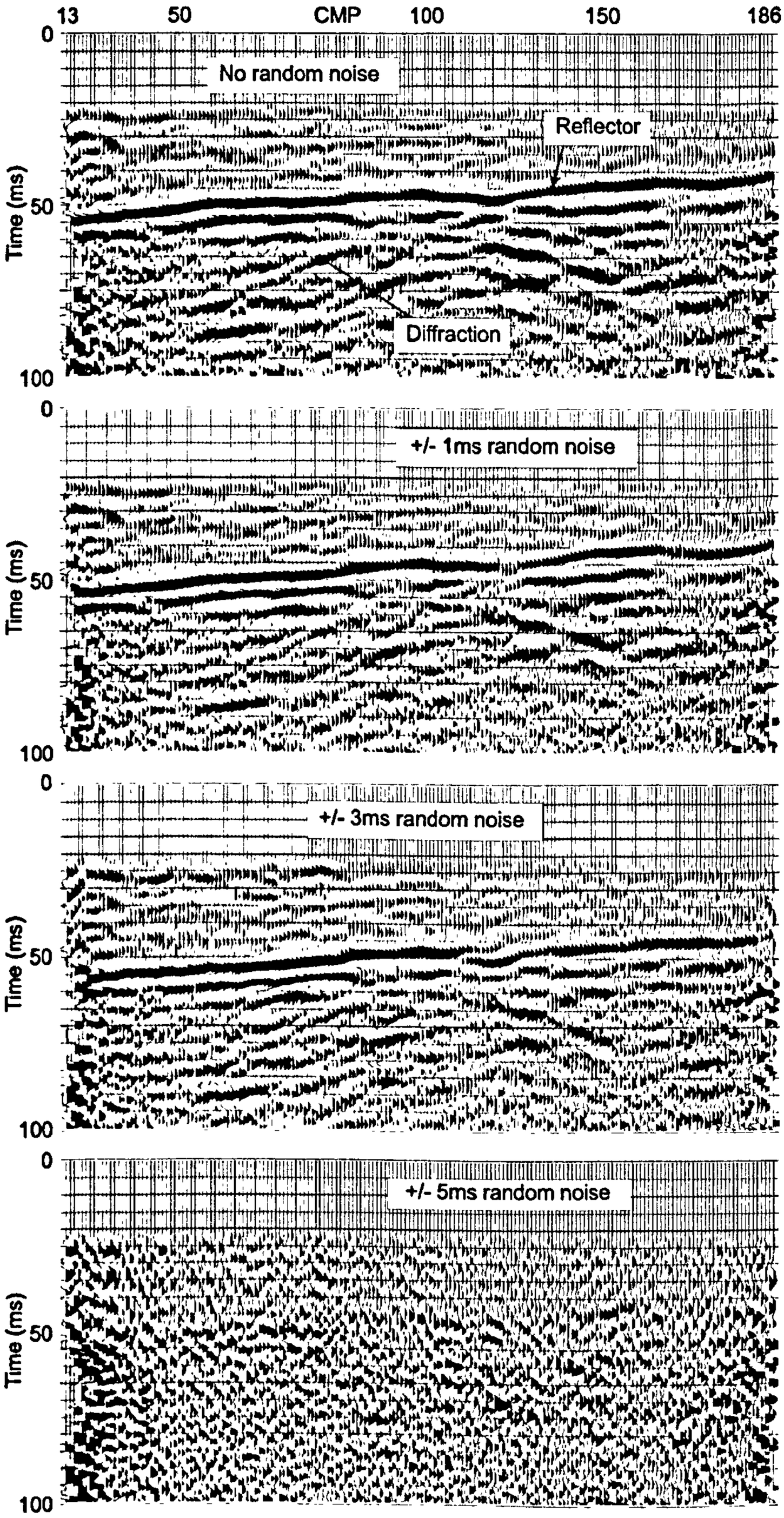

Figure 5.26: Stack sections of Hell Kettles profile 05 with varying amounts of additive noise. Sections are displayed with a scalar multiplier.

In the first trial the additive random noise was limited to a range of ±1 ms. In this case the RMS convergence criterion of 0.5 ms was satisfied after three iterations where the maximum movement of each individual trace was limited to ±4 ms. The shapes of the main features are very similar compared to the original section but with subtle differences.

With the additional random noise component restricted to a range of ±3 ms, the diffraction curves are still present and the general trend of the reflection horizon is preserved; however, the smaller undulations within the main reflection event are considerably altered. To achieve a residual statics solution the RMS convergence criterion was increased to 1.0 ms and required maximum trace movement limits of ±5 ms. When the random noise variation was increased to a range of ±5 ms, no residual statics solution was possible and all structures were completely destroyed (Figure 5.26, lower panel).

5.3 Interpretation

The digital data processing of the 2D and 3D data collected at Hell Kettles was achieved using standard techniques (Figure 4.31). A detailed account of the processing sequence was given in chapter four. In this section an interpretation of all the data acquired at the Hell Kettles site is given starting with the tie line to the North Oxen-le-Fields borehole. Then all the 2D lines are dealt with before giving the interpretation of the 3D survey.

5.3.1 Borehole tie line

Profile 07 links the network of 2D profiles encompassing the Hell Kettles ponds to the North Oxen-le-Fields borehole, located next to the main farmhouse building (Figure 5.3). The tie line is orientated approximately parallel to a line of trees bordering the ancient river meander, and terminates 30 m west of the borehole. An apron of concrete and fencing precluded acquiring a seismic line directly next to the borehole.

The North Oxen-le-Fields borehole was drilled to tap the artesian aquifer of the Seaham Formation. The Seaham Limestone is overlain by three different formations. Starting at the surface, there is a 20 m thickness of drift, followed by 10 m of siltstone at the base of the Triassic Sherwood Sandstone Group, and then 45 m of the Permian red-brown mudstones of the Roxby Formation. For the water saturated overburden the P-wave the

interval velocity is estimated as about 1800 m s^{-1} by reference to the refraction velocity below the water table at Hell Kettles with a small correction for compaction with depth. The P-wave interval velocity through water saturated Sherwood Sandstone is typically 2000 m s^{-1} (Fairbairn et al., 1986). At the deep Seal Sands borehole (Figure 2.6) the sonic log measured a P-wave interval velocity of 3400 m s^{-1} through the Roxby Formation mudstones, with uplift and erosion the Roxby P-wave interval velocity is estimated at 2100 m s^{-1}. Using these values, the two-way travel time (TWT) to the top of the Seaham Limestone from the reference datum, the water table, is estimated as 74 ms at the North Oxen-le-Fields borehole.

The most striking feature in the final time migrated stacked section of the borehole tie line (Figure 5.27) is the strong reflection event indicated by the black loop that dips gently from 50 ms at the start of the profile to 66 ms at the end of the profile. Running parallel about 6 ms deeper is another black loop, varying in strength and having a more broken appearance. These two positive amplitude loops are separated by a strong and continuous white loop. Above the top black, positive amplitude loop of is a broad low amplitude negative trough, which is probably a side lobe from bandpass filtering.

It is established that the strong reflection wavelet is related to the Roxby-Seaham geological boundary since the lower black leg is near to the estimated TWT of 74 ms to the top of the Seaham Limestone. However, no specific point on the wavelet, which spans 8 ms, can be related directly to the actual boundary between the Roxby and Seaham formations. If sonic and density logs are available in a local borehole, they can be used to match the local geology to the seismic data using the convolutional model and least squares matching techniques (White, 1980). The matching filter corresponds to the estimated effective wavelet in the data, so an operator can then be designed to alter the estimated wavelet to the desired wavelet shape with a time shift to place the reflection horizons with more precision. Without the wireline log information, the computed deconvolution filter applied here, as described in section 4.2.7, was unable to compress the effective wavelet in the data into a sharp impulsive wavelet.

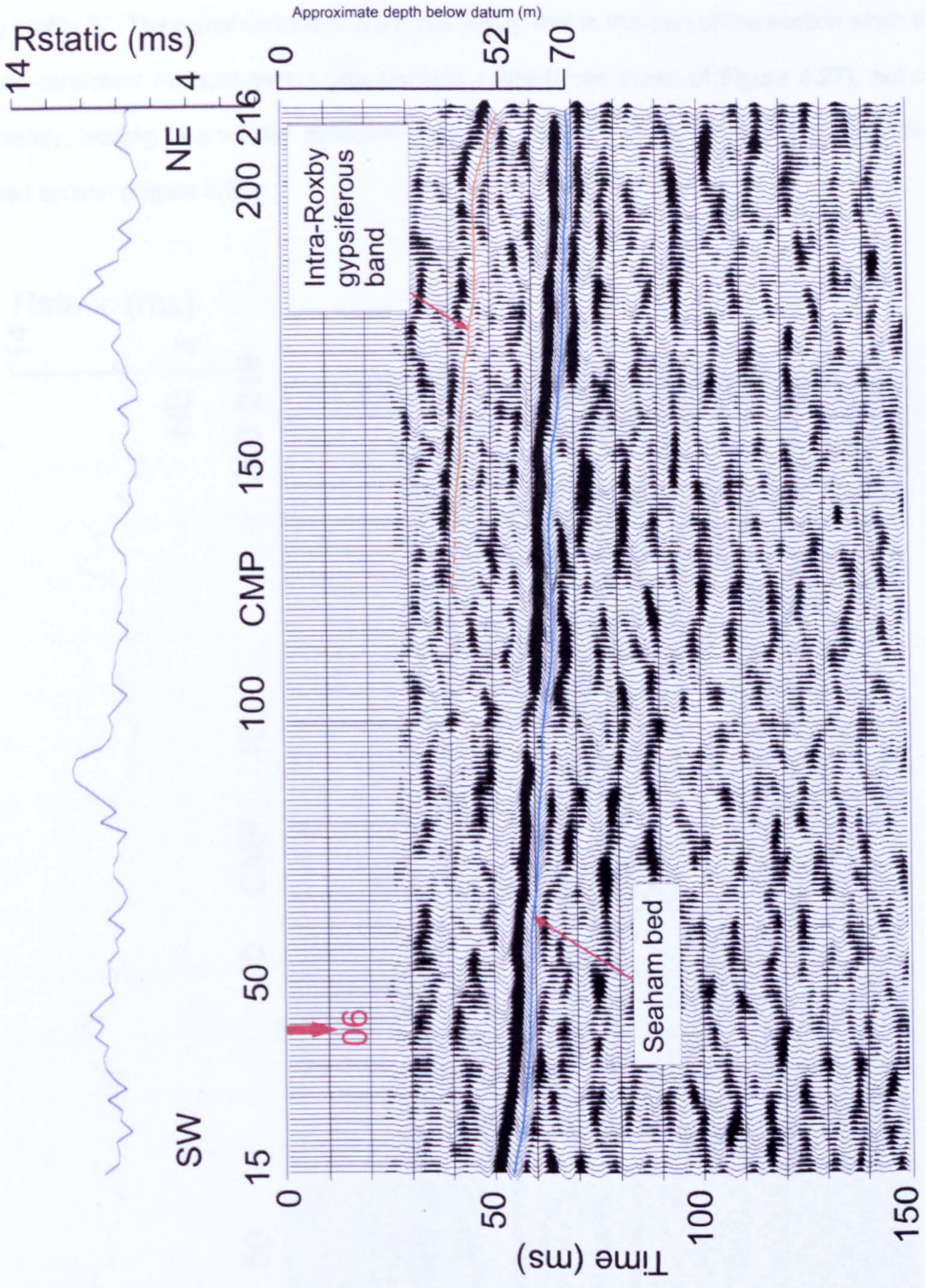

Figure 5.27: Interpreted final migrated stack section of profile 07, the borehole tie line. The distance between CMP traces is 1 m for all Hell Kettles 2D profiles. The CMP numbering has been adjusted to the distance along the profile from the first receiver station. The sections are overlaid with the receiver static solution and displayed with a scalar multiplier.

The main reflection event along profile 07 is smooth with only minor fluctuations in the topography of around 1 ms, which equates to a variation in height of about 1 m. There is also a slight alteration in the character of the reflection response across a 10 m length centred on

CMP 100. This is due to an area of pebble beds at the shot depth between 70 m and 140 m along profile 07. The signal was recovered reasonably well in this part of the section when the surface-consistent residual statics process was applied (see insert of Figure 4.27), but not completely, leading to a weaker reflection response between CMPs 60 and 110 in the final stacked section (Figure 5.28).

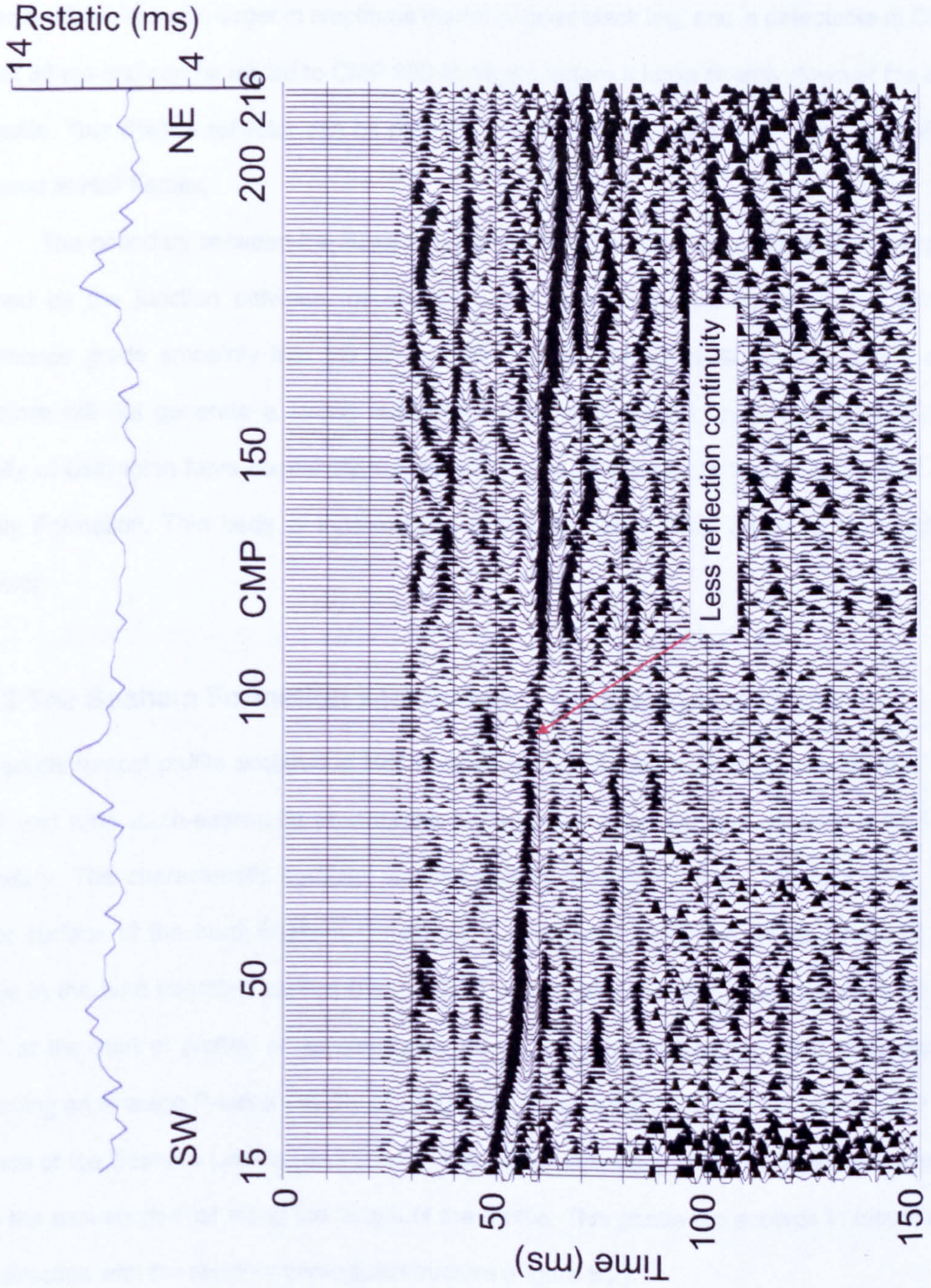

Figure 5.28: Final stack section of Hell Kettles profile 07, the borehole tie line.

The reflection generated by the difference in physical properties between the Roxby Formation and the Seaham Formation is the most prominent horizon imaged at Hell Kettles and is easily mapped across all the 2D profiles and the 3D volume. A shallower, much weaker, second reflection signal is observable in the borehole tie line, and runs sub-parallel to the Seaham Limestone surface. It has a similar character to the strong reflection event; two black positive amplitude loops are separated by a broader negative amplitude trough. The upper black leg is much larger in amplitude than the lower black leg, and is detectable at CMP 125 at 38 ms and can be traced to CMP 200 at 44 ms, where it kinks sharply down at the end of profile. This shallow reflector can be partially traced across a number of other 2D profiles acquired at Hell Kettles.

The boundary between the Roxby Formation and the Sherwood Sandstone Group is defined as the junction between the Permian and Triassic strata. However, the Roxby mudstones grade smoothly into the lower beds of the Sherwood Sandstone Group and therefore will not generate a strong reflection event. High quality cored boreholes in the vicinity of Darlington have commonly logged thin bands of gypsum in the mudstones of the Roxby Formation. Thin beds of intra-mudstone gypsum are a likely cause of the shallow reflector.

5.3.2 The Seaham Formation and evidence for sub-surface gypsum

The southernmost profile acquired at Hell Kettles, profile 08, starts on the grass verge of the A167 and runs south-eastwards towards the ancient river meander, sub-parallel to the field boundary. The characteristic complex wavelet seismic signature of the reflection from the upper surface of the hard Seaham Limestone is prominent along the whole length of the profile in the time migrated section (Figure 5.29). The surface of the limestone is at 40 ms TWT at the start of profile, or approximately 40 m below the reference water table datum assuming an average P-wave velocity of 2000 m s^{-1} through the overlying formations. The top surface of the Seaham Limestone is smooth but mildly undulating, deepening an estimated 5 m to the east-south-east along the length of the profile. This gentle dip accords in magnitude and direction with the regional geological structure (Figure 5.2).

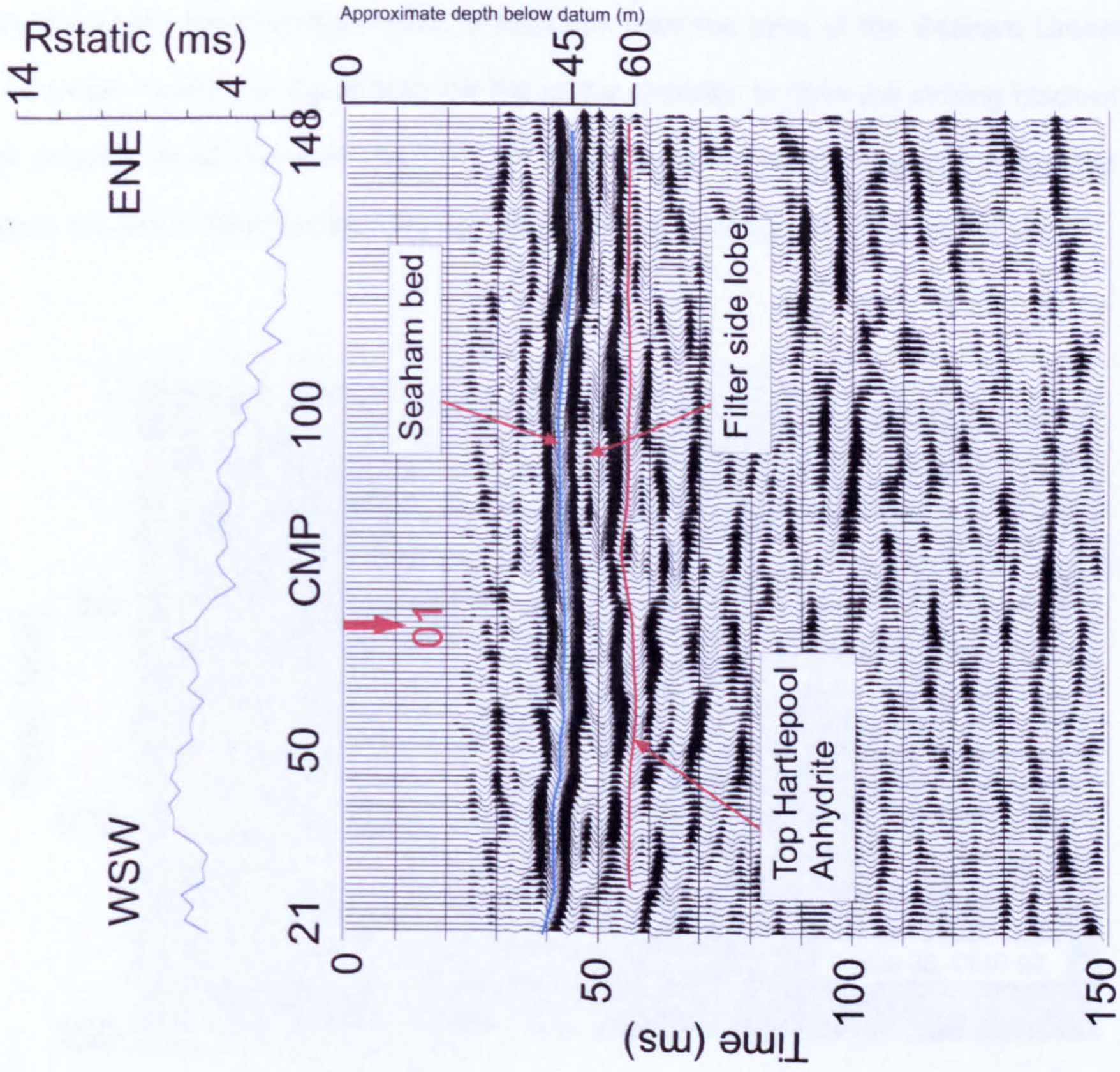

Figure 5.29: Interpreted final migrated stack section of Hell Kettles profile 08.

In the general geological succession at Darlington (Table 2.1) the Seaham Formation limestone is sandwiched between the Roxby and Edlington formations. These formations are lithologically similar, although the Edlington mudstones are likely to be slightly more compacted than the Roxby mudstones, and therefore have an estimated P-wave interval velocity of 2500 m s^{-1}. The limited number of boreholes in the vicinity of Darlington that cut completely through the Seaham Formation record thicknesses for the limestone of between 14 m and 20 m, suggesting that a reflection signal from the base of the Seaham Limestone should be present in the seismic data.

A second reflection event below the event interpreted as the top of the Seaham Limestone at around 52 ms can be picked with confidence in interactive velocity analyses along profile 08 (Figure 5.30). However, the Dix interval velocity between these two picks is around 2700 m s^{-1}. This value is very low for a thick, competent bed of limestone. If only a

thin bed of Seaham Limestone about 5 m thick is present at Hell Kettles, underlain by 10 m of Edlington mudstones then the reflection response from the base of the Seaham Limestone will be mixed in with the signal from the top of the Seaham to form the striking black-white-black package at 40 ms to 45 ms TWT. If this scenario is true then the pick below the top Seaham is likely to originate from the top surface of the Hartlepool Anhydrite Formation.

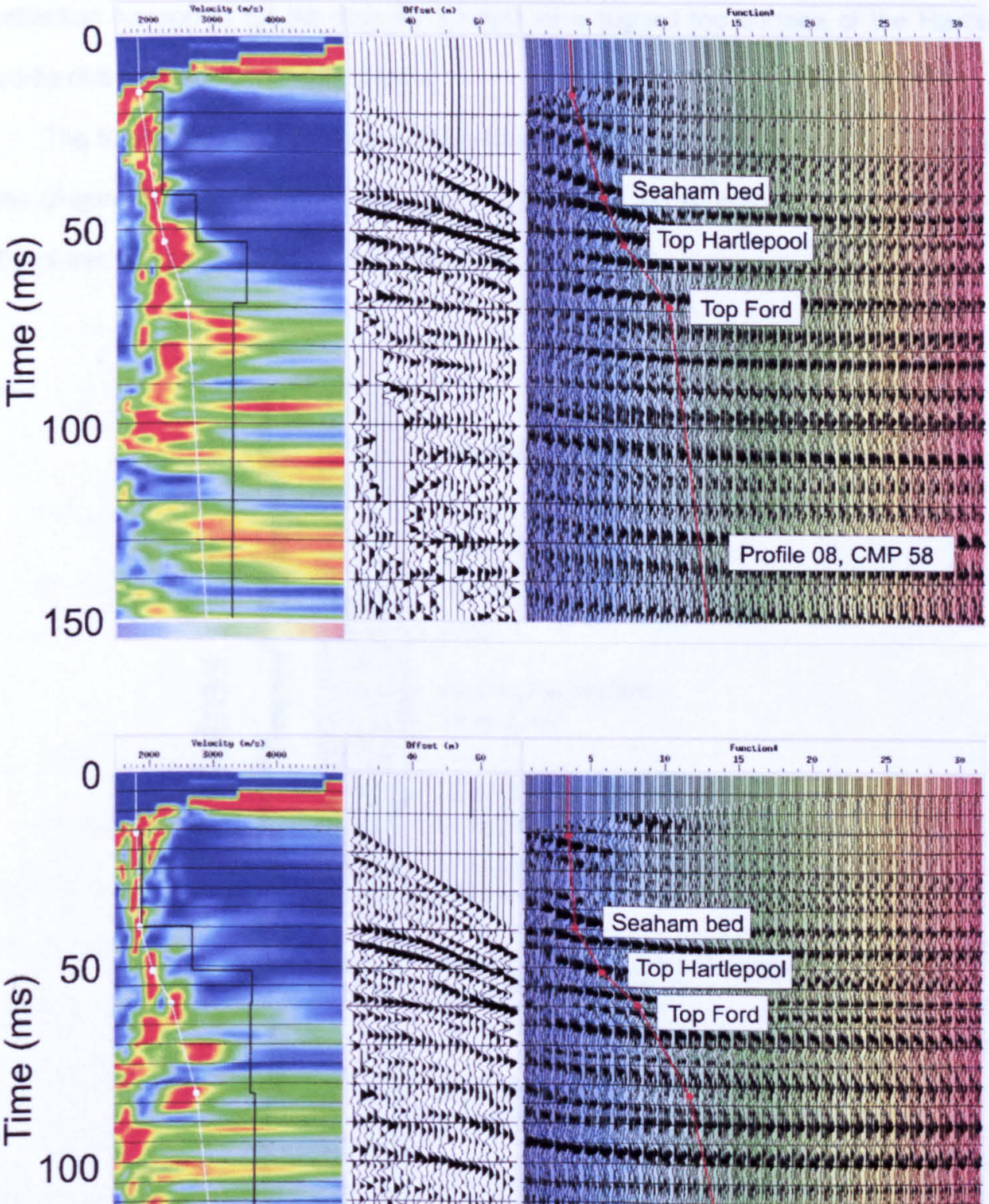

Figure 5.30: Interpreted interactive velocity analyses from Hell Kettles profile 08.

In the interactive velocity analysis at CMP 108 a third event can be picked at 60 ms. This yields a Dix interval velocity of 3600 m s^{-1}. This velocity is at upper value in the range of velocities through gypsum given by Sheriff and Geldart (1995), adding weight to the idea that the reflection event at 52 ms may be the top surface of the Hartlepool Anhydrite Formation, with the third event arising from the top of the Ford Limestone. If this is the case, then the thickness of gypsum must be approximately 15 m. The lumpy discontinuous appearance of the reflection horizon at 52 ms may be a result of a rugged top surface of the Hartlepool Anhydrite due to dissolution of the gypsum.

The interpretation of the sub-surface geology from the seismic data acquired at Hell Kettles (Figure 5.31) has 15 m thick bed of gypsum at 60 m below ground surface. The validity of this interpretation could only be proved by drilling.

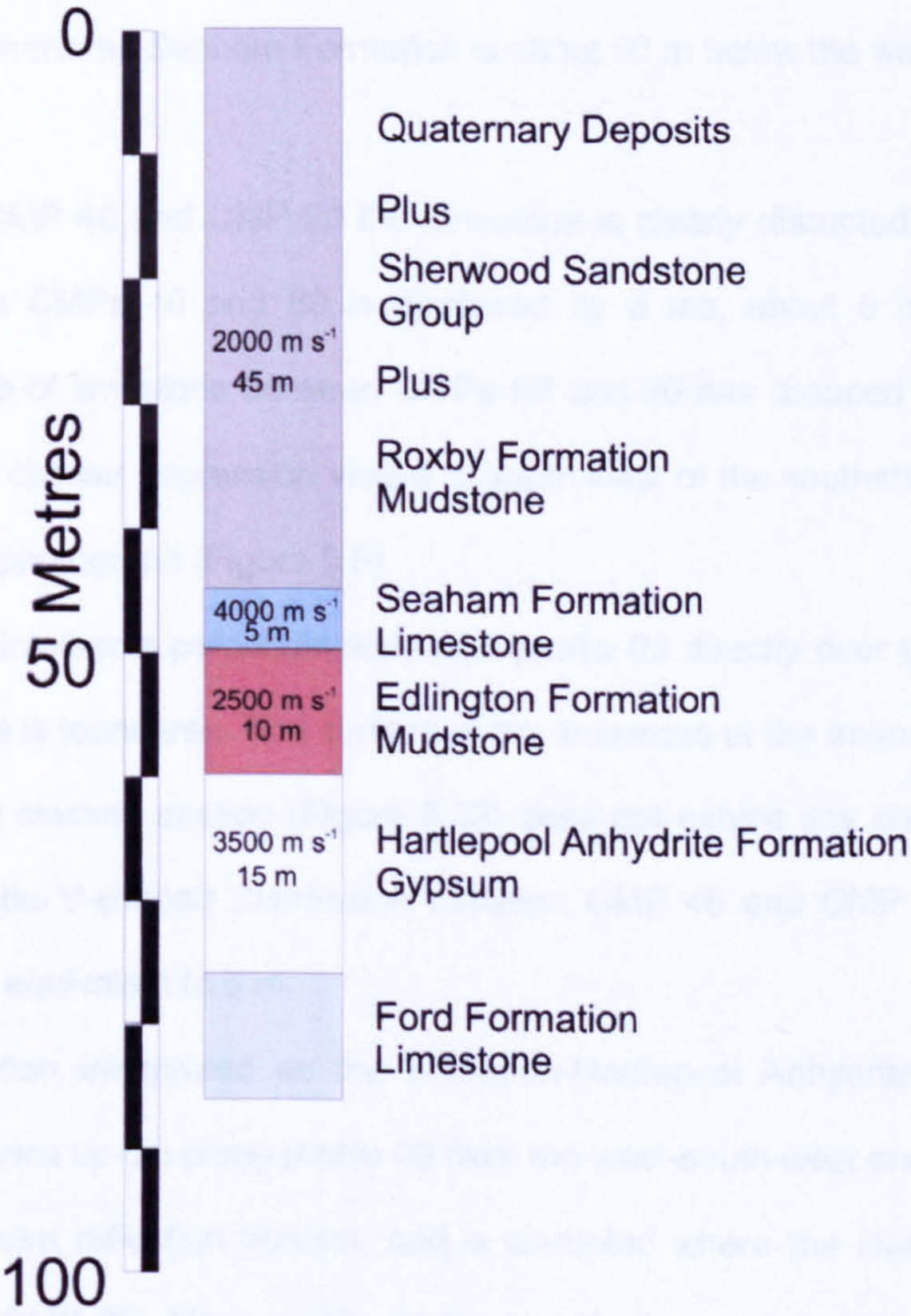

Figure 5.31: Hell Kettles seismically interpreted geological succession.

It has only been possible to pick the top surface of the Hartlepool Anhydrite Formation gypsum bed on the 2D profiles acquired in the field containing the Hell Kettles ponds. In the silage field to the north, only the top surface of the Seaham Limestone is imaged. This is because the shot coupling conditions are poorer in the silage field, where the soil is drier with increased gravel content and has been ploughed in recent years. The Hartlepool Anhydrite-Ford interface cannot be traced along the profiles at Hell Kettles with any confidence.

5.3.3 Sub-surface foundering

The characteristic seismic reflection package from the Seaham Limestone is prominent across the final time migrated stacked section of profile 03 (Figure 5.32). The limestone dips by 12 ms, or approximately 12 m, from the A167 at the eastern end of the line towards the dry ancient river bed where the Seaham Formation is about 50 m below the water table reference datum.

Between CMP 40 and CMP 90 the limestone is clearly disrupted. A 20 m length of limestone between CMPs 40 and 60 is displaced by 5 ms, about 5 m, downwards. An adjacent 30 m slab of limestone between CMPs 60 and 90 has dropped by some 2 m and correlates with the circular depression visible to south-west of the southern Hell Kettles pond on the 1940 aerial photograph (Figure 5.5).

Profile 01 intersects perpendicularly with profile 03 directly over the area where the Seaham Limestone is foundered. The surface of the limestone at the intersection point on the final time migrated stacked section (Figure 5.33) does not exhibit any sharp discontinuities, but there is a subtle V-shaped depression between CMP 45 and CMP 90 with maximum amplitude of 5 ms, equivalent to 5 m.

The reflection interpreted as the Edlington-Hartlepool Anhydrite interface can be traced with confidence up-dip along profile 03 from the west-south-west end of profile, parallel to the Roxby-Seaham reflection horizon, and is disrupted where the Seaham Limestone is foundered around CMP 80. Along profile 01 the top Hartlepool Anhydrite reflection event is more rugose than along profile 03. At the intersection with profile 03, the point of maximum limestone displacement, the top of the Hartlepool Anhydrite also lacks continuity.

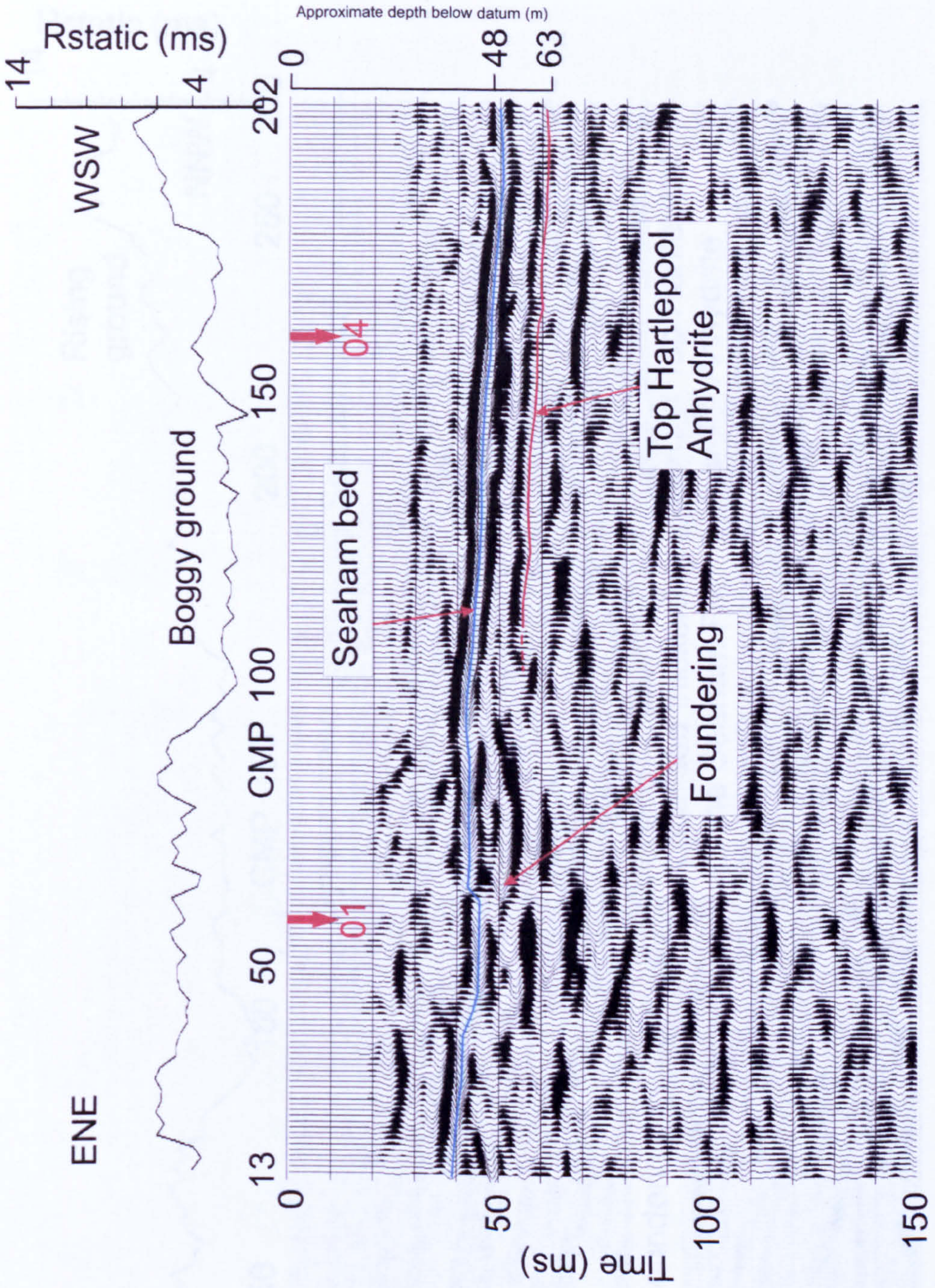

Figure 5.32: Interpreted final migrated stack section of Hell Kettles profile 03.

Interactive velocity analyses centred at CMP 135 on profile 01 and CMP 165 on profile 03 (Figure 5.34) have the same Dix interval velocity structure as seen on profile 08. The velocity analyses reinforce the idea that the Seaham Limestone is a thin bed at Hell Kettles. Between CMPs 110 and 150 along profile 01 there appears to be slight thickening of the Seaham Formation.

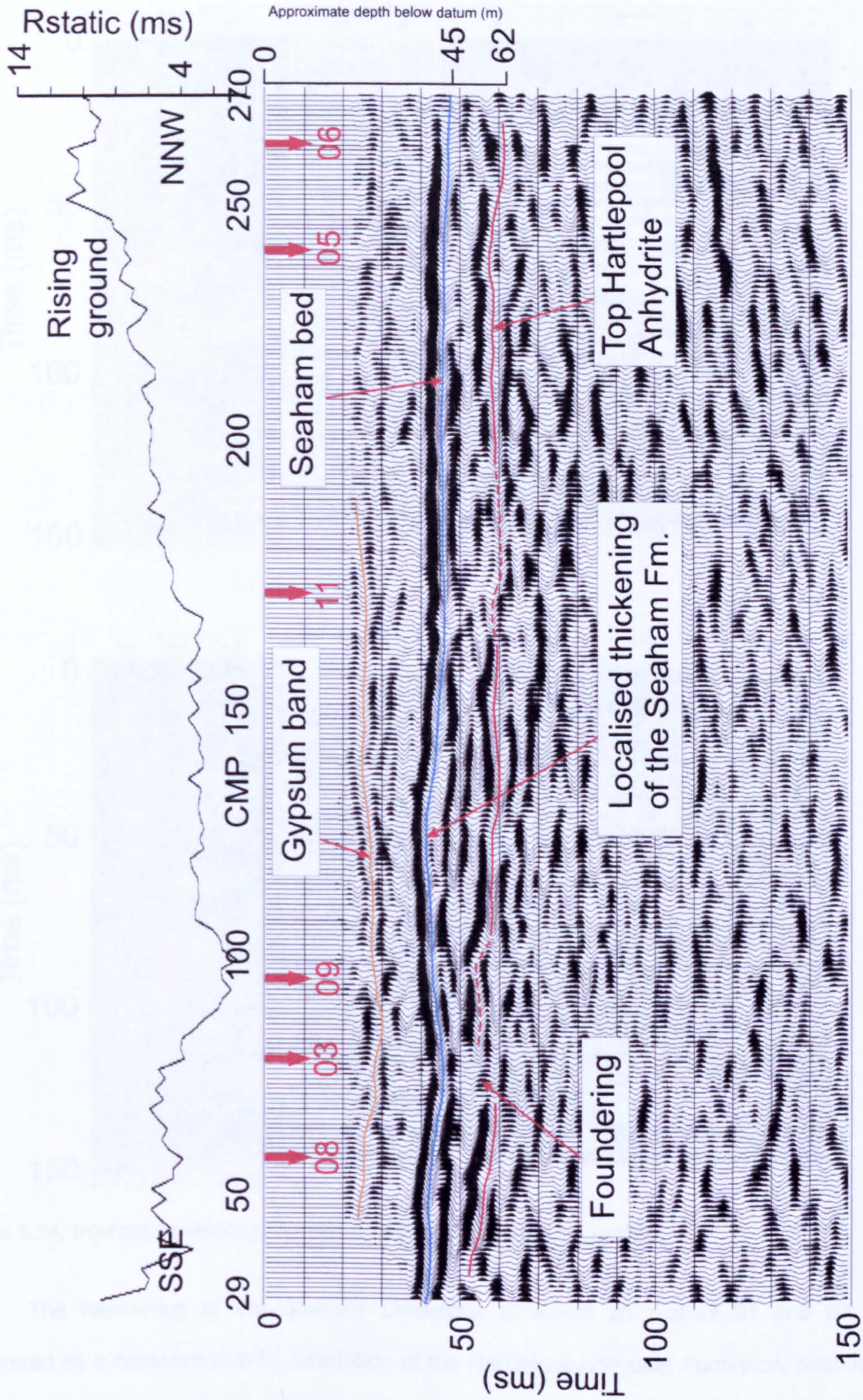

Figure 5.33: Interpreted final migrated stack section of Hell Kettles profile 01.

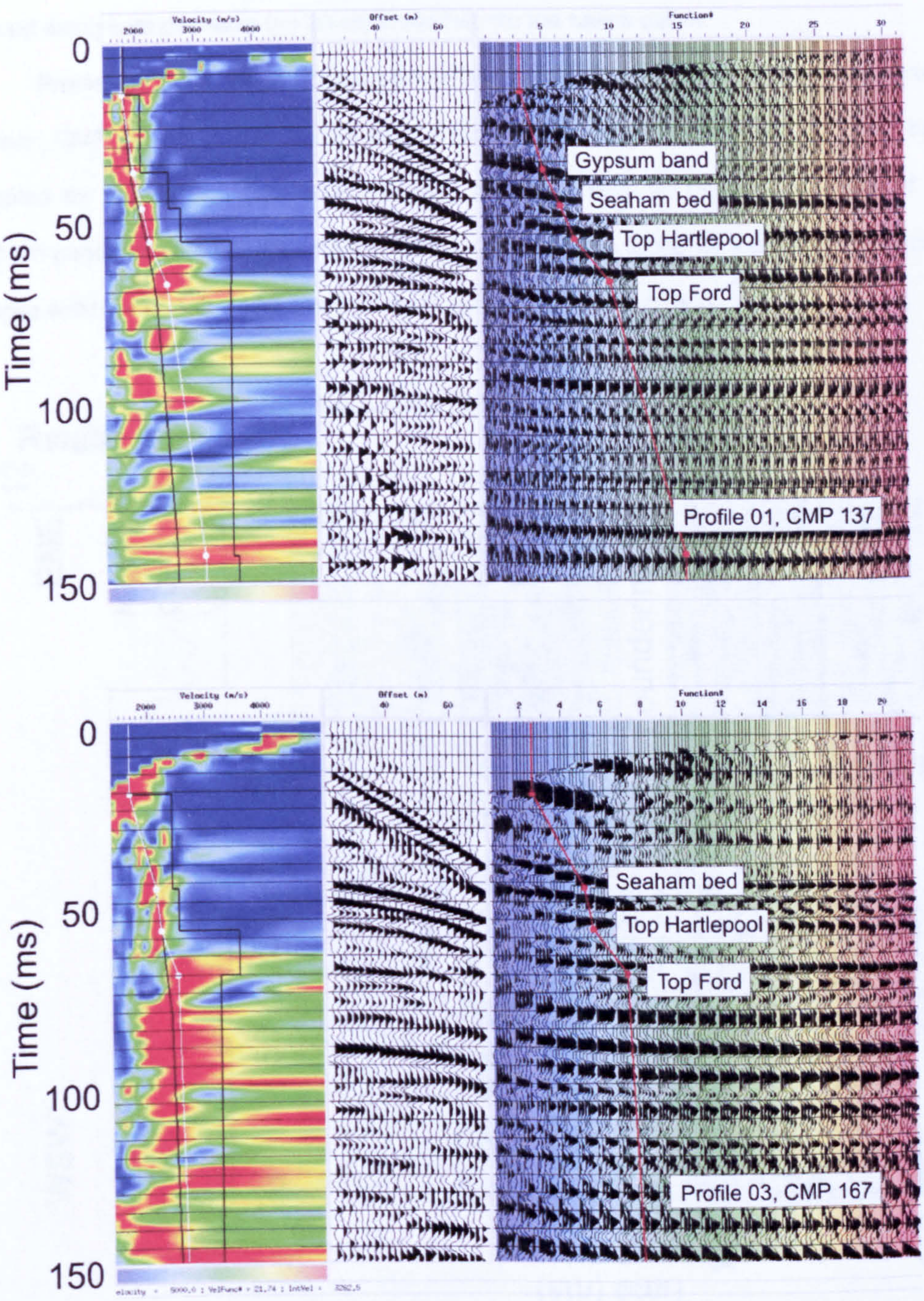

Figure 5.34: Interactive velocity analysis at points on profiles 01 and 03.

The foundering of the Seaham Limestone observed on profiles 01 and 03 is interpreted as subsidence due to dissolution of the Hartlepool Anhydrite Formation, because gypsum is easily dissolved by the passage of flowing water. The Edlington Formation mudstones may easily have slumped into the space created by dissolution, leaving a void immediately below the massive competent Seaham Limestone. When the void became large

enough, the limestone slab above was no longer strong enough to arch over the cavity, and sheared along joint planes in the limestone to fall into the space below.

Profile 09, 15 m north of and parallel to profile 03, exhibits significant disturbance between CMP 60 and CMP 100 (Figure 5.35), so the limestone appears to have been disrupted by foundering. The east-north-east end of profile 09 passes the edge of the southern pond, indicated by the receiver statics close to zero. Here, very close to the sudden collapse sinkhole of A.D. 1179, the Seaham Limestone appears intact.

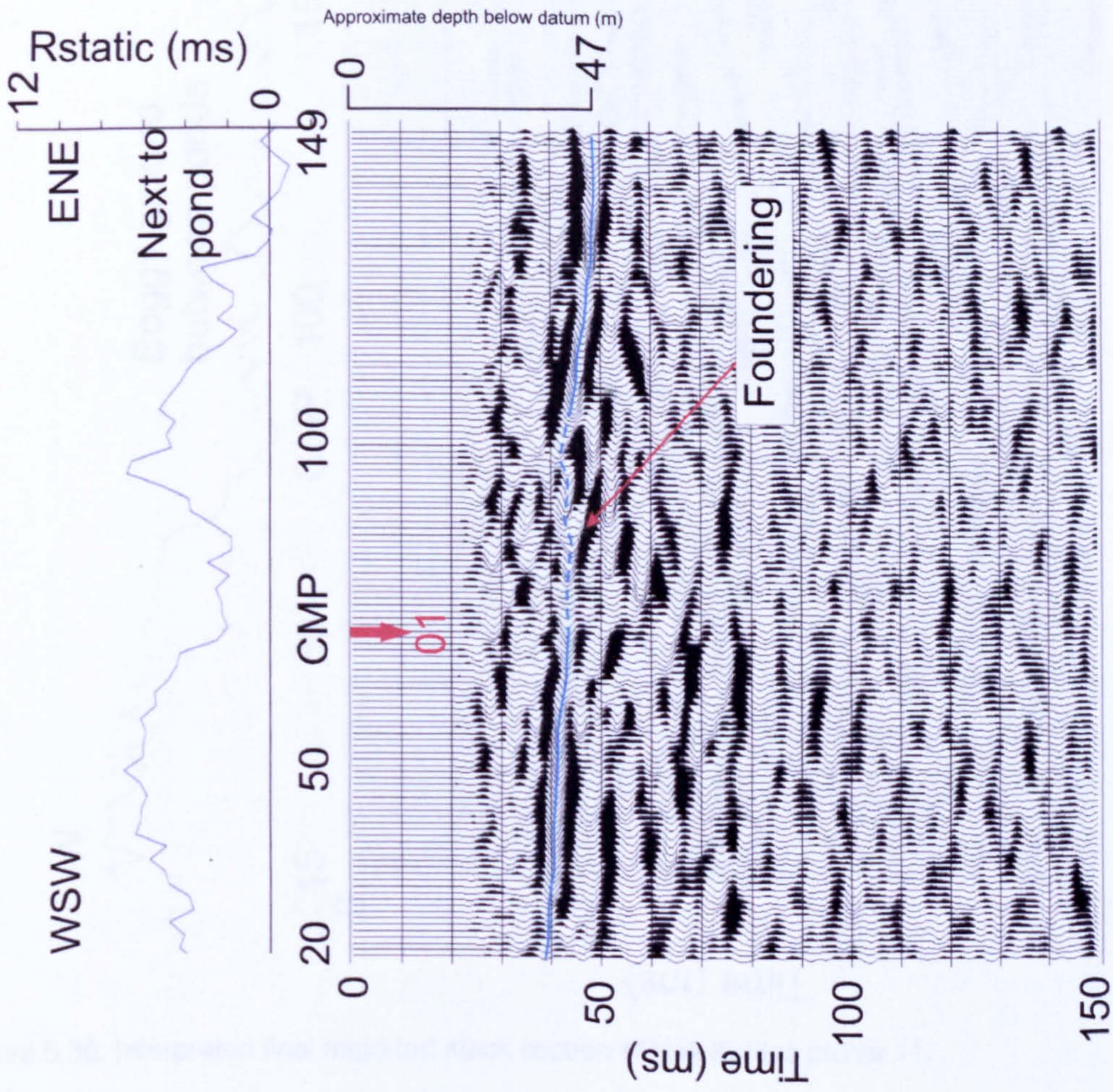

Figure 5.35: Interpreted final migrated stack section of Hell Kettles profile 09.

The surface of the Seaham Limestone is also intact along the complete length of profile 11 (Figure 5.36), which passes between the northern and southern Hell Kettles ponds. The reflection event from the Edlington-Hartlepool Anhydrite interface is also traced across

the majority of the profile without any disruption, although it was not imaged at each end of the profile where the shot coupling was poor.

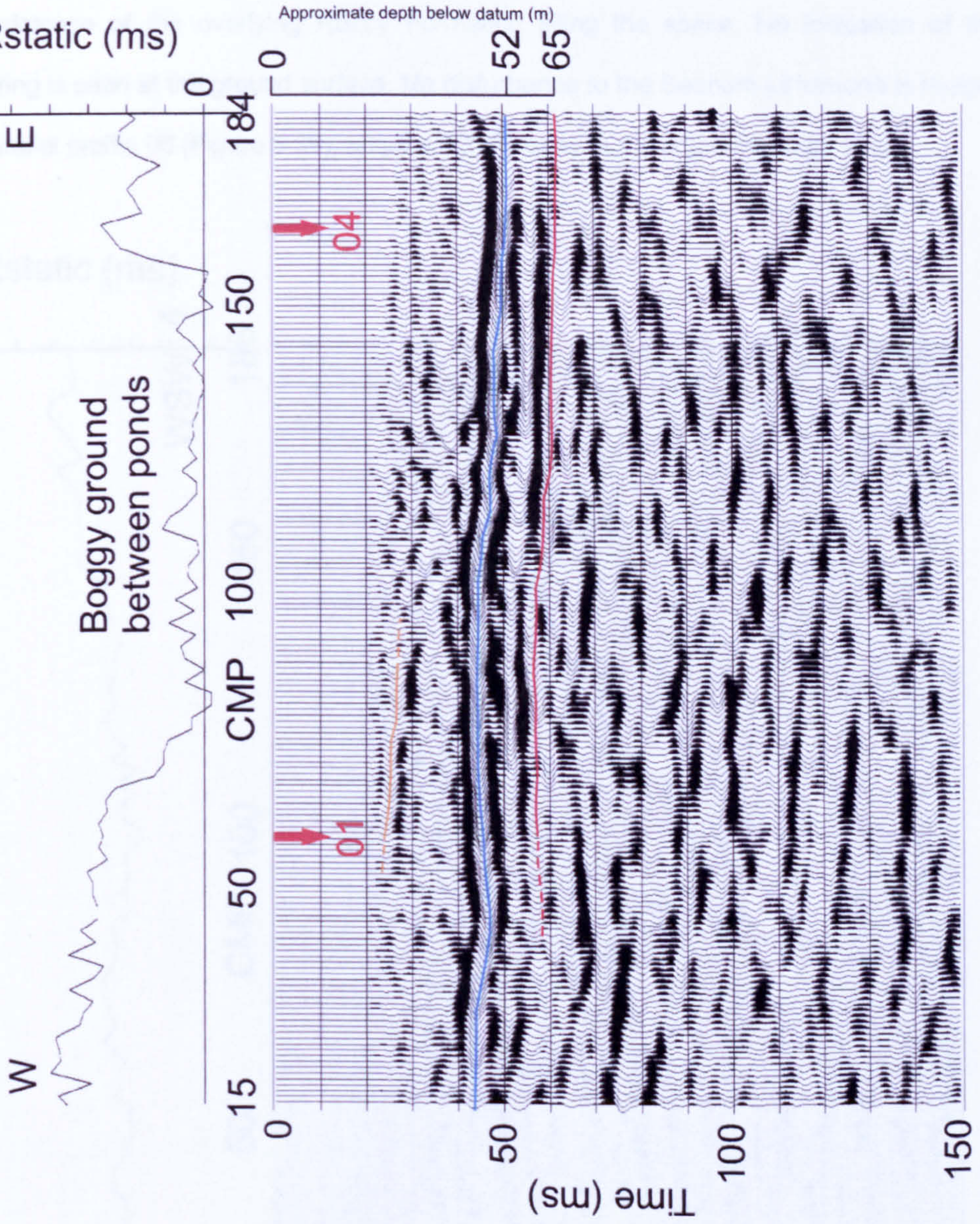

Figure 5.36: Interpreted final migrated stack section of Hell Kettles profile 11.

Profile 05 was shot parallel to the field boundary on the north side of the Hell Kettles ponds. Diffraction curves are present in the final stacked section (Figure 5.37), emanating from around CMP 118, suggesting the presence of sharp discontinuities within the geology. On migration, the diffracted energy is collapsed back to its origin. A large, 8 m wide, break in the Seaham Limestone is imaged around CMP 120 m on the final time migrated stacked

section (Figure 5.38), opposite the more westerly pond of the northern Hell Kettles double pond. This sub-surface geological feature is interpreted as an upward migrating cavity that has broken through the limestone. The upward progress of the void was probably stifled by the mudstones of the overlying Roxby Formation filling the space. No indication of this foundering is seen at the ground surface. No disturbance to the Seaham Limestone is imaged on a parallel profile 06 (Figure 5.39), acquired 20 m away in the adjacent silage field.

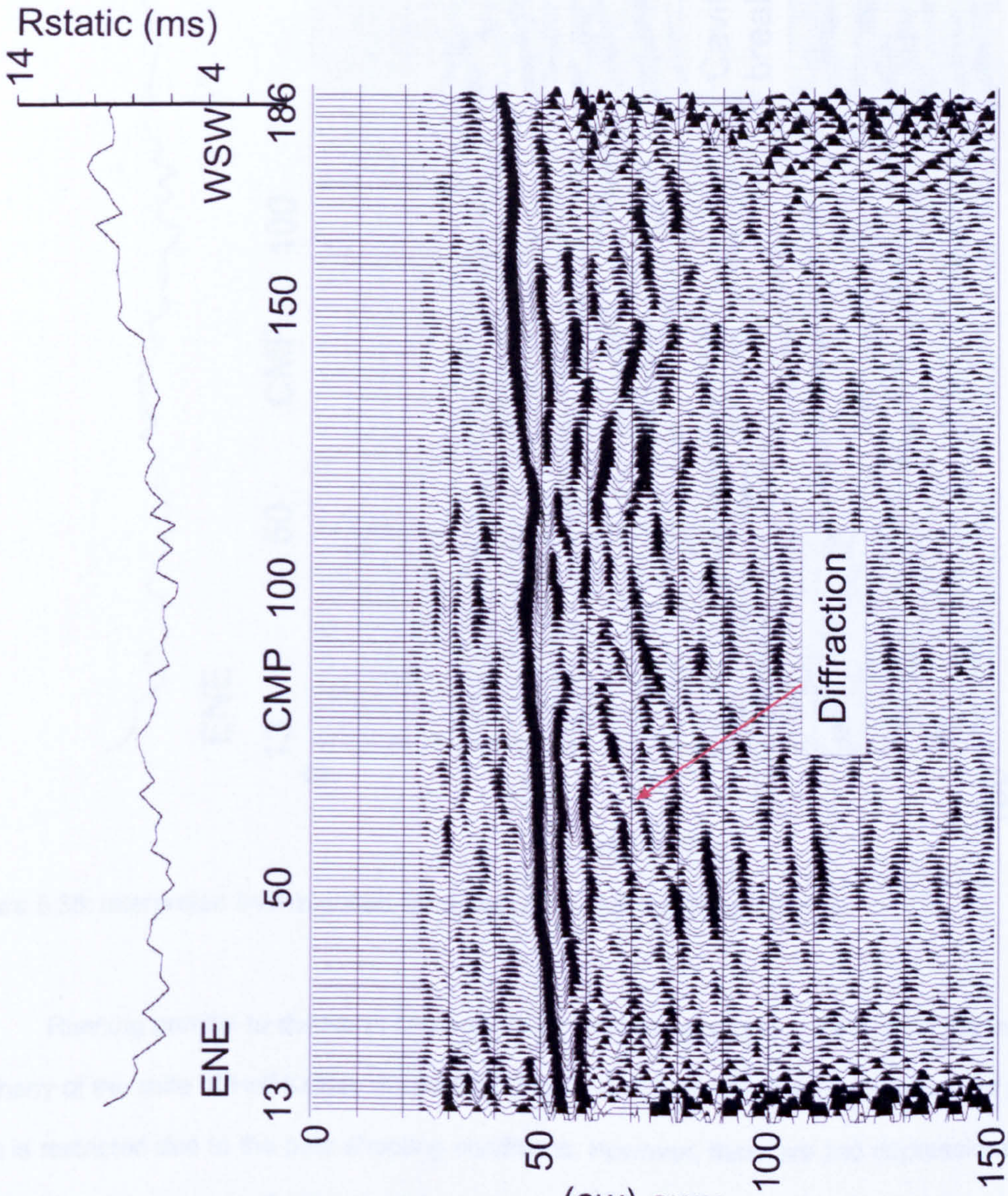

Figure 5.37: Final stack section of Hell Kettles profile 05.

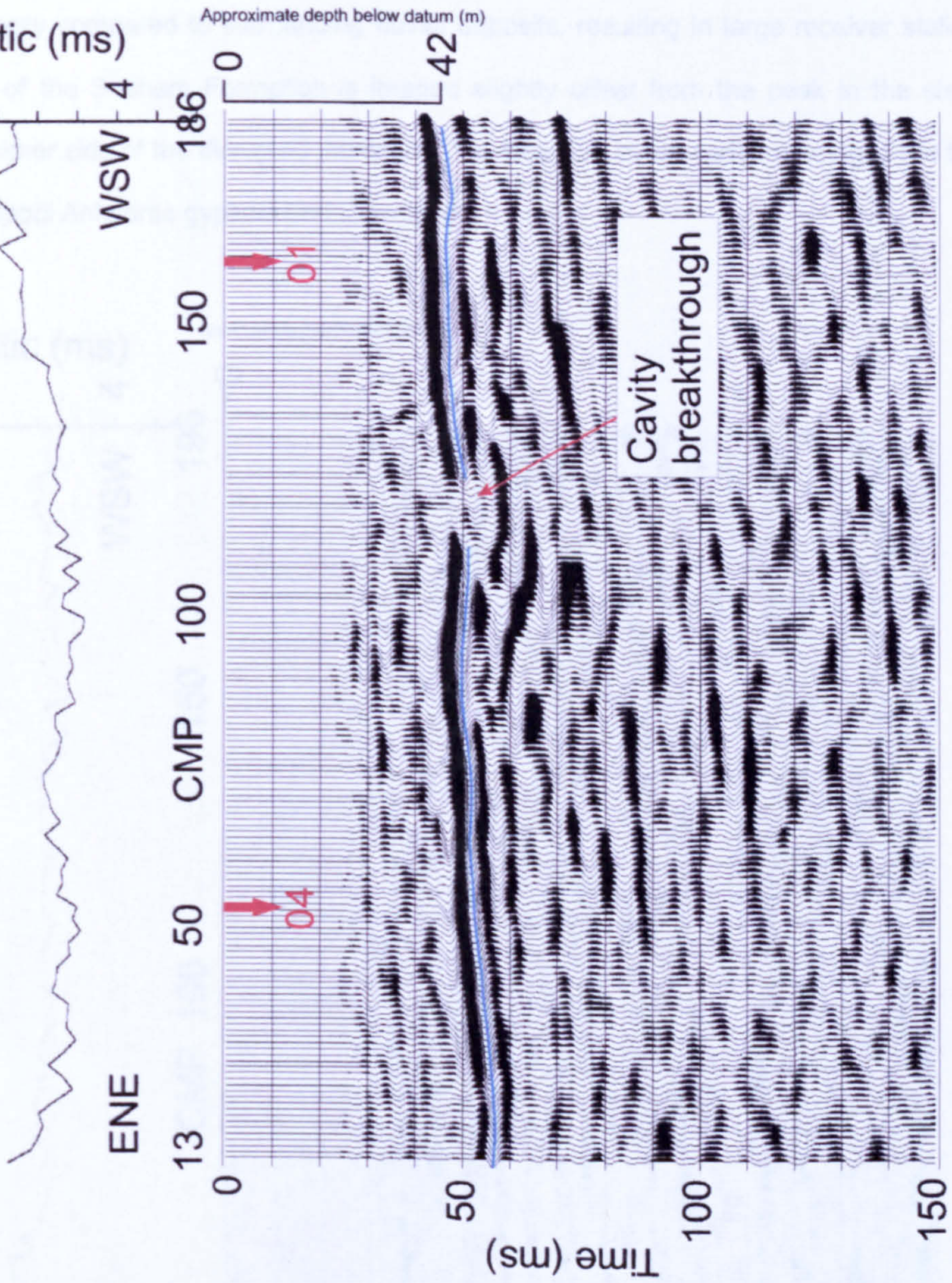

Figure 5.38: Interpreted final migrated stack section of Hell Kettles profile 05.

Running parallel to the North Oxen-le-Fields farm access road, profile 10 is the most northerly of the suite of Hell Kettles 2D profiles (Figure 5.40). The frequency bandwidth of the data is restricted due to the poor shooting conditions. However, there are two depressions in the Seaham Limestone reflection event, interpreted as foundering, between CMPs 20 and 100. Their maximum downward displacement is 6 m.

The position of the in-filled depression on the dog leg profile 16 is picked out by the receiver statics values (Figure 5.41). The hollow was filled in during a widening scheme for

the A167 and is difficult to pick out in the present-day ground topography. The fill has a lower P-wave velocity compared to surrounding fluvial deposits, resulting in large receiver statics. Foundering of the Seaham Formation is imaged slightly offset from the peak in the static values. To either side of the disrupted limestone, the reflection event corresponding to the top of the Hartlepool Anhydrite gypsum bed is traceable.

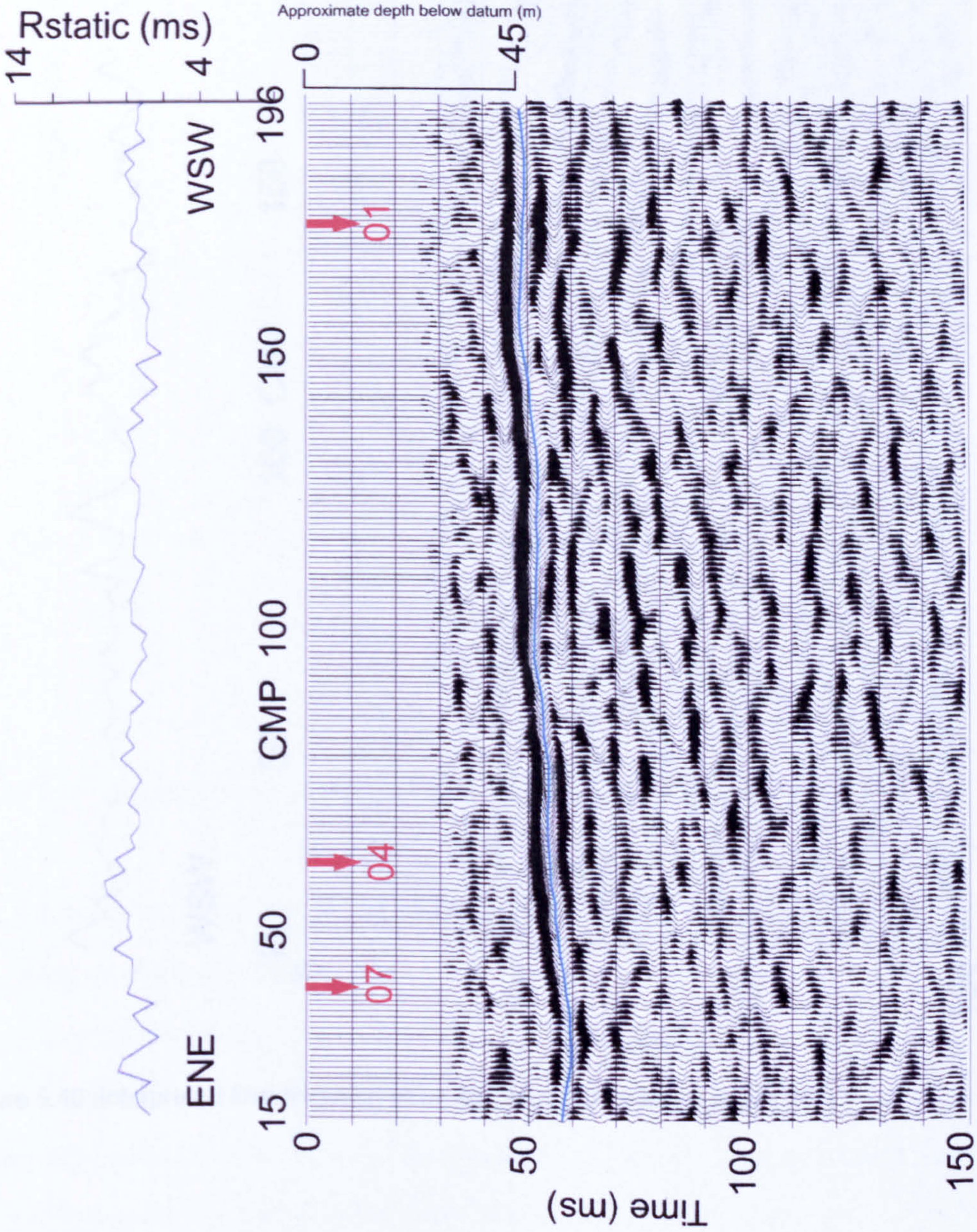

Figure 5.39: Interpreted final migrated stack section of Hell Kettles profile 06.

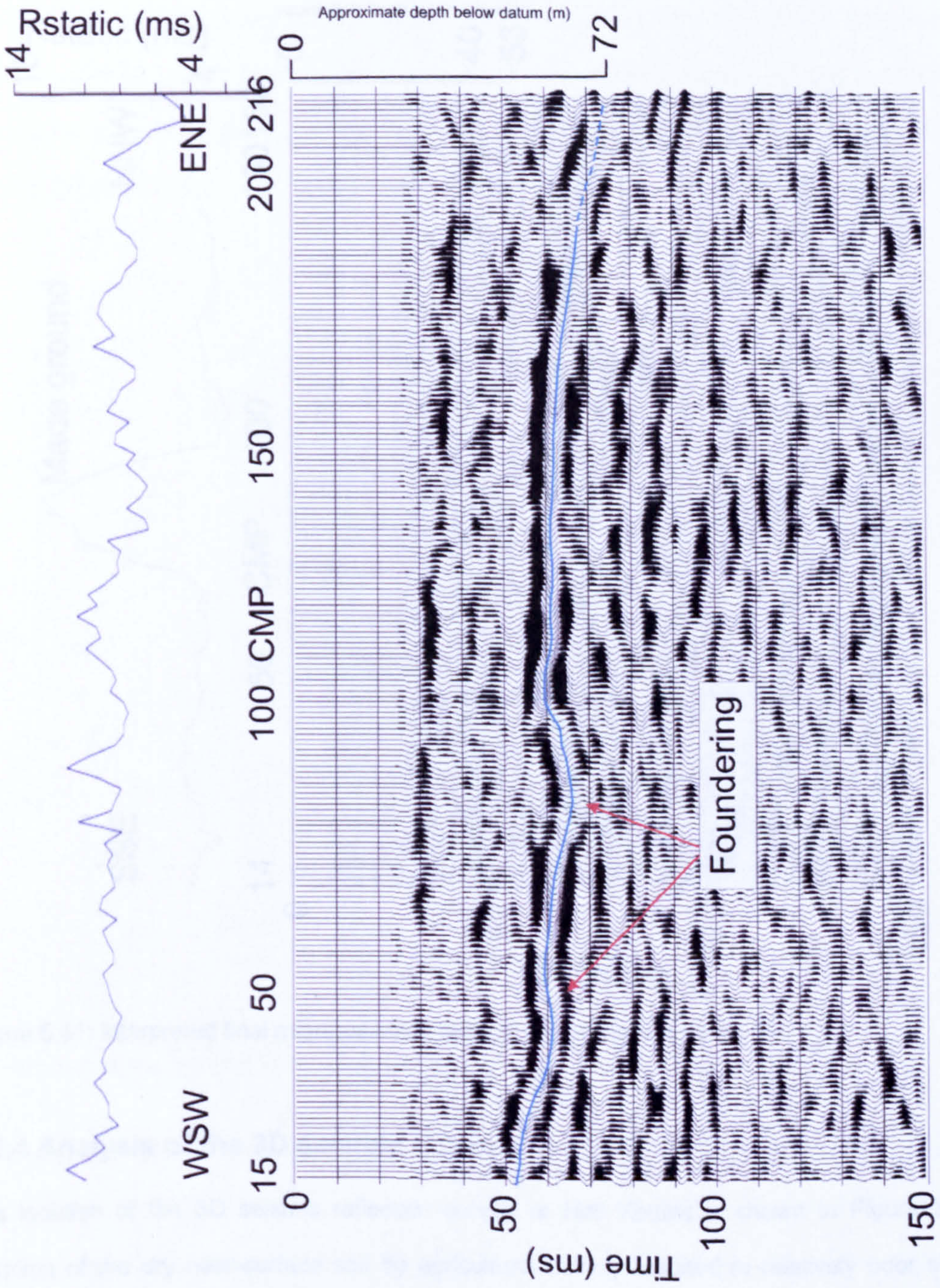

Figure 5.40: Interpreted final migrated stack section of Hell Kettles profile 10.

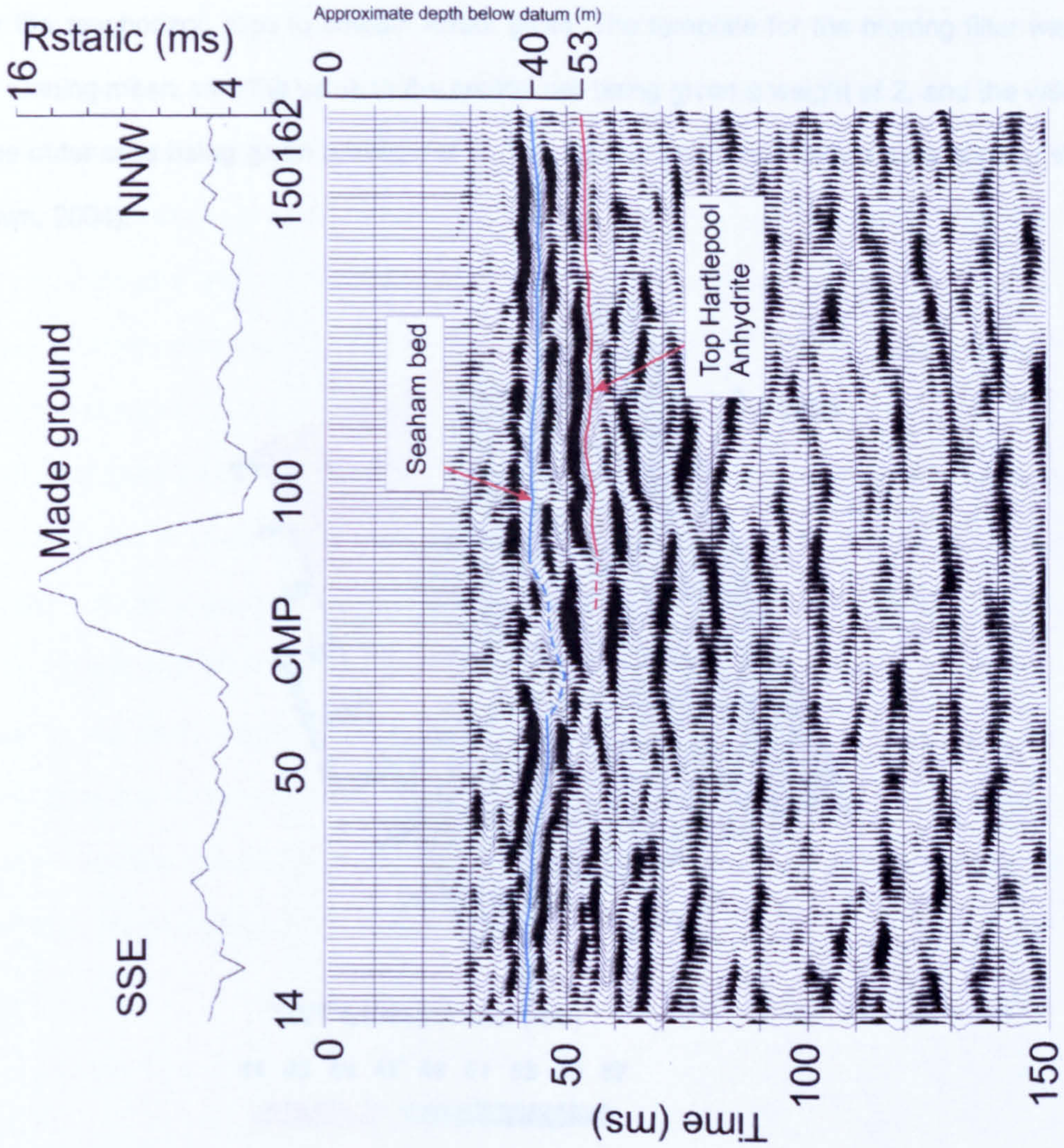

Figure 5.41: Interpreted final migrated stack section of Hell Kettles profile 16.

5.3.4 Analysis of the 3D seismic volume

The location of the 3D seismic reflection survey at Hell Kettles is shown in Figure 5.3. Aeration of the dry near-surface soil by agricultural activity resulted in relatively poor shot coupling conditions in the silage field. As with 2D profiles 06 and 10, only the top surface of the limestone of the Seaham Formation was interpretable across the whole of the 3D seismic volume. The deeper Hartlepool Anhydrite bed was not imaged.

A smooth contoured map of the TWT to the top of the Seaham Formation (Figure 5.42) was established by manually picking the zero-crossing just before the upper positive loop of the limestone reflection response over all in-line and cross-line sections of the 3D Hell

Kettles seismic volume. This procedure was followed by running a light 3×3 2D blurring filter over the raw horizon slice to smooth errant picks. The template for the blurring filter was a 3×3 running mean, with the value in the central cell being given a weight of 2, and the values in the outer cells being given a weight of 1. This type of surface is known as a horizon slice (Brown, 2004).

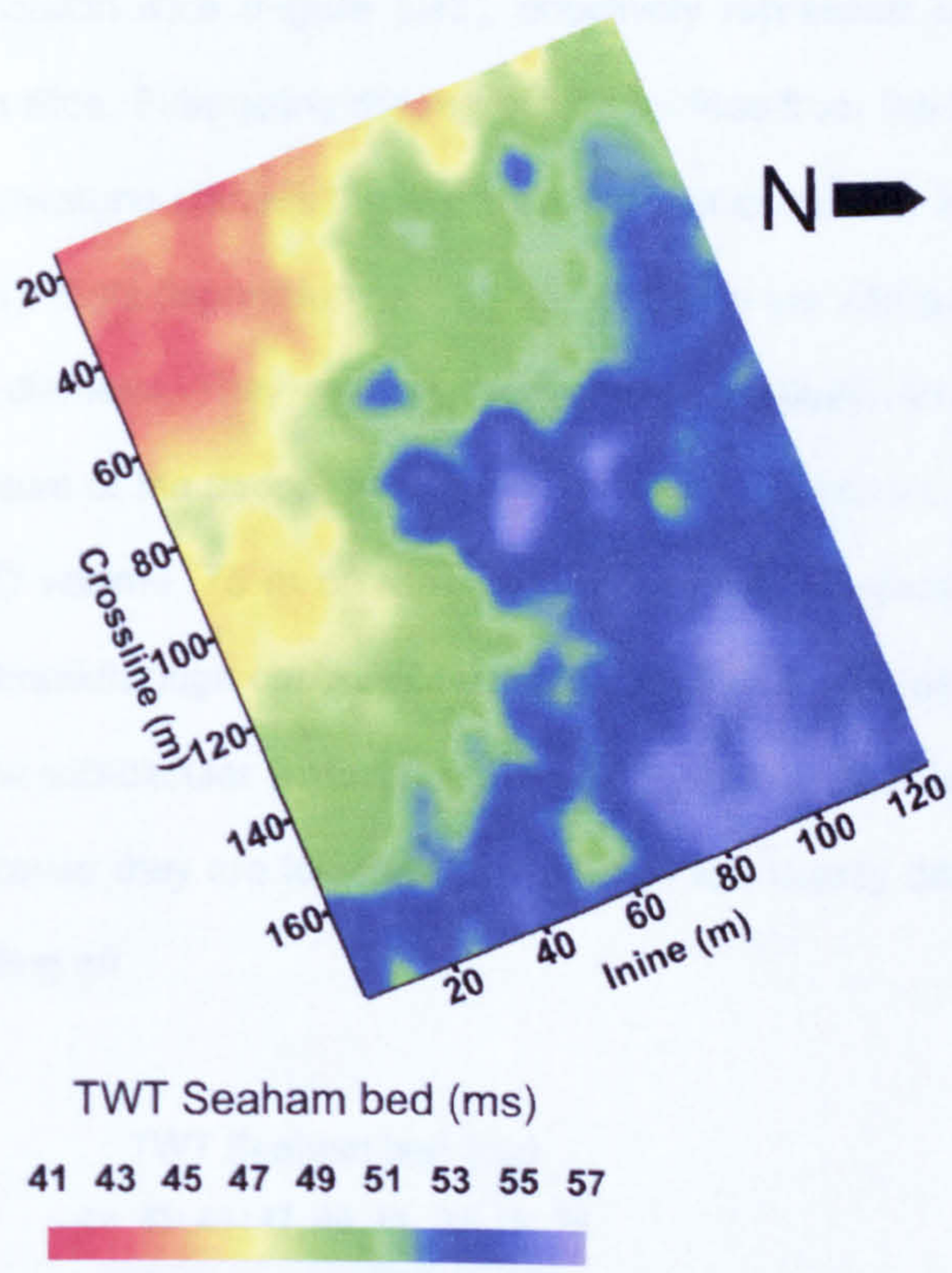

Figure 5.42: Hell Kettles 3D top Seaham Formation horizon slice.
The contour plot is orientated at the same angle as the direction of acquisition.

The overall dip direction of the Seaham Formation limestone across the 3D area is from the south-west towards the North Oxen-le-Fields borehole, with the TWT to the limestone increasing from 41 ms to 57 ms. The magnitude and direction of the dip are consistent with the regional dip at Hell Kettles shown on the solid geological map (Figure 5.2). Assuming an overburden velocity of 2000 m s^{-1}, the depth to the picked horizon slice below the water table varies across the imaged area of the 3D survey from 41 m to 57 m. The actual onset of the Roxby-Seaham interface within the reflection wavelet is unknown and so the depth to the top of the limestone may be a few metres shallower or deeper.

There is evidence of short wavelength variations in the horizon slice surface (Figure 5.42). Three lobes of blue, indicating greater depth to the limestone encroach within the green contour zone. There are also two smaller, but prominent, isolated blue sub-circular features in the green contour zone, indicating that the limestone is deeper there.

A quadratic polynomial regression surface, computed from the raw TWT data of the Seaham Formation horizon slice (Figure 5.43), effectively represents the long-wavelength content of the horizon slice. Subtracting the regression surface from the horizon slice for the top of the Seaham Limestone clarifies the short-wavelength deviations in the surface of the limestone (Figure 5.44). Eight depressions within the limestone are interpreted, varying in size from 5 m to 20 m in diameter. They are assumed to have resulted from foundering due to dissolution of the gypsum of the deeper Hartlepool Anhydrite Formation. A lesser depression at the edge of the 3D volume, 75 m cross-line, 10 m in-line, is adjacent to, and probably related to, the cavity breakthrough observed on profile 05. At the very eastern end of the 3D survey there are a few sub-circular features which are not interpreted as real hollows in the limestone surface because they are located in an area of low quality data where the fold of coverage is rapidly falling off.

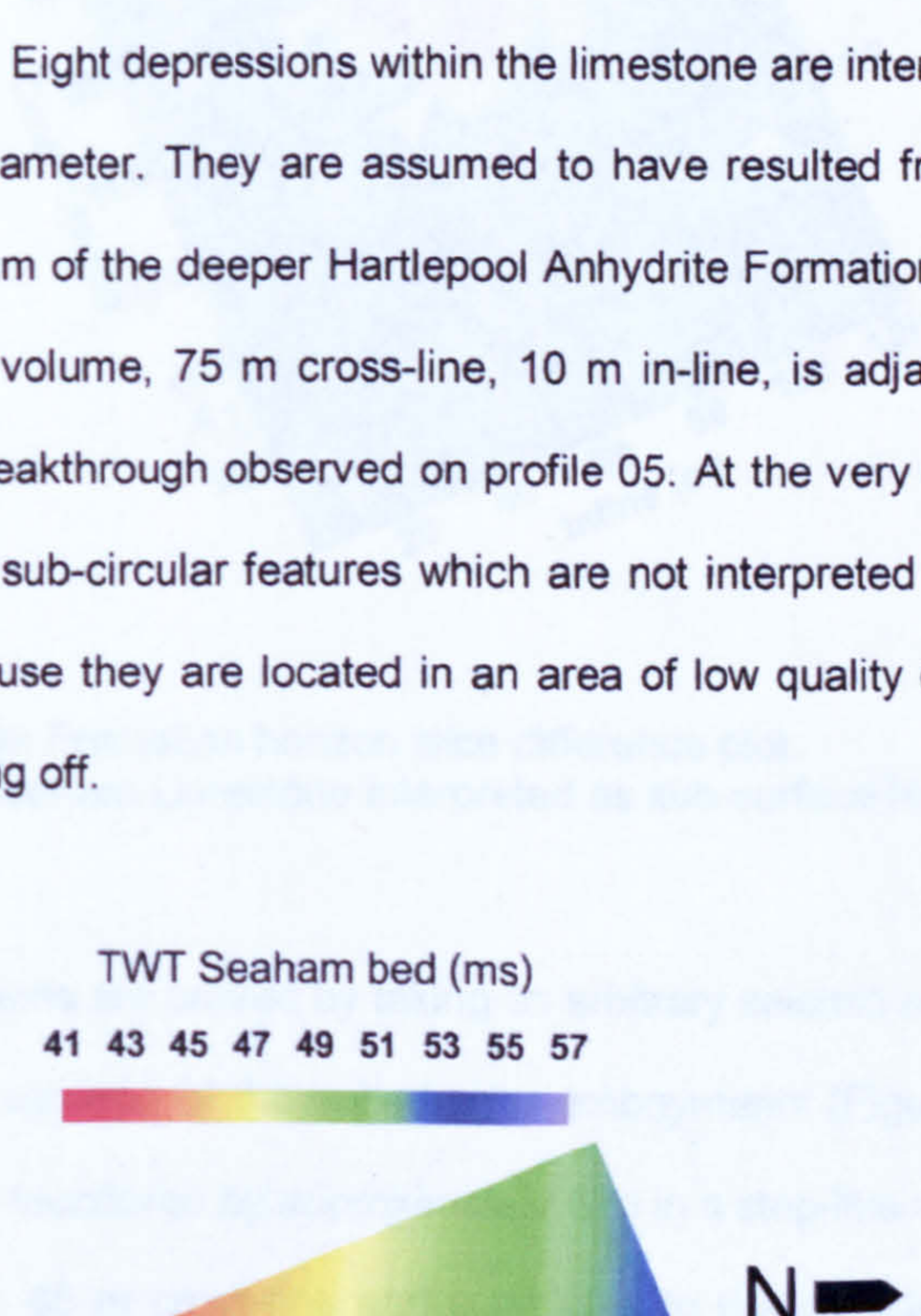

Figure 5.43: Top Seaham Formation horizon slice quadratic polynomial regression plot.

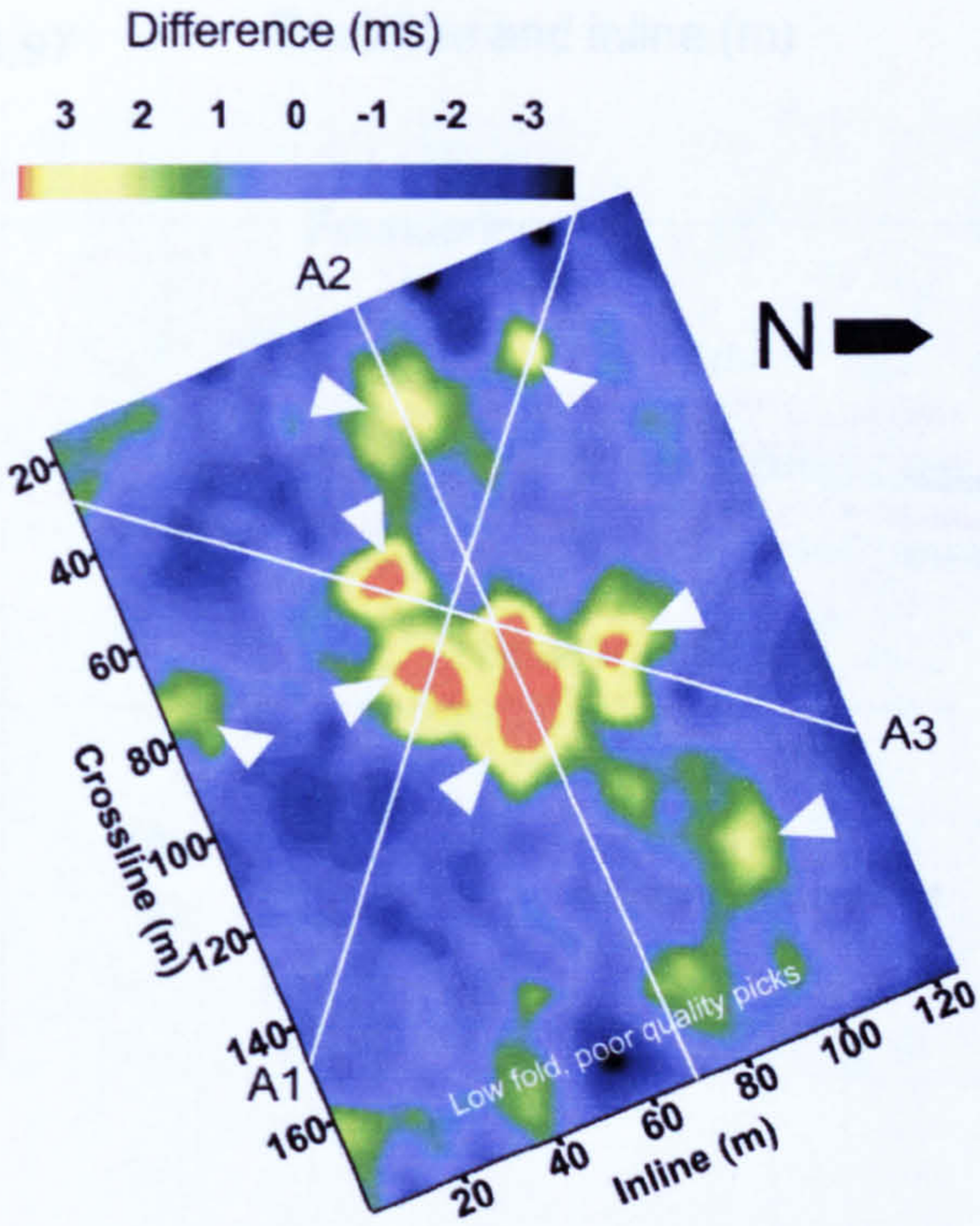

Figure 5.44: Top Seaham Formation horizon slice difference plot.
The eight areas in the Seaham Limestone interpreted as sub-surface foundering are indicated by the short arrows.

These observations are proved by taking an arbitrary seismic section through the Hell Kettles 3D volume through one of the sub-circular embayments (Figure 5.45). It shows the Seaham Limestone has foundered by approximately 6 m in a step-like manner. This feature is centred at 50 m in-line, 85 m cross-line and correlates to the pit visible in the 1940 aerial photograph (Figure 5.5). The amount and shape of the foundering can be assessed by visually comparing the smoothed manual picks shown by the red line with the polynomial regression surface displayed in yellow. Furthermore, the amplitude strength of the Seaham reflection event across the 3D volume is given by the gradational colour scheme. Further arbitrary time sections through the Hell Kettles 3D seismic volume display interesting variations in the forms of foundering (Figure 5.46). The arbitrary time sections were developed by importing the final time migrated cube into the Landmark Graphics SeisWORKS interpretation package.

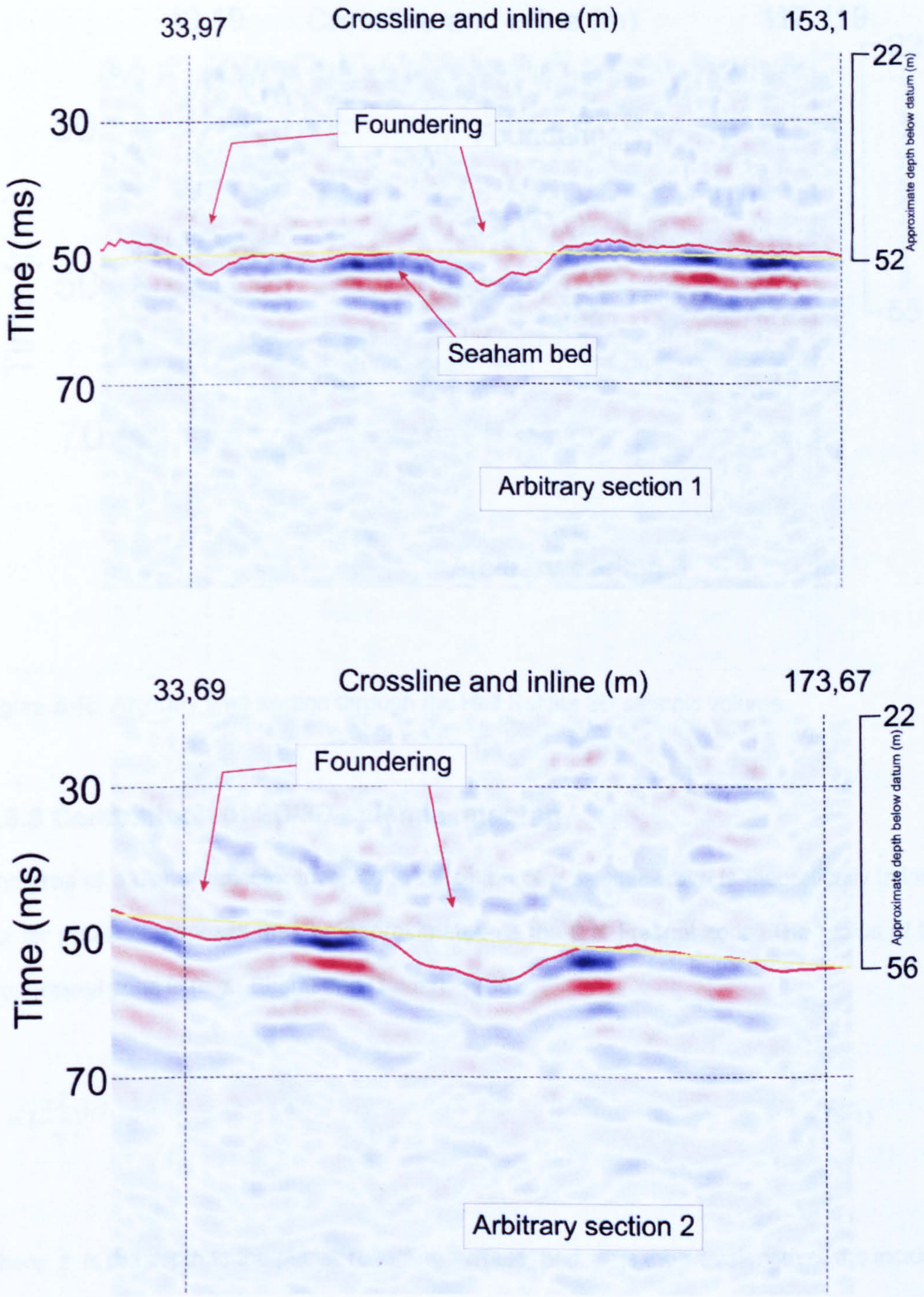

Figure 5.45: Arbitrary time sections through the Hell Kettles 3D volume.

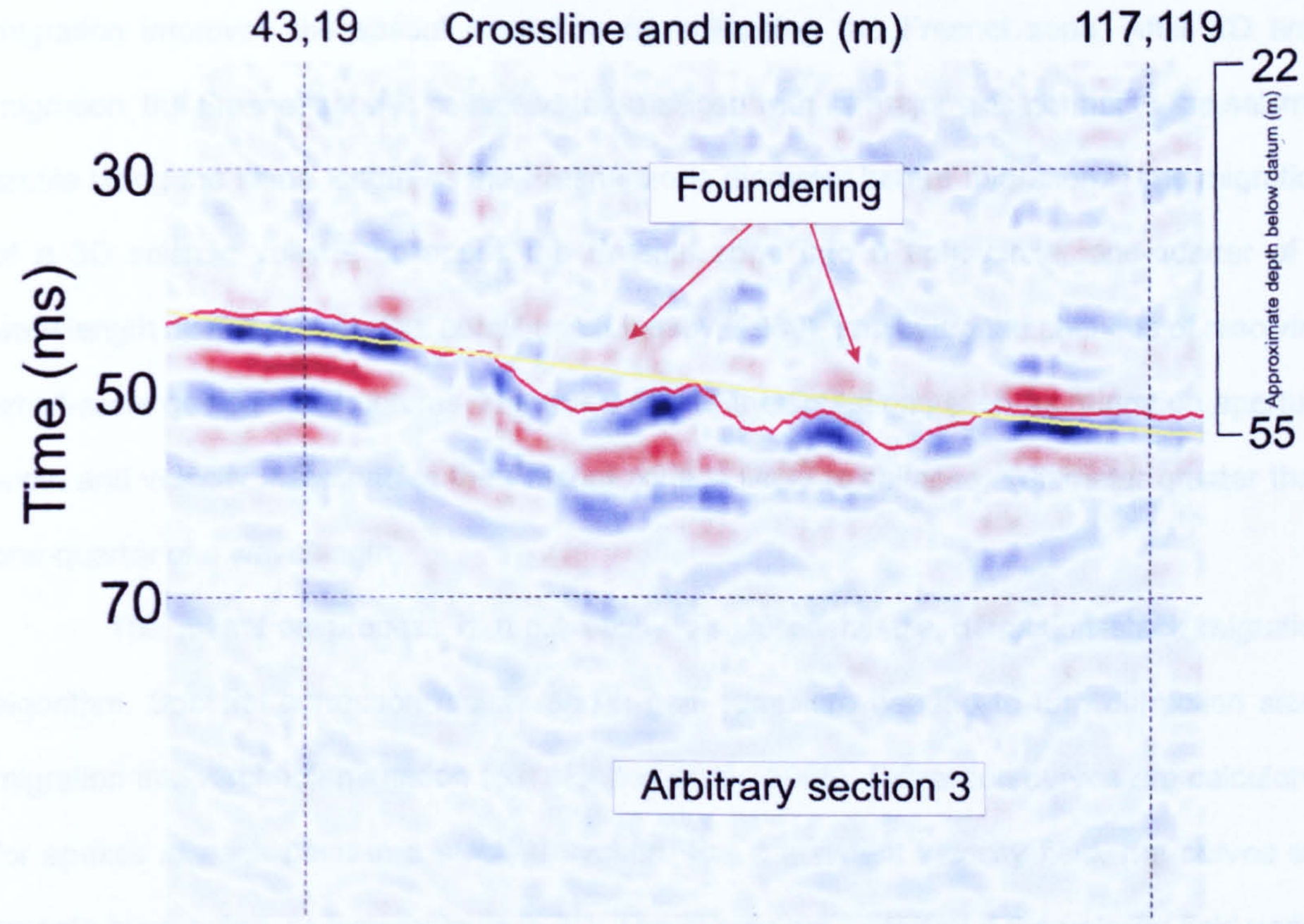

Figure 5.46: Arbitrary time section through the Hell Kettles 3D seismic volume.

5.3.5 Comparison of 2D/3D seismic imaging

The area of a planar reflector involved in reflection of a seismic wave is theoretically infinite, but for practical purposes may be approximated as the first Fresnel zone. The radius of the first Fresnel zone is (e.g., Sheriff and Geldart, 1995):

$$r = (\frac{z\lambda}{2})^{1/2} \qquad (5.1)$$

where z is the depth to the planar reflecting surface, and λ is the wavelength of the incident wave.

For a 200 Hz wave travelling at 2000 m s^{-1} incident on a reflecting boundary at 50 m depth, values typical of shallow seismic reflection investigation at Hell Kettles, the diameter of the first Fresnel zone is 32 m. For frequencies at the lower end of the recorded seismic passband, the diameter of the Fresnel zone is greater. The first Fresnel zone is normally

considered to be the limit of horizontal resolution in unmigrated seismic data. Fortunately, migration improves the spatial resolution by collapsing the Fresnel zone. After 2D time migration, the Fresnel zone is collapsed to an ellipse with its major axis normal to the seismic profile being the same length as the Fresnel zone diameter before migration. Time migration of a 3D seismic volume collapses the Fresnel zone into a tight circle, one-quarter of a wavelength diameter in perfect conditions (Lindsey, 1989), improving the chances of resolving small-scale geological structures. However, due to the limitations such as migration aperture width and velocity inaccuracies the Fresnel zone is likely to collapse a diameter greater than one-quarter of a wavelength.

The migration process is most easily visualised by the diffraction stack migration algorithm. Spectral correction factors and a gain ramp are needed to turn diffraction stack migration into Kirchhoff migration (e.g., Hatton et al., 1986). Diffraction curves are calculated for apexes at each point in a stacked section. For a constant velocity field, the curves are smooth hyperbolae, or hyperboloids in 3D. The curves are distorted if the velocity field varies in space. The data lying along the diffraction curves are summed to give the amplitude at the apex on the migrated section. Therefore, the migration process can be viewed as a stacking process.

Built in to the design of the Hell Kettles 3D survey are two 2D profiles (Figure 4.34) which were processed with exactly the same flow as the 3D dataset. The 2D profiles were acquired with a symmetric split-spread geophone arrangement with geophone spacing of 4 m (Figure 4.33). The shot spacing was 4 m on these two profiles, yielding a CMP fold of 12 with a CMP spacing of 2 m. The first twelve-fold 2D comparison profile is located along the south-east edge of the six-fold 3D volume, parallel to the field boundary adjacent to the ponds. The quality of the image of the Seaham Limestone reflector in the final stacked section of this 2D profile is marginally superior to the equivalent 3D sub-line (Figure 5.47, upper panel). The upper black leg of the reflection signal is tighter, the frequency content is higher, and the undulations in the surface of the limestone are better defined. After migration, the shape of the 2D profile is little altered. However, in the comparison 3D sub-line, the character of the surface of the limestone has become blockier and disjointed (Figure 5.47, lower panel). The comparison 3D sub-line is extracted from the very edge of the 3D volume, so the beneficial

effect of 3D migration is not fully realized. Energy is collapsed from only one half of the Fresnel zone that constitutes the reflection from the top surface of the Seaham Formation limestone. Even so, the 3D sub-line shows more detailed structure in the surface of the limestone.

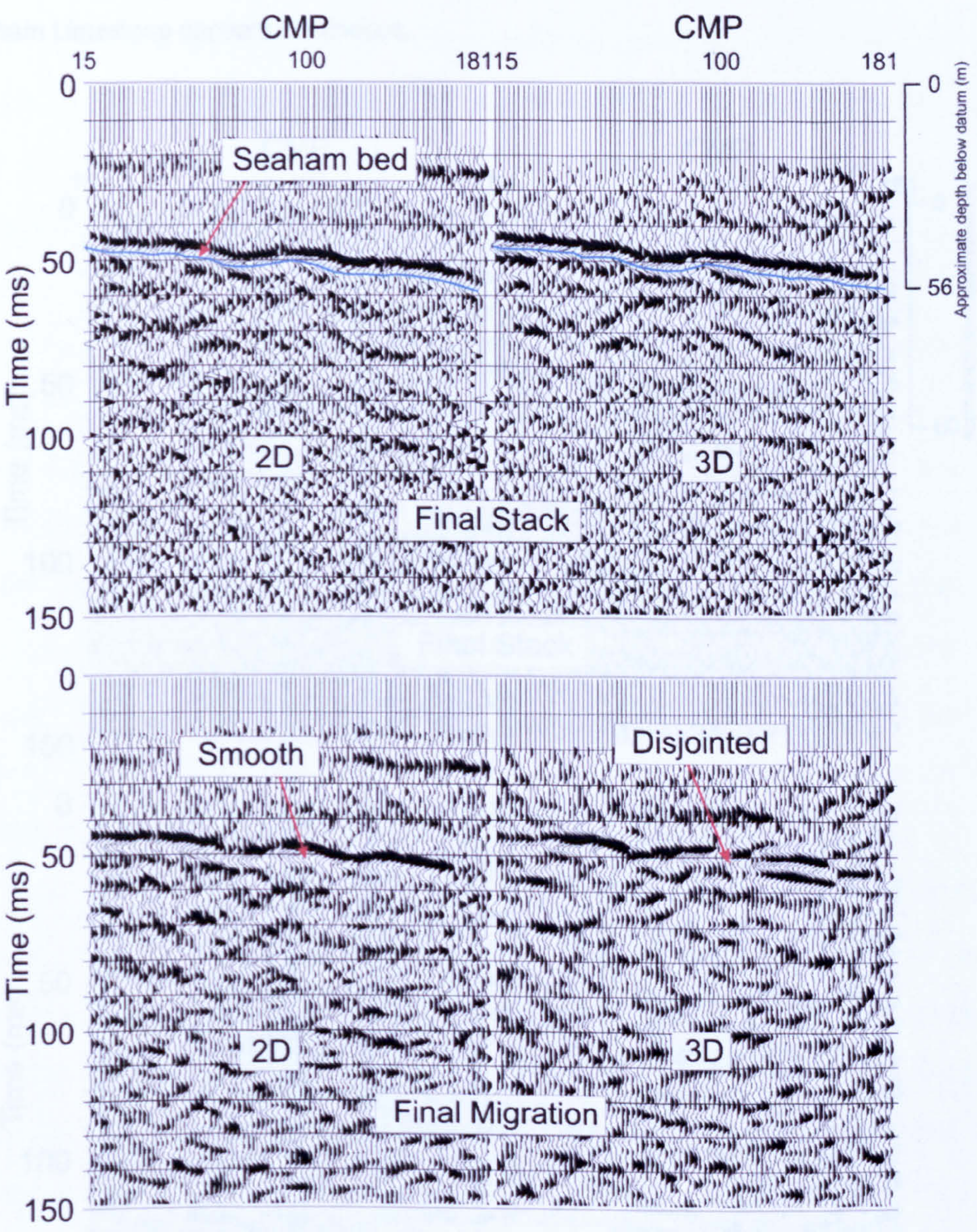

Figure 5.47: 2D and 3D comparison sections parallel to the silage field southern fenceline. Sections are displayed with a scalar multiplier. The distance between CMP traces is 2 m for all the comparison profiles. The CMP numbering has been adjusted to the distance along the profile from the first receiver station

The second embedded 2D profile runs through the very slight depression in the working silage field, the target of the 3D seismic volume. The final stacked section (Figure

5.48, upper panel) for this 2D profile and the equivalent 3D sub-line over the depression are very similar in shape, character, frequency and noise content. After migration, detailed structures within the Seaham Limestone are resolved in the 3D dataset (Figure 5.48, lower panel). Diffraction tails in the 2D and 3D final stacked sections hinted at sub-surface geological discontinuities, but 2D migration is unable to resolve them and the surface of the Seaham Limestone appears continuous.

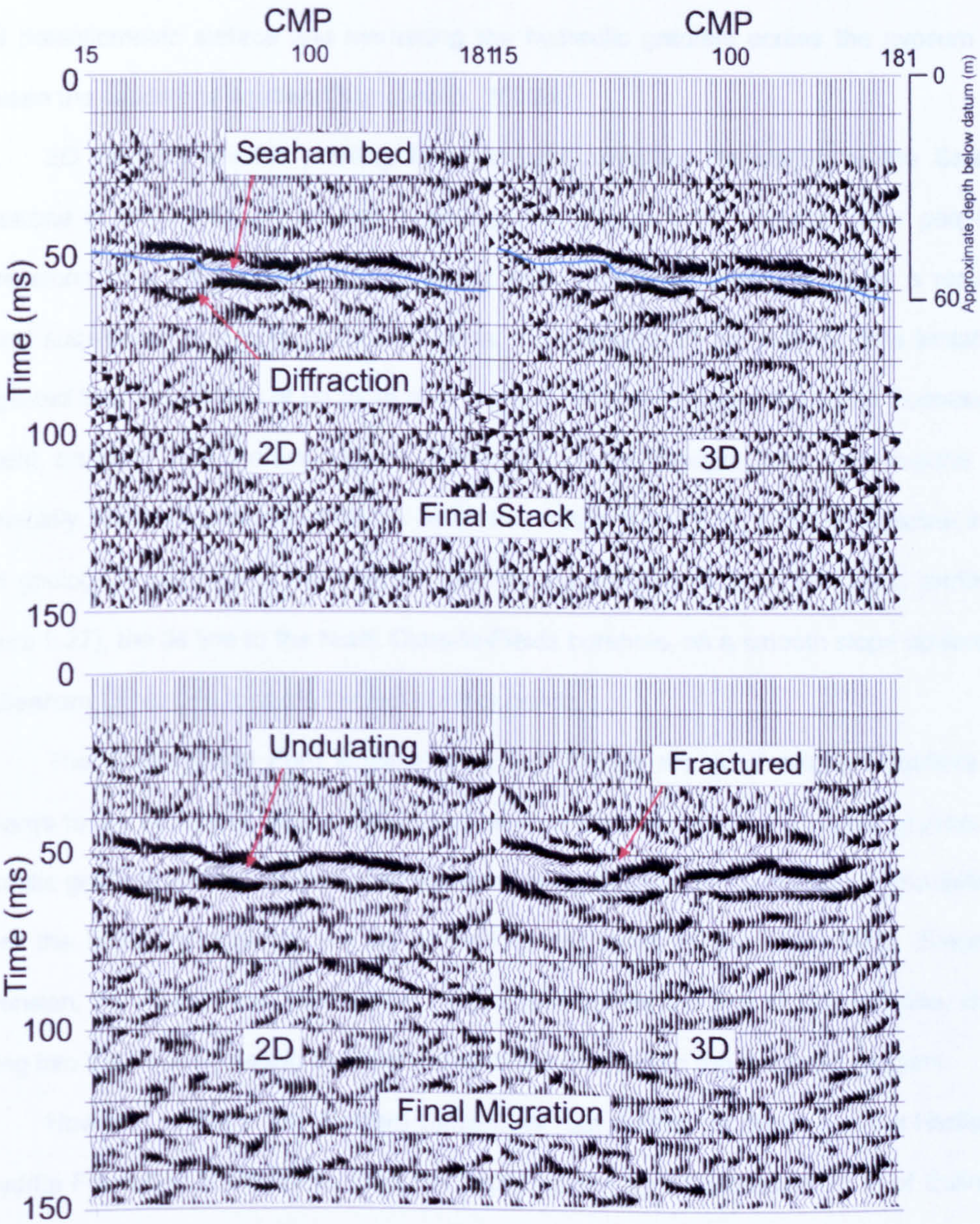

Figure 5.48: 2D and 3D comparison sections through the silage field shallow depression.

5.3.6 Mechanisms of gypsum dissolution

Extensive gypsum maze caves occur in the Western Ukraine where a thick gypsum bed is bounded by two sandstone aquifers (Klimchouck, 2000b). The water in the artesian aquifers is under-saturated with respect to calcium sulphate. Field relationships (Klimchouck, 2000b) and modelling (Birk et al., 2005) suggest that the Ukrainian maze caves developed slowly where the hydraulic gradient between the two bounding aquifers is greatest. The maze caves are generally coincident with river systems cutting down through the local terrain, altering the local potentiometric surface and increasing the hydraulic gradient across the gypsum bed between the sandstone aquifers (Klimchouck, 2000b).

2D and 3D seismic profiling have imaged extensive foundering of the Seaham Limestone in the vicinity of the Hell Kettles ponds (Figure 5.49). Several other peat-filled depressions lie a few hundred metres to the north-west (Figure 5.1), probably a result of ground subsidence due to gypsum dissolution. Interpretation of the seismic data tentatively suggested that a thickness of up to 15 m of gypsum of the Hartlepool Anhydrite Formation is present beneath Hell Kettles (Figure 5.31). All of the topographical depressions and seismically imaged foundering features lie on the axis of an NW-SE trending anticline in the solid geology (Figure 5.2). The northern limb of the anticline is observed along profile 07 (Figure 5.27), the tie line to the North Oxen-le-Fields borehole, as a smooth slope upwards in the Seaham Limestone towards the Hell Kettles ponds.

The Seaham and Ford limestones at Hell Kettles are good artesian aquifers and recharge to the north and west of Darlington where they crop out on the higher ground. The hydraulic gradient across the limestone aquifers will be greatest along the axis of the anticline where the limestone aquifers will be at their closest point to the water table. Since the Devensian, the River Tees would have meandered across the line of the anticline, down-cutting into the Permo-Triassic sediments and further increasing the hydraulic gradient.

However, unlike in the Western Ukraine, at Hell Kettles the gypsum of the Hartlepool Anhydrite Formation is separated from the upper aquifer by an estimated 10 m of Edlington Mudstone. Although the mudstones do not form a completely impermeable barrier to water percolating down from the Seaham Limestone aquifer, it is likely that the vertical rate of fluid flow is severely restricted by their low permeability. Thus, the hydrological conditions at Hell

Kettles do not seem suitable for the formation of rectilinear maze caves, although the possibility that they may be present cannot be fully discounted. For instance, the gypsum cave system discovered at Houtsay, Cumbria although of limited lateral extent was formed in a gypsum bed sandwiched between mudstones of low permeability (Ryder and Cooper, 1993), and so the permeability structure is different from that present at the Ukrainian maze cave system. Therefore, conditions other than those described by Klimchouck (2000b) and Birk et al. (2005) may allow the formation of maze caves in gypsum beds under confined conditions.

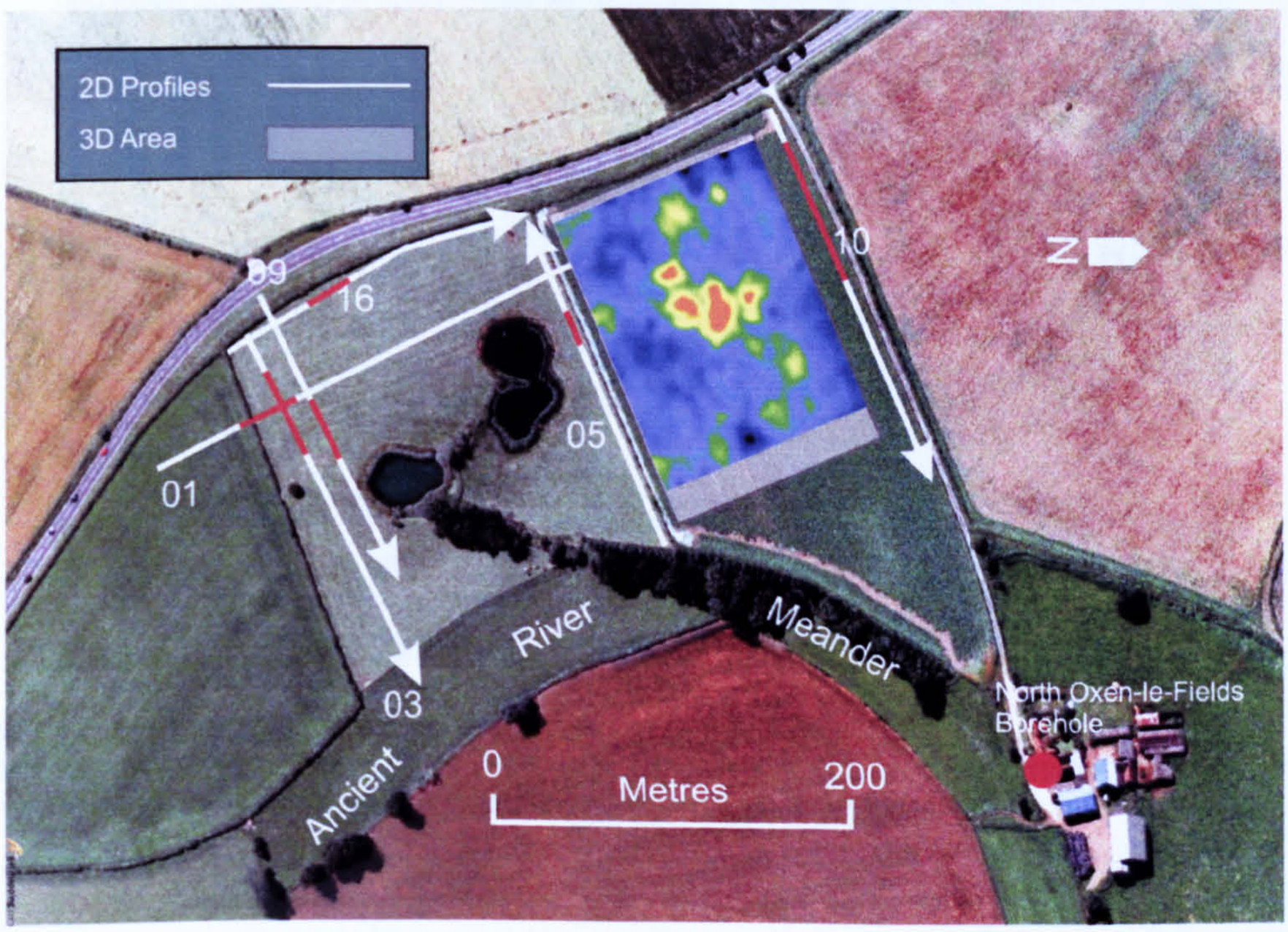

Figure 5.49: Distribution of sub-surface foundering imaged at Hell Kettles.

The random distribution of foundering suggests that the sub-surface at Hell Kettles is punctuated by breccia pipes (Figure 5.50), some of which have caused the foundering of the Seaham Limestone imaged in the 2D and 3D seismic data. A few pipes have broken through to the ground surface, as in the 1179 A.D. historic event (Figure 5.5). Discrete voids have been encountered in mining activities at depths of 400 m at the base of the Zechstein gypsum in Germany (e.g., Klimchouk, 2000c) and are thought to be caused by natural convection due to density differences within the underlying aquifer water. The Hartlepool Anhydrite rests directly on top of the Ford Limestone aquifer, so discrete voids may have developed at the

base of the gypsum bed. Eventually some of the cavities become large enough so that the internal forces within the strata arching over the fluid filled space are much less than the downward gravitational force, resulting in pieces of rock collapsing into void below. The Ford Limestone aquifer bed dips gently to the south-east. The water will flow eastwards under the hydraulic gradient, carrying any dissolved gypsum away.

Figure 5.50: A breccia pipe in cross-section.
The feature is approximately 5 m high and 3 m wide and progressed through the Permian Roker Dolomite Formation at Marsden near Sunderland, Tyne and Wear

6.0 Parkside

6.1 Site description

The Parkside [NZ 2992 1289] investigation site is on the southern outskirts of Darlington, County Durham, approximately 2 km south-east of the town centre. The survey site is located in the northern part of a triangular shaped field (Figure 6.1) immediately south of the Darlington to Middlesborough railway branch line. The field is bounded on the north side by a single track road parallel to the railway embankment. Neasham Road, which connects the centre of Darlington to the outer ring road, bounds the eastern edge of the triangular field, and there are pasture fields belonging to a riding school to the south-west. The terrain is generally flat rough pasture bisected by a rough track running from the gate in the Neasham Road boundary north-west past the Geneva borehole. The north-west corner of the field is topographically lower than the survey area, and comprises rush-filled boggy ground. At this locality, the Ordnance Survey map shows a pond that covered a more extensive area than the present-day the boggy ground. From the presence of this boggy ground, it is estimated that the water table is approximately 2 m below the ground surface where the seismic data were acquired at Parkside.

Aerial photography does not reveal any obvious depressions in the terrain at the Parkside site; however 80 m south-east of the Geneva Borehole beyond the rough track profiles 01 and 04 cut a shallow depression where the ground surface falls by 1 m (Figure 6.1). This feature was noted by Thompson et al. (1996) as a possible subsidence hollow and the British Geological Survey assessment of the superficial deposits in the area indicates foundering (Figure 6.2). The underlying solid geology is of Permian age and the Parkside site is located on the southern limb of the easterly dipping Darlington syncline (Figure 6.3).

Geological control is provided by the Geneva borehole (Figure 6.4). A thickness of 50 m of Quaternary till, silts, sands and clays rests almost directly on top of gypsum beds of the Hartlepool Anhydrite Formation, separated only by a 1 m thickness of mudstone of the Edlington Formation. The Geneva borehole penetrated 18 m of the Hartlepool Anhydrite Formation, and was terminated before reaching the base of the formation. Within the thick

Hartlepool Anhydrite Formation, at 66 m below ground surface, a 2 m deep cavity was encountered. Although an investigation into the subsidence of several houses on a nearby estate as part of the European Community funded ROSES (Risk of Subsidence due to Evaporite Solution) project concluded that gypsum dissolution does not present a risk of subsidence in Darlington (Lamont-Black et al., 2005), dissolution of the Hartlepool Anhydrite gypsum bed may be the cause of the ground surface foundering at the Parkside site.

To investigate the condition of the sub-surface gypsum, a loose grid of four 2D profiles was acquired in 2005, with a follow up 3D seismic survey in 2006 acquired over the Geneva borehole (Figure 6.1). For a fuller account of the acquisition parameters the reader is referred to Chapter 3.

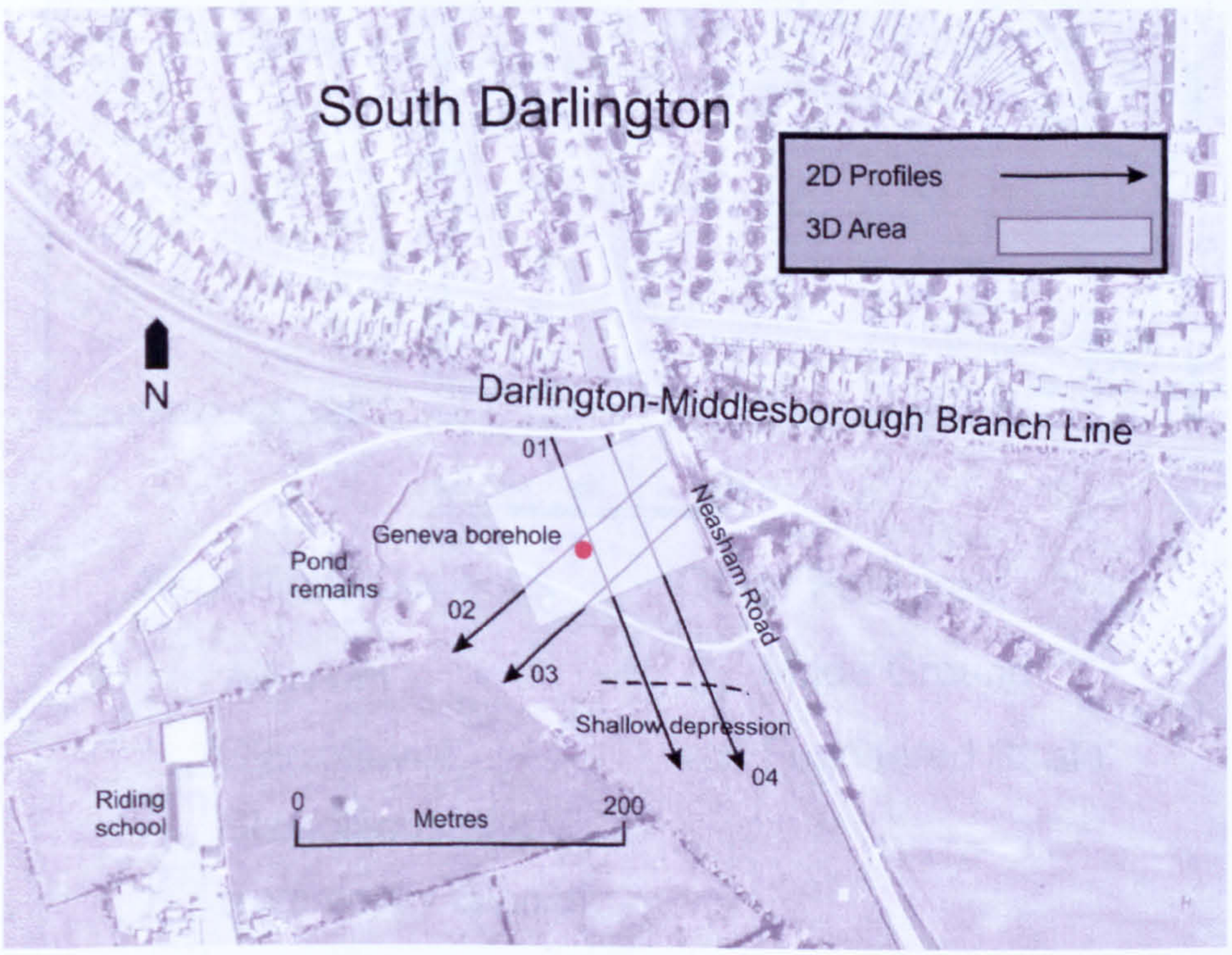

Figure 6.1: Aerial photograph taken in 1988 of the Parkside survey site.

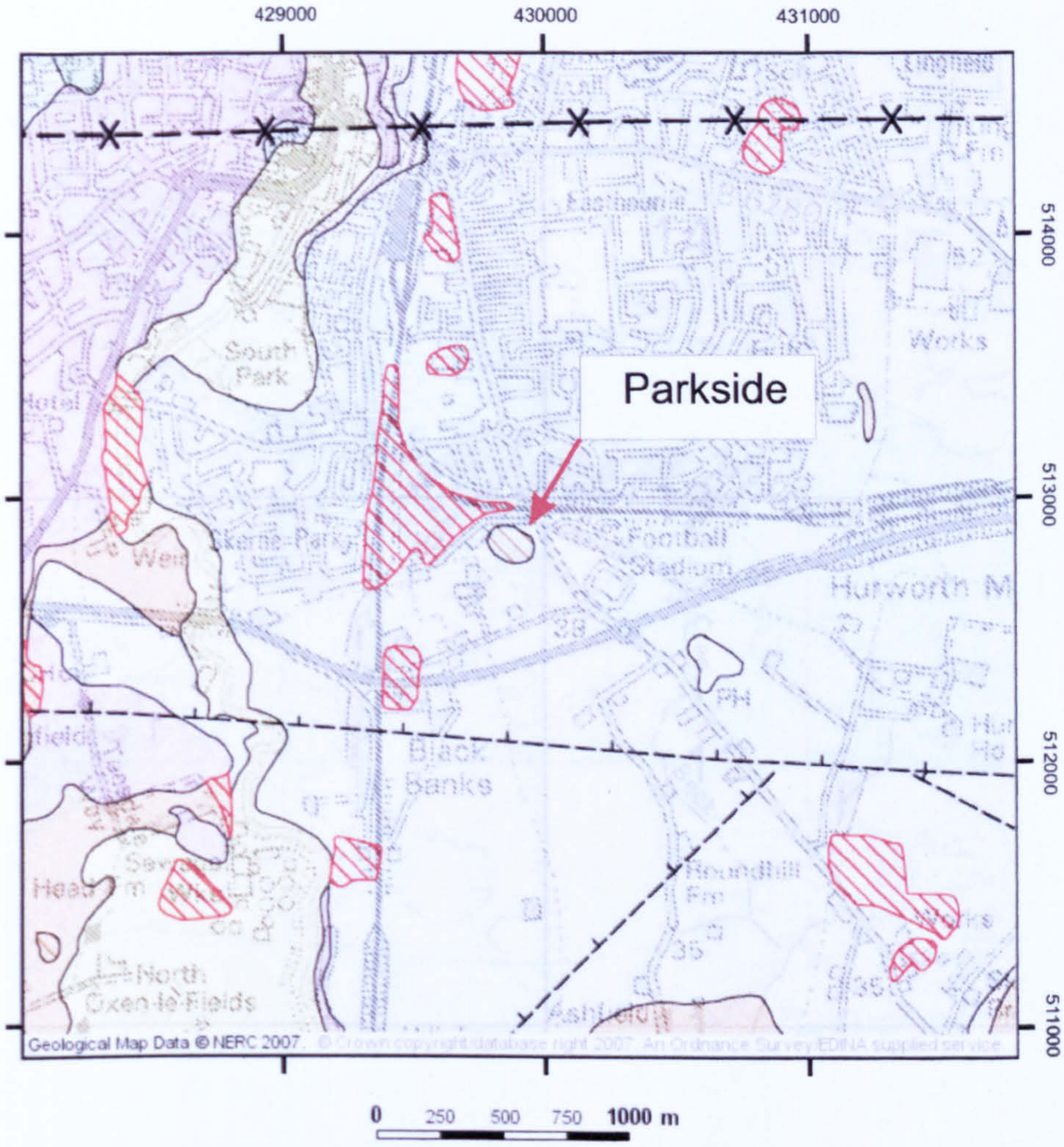

Figure 6.2: Superficial geology at the Parkside survey site.
Data supplied by Ordnance Survey/EDINA service © Crown Copyright Database 2007.

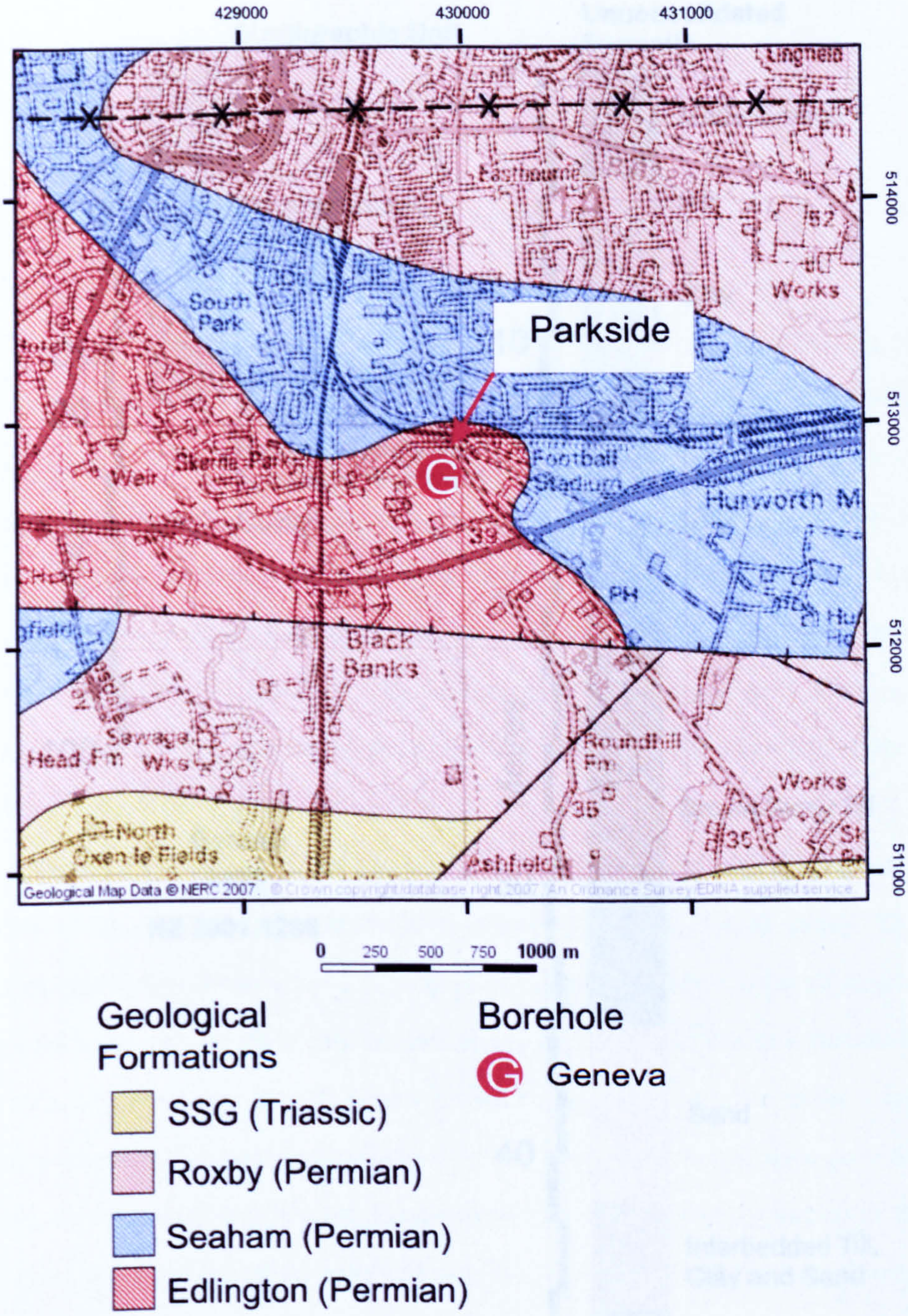

Figure 6.3: Solid geology beneath the Parkside survey site.
Data supplied by Ordnance Survey/EDINA service © Crown Copyright Database 2007.

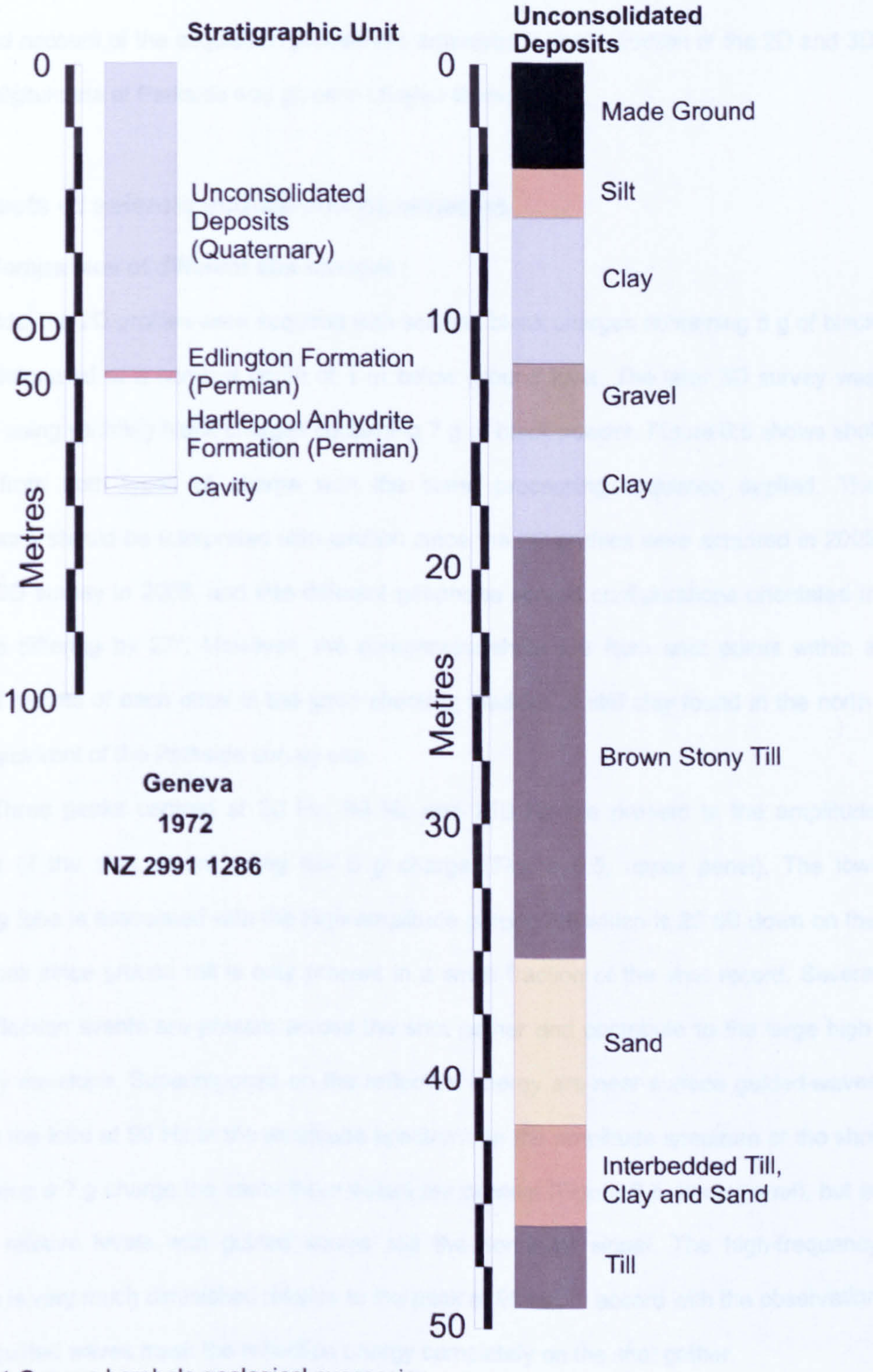

Figure 6.4:Geneva borehole geological succession.
Quaternary unconsolidated deposits expanded to show layering details.

6.2 Acquisition

A detailed account of the acquisition procedures employed in the collection of the 2D and 3D seismic digital data at Parkside was given in chapter three.

6.2.1 Tests of seismic acquisition parameters

6.2.1.1 Comparison of different size charges

At Parkside, the 2D profiles were acquired with saluting blank charges containing 5 g of black powder detonated at a nominal depth of 1 m below ground level. The later 3D survey was collected using yachting blank charges containing 7 g of black powder. Figure 6.5 shows shot records from both types of charge with the same processing sequence applied. The comparisons should be interpreted with caution since the 2D profiles were acquired in 2005 and the 3D survey in 2006, and into different geophone spread configurations orientated in directions differing by 27°. However, the comparison shots are from shot points within a couple of metres of each other in the good shooting medium of stiff clay found in the north-eastern quadrant of the Parkside survey site.

Three peaks centred at 30 Hz, 90 Hz and 210 Hz are present in the amplitude spectrum of the shot record using the 5 g charge (Figure 6.5, upper panel). The low-frequency lobe is associated with the high-amplitude ground roll which is 20 dB down on the 90 Hz peak since ground roll is only present in a small fraction of the shot record. Several sharp reflection events are present across the shot gather and contribute to the large high-frequency envelope. Superimposed on the reflection energy are near-surface guided-waves that form the lobe at 90 Hz in the amplitude spectrum. In the amplitude spectrum of the shot record using a 7 g charge the same three peaks are present (Figure 6.5, lower panel), but at different relative levels with guided waves still the dominant signal. The high-frequency envelope is very much diminished relative to the peak at 95 Hz, in accord with the observation that the guided waves mask the reflection energy completely on the shot gather.

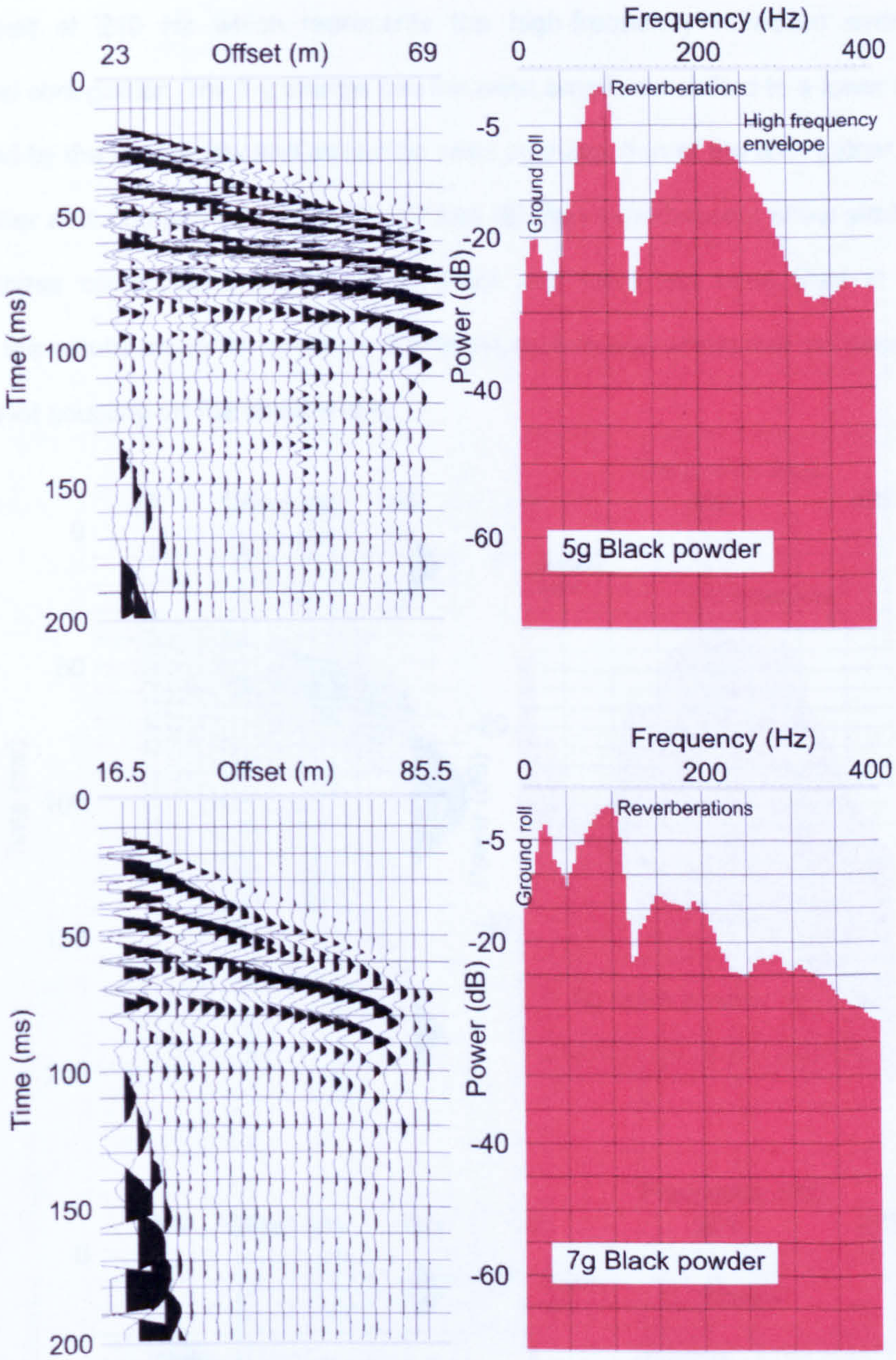

Figure 6.5: Shot charge size comparison at Parkside.
Amplitude spectra are for the complete 200 ms window displayed.

For the shot gathers in Figure 6.6, the ground roll and reflection arrivals are separated from the total signal contribution by muting, whilst the strong guided waves centred at 95 Hz are removed by bandpass filtering with corner frequencies of 100 Hz, 140 Hz, 330 Hz and 350 Hz. The amplitudes are normalised to range between +1 and -1 over the total length of 512 ms of each shot record, after which the same low-frequency dummy trace is appended. The dummy trace is designed so that the spectral analysis normalises the

amplitude spectra relative to this high peak. The 5 g charge has a broad smooth amplitude peak centred at 210 Hz which represents the high-frequency reflection events in the manipulated shot gather. The 7 g charge has the peak amplitude shifted to a lower frequency, as predicted by the scaling law and as can be seen by inspection of the shot gather.

Other shot comparisons from the 2D and 3D Parkside datasets show similar results. Although these comparisons are between shots that have not been fired in the same shotholes, the results are in fair agreement with the scaling law, which may be because of the excellent shot coupling on the shallow clay.

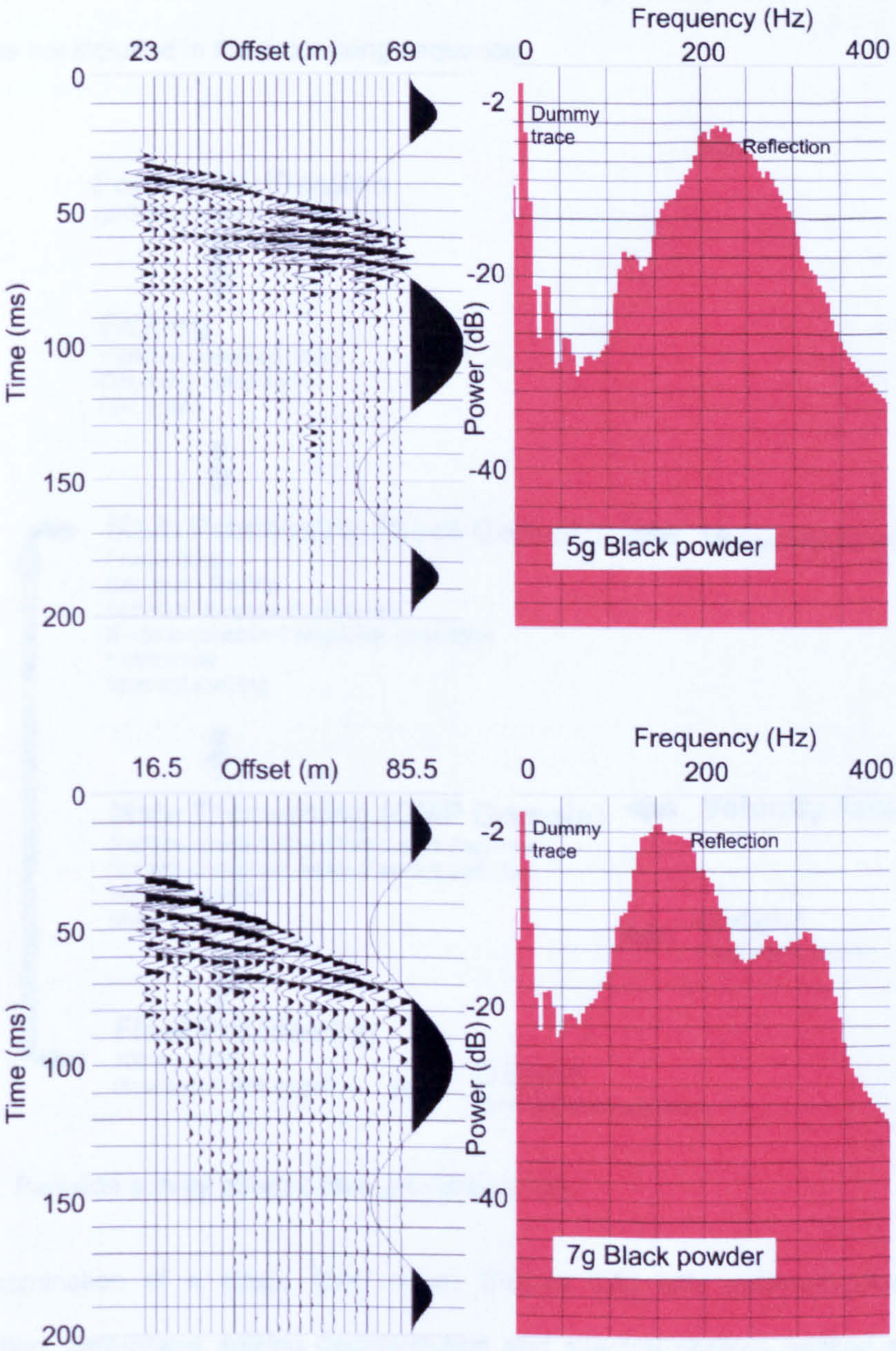

Figure 6.6: Filtered and muted shot charge size comparison at Parkside. Amplitude spectra are for the complete 200 ms window displayed.

6.3 Processing

There are three main differences in the digital processing sequence of the 2D and 3D seismic data collected at the Parkside survey site (Figure 6.7) compared to the seismic processing flow applied to the Hell Kettles seismic dataset (Figure 4.31). In the shot domain, spectral shaping was preferred to zero-phase spiking deconvolution to expand the dataset frequency bandwidth and improve the temporal resolution. In the common midpoint (CMP) domain, two passes of surface-consistent residual statics were preferred to tune the reflection continuity, with each pass separated by a refinement of the stacking velocity field. *F-x* deconvolution filtering was not included in the processing sequence.

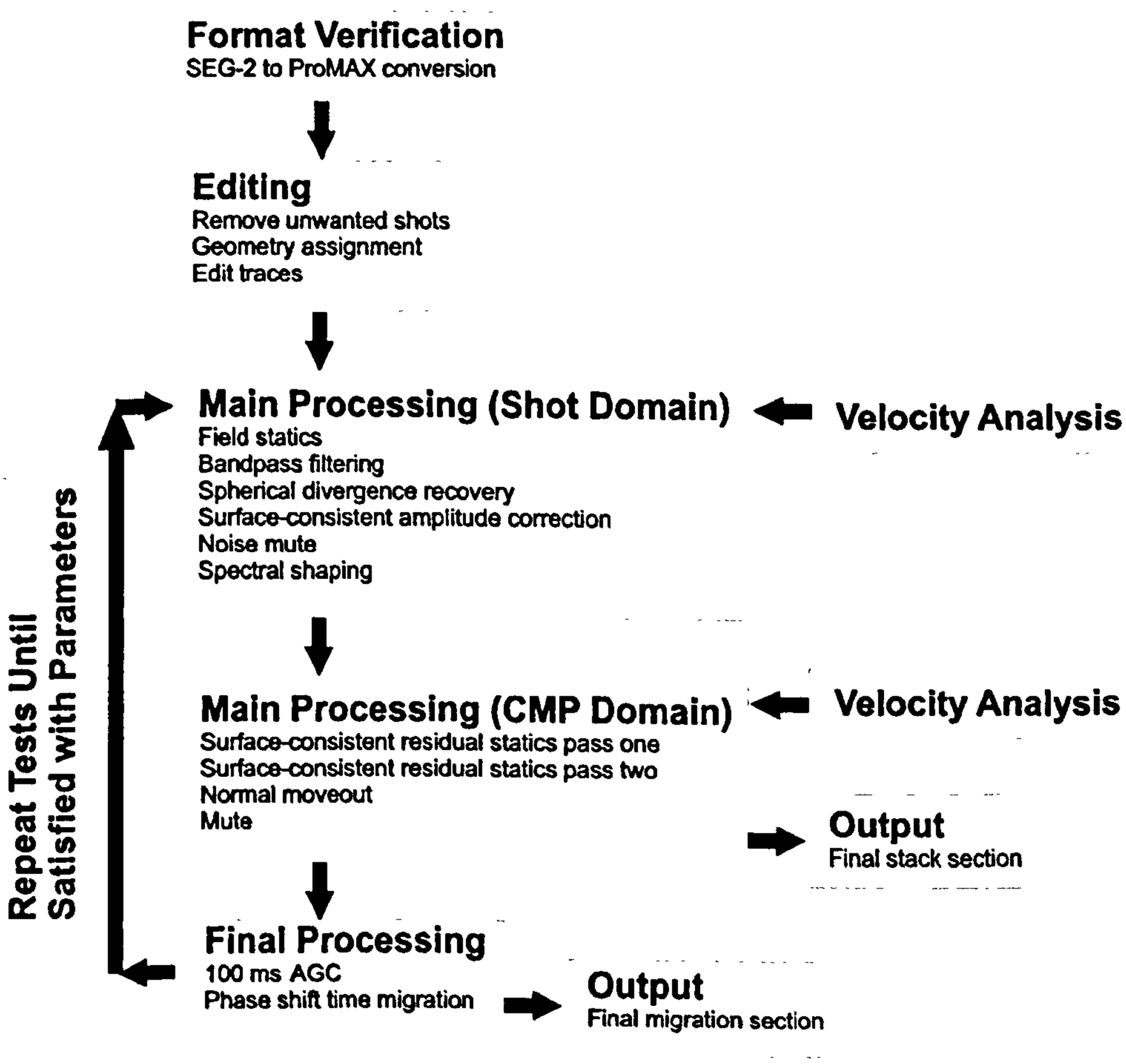

Figure 6.7: Parkside survey seismic data processing flow.

Examination of a single shot record (Figure 6.8) with minimum-phase spiking deconvolution, zero-phase spiking deconvolution and spectral shaping applied shows that each method sharpens the reflection events effectively. Spectral shaping boosts or

suppresses the amplitude of each discrete frequency determined by a user defined design. At Parkside frequencies of less than 60 Hz and more than 350 Hz were assigned 0% amplitude response, to minimise the effect of any seismic noise beyond these limits. The amplitudes of frequencies between 100 Hz and 330 Hz were set to the same maximum value, and the amplitude spectrum had linear ramps between the corner points of 60 Hz to 100 Hz and 330 Hz to 350 Hz. During this procedure the phase spectrum of the signal is left unchanged. The frequency content of the filtered shot gathers is very similar with only subtle differences in the character of the reflection signal. Although the spectral shaping result is much noisier in the individual shot gathers, after viewing the results of the different approaches at the stack section level, spectral shaping was the preferred option.

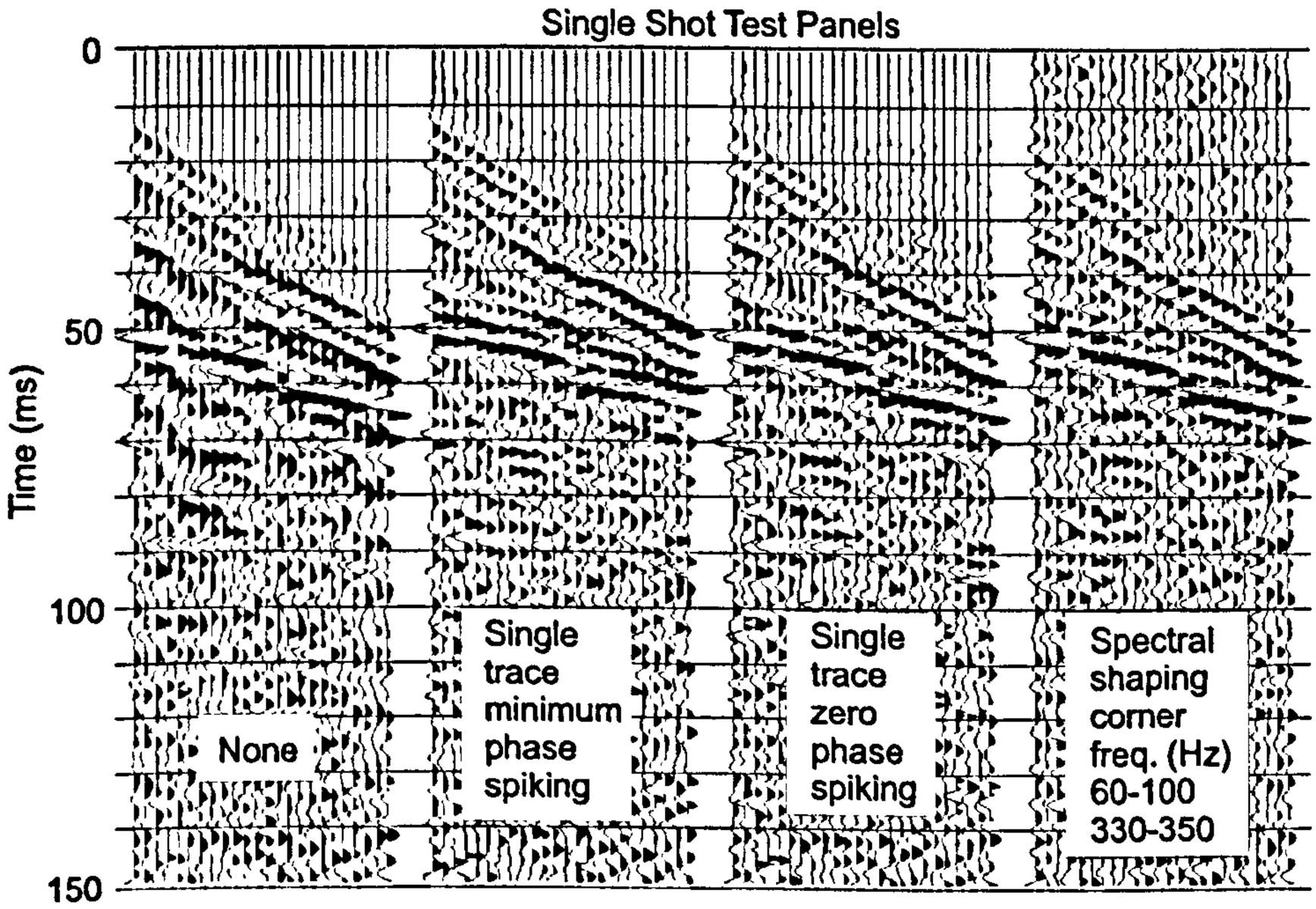

Figure 6.8: Shot record deconvolution type scan on Parkside data.
The single trace spiking variations both have a 10 ms operator length. Data are displayed with a 200ms AGC window before being cropped.

Several reflectors are present in the Parkside data from a shallow horizon at 30 ms through to 70 ms. To define the fine detail of the reflection events, it was decided to tune the reflection signal on the individual traces within the CMP gathers progressively with two passes of surface-consistent residual statics (Figure 6.9). Each pass was constrained by the

same convergence criteria, but separated by a refinement of the velocity field and the horizon about which the residual statics are computed.

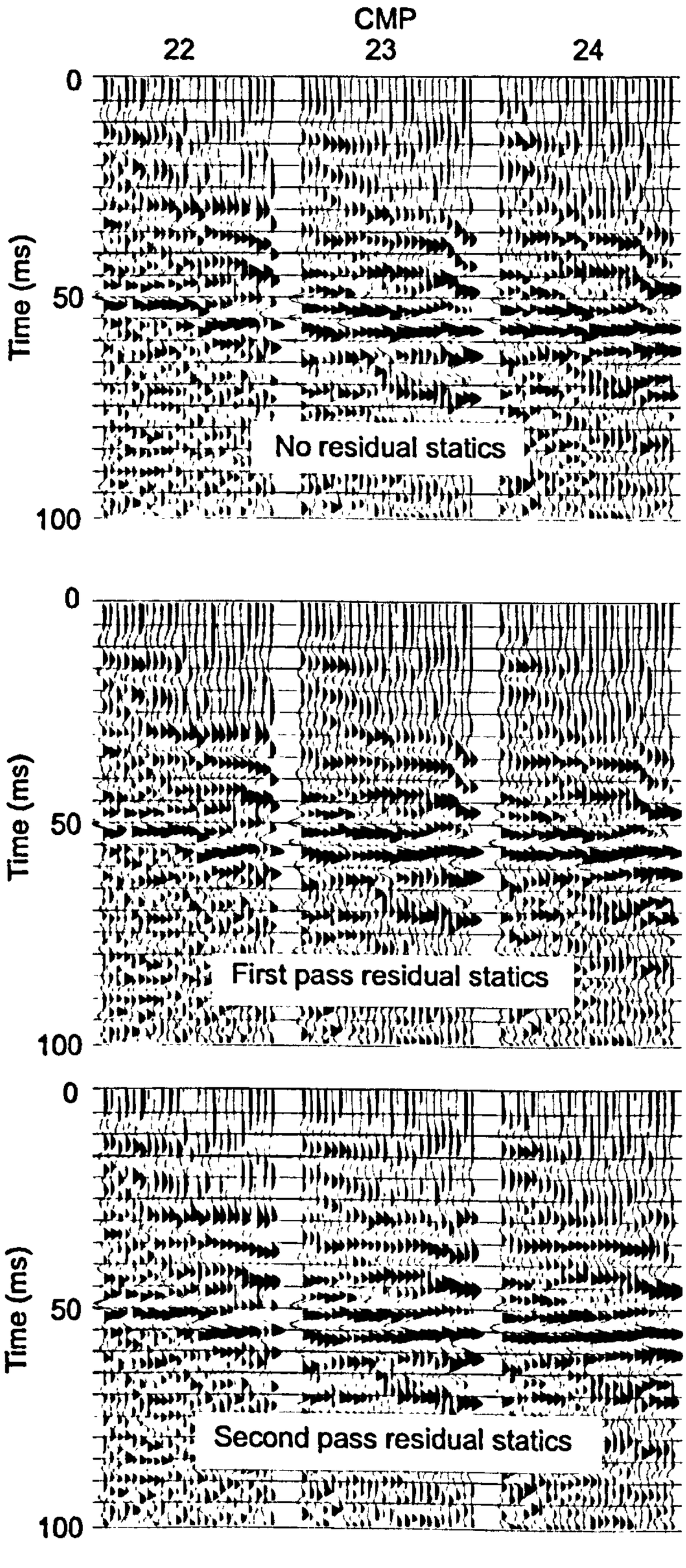

Figure 6.9: Improvement in reflection continuity with surface-consistent residual statics. Data are displayed with a 200 ms AGC window before being cropped.

Low-velocity high-amplitude ground roll noise is prevalent on all the raw shot records acquired at Parkside (Figure 6.10). Only weak air-waves are observed. The ground roll noise is removed by passing a simple bandpass filter over the shot gathers, leaving some disorganised high-frequency noise at later travel times which has low-amplitude in the stacked section. Hence, no *f-x* deconvolution filtering is required.

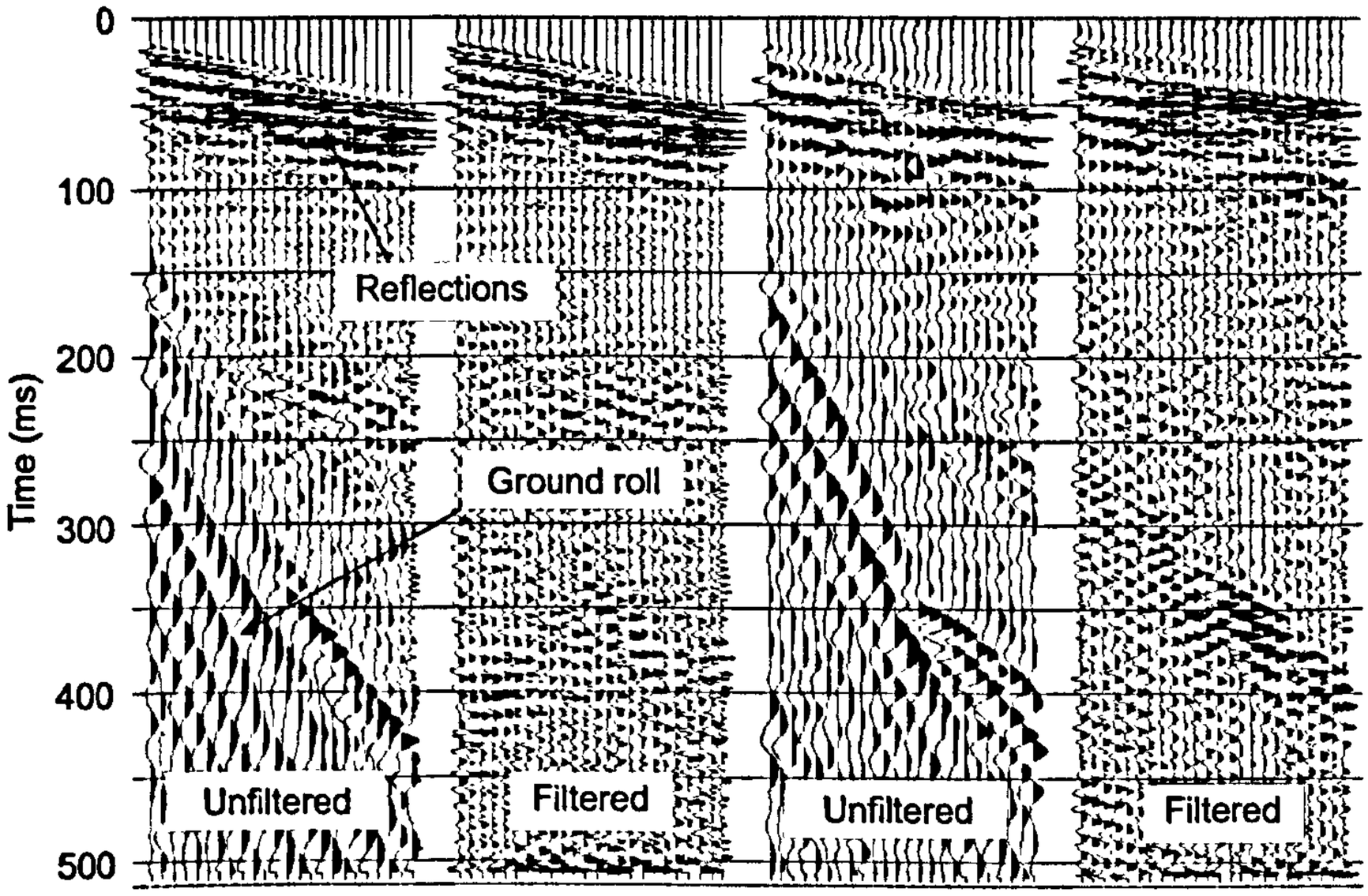

Figure 6.10: Bandpass filtered shot records from the Parkside survey profile 04.
The bandpass filter used is a simple non-variant filter with corner frequencies of 60 Hz, 100 Hz, 330 Hz and 350 Hz. Shots are displayed with a 200 ms AGC window.

6.4 Interpretation

6.4.1 Reflections from the Permian formations

Several reflection events are observed in the time migrated section from profile 04 (Figure 6.11). The deepest interpretable reflecting horizon is at 70 ms between CMPs 63 and 113. It has a black-white-black seismic signature that has been picked in blue on the central white loop. In the velocity analysis at CMP 85 (Figure 6.12) the 70 ms horizon is represented by a strong continuous event, and there appears to be a surface multiple of it at 140 ms.

The blue reflection event at 70 ms is too deep to be a reflection from the top surface of the gypsum-rich Hartlepool Anhydrite Formation, which is at approximately 50 ms assuming a P-wave interval velocity of 1800 m s^{-1} through the Quaternary deposits. The

Geneva borehole proves 18 m of gypsum-rich Hartlepool Anhydrite Formation exists at Parkside. It did not reach the base of the Hartlepool Anhydrite, which overlies the Ford Limestone; therefore, the interface between these two formations is the likely candidate responsible for the blue event.

The P-wave velocity through the Permian Zechstein limestones is 6400 m s^{-1} on the sonic log in the Seal Sands borehole (Figure 2.6). This velocity is likely to be lower at Darlington due to relaxation, following uplift and erosion of the overlying rock mass, and dissolution by ground water because the Ford Formation is an artesian aquifer. Fairbairn et al. (1986) gave 4000 m s^{-1} as the average P-wave velocity through the Permian sequence in the Selby coalfield, where more than half the thickness of strata comprised limestone, so the velocity in the Ford Limestone at Darlington may be around 4500 m s^{-1}. Gypsum is of lower density than limestone and has also lower P-wave interval velocities of between 2000 m s^{-1} and 3500 m s^{-1} (e.g. Sheriff and Geldart, 1995), so its acoustic impedance must be lower too. Therefore, the Hartlepool Anhydrite-Ford interface will have a positive reflection coefficient.

The top of the Ford Formation limestone is not picked with any confidence along the other three Parkside 2D profiles 01, 02 and 03 (Figures 6.13, 6.14 and 6.15). However, 3D time migration resolves the top Ford horizon as a dipping surface on an in-line 3D sub-profile (Figure 6.16). The Hartlepool Anhydrite-Ford interface is imaged across approximately half of the 3D volume dipping to the west (Figure 6.17), contrary to the expected local dip to the north-east towards the Darlington Syncline.

Only a very thin bed of Edlington Formation mudstones is recorded the Geneva borehole, so the Hartlepool Anhydrite Formation is almost in direct contact with the Quaternary deposits at that location. At the borehole intersection point on profile 01, there is a black-white-black seismic package that has been picked in red on the central white loop at 54 ms travel time (Figure 6.13), which coincides with the depth to the Hartlepool Anhydrite Formation assuming a P-wave interval velocity of 1800 m s^{-1} through the overlying water-saturated Quaternary deposits. In character, the red event is similar to that from the top Ford and presumably represents a positive acoustic impedance contrast. Beyond the intersection point with profile 03 the character of this reflection event alters, becoming more rugged, and cannot be traces with any confidence beyond CMP 150.

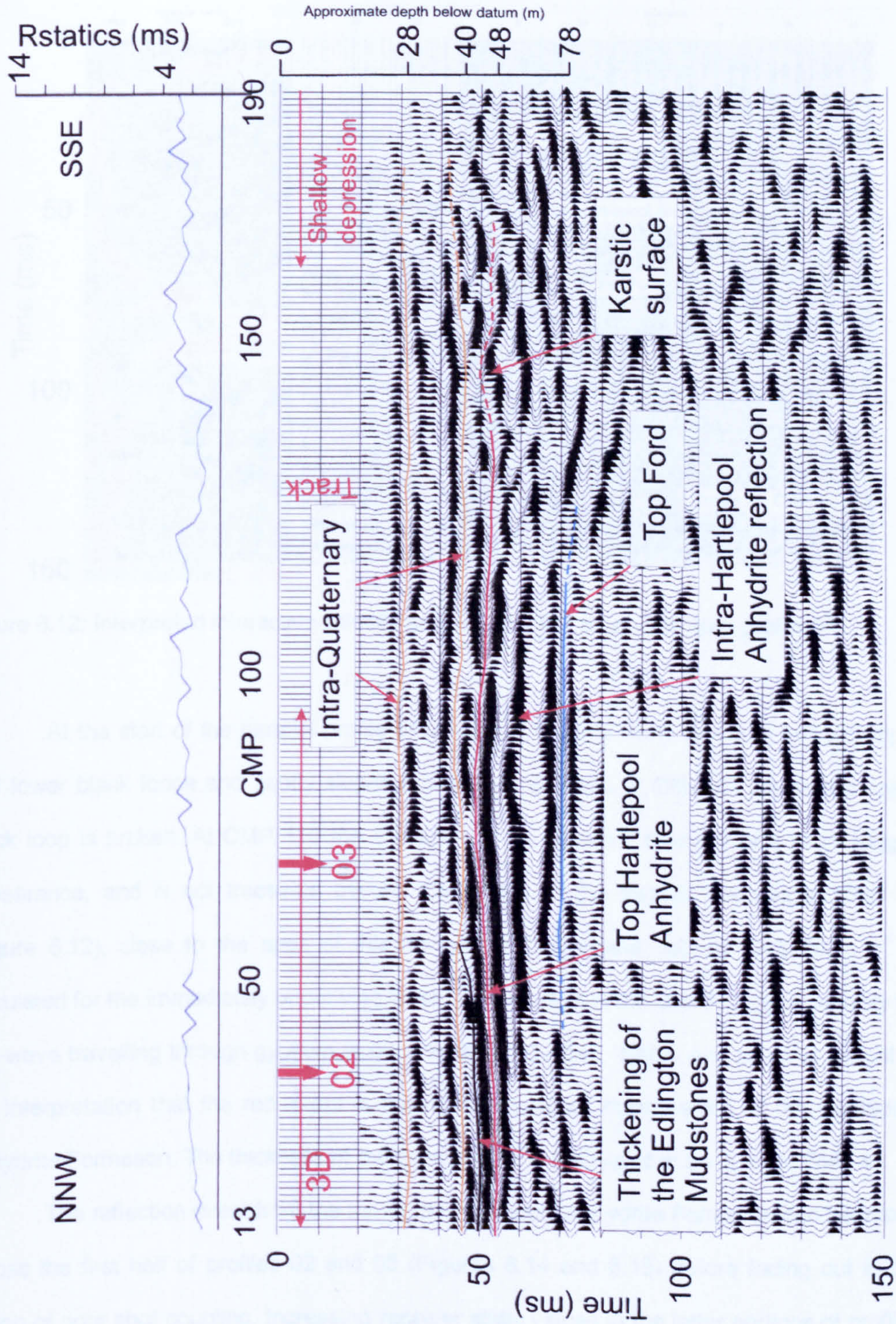

Figure 6.11: Interpreted final migrated section of Parkside profile 04.
The distance between CMP traces for all Parkside 2D profiles is 1 m. The CMP numbering has been adjusted to represent the distance along the profile from the first receiver station. Section is displayed with a scalar multiplier.

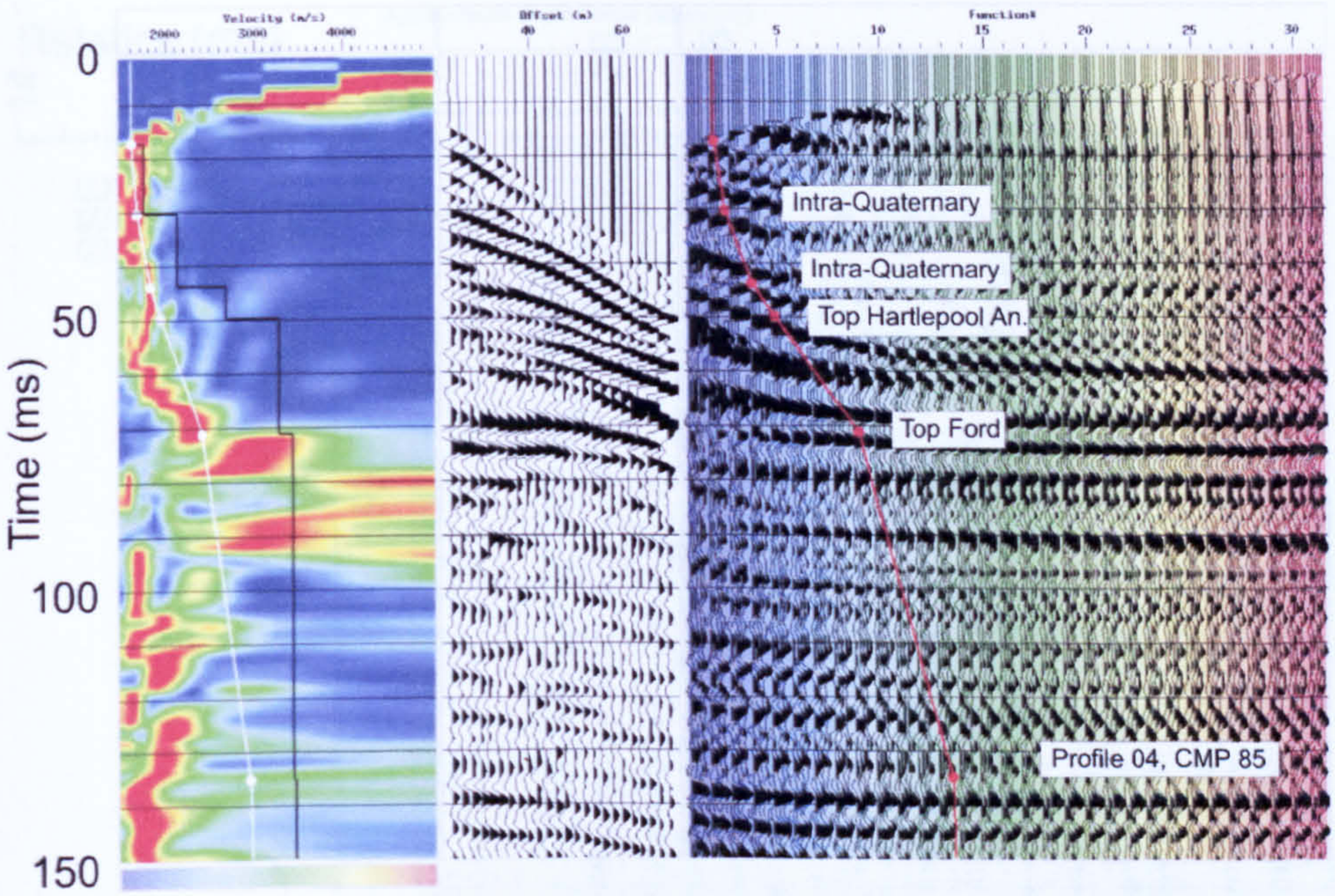

Figure 6.12: Interpreted interactive velocity analysis at CMP 85 on Parkside profile 04.

At the start of the parallel profile 04 (Figure 6.11) this event has well defined upper and lower black loops and gently slopes upwards to an apex at CMP 80 where the upper black loop is broken. At CMP 113 the character of the reflector changes to a more rugged appearance, and is not traceable beyond CMP 163. In the velocity analysis at CMP 85 (Figure 6.12), close to the apex of this horizon, a Dix interval velocity of 3500 m s^{-1} is calculated for the immediately underlying layer. This value is at the upper range of velocity for a P-wave travelling through gypsum (e.g., Sheriff and Geldart, 1995), and so gives weight to the interpretation that the red event is the reflection signal from the top of the Hartlepool Anhydrite Formation. The thickness of the gypsum bed is estimated to be 30 m at CMP 85.

The reflection event from the top of the Hartlepool Anhydrite Formation can be traced across the first half of profiles 02 and 03 (Figures 6.14 and 6.15) before fading out in the region of poor shot coupling. Increasing receiver static values in the latter portions of profiles 02 and 03 are due to the very dry sandy soil which also has the effect of attenuating high-frequency seismic signal.

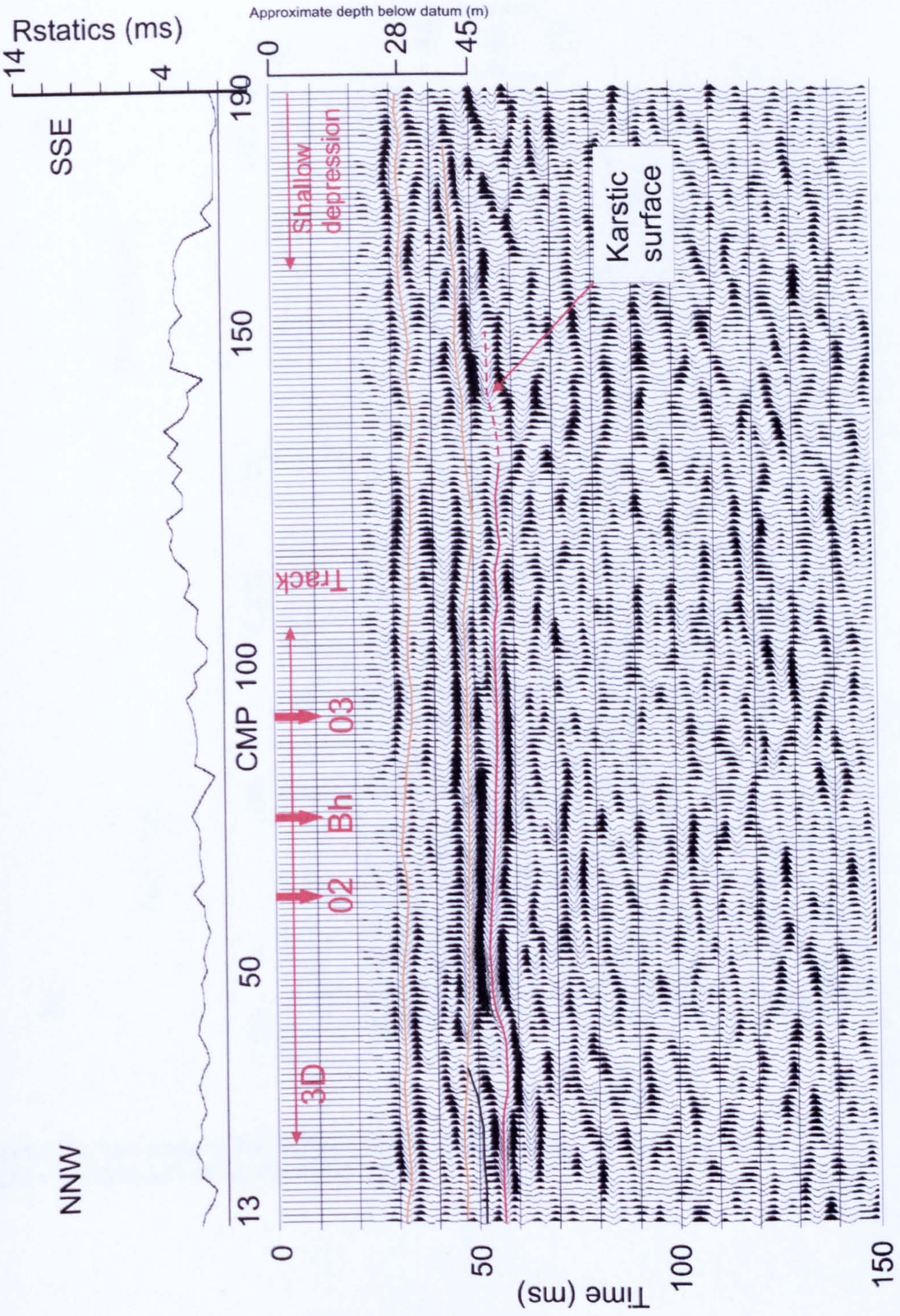

Figure 6.13: Interpreted final migrated section of Parkside profile 01.
Section is displayed with a scalar multiplier.

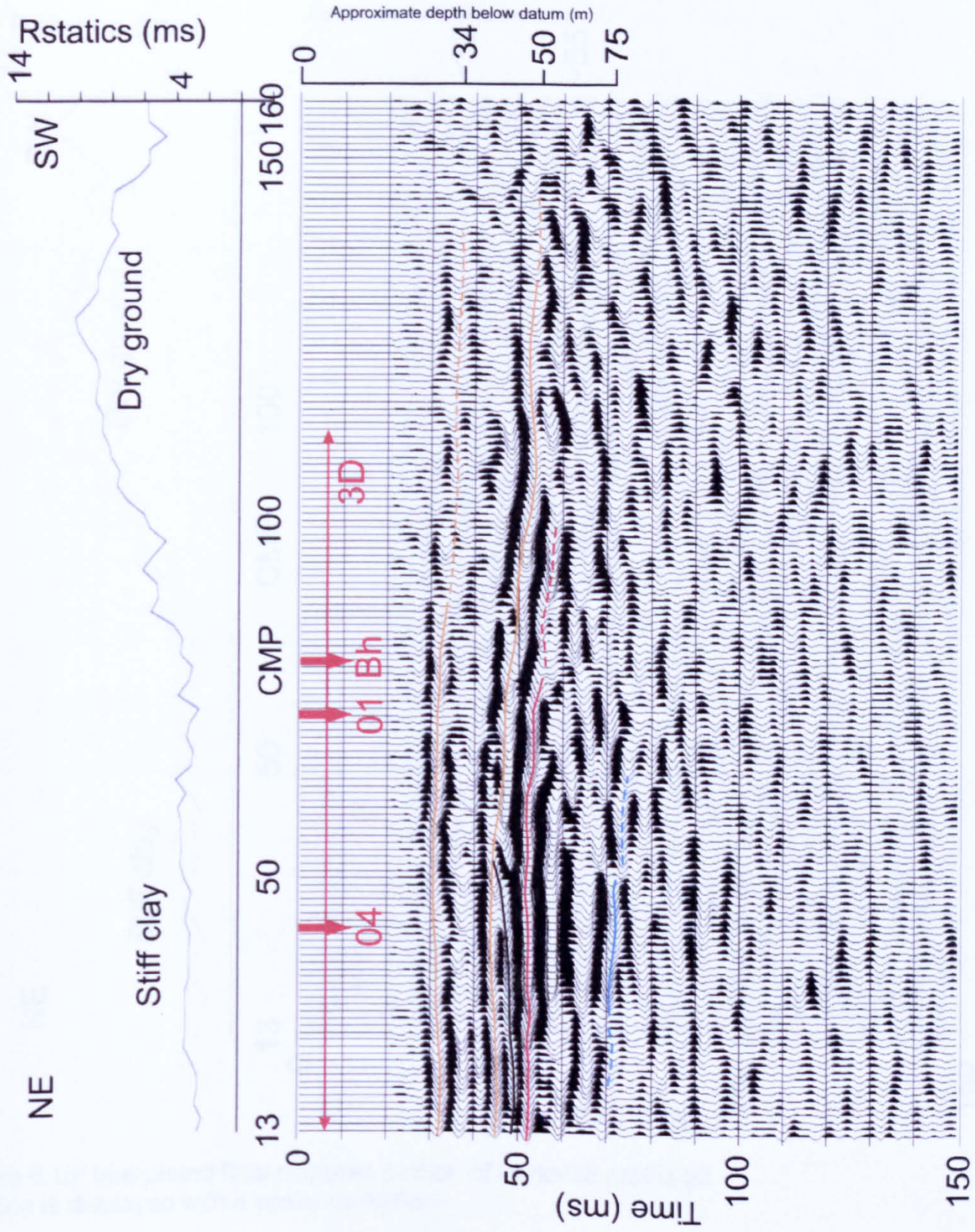

Figure 6.14: Interpreted final migrated section of Parkside profile 02.
Section is displayed with a scalar multiplier.

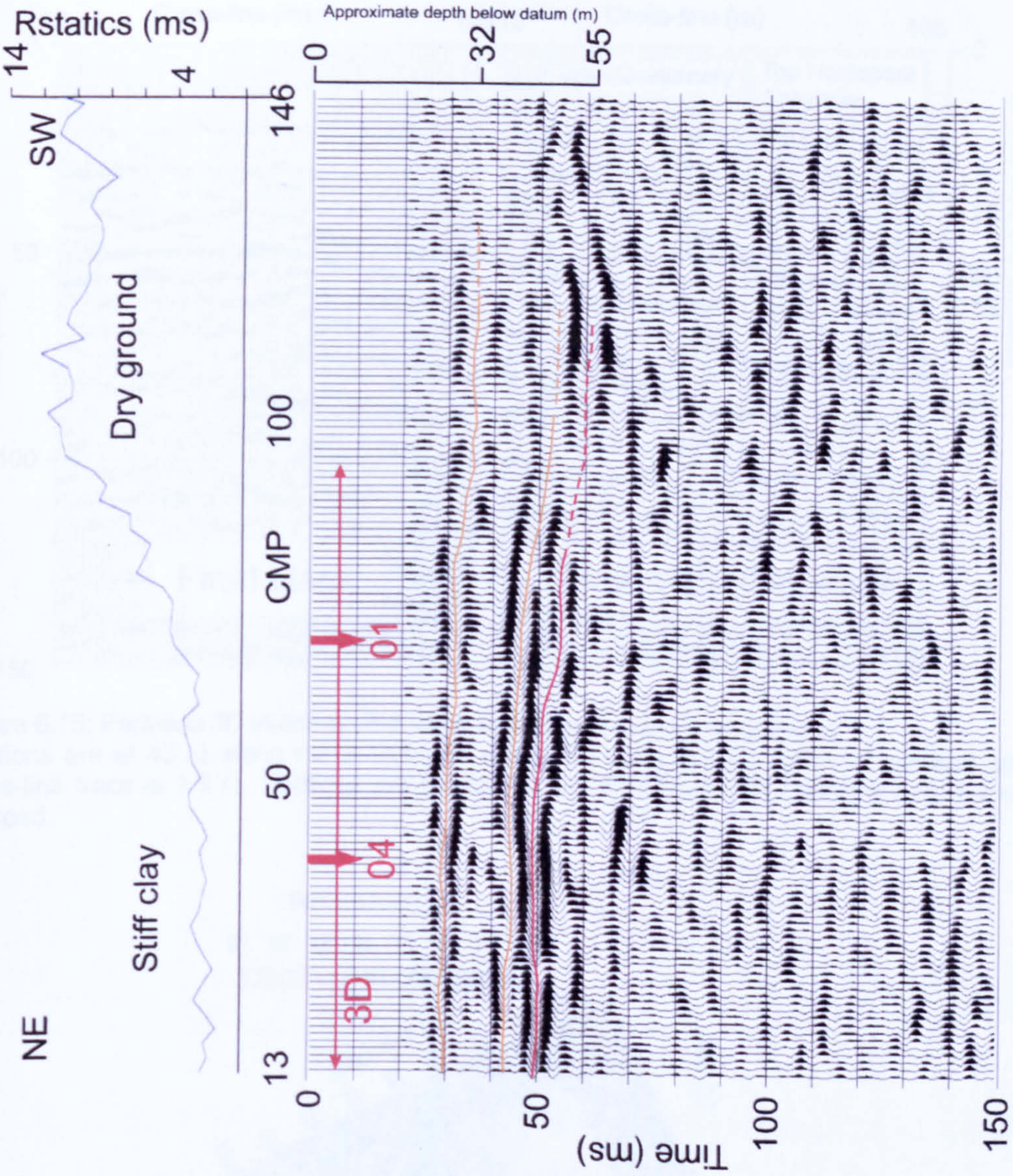

Figure 6.15: Interpreted final migrated section of Parkside profile 03.
Section is displayed with a scalar multiplier.

When mapped across the 3D seismic volume, the top surface of the Hartlepool Anhydrite Formation (Figure 6.18) is closest to the ground surface in the eastern quadrant of the 3D survey area. The gypsum surface dips to the north and west by approximately 10 ms, in concordance with the underlying Ford Formation limestone but differing from the local geological trend. The change in dip direction is expressed on the geological map (Figure 6.3) as a sharp deviation in the strike of the Edlington-Seaham interface at rockhead, and it is possible that there is an unidentified fault present to the north-west of the Geneva borehole, striking approximately NE–SW and downthrown to the south-east.

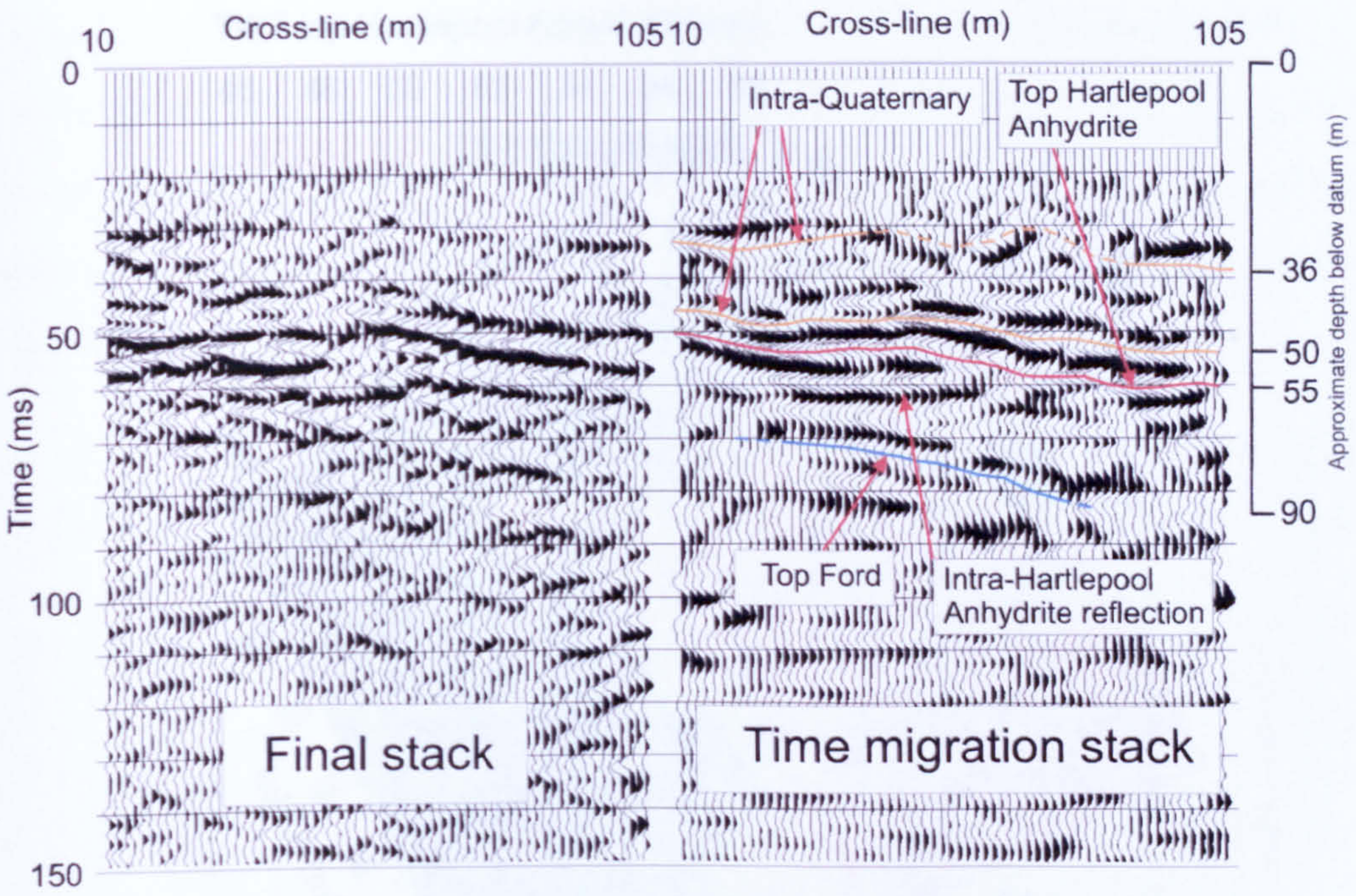

Figure 6.16: Parkside 3D in-line-profile stack and time migrated comparison.
Sections are at 45 m along the in-line axis of the 3D volume. The distance between each cross-line trace is 1.5 m. Sections are displayed with a 200 ms AGC window before being cropped.

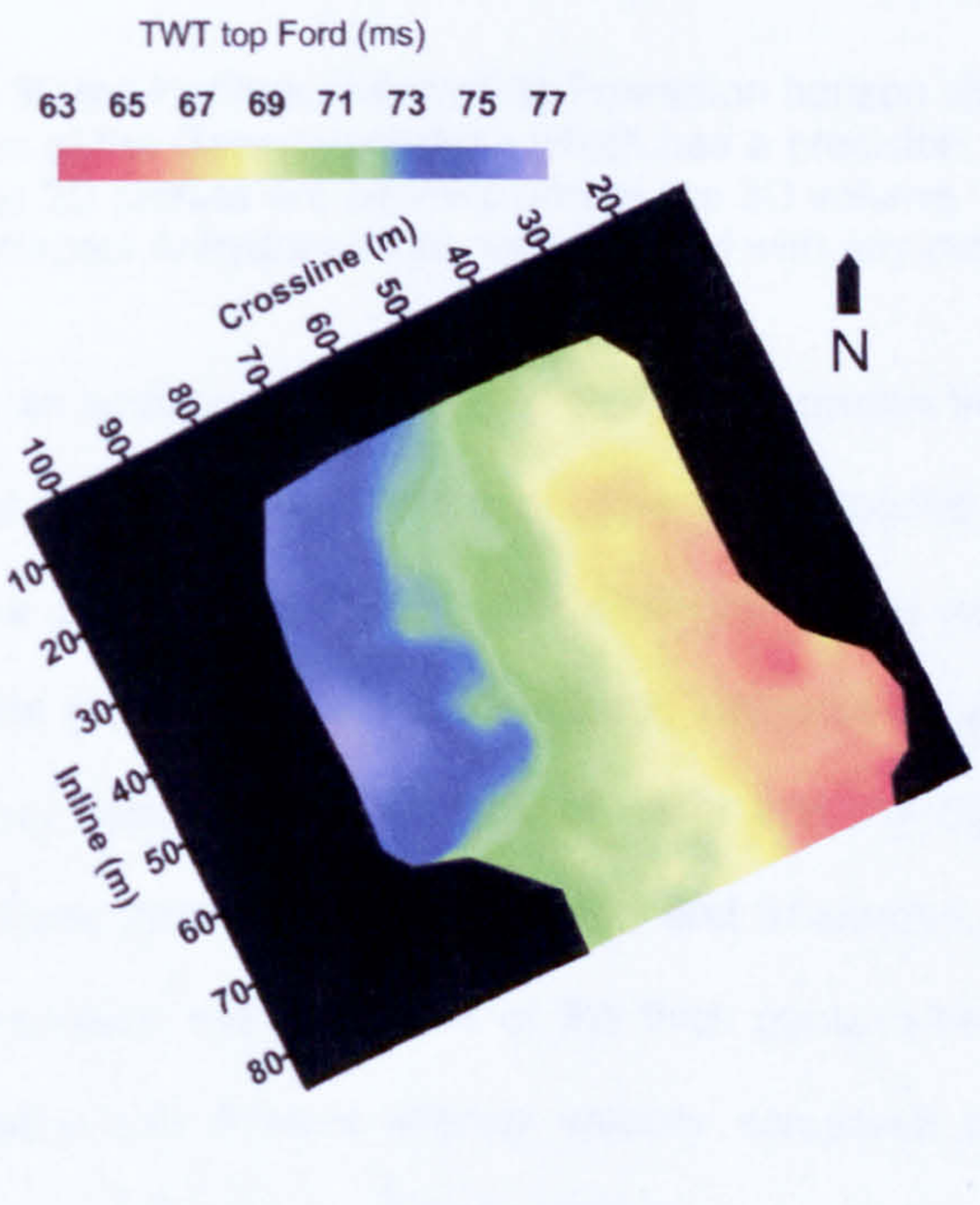

Figure 6.17: Parkside 3D top Ford Formation horizon slice.
The blanked out areas are where the top Ford could not be picked with any certainty.

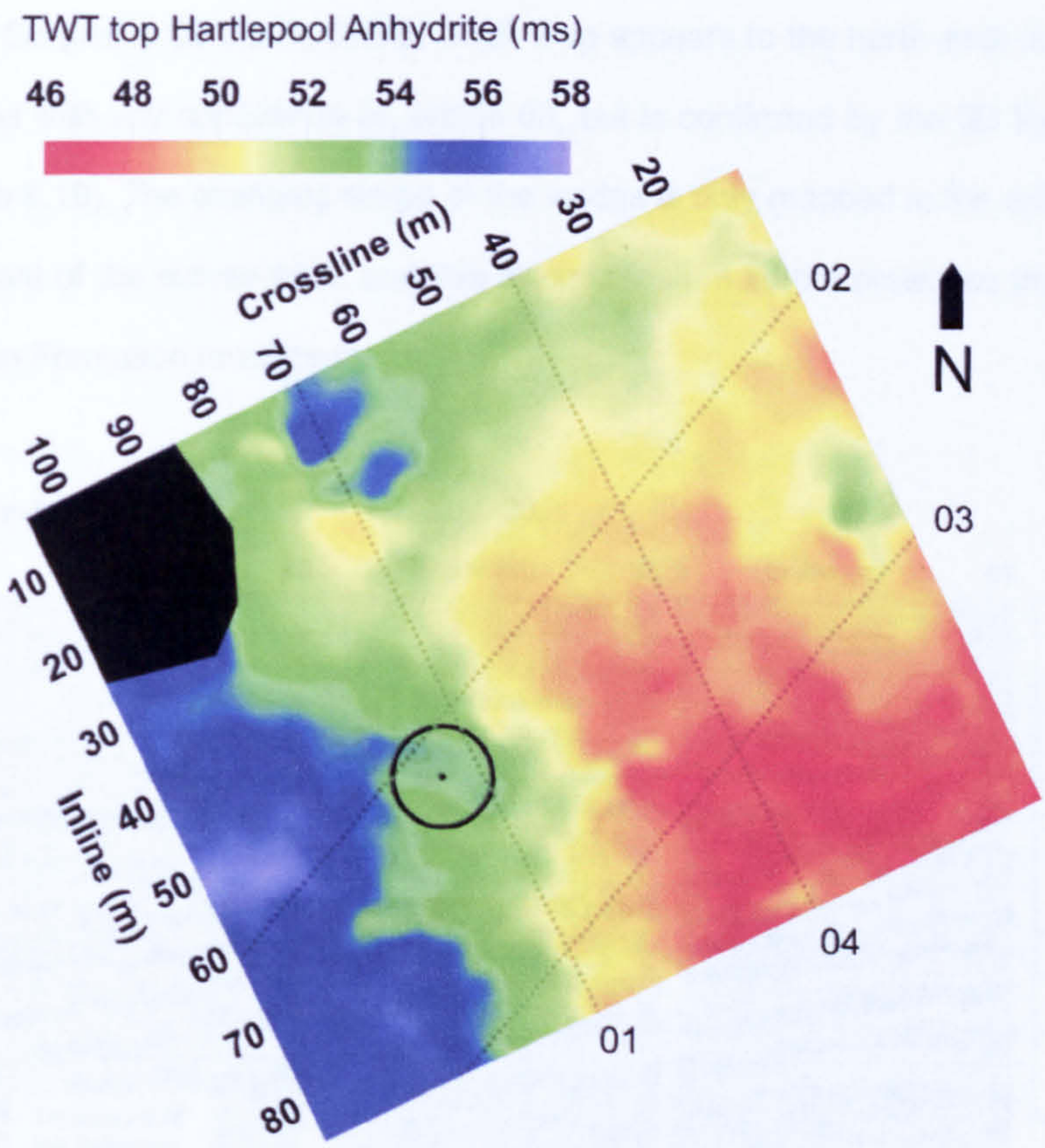

Figure 6.18: Parkside 3D top Hartlepool Anhydrite Formation horizon slice.
Overlaid is the location of the Geneva borehole which has a precision of 10 m given by error circle. The paths of the 2D profiles are overlaid across the 3D volume. The blanked out areas are where the top Hartlepool Anhydrite could not be picked with any certainty.

On profile 04 an additional black loop is observed between the horizons interpreted as the top Ford and top Hartlepool Anhydrite. This is interpreted as the result of the stratification within the gypsum bed. The rugose character of the top Hartlepool Anhydrite Formation is where the gypsum is likely to have been infiltrated by water percolating down through the Quaternary deposits. The addition of water into the calcium sulphate crystal lattice results in a volume increase of 63% (Mossop and Shearman, 1973), resulting in an undulating surface. However, the inner core of the thick gypsum bed could be still intact, having a higher density and P-wave interval velocity compared to mechanically weak, hydrated gypsum at the top of the bed, resulting in an internal reflection event.

On profile 04, an additional thin black loop appears above the top Hartlepool Anhydrite reflection event to the north-north-west of CMP 63 (Figure 6.11). There is a similar

change of seismic character to the north-north-west of CMP 45 on the parallel long profile 01 (Figure 6.13). On profile 02 the additional black loop appears to the north-east of CMP 73. It is not observed with any confidence on profile 03, but is confirmed by the 3D time migrated volume (Figure 6.19). The changing shape of the wedge is only mapped in the extreme north-eastern quadrant of the survey area, and this seismic feature is interpreted as the thickening of the Edlington Formation mudstones.

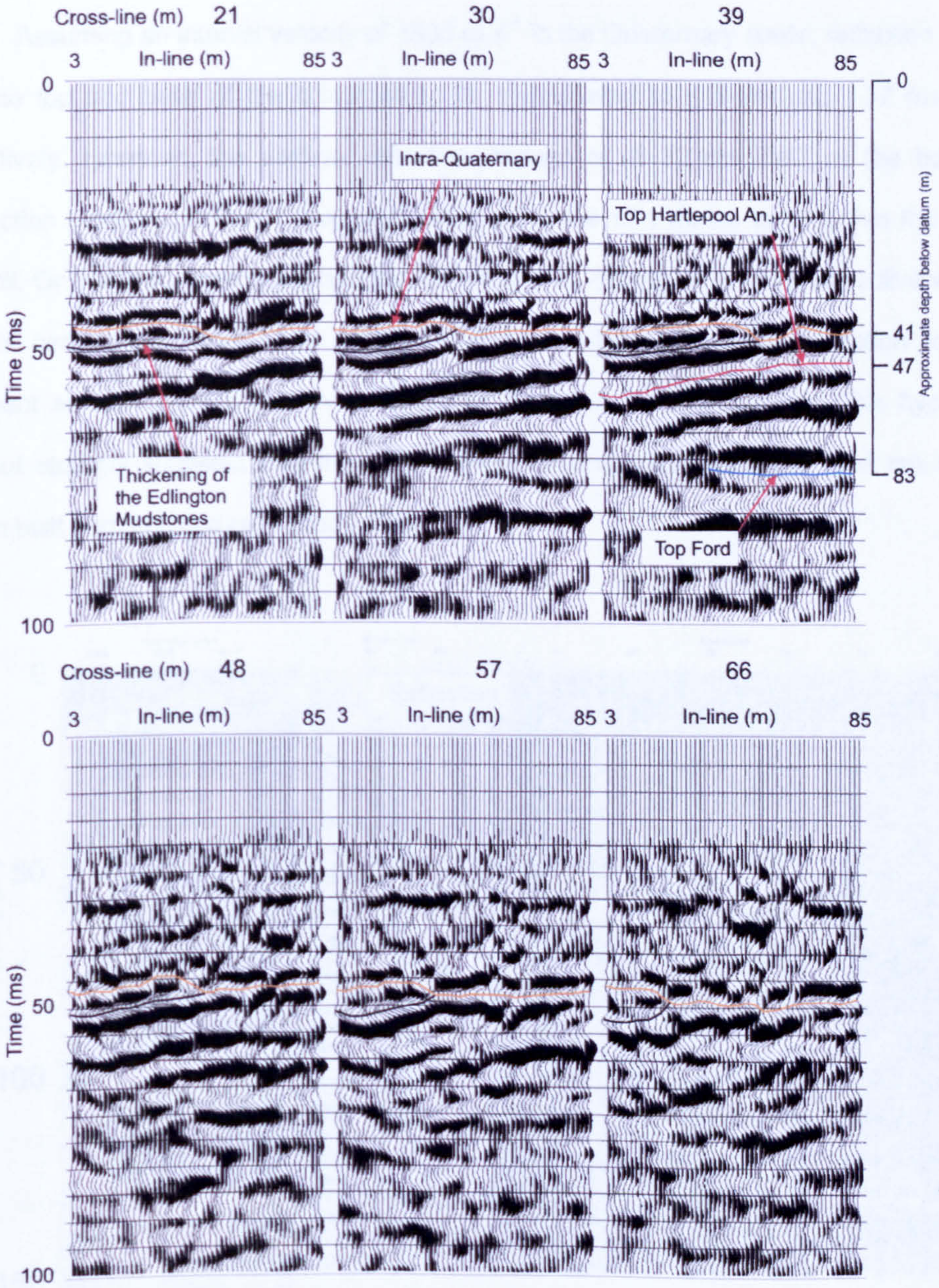

Figure 6.19: Thickness variation of the Edlington Formation over the Parkside 3D volume. Distance between in-line traces is 1.5 m. Sections are displayed with a scalar multiplier.

6.4.2 Shallow intra-Quaternary reflections

In the time migrated stacked sections of the four 2D profiles (Figures 6.11, 6.13, 6.14 and 6.15), there are two shallower reflection events, picked in orange, above the reflection horizon interpreted as the top of the gypsum-rich Hartlepool Anhydrite Formation. These two events must originate within the thick Quaternary deposits, but from comparison with the stratigraphy logged in Geneva borehole (Figure 6.4) it is not obvious which stratigraphic horizons are responsible for them. The upper reflection appears to have a positive reflection coefficient.

Assuming an interval velocity of 1800 m s^{-1} in the Quaternary strata, reflection events from the top and base of the brown stony till should start at ~18 ms and ~37 ms TWT, respectively. However, the shallow reflection horizon is at 32 ms TWT at the borehole intersection point on profile 01, suggesting the presence of a dense layer within the brown stony till. Only a few traces contribute to this event after muting, yet in the interactive velocity analysis centred on CMP 35 in profile 04 (Figure 6.20) the shallow reflection forms a prominent smooth hyperbolic curve starting at 30 ms on the near trace. This hyperbolic moveout strongly suggests that the very shallow reflection event is real, and not a false horizon built from stacked refraction arrivals.

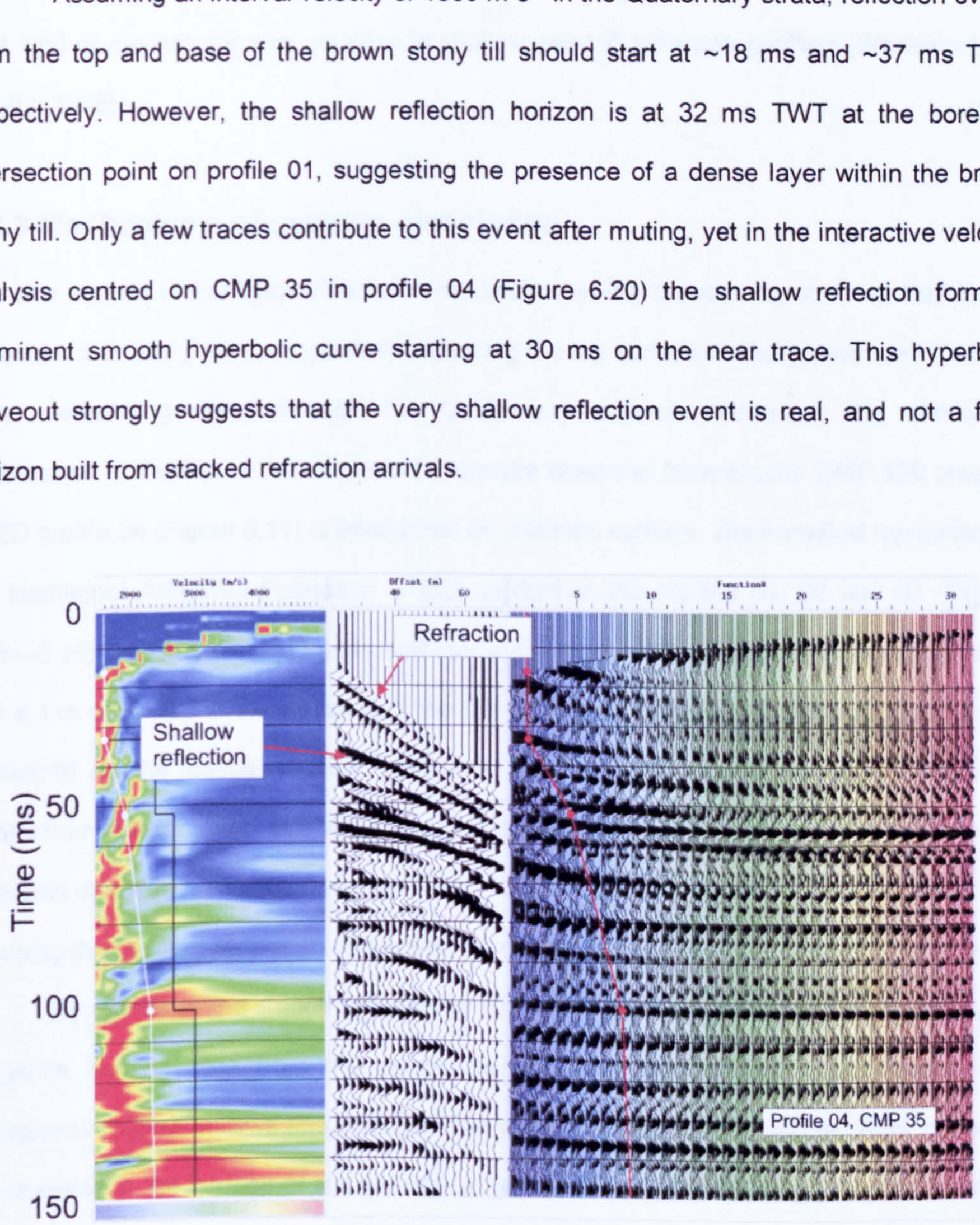

Figure 6.20: Interactive velocity analysis centred at CMP 35 on Parkside profile 04.

The strength and continuity of the black leg at 42 ms TWT in the region of CMP 140 of profile 04 above the undulating top Hartlepool Anhydrite event confirms the presence of the deeper intra-Quaternary reflection rather than a filter side lobe. The time difference between this event and rockhead at the borehole intersection point on profile 01 suggests that this reflection is related to the base of the 6 m sand layer.

At Parkside, the shooting conditions in the near-surface stiff clay enabled enough P-wave energy to be generated to image interfaces with low acoustic impedance contrasts within the Quaternary deposits. Very fine grained soils such as clay are recognised as the best kind of medium for shot coupling in shallow seismic reflection profiling (Bredewout and Goulty, 1986).

6.4.3 Mechanisms of gypsum dissolution

The thin veneer of Edlington Formation mudstones in the Geneva borehole at Parkside is likely to act as leaky aquitard, partially protecting the top surface of the gypsum bed from any water percolating down through the Quaternary deposits. However, the convoluted appearance of the top of the Hartlepool Anhydrite observed from around CMP 120 onwards on 2D profile 04 (Figure 6.11) is interpreted as a karstic surface. The karstified top surface of the Hartlepool Anhydrite Formation is also evident in 2D profiles 01, 02 and 03 (Figures 6.13—6.15). The onset of the karstic surface on the long profiles 01 and 04 does not coincide with a 1 m downstep in the elevation of the ground surface intercepted at the southern end of profiles 01 and 04 (dashed line on Figure 6.1). Also, above the rockhead interface, the intra-Quaternary reflections do not show any disturbance, but are smooth and continuous. The Edlington mudstones may not be present in this area, having been removed by glacial action, exposing the gypsum surface to dissolution from the melt waters of the retreating glaciers.

By differencing a smooth polynomial surface (Figure 6.21) fitted to the top Hartlepool Anhydrite horizon slice from the picked horizon slice itself (Figure 6.18), some large amorphous shallow hollows and a smaller but deeper hollow at 10 m in-line, 70 m cross-line are revealed in the surface of the gypsum (Figure 6.22). Sections through the middle of the 3D time migrated volume in the cross-line direction (Figure 6.19) show the top of the Hartlepool Anhydrite Formation gypsum bed to be approximately planar, with minor

undulations, dipping towards the north-west. In the 3D in-line direction the shape of the surface of the Hartlepool Anhydrite is variable, ranging from approximately planar at 30 m in-line distance (Figure 6.23) to more S-shaped through the borehole location. Associated with the large depressions are changes in character of the reflection from the top surface of the gypsum bed, such as the in-line section at 52 m and 75 m (Figure 6.23).

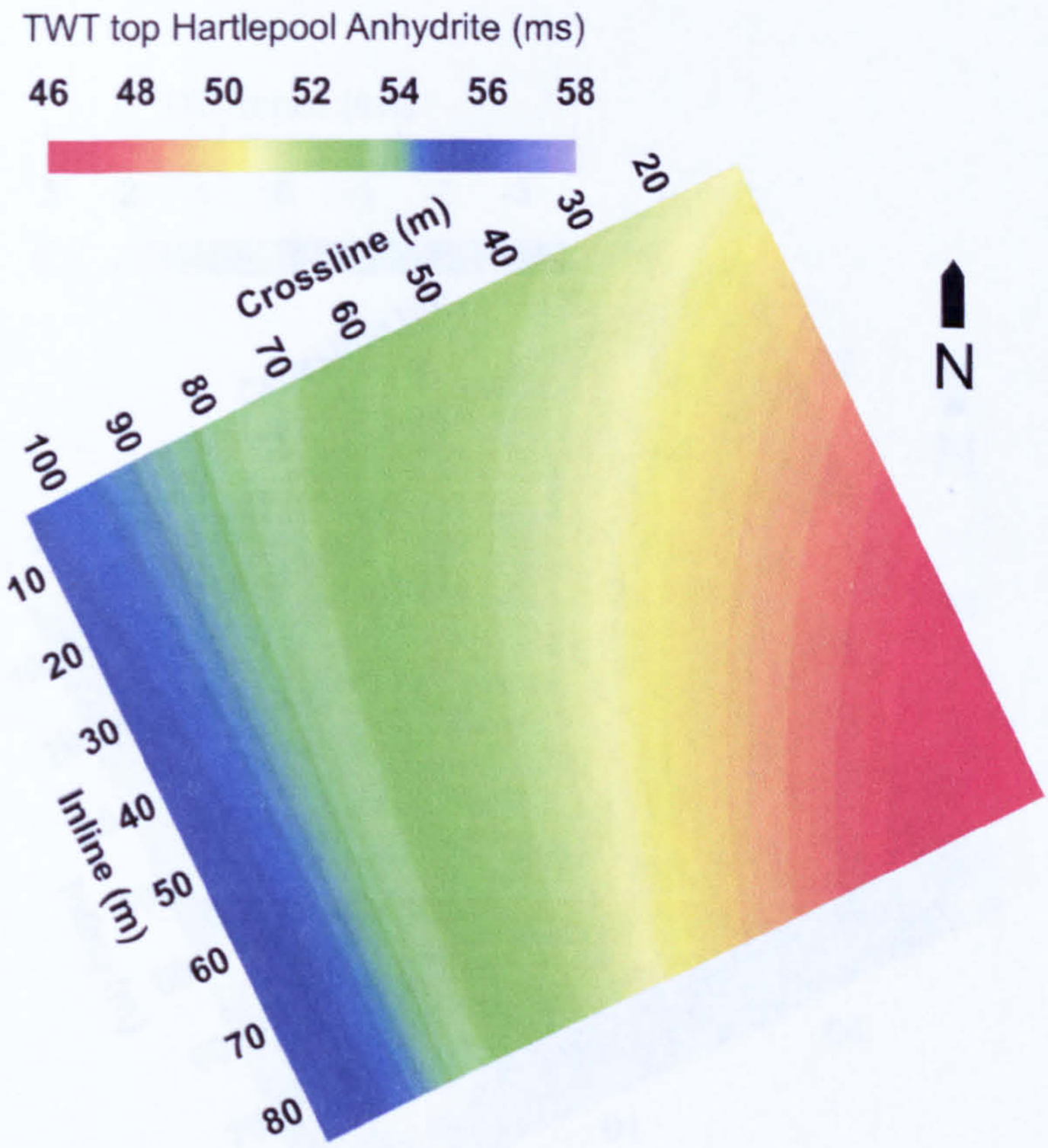

Figure 6.21: Top Hartlepool Anhydrite horizon slice quadratic polynomial regression plot.

Below the Hartlepool Anhydrite Formation is the Ford Limestone artesian aquifer. Water flowing through the aquifer may have dissolved and transported gypsum from the base of the Hartlepool Anhydrite Formation. Potentially, overlying blocks of gypsum may fall into large cavities formed at the base of the thick gypsum. The depression at 70 m cross-line, 10 m in-line correlates with the depression in the top surface of the Hartlepool Anhydrite Formation imaged at CMP 40 profile 01 (Figure 6.13). It is not interpreted as the Hartlepool Anhydrite Formation collapsing into a cavity since the overlying beds of Edlington Mudstones and Quaternary deposits do not exhibit any downward deflection. It is unclear whether the two

larger sub-circular shallow hollows in the south-west of the 3D survey and another at the north-eastern edge are the result of the Hartlepool Anhydrite gypsum falling into an upward migrating cavity. But the two south-western shallow hollows are associated with a weakening of the upper black leg of the top Hartlepool Anhydrite reflection (Figure 6.23), suggesting that gypsum dissolution from water percolating through the Quaternary deposits may have occurred at these locations.

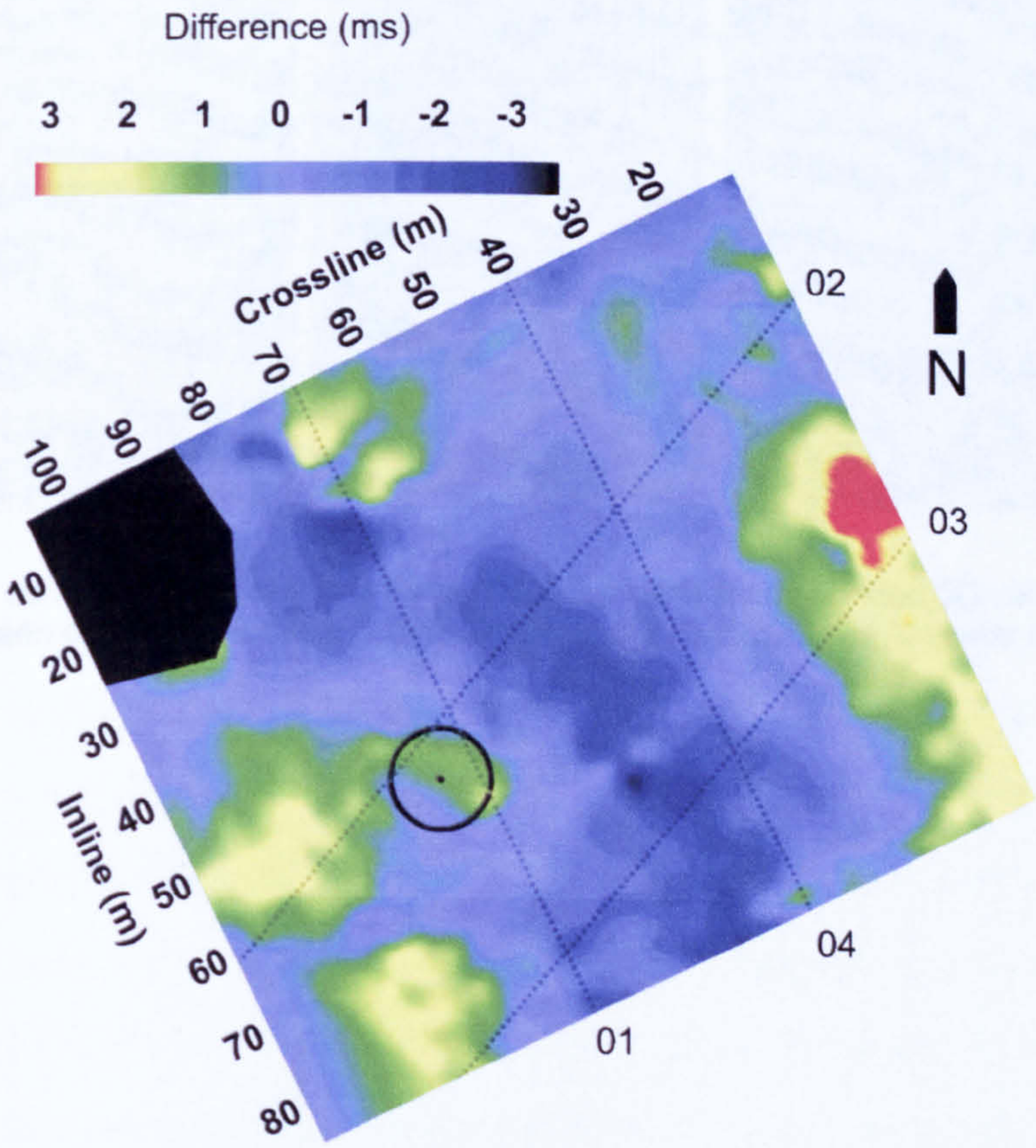

Figure 6.22: Top Hartlepool Anhydrite horizon slice difference plot.

The presence of the 2 m deep cavity logged in the Geneva borehole, plus 4 m of made ground at the surface provides circumstantial evidence that sub-surface gypsum dissolution has caused foundering at the ground surface. No patterns can be discerned within the seismic data to indicate the existence of a network of conduits within the thick Hartlepool Anhydrite Formation.

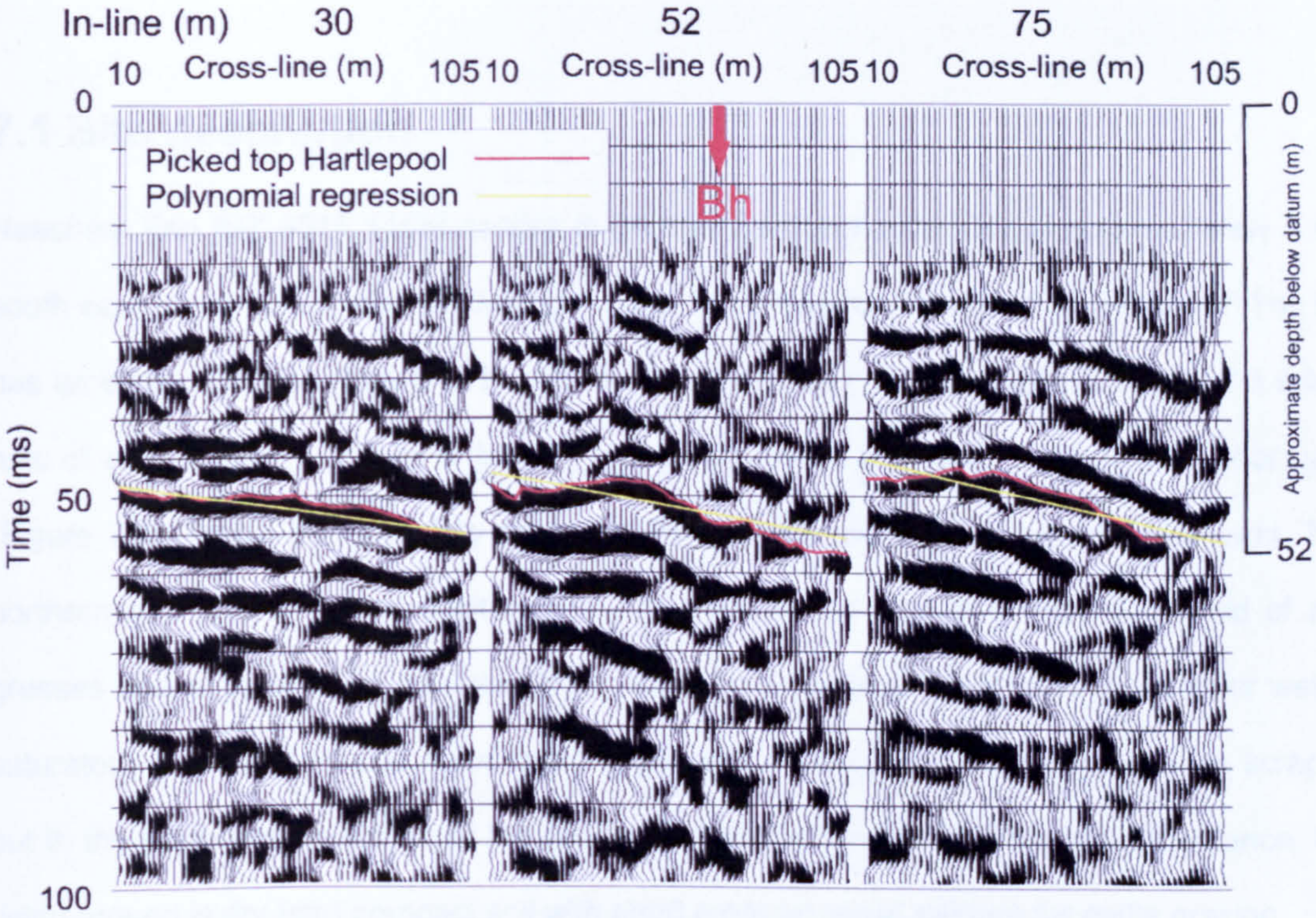

Figure 6.23: A series of in-line sections through the Parkside time migrated 3D volume. Distance between cross-line traces is 1.5 m. Sections are displayed with a scalar multiplier.

7.0 Neasham Fen

7.1 Site description

Neasham Fen [NZ 3315 1155] nestles in gently rolling agricultural land approximately 5 km south-east of the town centre of Darlington and 1 km north of the village of Neasham. The fen has an elliptical shape (Figure 7.1), with a west-east major axis of about 200 m and a minor axis of approximately 150 m in length, and is located at the centre of a much wider bowl (Figure 7.2). Inside the boundary fence the fen can be roughly divided into two parts. The northern and central part is sheltered by trees where the ground surface is devoid of any grasses and is covered by tree leaf litter. The remaining ground consists of damp or water-saturated, peaty ground populated by long grasses. A large shallow lake has been scraped out in the north-west quadrant of the fen by the landowner. Outside the boundary fence, the rising ground is dry hard compact soil with short cropped grass pasture for cattle grazing.

Shallow coring (Figure 7.3) shows that in the centre of Neasham Fen the uppermost 2 m of the sub-surface is peat-dominated, underlain by 4 m of fine detritus material, and then 6 m of fine pink clay (Bartley et al., 1976). Boulder Clay is logged at 14 m below ground surface, shallowing to a depth of 8 m towards the boundary of the fen, and the Boulder Clay probably constitutes the ground level material before subsidence. The layers of material within Neasham Fen provide valuable evidence of the vegetation history for the lowlands of north-east England; hence Neasham Fen is classified by Natural England as a Site of Special Scientific Interest (SSSI).

The Neasham borehole (Figure 7.4), 300 m south-east of the fen, logged a 6 m thick bed of gypsum, the Billingham Anhydrite Formation, with its top surface at 52 m below the ground surface. A second massive deposit of gypsum, the 45 m thick the Hartlepool Anhydrite Formation, has its top surface at 80 m depth. The fen is located between two normal faults shown as downthrown to the north on the BGS map (Figure 7.5). Six other depressions to the north and east of Neasham Fen are marked on the geological map of the superficial deposits (Figure 7.6).

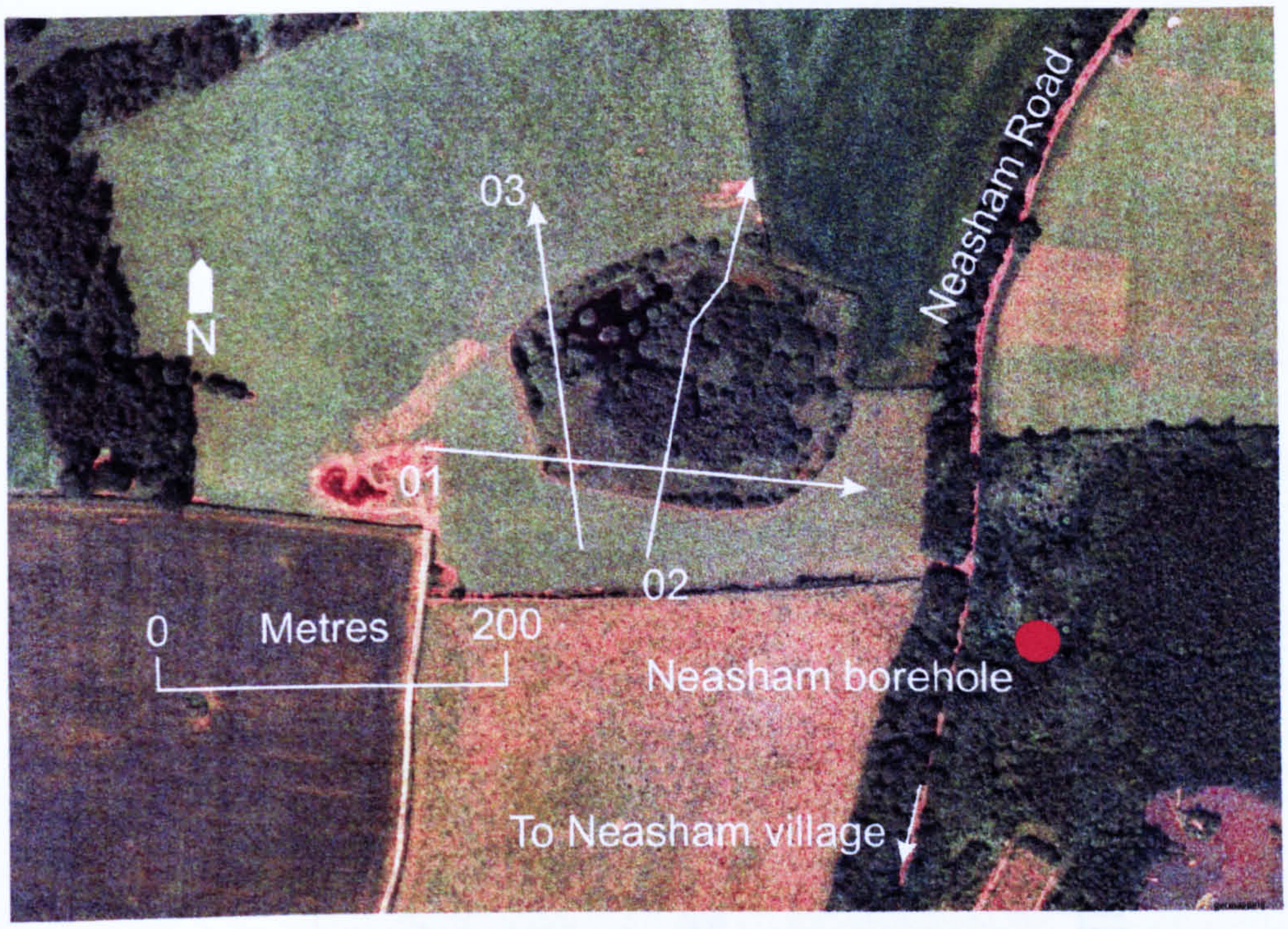

Figure 7.1: Aerial photograph taken in 2000 of the Neasham Fen survey site.

Figure 7.2: Panoramic view to the north-west across Neasham Fen.

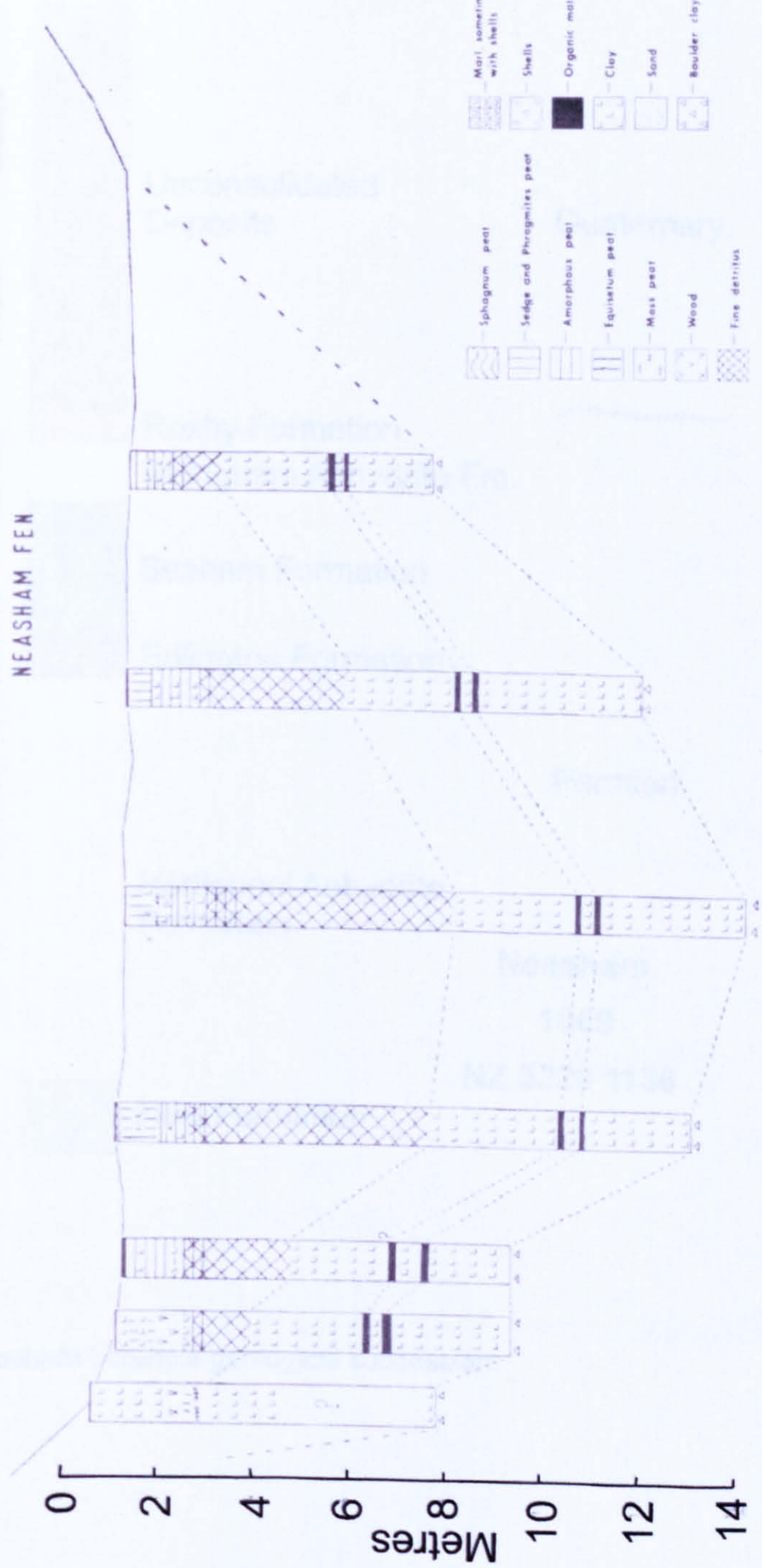

Figure 7.3: Shallow corings across Neasham Fen.
Modified from Bartley et al. (1976).

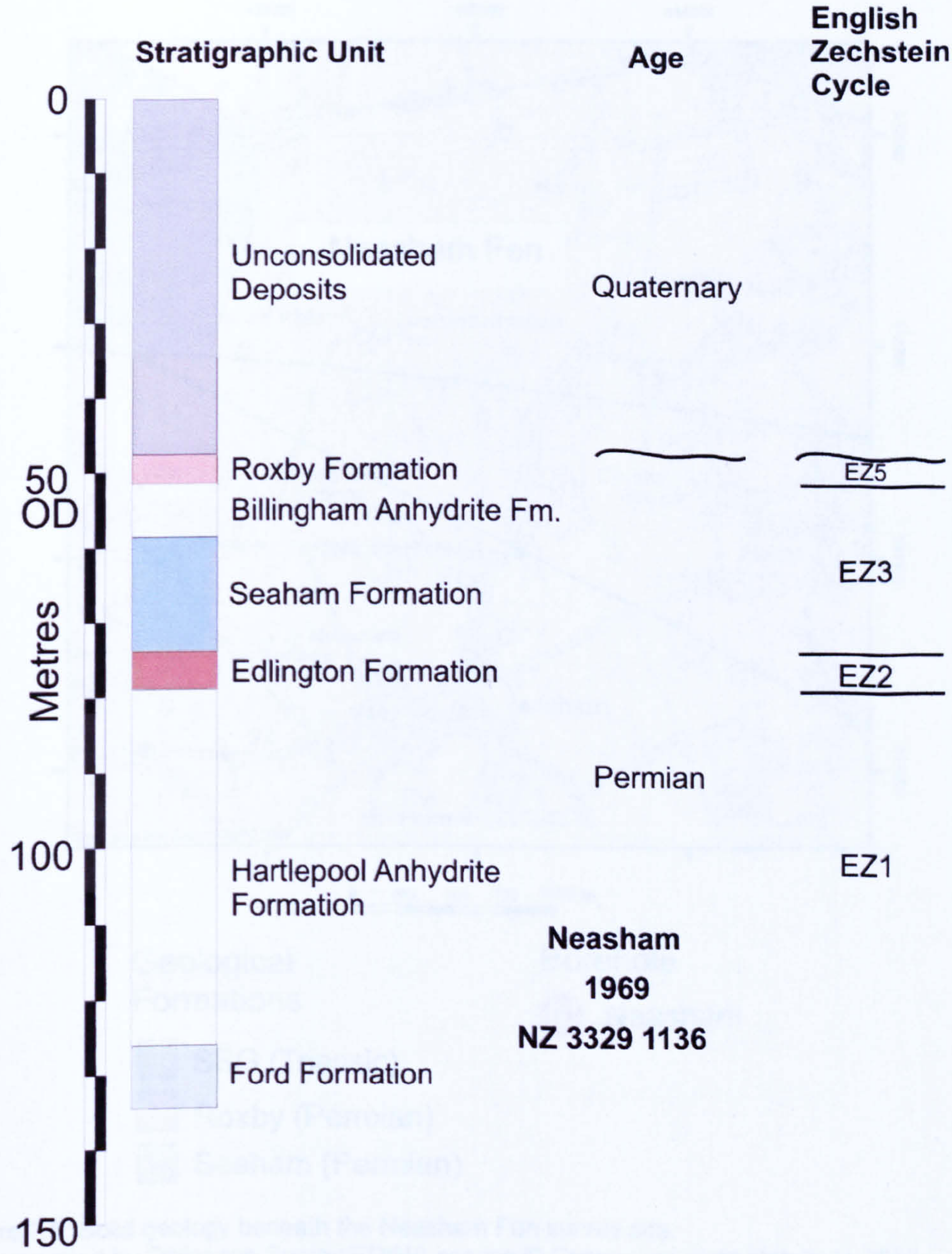

Figure 7.4: Neasham borehole geological succession.

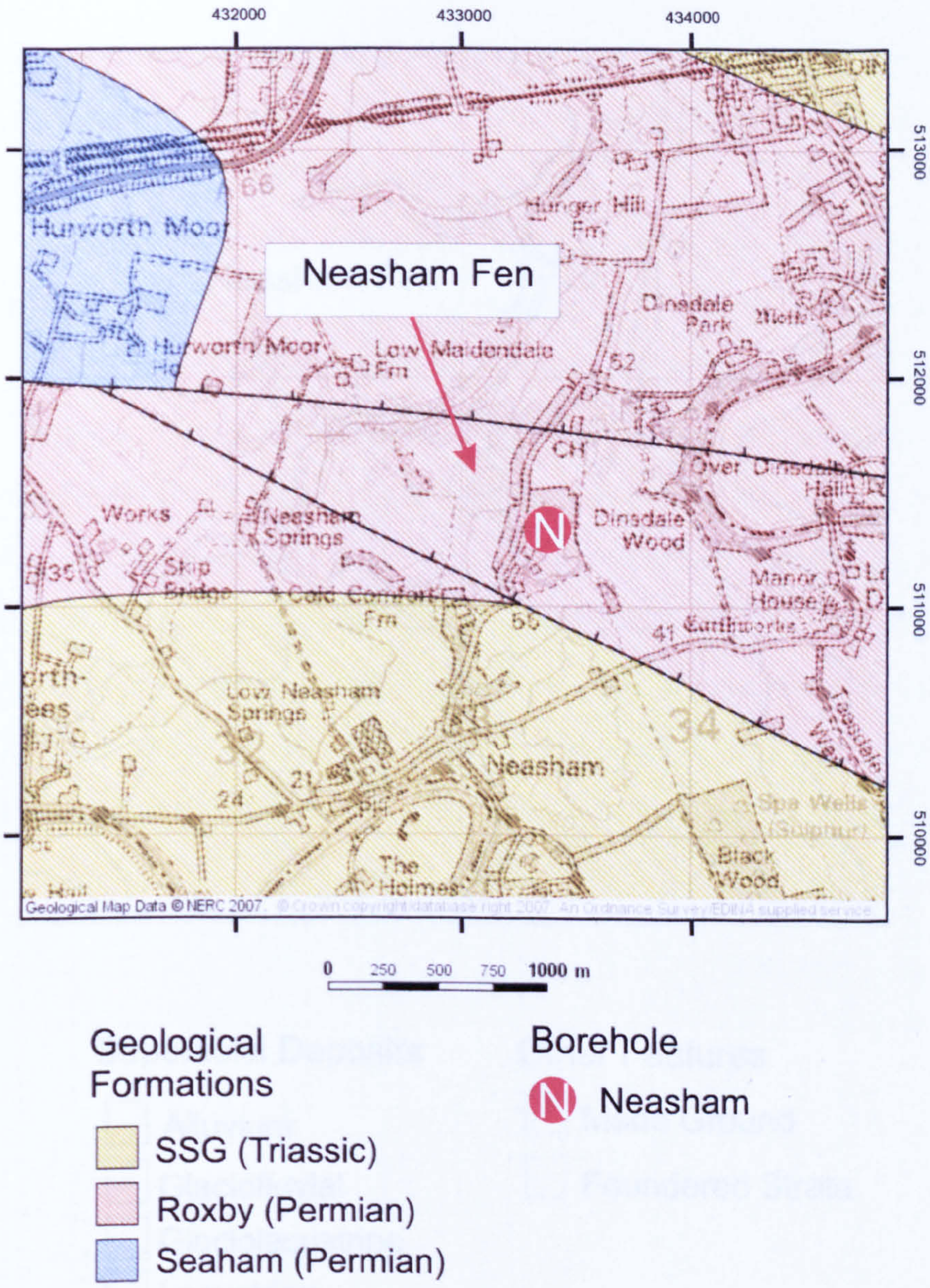

Figure 7.5: Solid geology beneath the Neasham Fen survey site.
Data supplied by Ordnance Survey/EDINA service © Crown Copyright Database 2007.

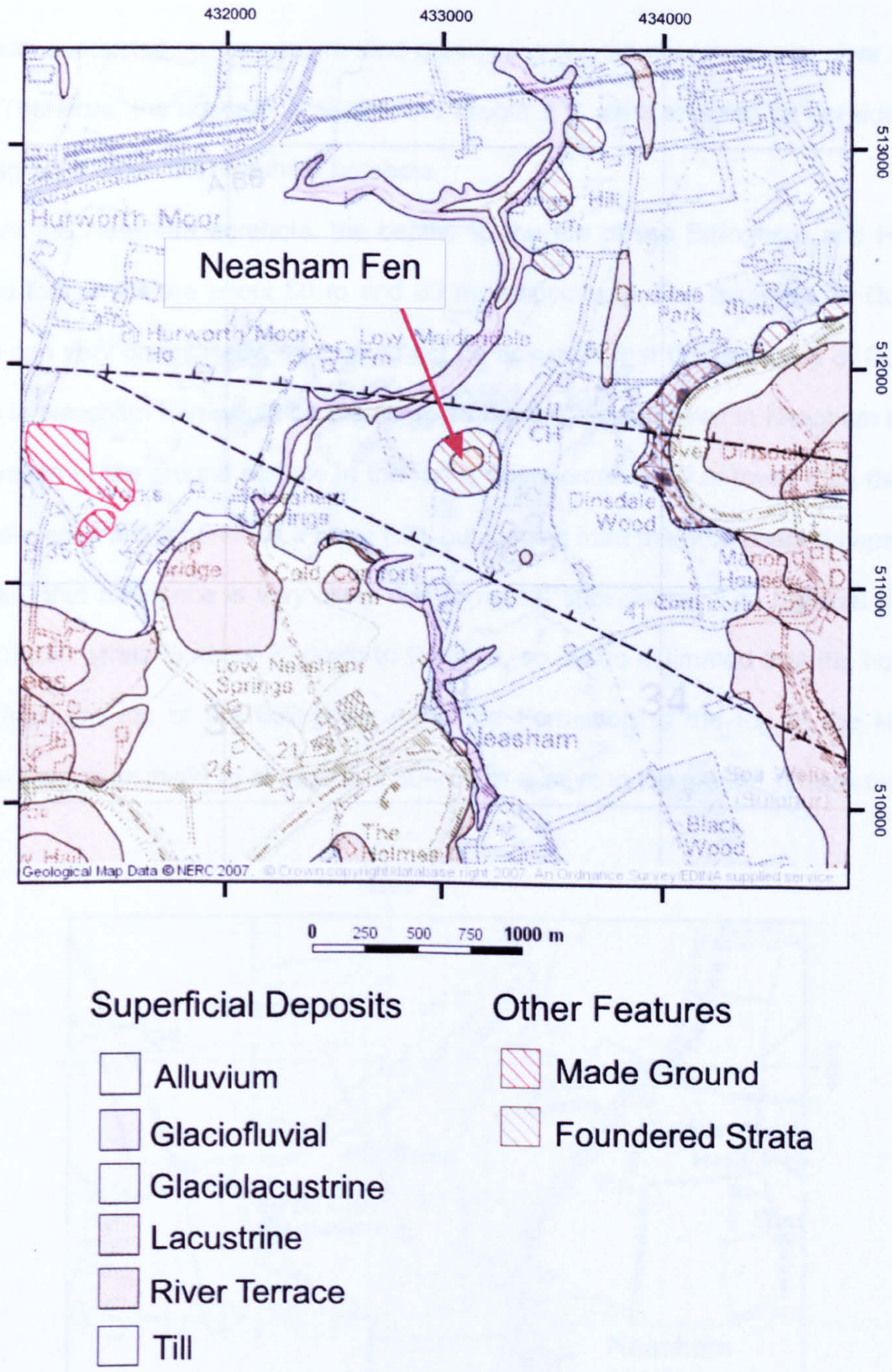

Figure 7.6: Superficial geology at the Neasham Fen survey site.
Data supplied by Ordnance Survey/EDINA service © Crown Copyright Database 2007.

7.2 Acquisition

Wave tests conducted on the pasture land outside the fen did not reveal any clear reflection events. Therefore, the acquisition parameters (Table 7.1) were selected by consideration of the stratigraphy within the Neasham borehole.

At the Neasham borehole, the depths to the top of the Billingham and Hartlepool Anhydrite formations are about 50 m and 80 m, respectively. The thickness of Quaternary deposits can vary dramatically, so it could not be assumed that the thickness of Quaternary deposits in Neasham Fen would be the same as the thickness proved in Neasham borehole. The elevation of the ground surface in the fen is approximately 10 m lower than the ground surface elevation at the borehole (Figure 7.7), but judging from the bowl-shaped depression in the terrain, that difference is very likely due to recent subsidence. The regional dip of the Permo-Triassic strata is about 3° down to the east, so it was estimated that the horizons of interest from the top of the Billingham Anhydrite Formation to the top of the Hartlepool Anhydrite Formation might lie at depths of 30—60 m relative to the ground surface in the fen.

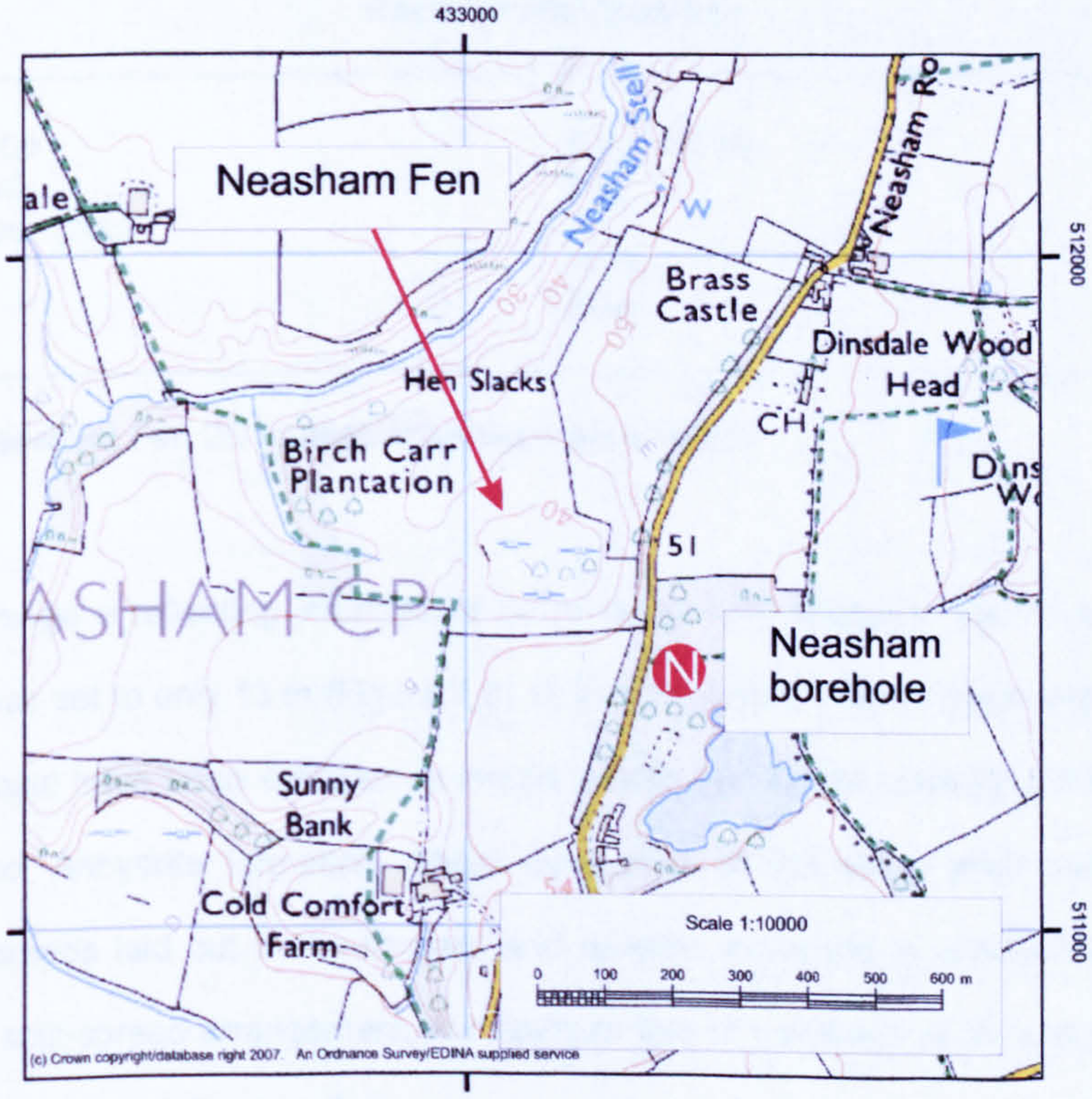

Figure 7.7: Ordnance Survey map of Neasham Fen.
Data supplied by Ordnance Survey/EDINA service © Crown Copyright Database 2007.

Instrument Parameters	
Recording instrument	Geometrics SmartSeis S12
Format	SEG-2
Data channels	24
Pre A/D converter low cut filter	10 Hz
Pre A/D converter high cut filter	500 Hz
Sample rate	0.5 ms
Record length	512 ms
Delay	0 ms

Source Parameters	
Source type	Buffalo gun, 5 g black powder blanks
Shot interval	2 m
Shot depth	1 m
Shot in-line skid relative to geophones	1 m
Shot cross-line offset relative to geophones	2 m

Off-end shooting arrangement, forward and reverse shots to simulate symmetric split-spread.
All shot holes tamped with water before firing.

Receiver Parameters	
Geophone type	SM-7/30 Hz
Group interval	2 m
Geophones per group	1
Near-offset	13 m
Far-offset	59 m

Table 7.1: Neasham Fen 2D profiles acquisition parameters.

To image a reflecting interface at 30 m depth with adequate fold of coverage, the near-offset was set to only 13 m (Figure 7.8). A 2 m geophone interval gave a far offset of 59 m, which should have been sufficient to image a reflection signal originating from the top of the Hartlepool Anhydrite formation. Shots were fired at the same shot point twice into geophone spreads laid out in the forward and reverse directions to simulate a 48-channel symmetrical split-spread arrangement. A maximum fold of coverage of 24 was possible with the shot point interval defined as 2 m.

Profile 01 was the longest 2D profile, and passed through the more open part of the fen without tree cover (Figure 7.1). Profile 02 bisected the fen from south to north, with the dog-leg in the middle of the profile a consequence of navigating around a dense thicket. The shorter profile 03 passed across boggy ground skirting the western edge of the man-made pond. All three profiles began and terminated in the surrounding pasture.

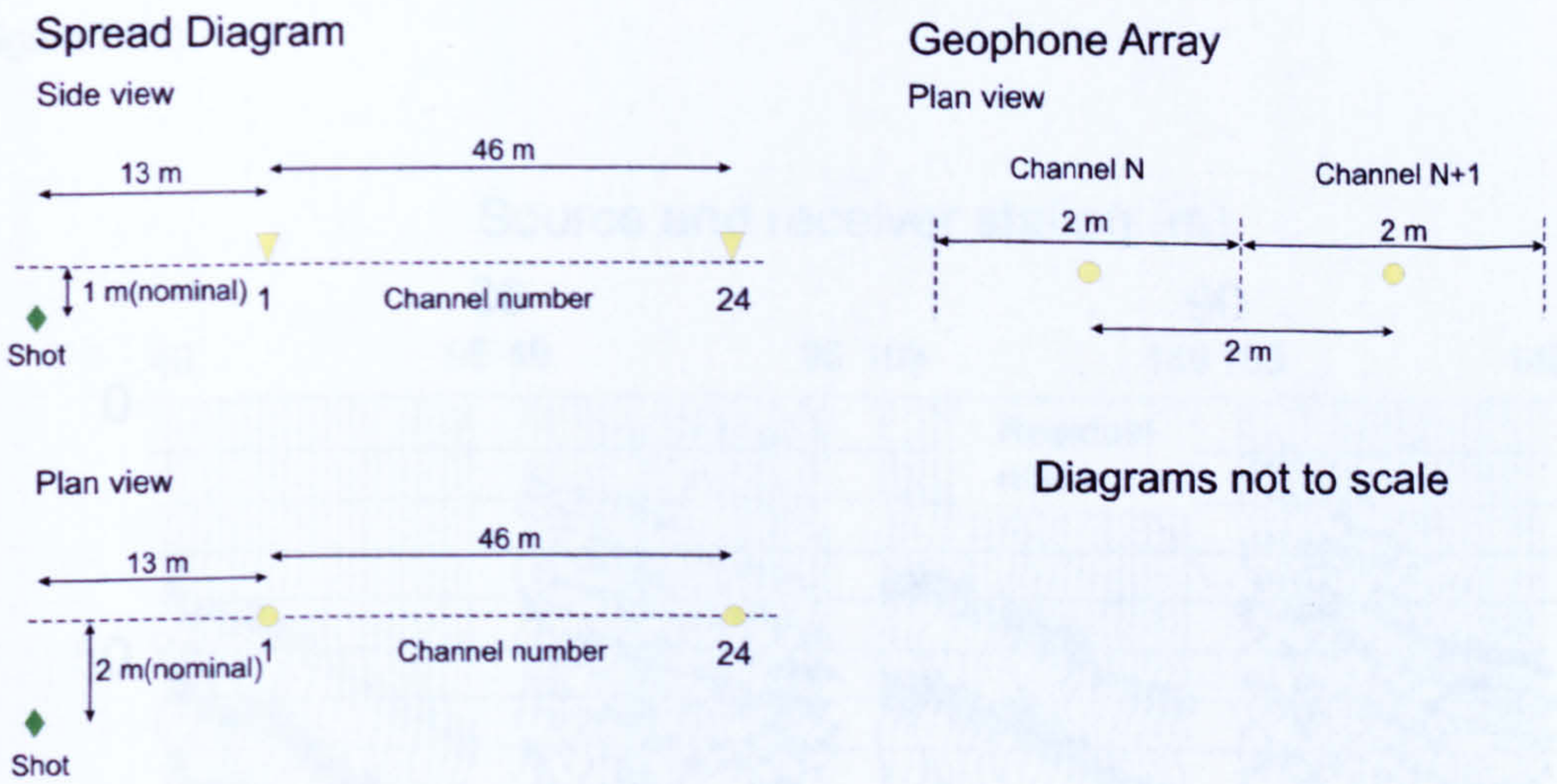

Figure 7.8: Neasham Fen 2D seismic profiles shooting template.

7.3 Processing

The peaty shooting conditions at Neasham Fen were significantly different from the alluvial soils encountered at Hell Kettles and Parkside. Raw shot records extracted from profile 03 are dominated by high-amplitude low-frequency reverberations (Figure 7.9). Suppression of the reverberations by simple bandpass filtering reveals some very weak reflection energy that is only visible on the far offsets after applying a gain function. The near-traces are masked by a combination of air-wave and remnant ground roll, whilst the mid-traces are often devoid of any type of signal.

On stacking, the reflection events are marred by the chequerboard effect of the high-energy ground roll (Figure 7.10, upper panel). The shot records were balanced individually with a sliding 100 ms AGC which suppressed the shot-generated noise (Figure 7.10, lower panel). Because reflection energy only accounts a small proportion of the energy on each shot record, the more sophisticated statistical approach of a surface-consistent amplitude

adjustment was not justifiable. However, the more brutal approach to shot gather balancing meant that no additional *f-x* deconvolution filtering was necessary to damp down remnant noise content.

Zero-phase spiking deconvolution appeared to give marginally better results on the ensembles of traces in CMP gathers, rather than on shot gathers, and two passes of surface-consistent residual statics were also computed in the Neaham Fen processing sequence (Figure 7.11).

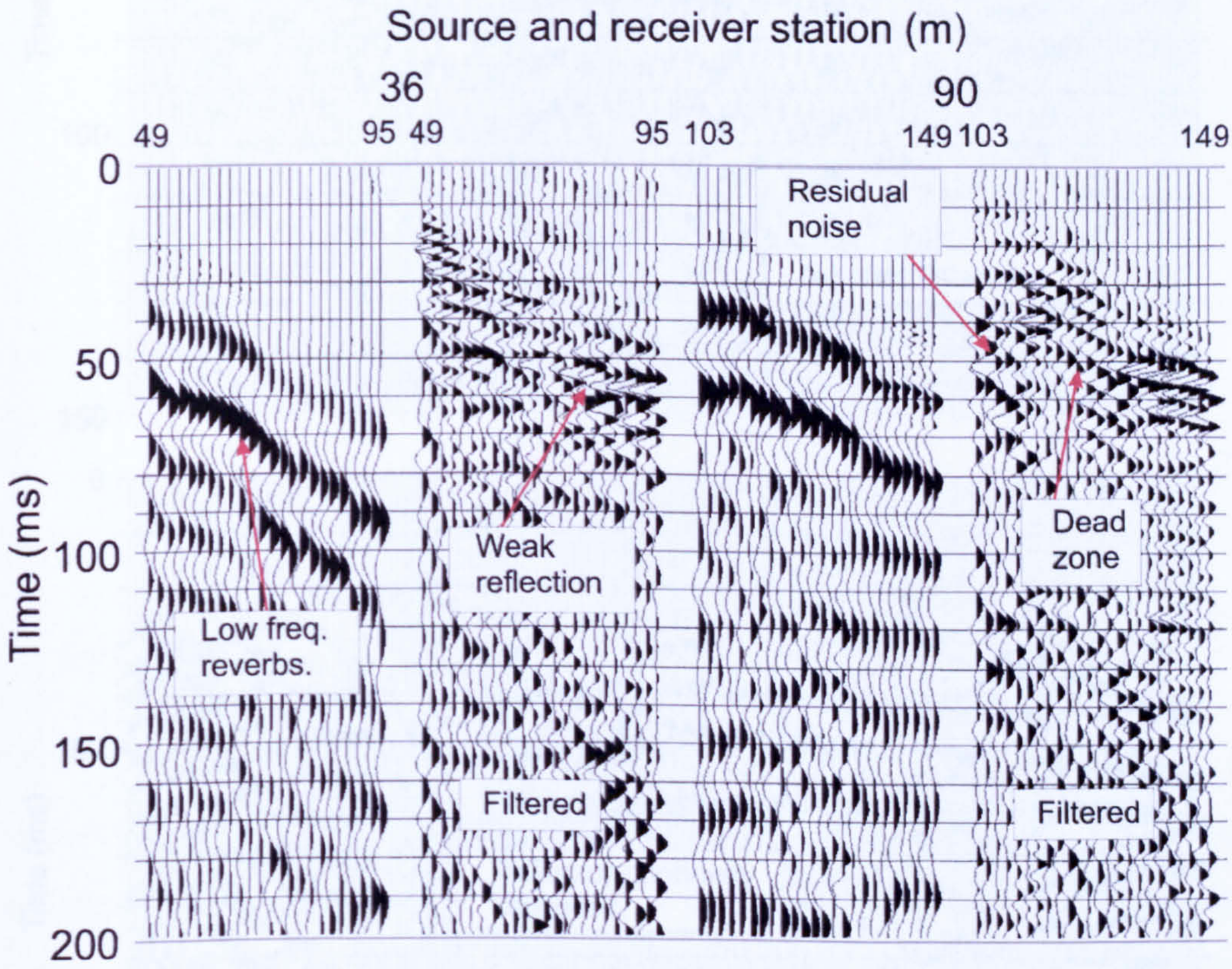

Figure 7.9: Raw and bandpass filtered shots from Neasham Fen profile 03.
Data are scaled with a 100 ms AGC sliding window before being cropped.

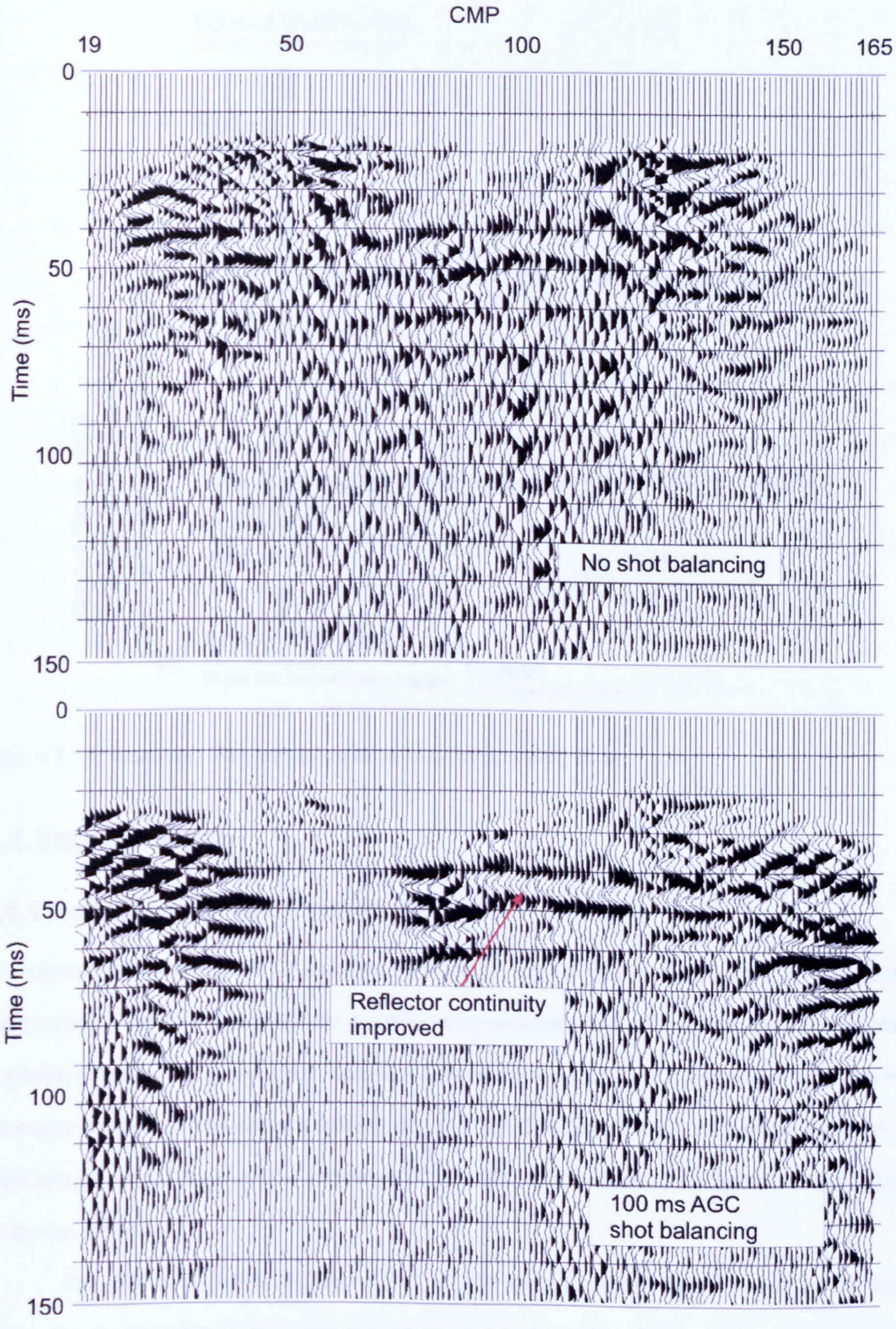

Figure 7.10: The effect of AGC shot balancing on the Neasham Fen data.
Data are displayed with a scalar multiplier.

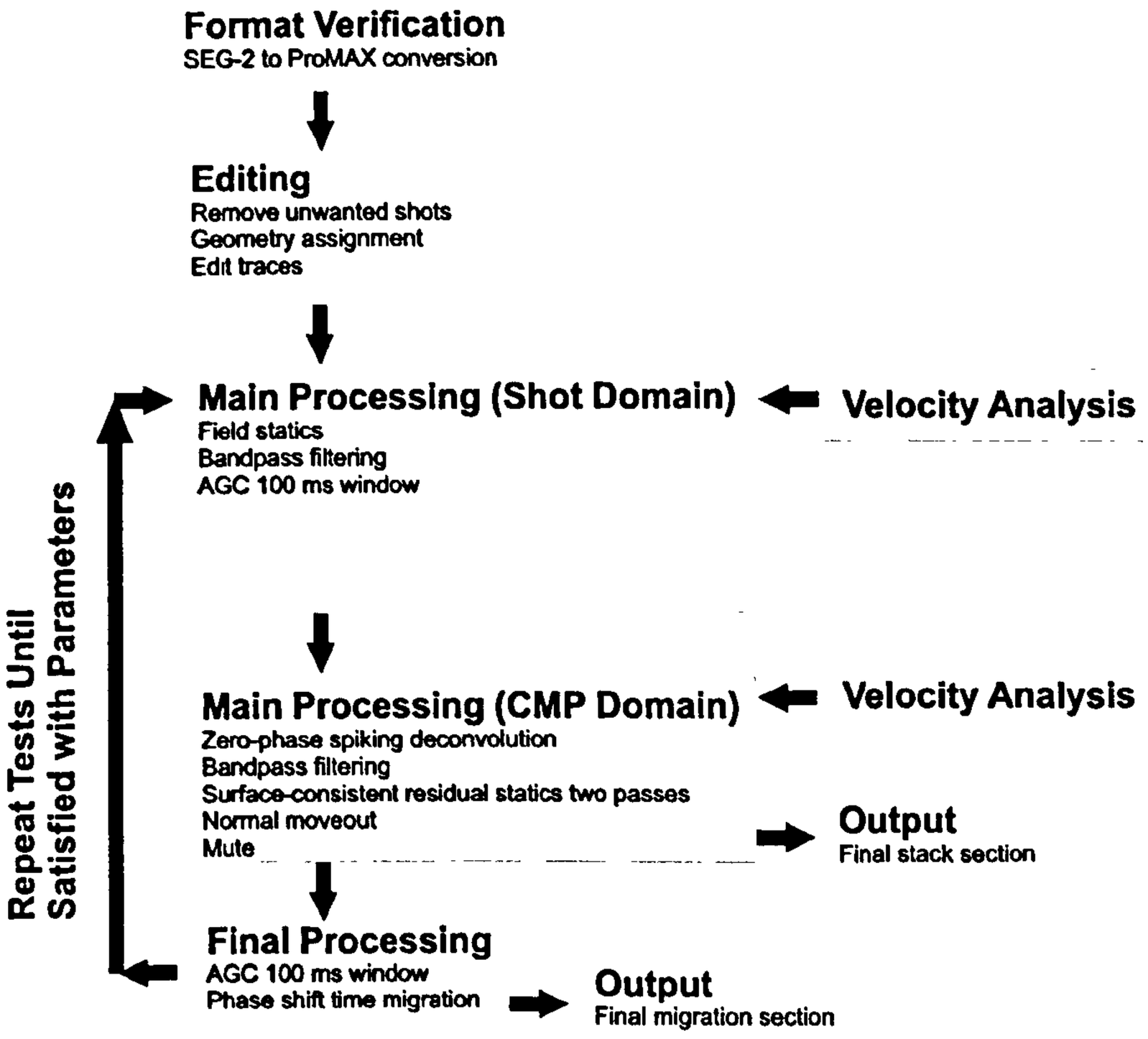

Figure 7.11: Neasham Fen survey seismic data processing flow.

7.4 Interpretation

7.4.1 Negative results on profile 02

The second panel of Figure 7.12 shows the seismic signal from a shot fired within the outer fen grasses. This shot was fired into a spread of geophones laid southwards towards the start of profile (Figure 7.1), geophones placed at receiver stations 1 m to 35 m are outside the fen boundary coupled on the upward sloping dry pasture. The first breaks are easily picked on all channels when displayed with a simple AGC function, and a possible reflection event occurs on the far offsets.

The first shot gather in Figure 7.12 is the seismic signal from a saluting cartridge detonated at a position just inside the southern fen boundary fence line in shot coupling conditions similar to those for the shot gather in panel two. The recording geophones for this shot were aligned towards the centre of Neasham Fen. Sharp first breaks are visible from the near-trace geophone through to the receiver station at 59 m. On the far-offset channels, all

the refracted energy completely disappears from the seismic record and the first identifiable shot-generated seismic signal comprises reverberations. The change in signal character coincides with the change of vegetation from long grasses to tree cover.

The final shot record, panel three in Figure 7.12, shows seismic data from a shot fired under the tree cover into a spread of receivers where the last geophone is only few metres from the southern fen boundary fence. The air-wave is prominent along with low-frequency reverberations; however, no refracted headwave arrivals are visible, even on the geophones beyond the tree line in the fen grasses.

No high-frequency refracted headwave arrivals arising from the water table are detected on receivers placed under the tree cover at Neasham Fen, regardless of the position of the shotpoint. No sub-surface geologic detail is imaged along profile 02 due to the complete absence of any useful seismic signal, which is likely to be due to the loss of high-frequency energy by friction as the seismic waves passed through the weakly bonded aerated leaf litter and peat above the water table.

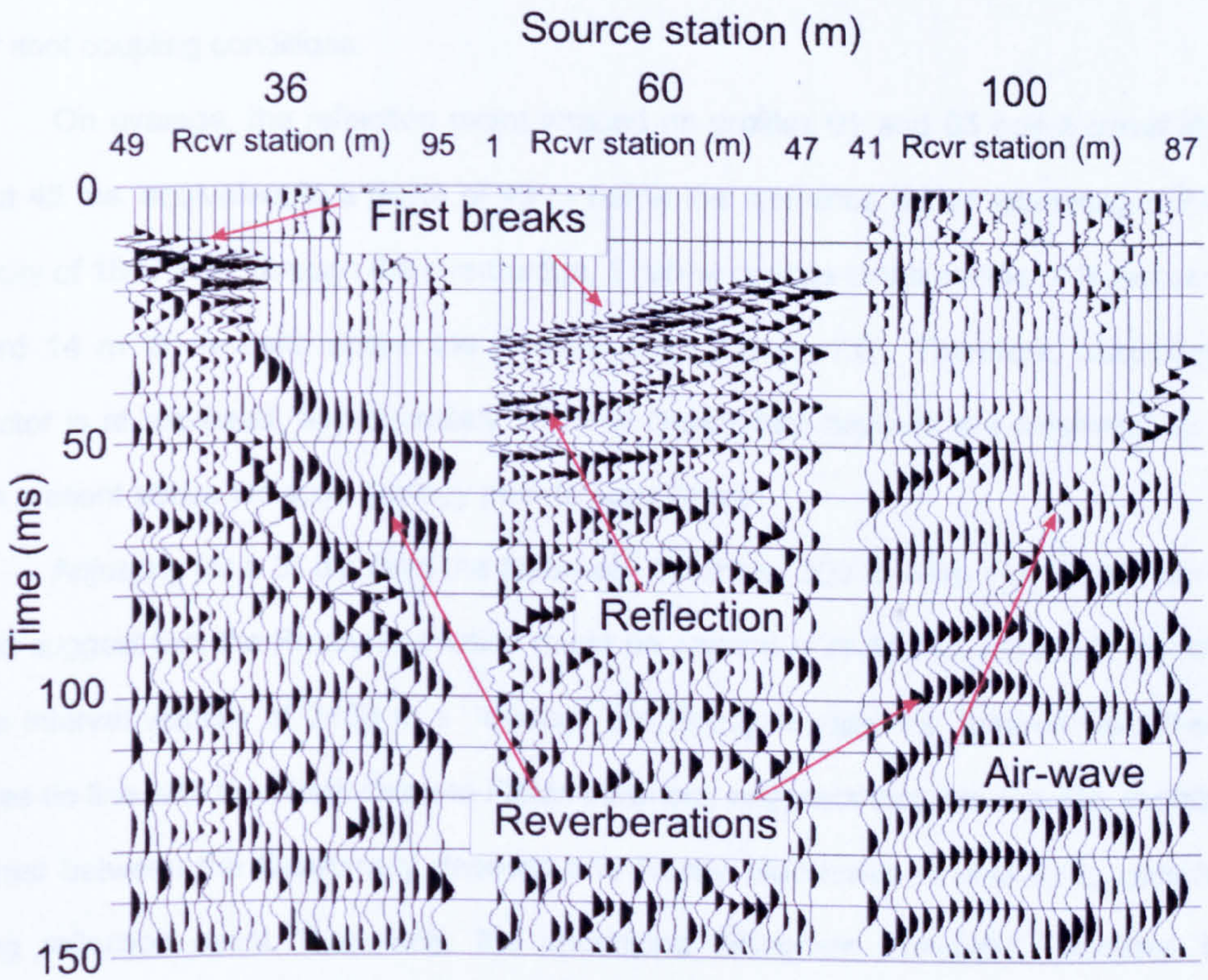

Figure 7.12: Raw shots from Neasham Fen profile 02.
The seismic data have been scaled with a 100 ms AGC sliding window before being cropped.

7.4.2 Foundered geology

Profiles 01 and 03 were acquired in challenging peaty shot coupling conditions. However, useful seismic energy is extracted from these datasets by data digital processing, each revealing a single reflection event.

On the final migrated section of profile 03 (Figure 7.13) the single reflection horizon is imaged between 40 ms and 50 ms dipping gently towards the north. The character of the reflection is a black-white-black signal with a lumpy variable-amplitude along the profile, and between CMP 60 and CMP 75 it has all but disappeared. At CMP 138 the reflection event is interpreted as having dropped down by 10 ms, or 9 m assuming a P-wave interval velocity of 1800 m s^{-1} for the overlying strata. The break in the reflection event is coincident with the fen boundary at the north end of the profile.

Around the intersection point with profile 03 on the perpendicular profile 01 (Figure 7.14) the reflection horizon has a similar character to that observed on profile 03. On the western half of profile 01, the character of the reflection is very disjointed and cannot be traced with confidence. Outside the fen boundary no useful signal was observed due to the poor shot coupling conditions.

On average, the reflection event imaged on profiles 01 and 03 has a travel time of about 45 ms, equivalent to a depth of 40 m below the reference datum assuming a P-wave velocity of 1800 m s^{-1} through the overburden. Shallow corings in the middle of Neasham Fen record 14 m of deposits above the Boulder Clay (Figure 7.3). Therefore, assuming the reflector is at rockhead, approximately 25 m of Quaternary deposits are estimated to have been present above the solid geology prior to subsidence.

Adjusting for a 3° dip from the Neasham borehole, 300 m away from Neasham Fen, would suggest that the Roxby Formation might be present at rockhead. However, the low P-wave interval velocity of 2100 m s^{-1} through the Roxby Mudstones, inferred from the Hell Kettles tie line with the North Oxen-le-Fields borehole, suggests that the acoustic impedance contrast between the Quaternary deposits and Roxby Mudstones is unlikely to generate a strong reflection event. Potentially, the underlying Billingham Anhydrite Formation could provide a reflecting interface, but it is likely that the majority of this gypsum bed would have been washed away during the subsidence process. Therefore, the top surface of the Seaham

Formation limestone is interpreted as the most likely cause of the reflection imaged in profiles 01 and 03. Along profile 01 the reflection event shows a gentle dip eastwards, towards the borehole in agreement with the local geology, but less than the 7° required between Neaham Fen and Neasham borehole for the Seaham Limestone interpretation. However, the disjointed appearance of the limestone imaged is the result of foundering that may have altered the local geological dip in the vicinity of Neasham Fen.

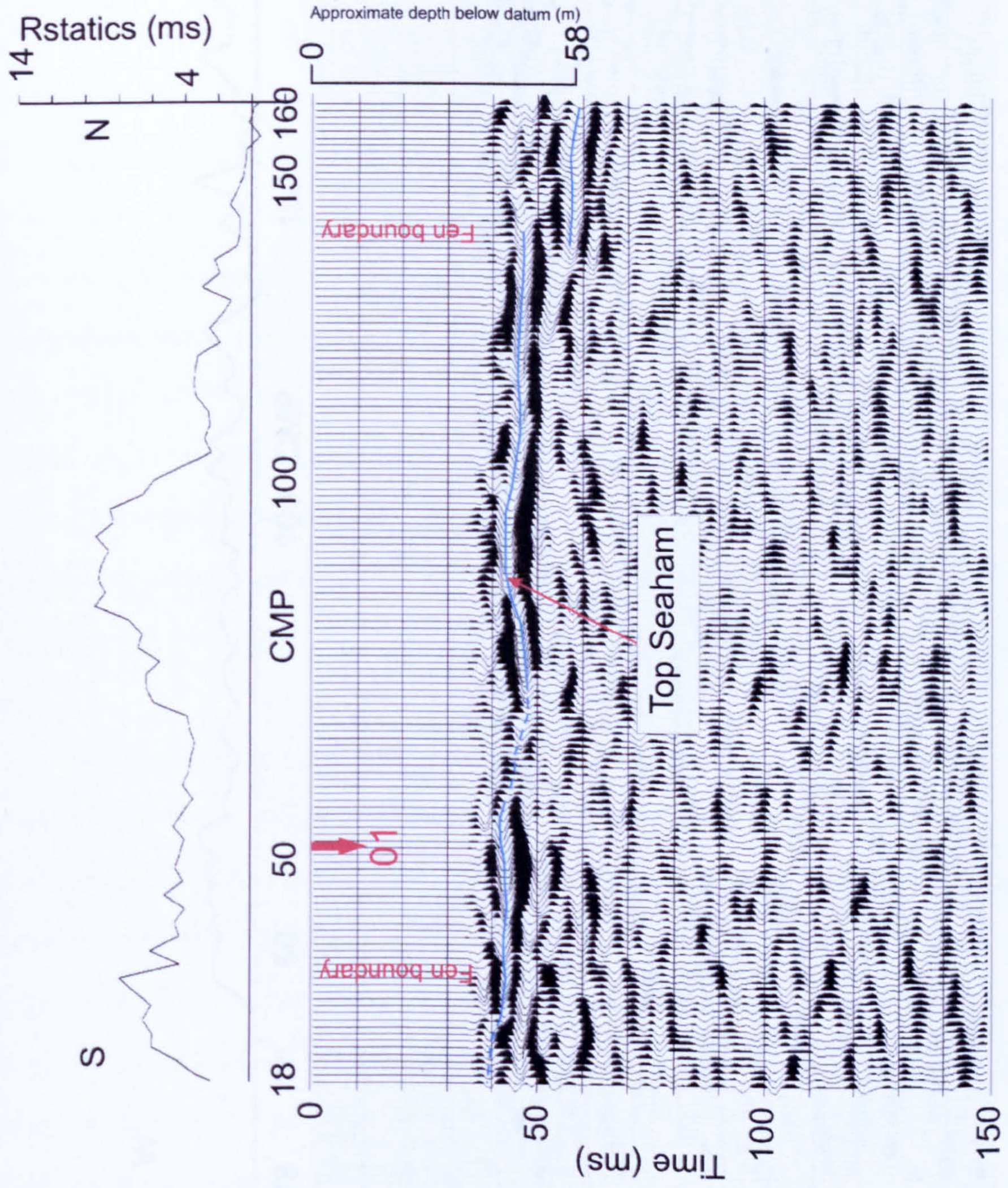

Figure 7.13: Interpreted final time migrated section of Neasham Fen profile 03.
The distance between CMP traces for all Neasham Fen 2D profiles is 1 m. The CMP numbering has been adjusted to represent the distance along the profile from the first receiver station. The section is displayed with a scalar multiplier.

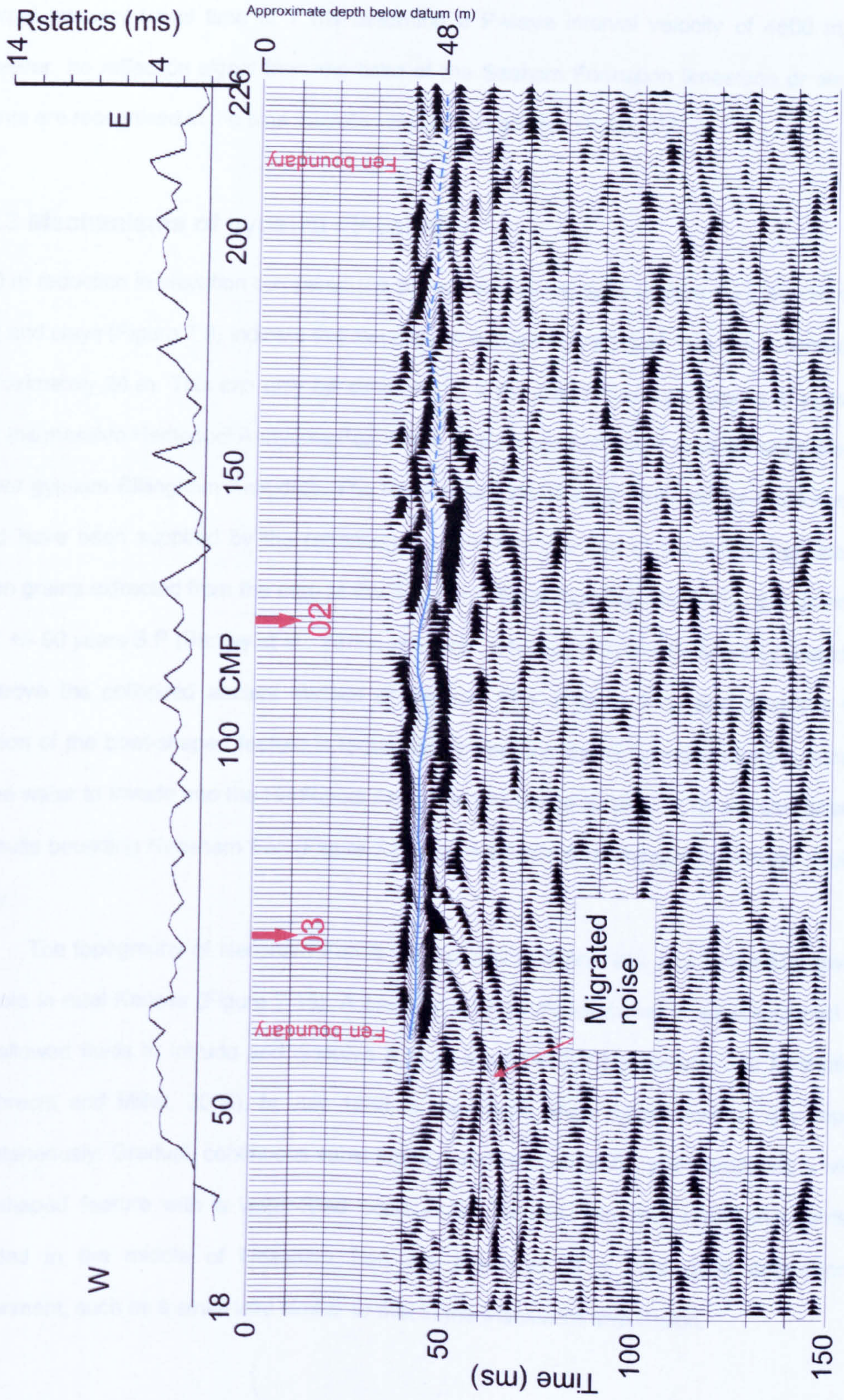

Figure 7.14: Interpreted final time migrated section of Neasham Fen profile 01.

The Seaham Limestone is 16 m thick in the Neasham borehole, equivalent to an internal two-way travel time of 7 ms assuming a P-wave interval velocity of 4500 m s^{-1}. However, no reflection signal from the base of the Seaham Formation limestone or deeper events are recognised in the time migrated sections of profiles 01 and 03.

7.4.3 Mechanisms of gypsum dissolution

A 10 m reduction in elevation compared the surrounding topography (Figure 7.7) plus 14 m of peat and clays (Figure 7.3) indicate that the ground surface at Neasham Fen has subsided by approximately 24 m. This can only be achieved by a scouring of a large volume of gypsum from the massive Hartlepool Anhydrite Formation, plus removal of some or all of the shallower thinner gypsum Billingham Anhydrite. The large quantities of water required for this to occur could have been supplied by the retreating ice sheet at the end of the Devensian stage. Pollen grains extracted from the core at the 6 m depth mark from Neasham Fen are dated at 9082 +/- 90 years B.P (Bartley et al., 1976). However, a further 8 m of very fine clay materials lie above the collapsed ancient surface of Boulder Clay (Figure 7.3), and therefore the creation of the bowl-shaped feature is much earlier than the dated organic material. Access for the water to invade into the Hartlepool Anhydrite Formation is likely to be via one or both the faults bounding Neasham Fen (Figure 7.5) and from the Ford Formation artesian aquifer below.

The topography of Neasham Fen is very similar in shape and size to the Macksville sinkhole in rural Kansas (Figure 7.15). A break in a brine disposal well in an abandoned oil field allowed fluids to intrude and dissolve a large cavity in the Hutchinson Salt Formation (Lambrecht and Miller, 2006). In July 1988, a very large sheer-sided sinkhole developed instantaneously. Gradual, continuous subsidence over the intervening years produced a wide bowl-shaped feature with a water-filled pond in the middle. The fine clays and detritus recorded in the middle of Neasham Fen are indicative of a very quiet depositional environment, such as a small lake similar to that in the Macksville depression.

Figure 7.15: The Macksville Sinkhole, Kansas.
Picture is extracted from Lambrecht and Miller (2006).

8.0 Ulleskelf Mires

8.1 Site description

The Ulleskelf Mires survey area (Figure 8.1) is sited amongst a swarm of shallow sub-circular hollows in very flat land approximately 2 km north of Church Fenton, North Yorkshire. A network of drainage ditches enables the cultivation of a diverse variety of crops on the rich farmland in the area, alongside cattle farming. During the winter months the depressions are highlighted by being water-filled (inset Figure 8.1) and cover an area of approximately 2 km^2. Thompson et al. (1996) suggested that these features are the result of sub-surface dissolution of gypsum within the underlying Permian strata.

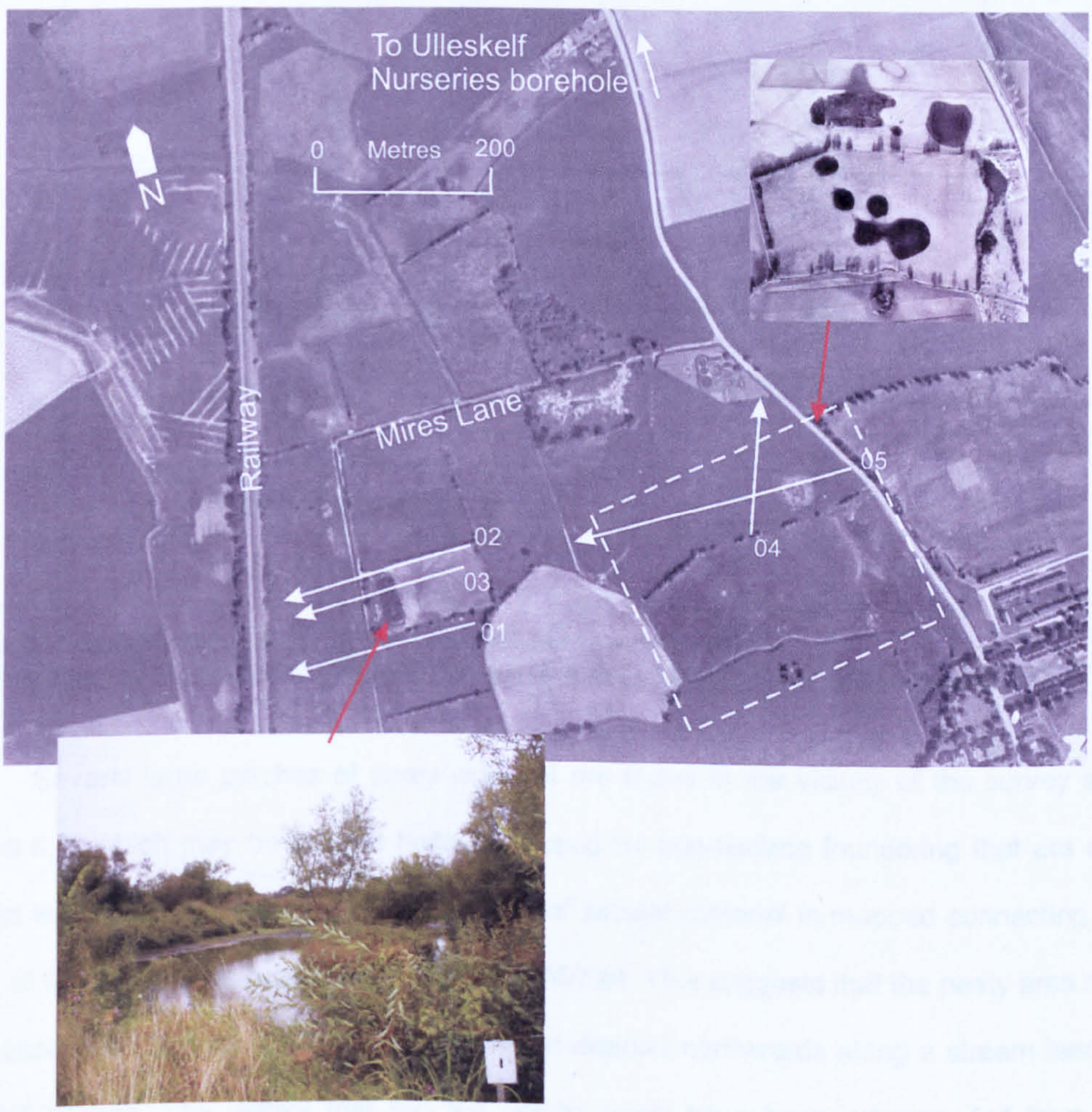

Figure 8.1: Aerial photograph taken in 1976 of the Ulleskelf Mires survey site.
Inset pictures show the broad shallow hollows water filled and a view across the target rectangular shaped pond.

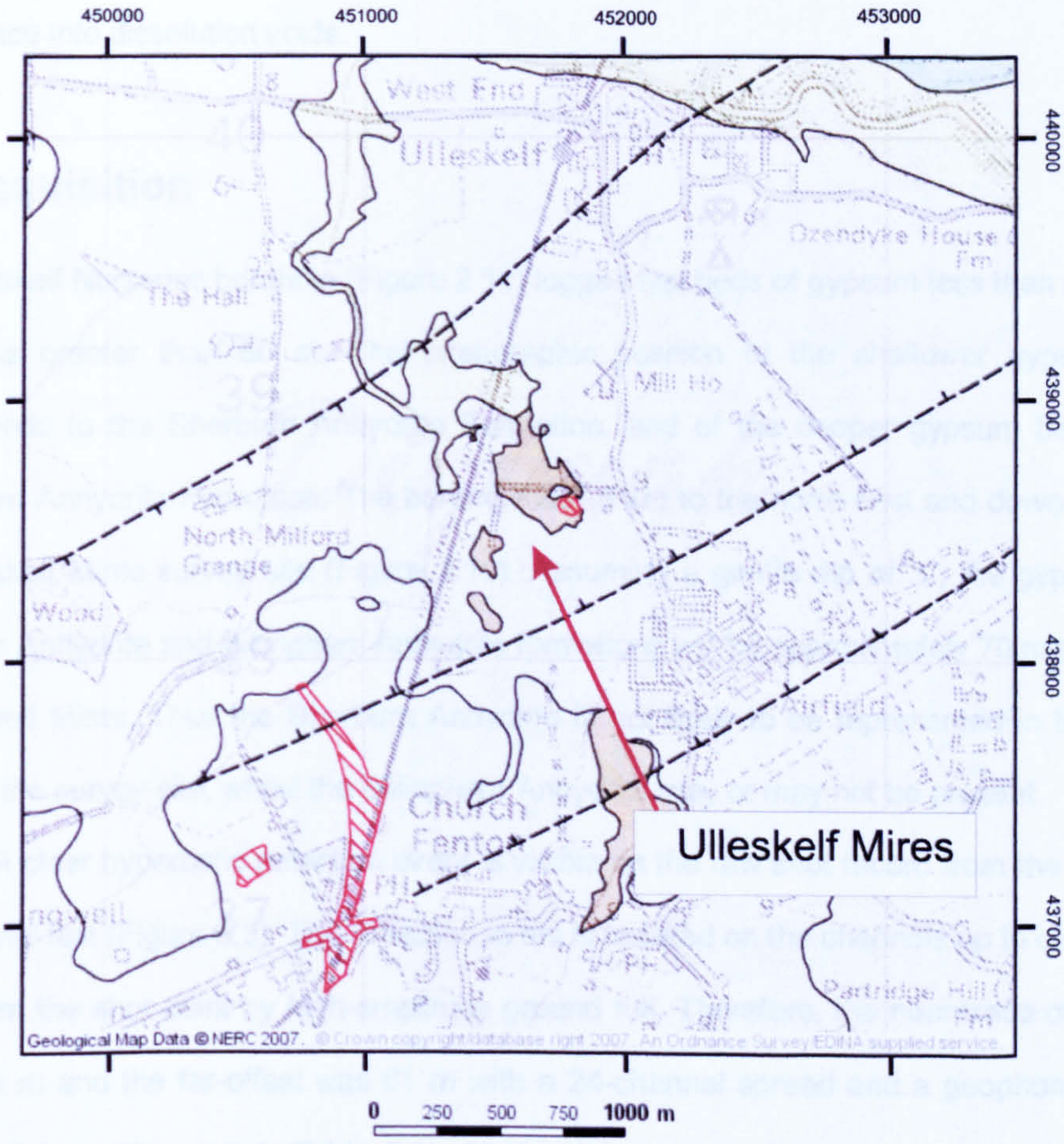

Figure 8.2: Superficial geology at the Ulleskelf Mires survey site.
Data supplied by Ordnance Survey/EDINA service © Crown Copyright Database 2007.

Several large patches of peaty material are found in the vicinity of the survey area (Figure 8.2) which may be ancient hollows caused by sub-surface foundering that are now filled in with organic material. A sinuous band of alluvial material is mapped connecting the larger of the amorphous peat areas to the River Wharf. This suggests that the peaty area may have once been a vigorous natural spring which drained northwards along a stream leading into the Wharfe. The waters that fed the spring could have been artesian, fed from the

underlying Permian limestones through the breccia pipes created by chimney-collapse subsidence into dissolution voids.

8.2 Acquisition

The Ulleskelf Nurseries borehole (Figure 2.11) logged two beds of gypsum less than 5 m thick at depths greater than 60 m. The stratigraphic position of the shallower gypsum bed corresponds to the Sherburn Anhydrite Formation, and of the deeper gypsum bed to the Billingham Anhydrite Formation. The borehole is 1.5 km to the north-east and down-dip from the Ulleskelf Mires survey site (Figure 2.10). Assuming a gentle dip of 3°, the gypsum-rich Sherburn Anhydrite and Billingham Anhydrite formations will be approximately 70 m shallower at Ulleskelf Mires. Thus the Sherburn Anhydrite is not likely to be represented in the strata beneath the survey site, whilst the Billingham Anhydrite may or may not be present.

A clear hyperbolic reflection event is visible on the raw shot record from the Ulleskelf Mires wave test (Figure 8.3). The reflection event is masked on the channels up to distance of 13 m from the shot point by high-amplitude ground roll. Therefore, the near-trace offset was set at 15 m and the far-offset was 61 m with a 24-channel spread and a geophone station interval of 2 m (Figure 8.4, Table 8.1). Shot points were placed at 2 m intervals midway between receiver stations and offset from the line of geophones by 2 m. Data were acquired by using this off-end shooting arrangement in the forward direction only, with the geophone spread laid out ahead of the shot, to yield a maximum fold of coverage of 12.

Three 2D profiles, 01, 02 and 03, each of approximately 230 m length between the first and last receivers, were arranged to investigate a 40 m × 20 m rectangular pond at the end of Mires Lane (inset Figure 8.1), near the main railway line embankment (Figure 8.1). Profile 03 crossed the pond with the parallel profiles 01 and 02 located immediately to the south and north of the pond. Two other 2D profiles were laid out in an adjacent field with the longer one, profile 05, traversing two broad shallow depressions, whilst the shorter one, profile 04, was acquired almost perpendicularly to profile 05 passing between the shallow hollows.

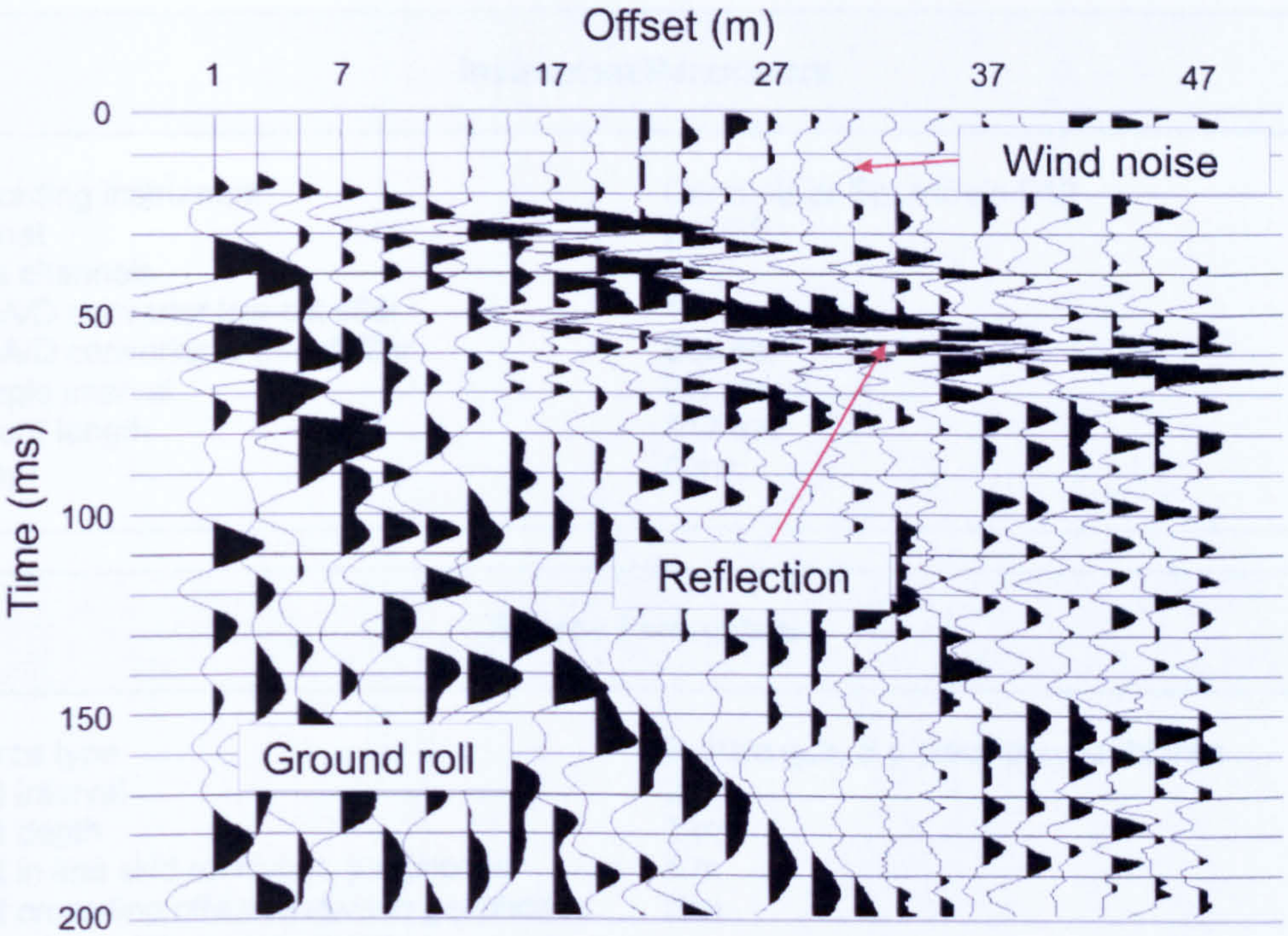

Figure 8.3: Ulleskelf Mires wave test shot record.
The data have been scaled with a 100 ms AGC window before being cropped.

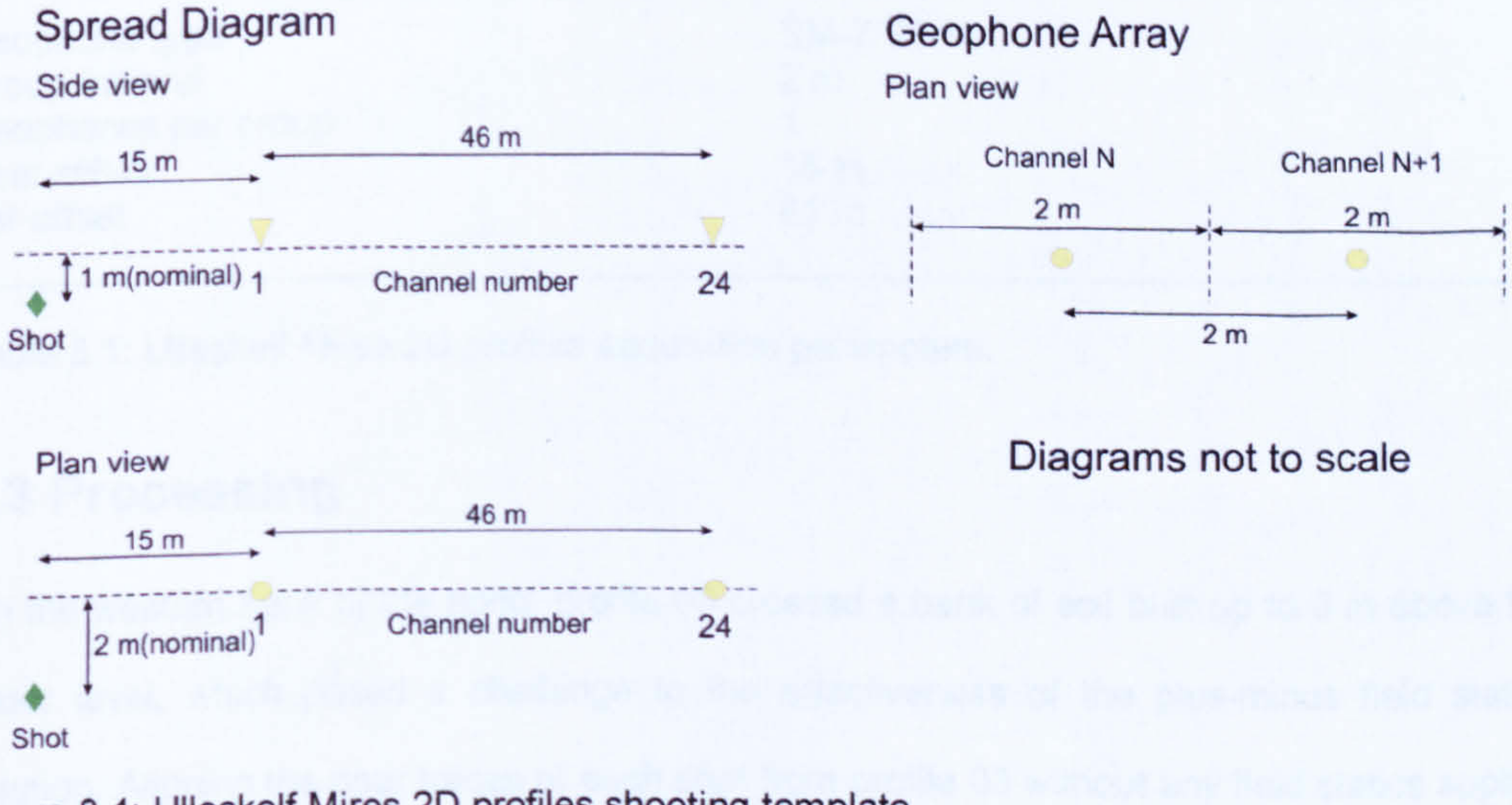

Figure 8.4: Ulleskelf Mires 2D profiles shooting template.

Instrument Parameters	
Recording instrument	Geometrics SmartSeis S12
Format	SEG-2
Data channels	24
Pre A/D converter low-cut filter	10 Hz
Pre A/D converter high-cut filter	500 Hz
Sample interval	0.5 ms
Record length	512 ms
Delay	0 ms
Source Parameters	
Source type	Buffalo gun, 5 g black powder blanks
Shot interval	2 m
Shot depth	1 m
Shot in-line skid relative to geophones	1 m
Shot cross-line offset relative to geophones	2 m
Off-end shooting arrangement.	
All shot holes tamped with water before firing.	
Receiver Parameters	
Geophone type	SM-7/30 Hz
Group interval	2 m
Geophones per group	1
Near-offset	15 m
Far-offset	61 m

Table 8.1: Ulleskelf Mires 2D profiles acquisition parameters.

8.3 Processing

On the western bank of the pond, profile 03 crossed a bank of soil built up to 3 m above the water level, which posed a challenge to the effectiveness of the plus-minus field statics solution. Aligning the near traces of each shot from profile 03 without any field statics applied shows the variation in first break timing (Figure 8.5, upper panel). Superimposed on the smoother changes in first break timing is a random larger variation that was caused by the shot triggering sensitivity not being set correctly for the shooting conditions. After application of the computed field statics, all the near-trace first breaks align neatly (Figure 8.5, lower

panel) and close to the expected arrival time of 9.5 ms for a calculated water table refractor velocity of 1571 m s^{-1} and a near-trace offset of 15 m.

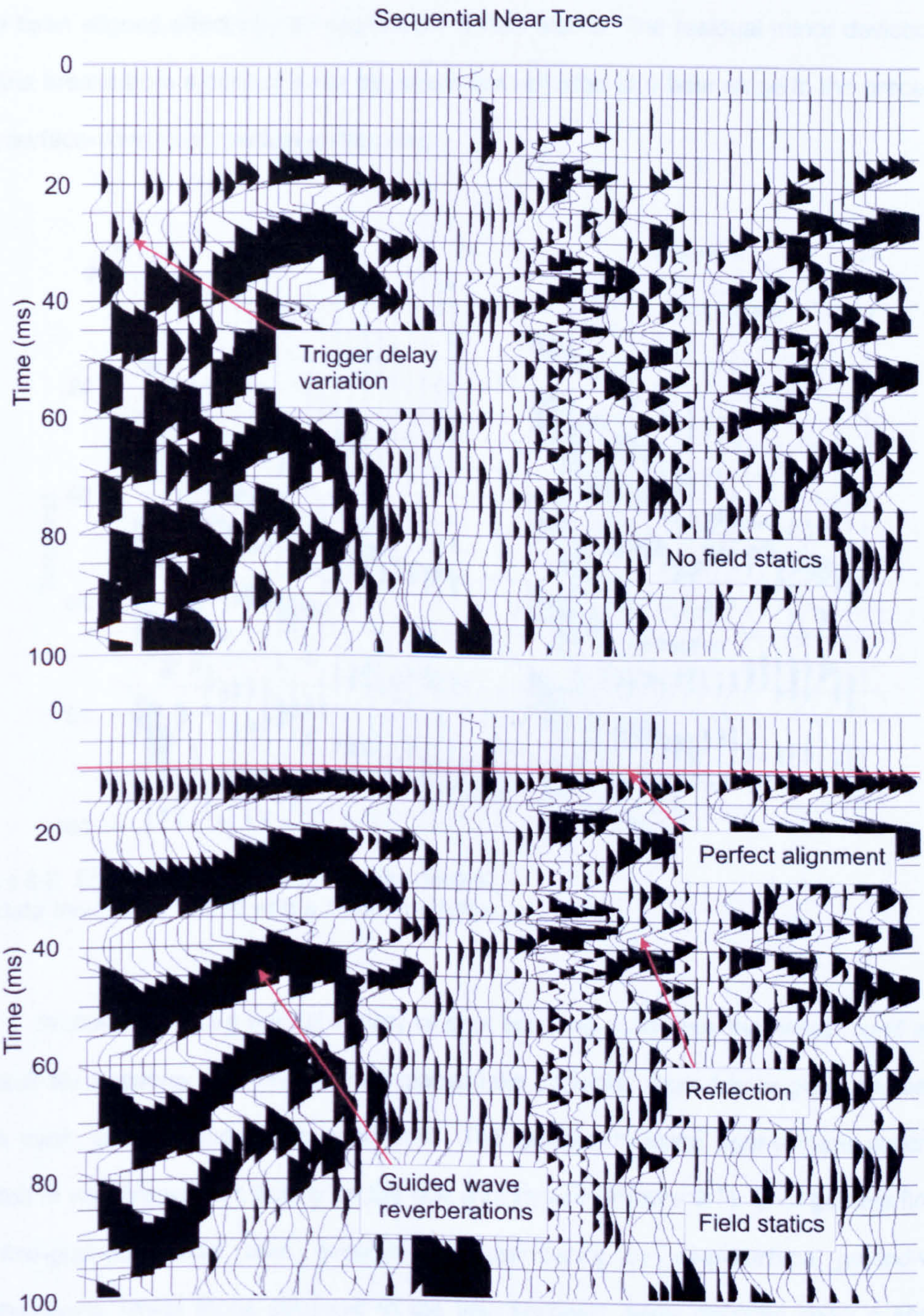

Figure 8.5: Near-trace field statics quality control.
The data have been scaled with a scalar multiplier.

An alternative quality control test of the field statics solution is to examine the shot gathers. The left panel in Figure 8.6 shows relatively late first breaks on the first 14 channels, where the geophones were planted on the bank. The right panel shows that the first breaks have been aligned effectively by application of field statics. The residual minor deviations in the first breaks from a perfect linear alignment are adjusted at a later stage in the processing by a surface-consistent residual statics step.

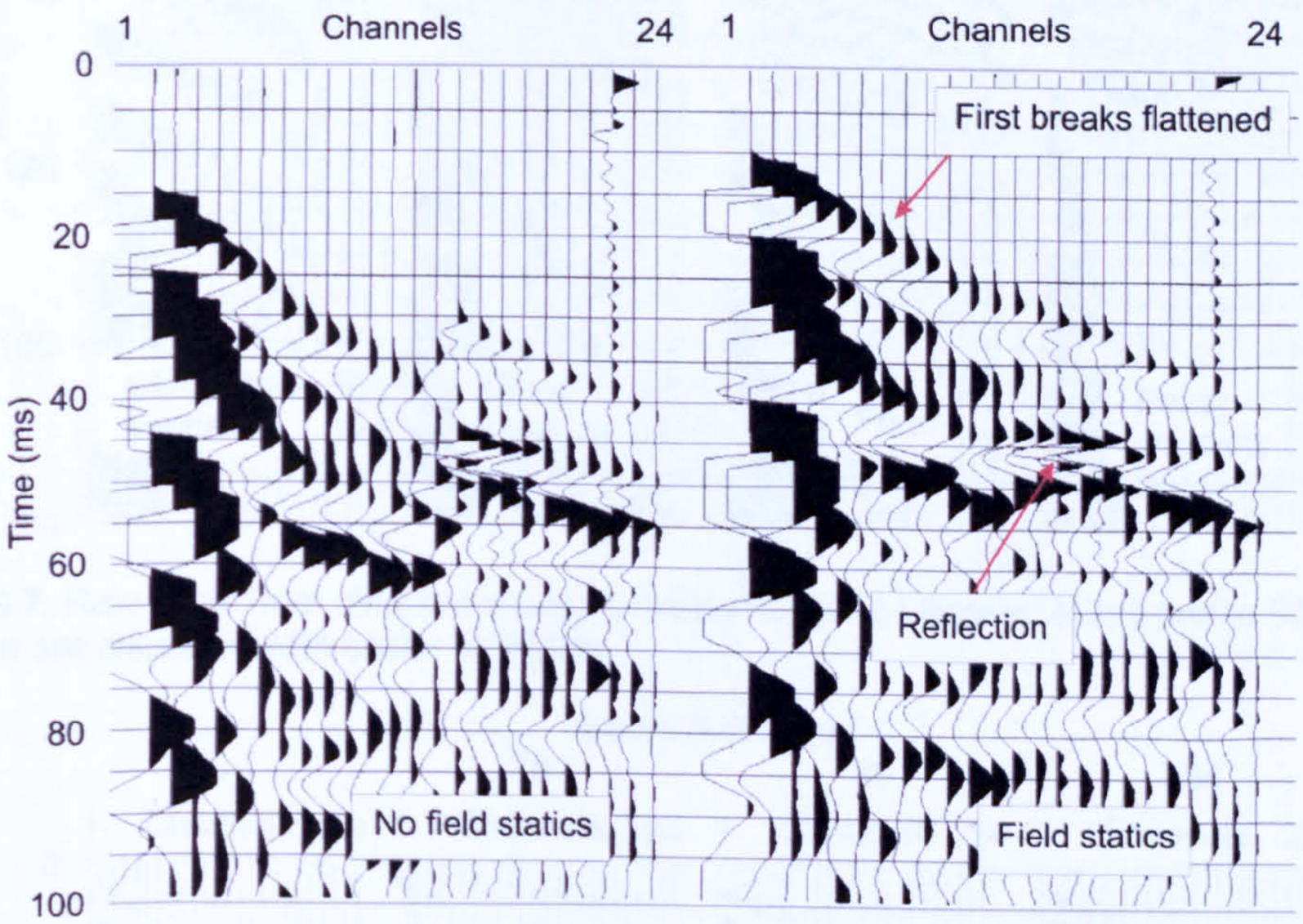

Figure 8.6: Shot record field statics quality control.
The data have been scaled with a scalar multiplier.

Profile 03 crossed the full variety of shot coupling conditions that were found at the Ulleskelf Mires survey site: fine-grained glacial lake deposits, more lumpy peaty material, a rough track, and the bed of the pond itself. The rapidly changing near-surface conditions resulted in variable seismic quality on the raw shot records (Figure 8.7). Shot gathers fired in the fine-grained glacial lake deposits are dominated by near-surface guided-wave reverberations, whilst those collected in the less compact peaty deposits show a shallow reflection event. Ground roll is present on all shot gathers, but at late arrival times so it does not interfere with the shallow reflection events. The low-frequency shot-generated noise can be removed effectively with bandpass filtering and reveals a shallow reflection event (Figure 8.8).

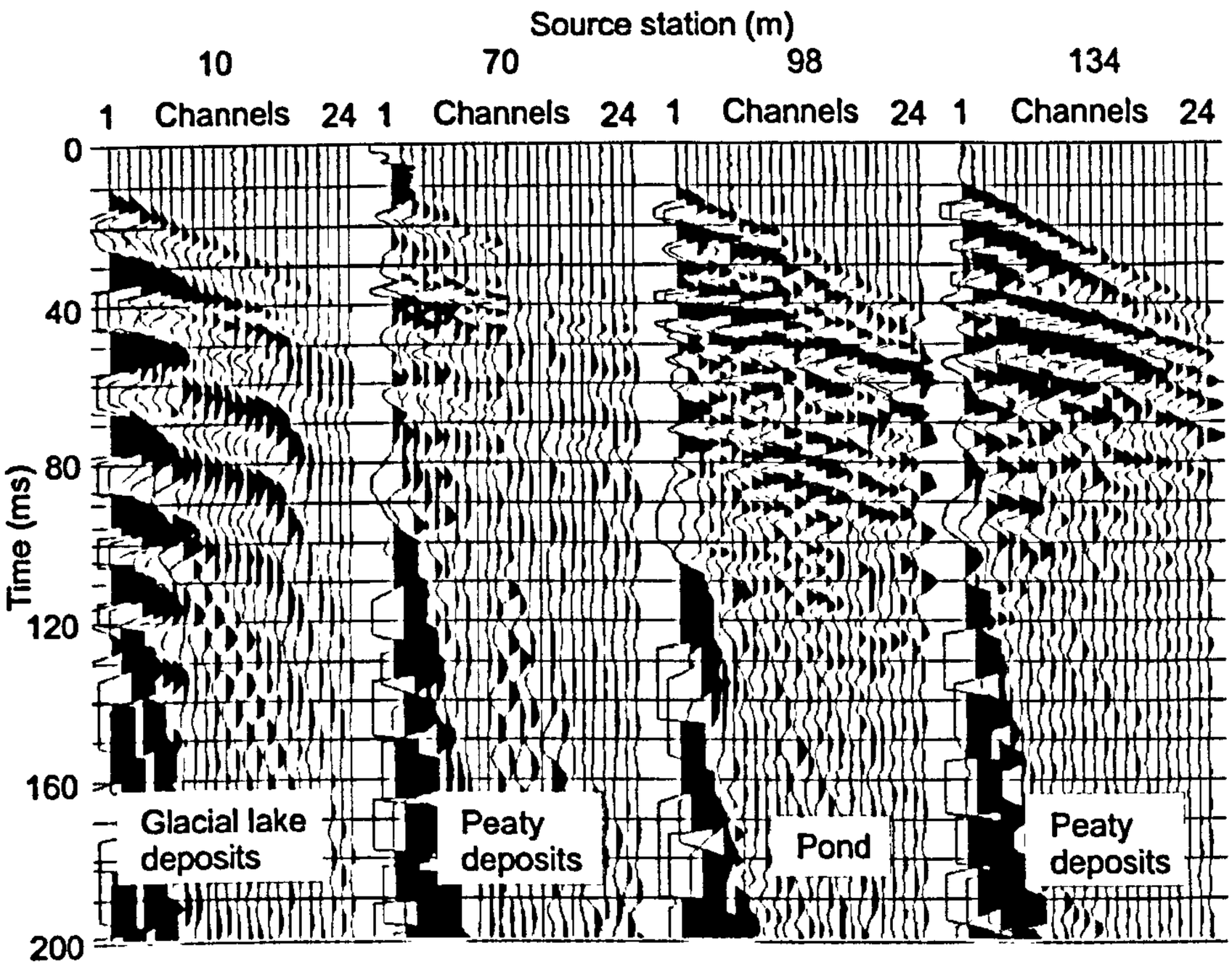

Figure 8.7: Raw shots from different shooting mediums along Ulleskelf Mires profile 03. The data are displayed with scalar multiplier.

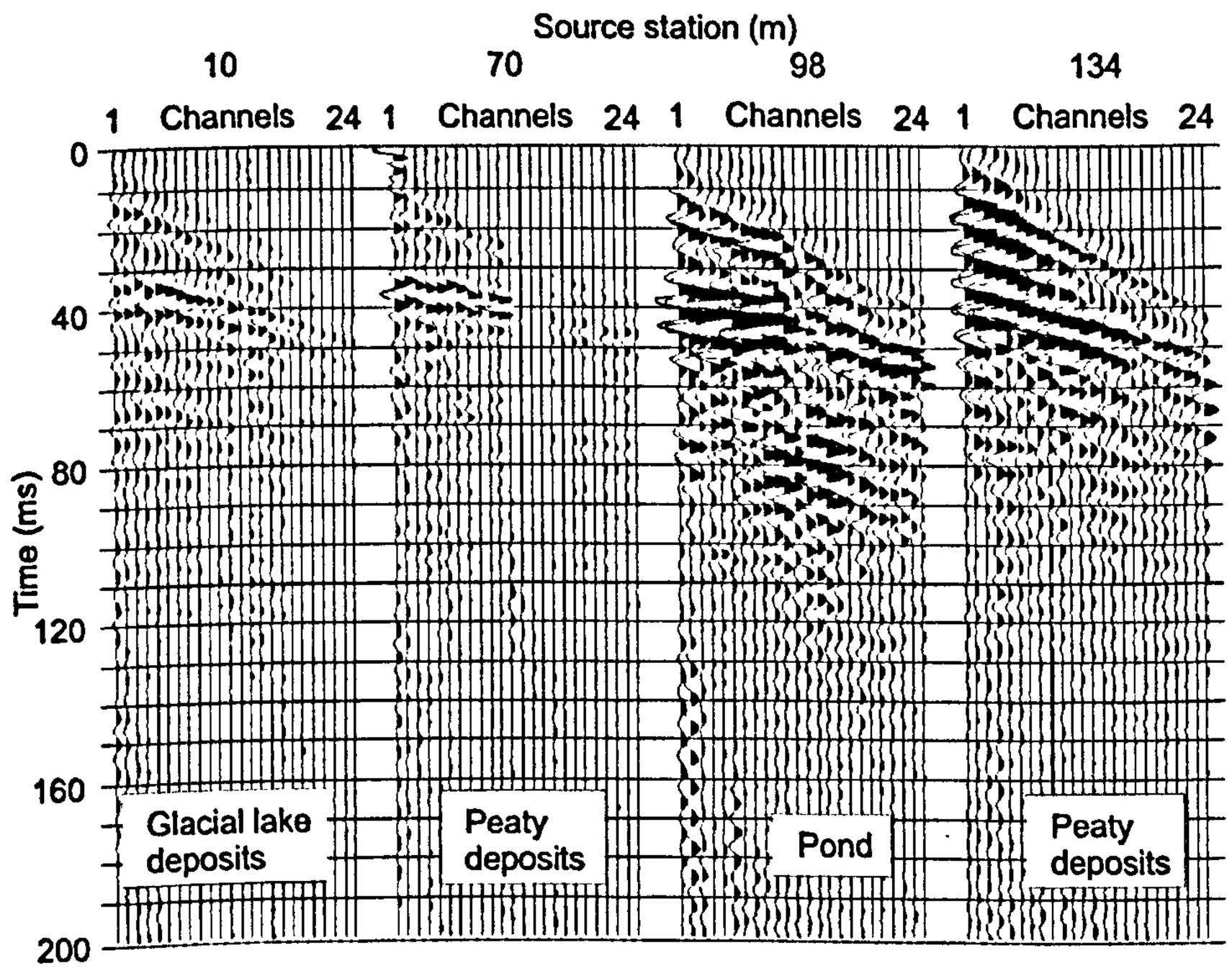

Figure 8.8: Shots records in different shooting mediums bandpass filtered. Bandpass filter applied withcorner frequencies with 100 Hz, 140 Hz, 330 Hz and 350 Hz. The data are displayed with scalar multiplier.

The filtered shot gathers are balanced with a 60 dB per second gain function followed by surface-consistent statistical adjustment of the gain for each shot and receiver station. Any remaining shot-generated noise boosted by the gain balancing is removed by judicious surgical muting and later in the common midpoint (CMP) domain by *f-x* deconvolution.

Testing shows that deconvolution improves the temporal resolution of the Ulleskelf Mires seismic dataset (Figure 8.9). The minimum-phase and zero-phase spiking deconvolution variations have slightly better frequency content than the spectral test panel, and so give a sharper main reflection event with its onset at 30 ms on the near channel. On the spectral shaping test panel, there is a black loop followed by a strong white loop riding on top of the main reflection event on the near-offset traces. This signal is also present on the zero-phase test panel, but only the negative trough is visible on the minimum-phase test panel. These precursory loops are side-lobes that have resulted from bandpass filtering. Comparing the results from different deconvolution filters on both shot gathers and stacked sections, for the Ulleskelf Mires survey minimum-phase spiking deconvolution with a 10 ms operator length was preferred. Phase shift time migration was the final processing step applied to the Ulleskelf Mires 2D profiles (Figure 8.10).

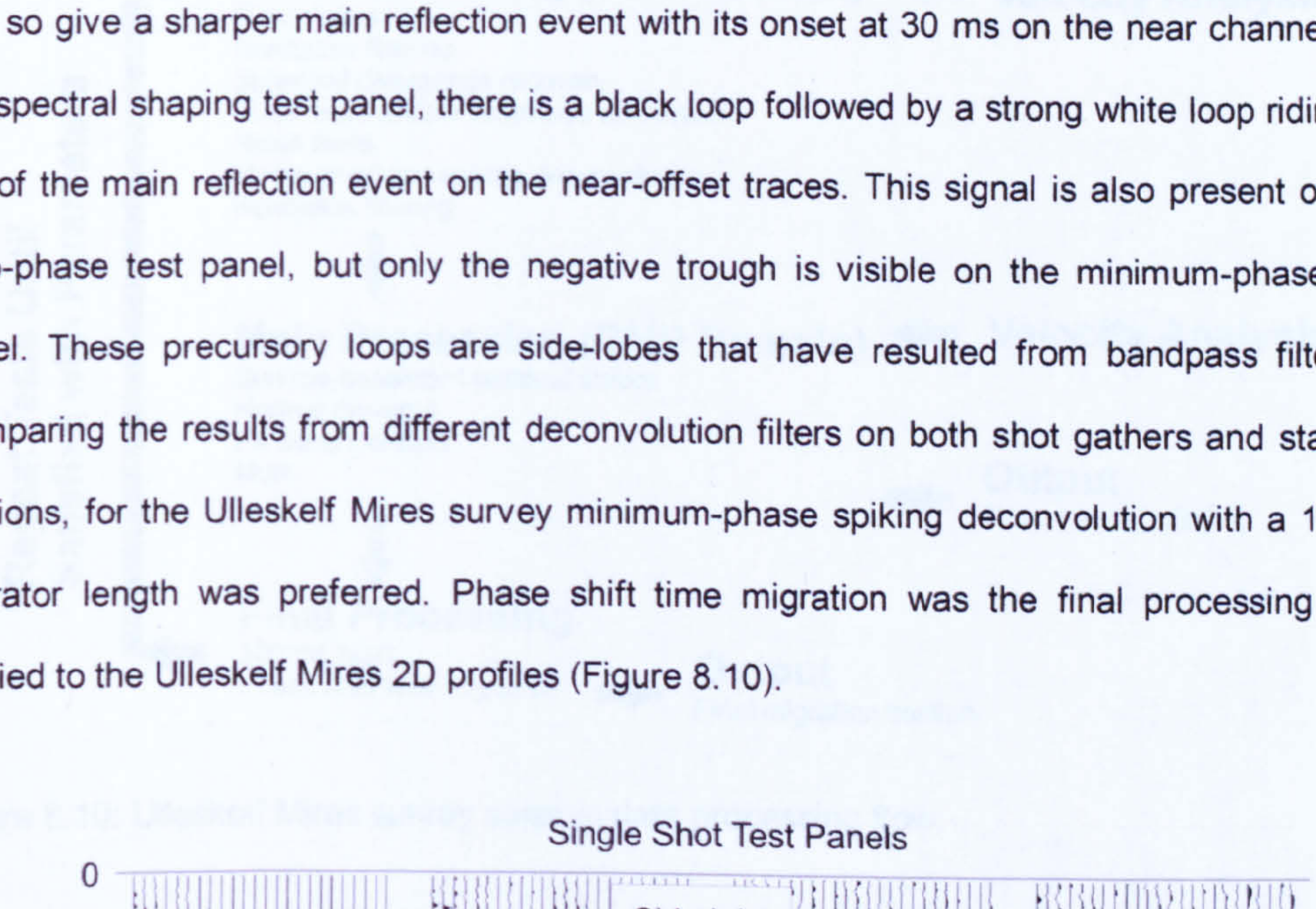

Figure 8.9: Deconvolution shot record test panels from Ulleskelf Mires profile 01. The data have been scaled with a 200 ms AGC before being cropped.

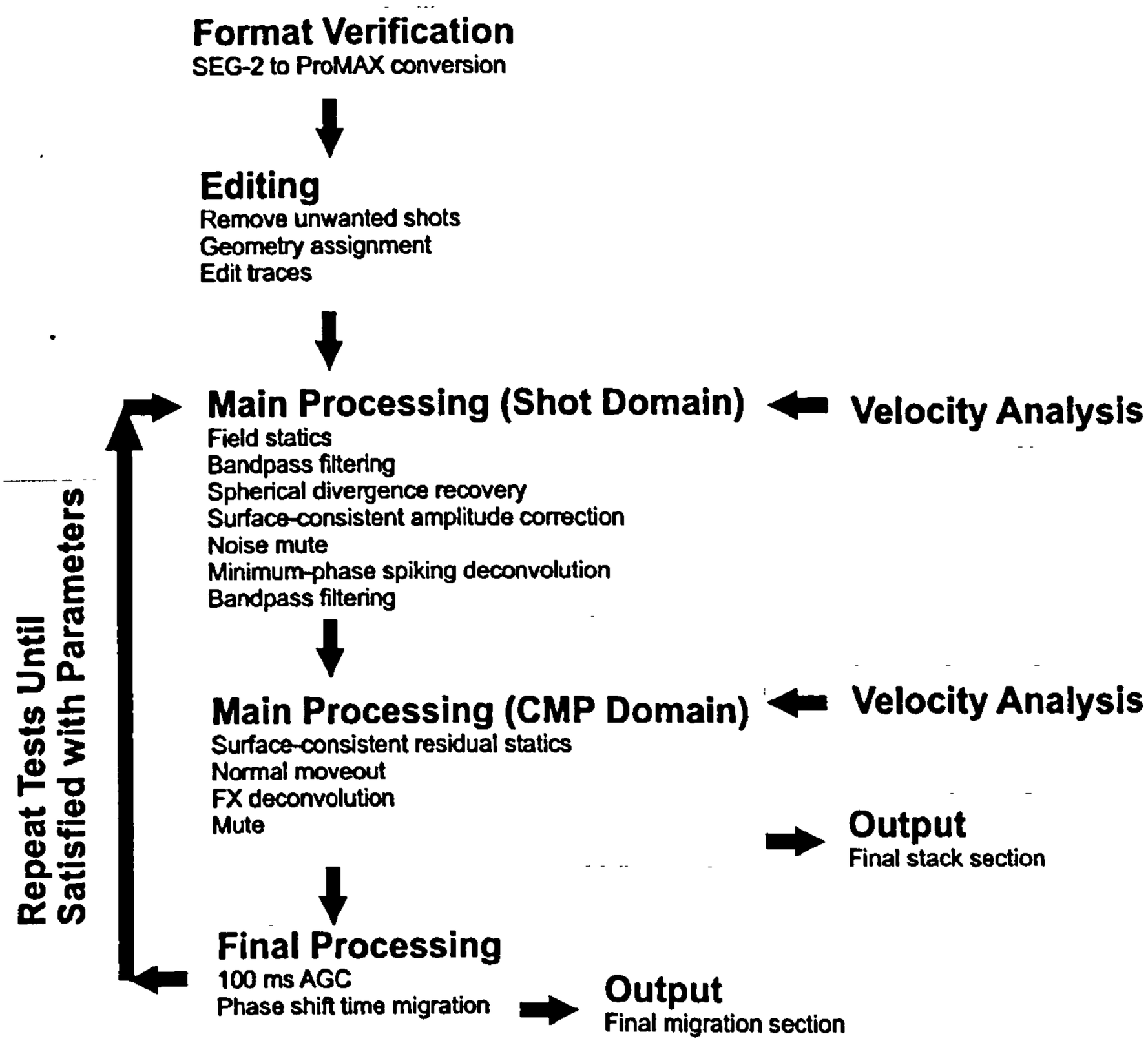

Figure 8.10: Ulleskelf Mires survey seismic data processing flow.

8.4 Interpretation

8.4.1 Brotherton Formation and sub-surface foundering

A prominent reflection event features along the complete length of the time migrated stack section of profile 02 (Figure 8.11). The upper black loop is at 30 ms at the beginning of the profile. Below and parallel to the upper black positive amplitude loop is a negative amplitude loop followed by another black loop. The upper black loop is very smooth up to CMP 75 where it drops down sharply by 3 ms. Then it continues towards the west end of profile at approximately the same two-way time but has a rippled surface with an amplitude of 1 ms, particularly around CMP 120. The lumps and bumps imaged on profile 02 do not correlate with the position of the pond which is adjacent to profile 02 between CMPs 110 and 130.

Boreholes BHP 71 and BHP 72 drilled by British Gypsum Limited are located about 1.5 km from the Ulleskelf Mires survey site, approximately along strike (Figure 8.12). The stratigraphy proved in these shallow boreholes is shown in Figure 8.13. In borehole BHP 72 the hard limestone of the Brotherton Formation is overlain by 28 m of Roxby Formation mudstones and Quaternary glacial lake deposits. In borehole BHP 71 a thin bed of BIllingham Anhydrite rests on top of the Brotherton Limestone.

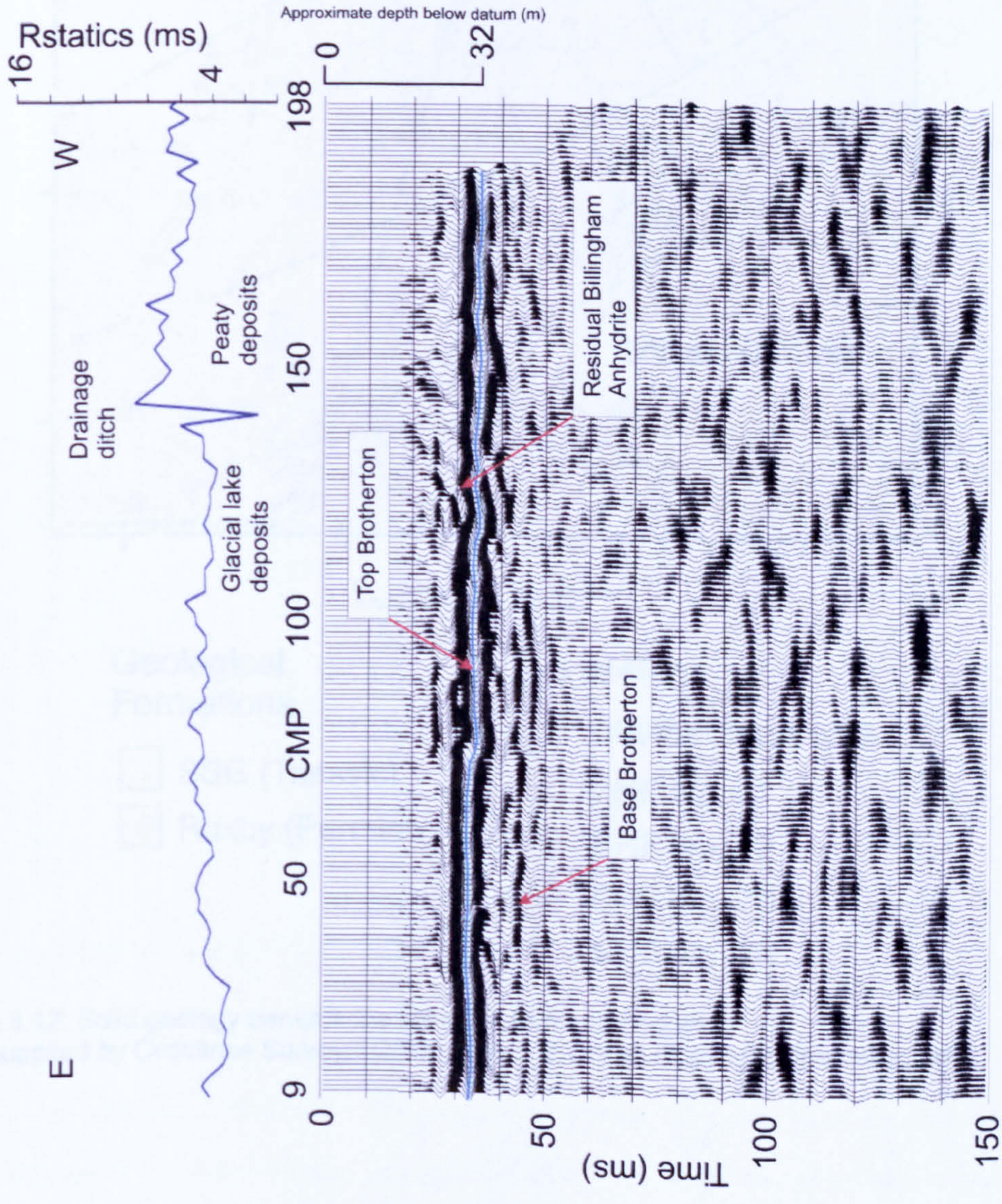

Figure 8.11: Interpreted final time migrated section of Ulleskelf Mires profile 02.
The distance between CMP traces for all Ulleskelf Mires 2D profiles is 1 m. The CMP numbering has been adjusted to represent the distance along the profile from the first receiver station. The section is displayed with a scalar multiplier.

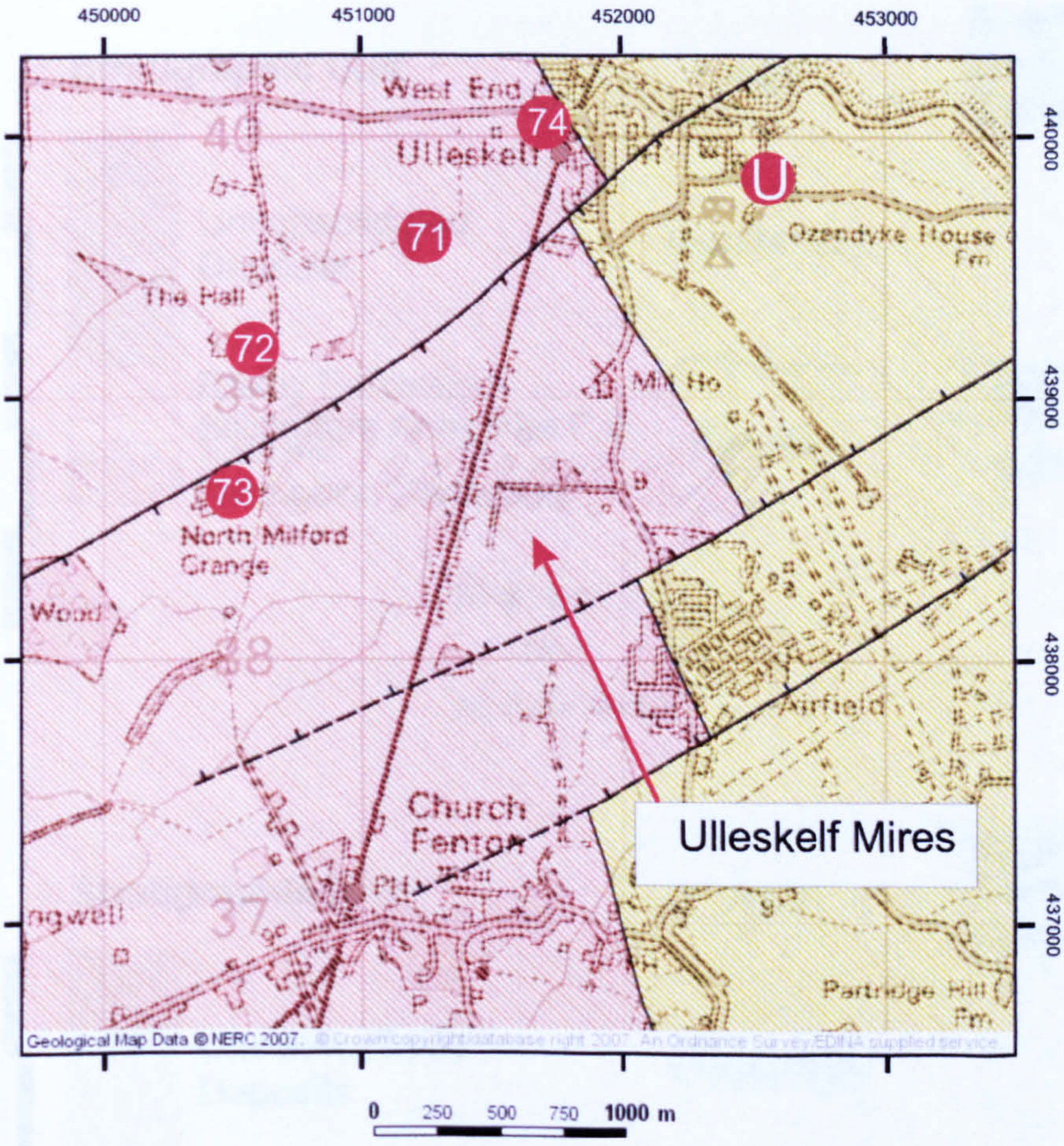

Figure 8.12: Solid geology beneath the Ulleskelf Mires survey site.
Data supplied by Ordnance Survey/EDINA service © Crown Copyright Database 2007.

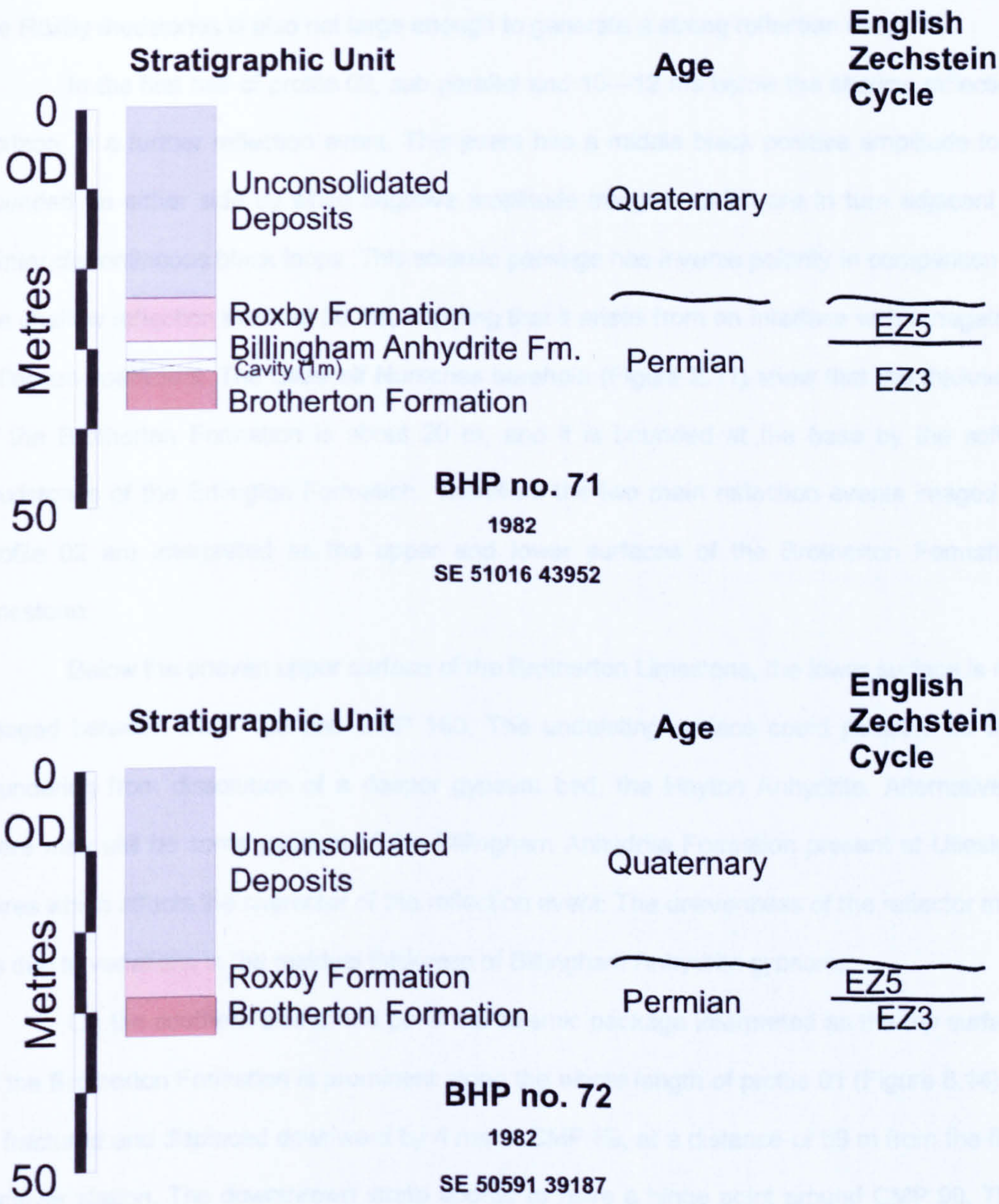

Figure 8.13: BHP 71 and 72 boreholes geological successions.

The shallow reflection event imaged in profile 02 could well be the seismic representation of the Roxby-Brotherton or Roxby-Billingham interface. It has previously been noted that the Roxby mudstones have a low P-wave interval velocity of around 2100 m s^{-1} (e.g., at Hell Kettles borehole) and so it is unlikely to have much of an acoustic impedance contrast with Quaternary Boulder Clay. The gypsum of the Billingham Anhydrite Formation at

Ulleskelf Mires may have taken up so much water that its acoustic impedance contrast with the Roxby mudstones is also not large enough to generate a strong reflection event.

In the first half of profile 02, sub-parallel and 10—12 ms below the shallow reflection horizon, is a further reflection event. This event has a middle black positive amplitude loop bounded on either side by white negative amplitude troughs, which are in turn adjacent to fainter discontinuous black loops. This seismic package has inverse polarity in comparison to the shallow reflection event at 30 ms, implying that it arises from an interface with a negative reflection coefficient. The Ulleskelf Nurseries borehole (Figure 2.11) show that the thickness of the Brotherton Formation is about 20 m, and it is bounded at the base by the softer mudstones of the Edlington Formation. Therefore the two main reflection events imaged in profile 02 are interpreted as the upper and lower surfaces of the Brotherton Formation limestone.

Below the uneven upper surface of the Brotherton Limestone, the lower surface is not imaged between CMP 100 and CMP 160. The undulating surface could possibly be due foundering from dissolution of a deeper gypsum bed, the Hayton Anhydrite. Alternatively, there may still be some gypsum of the Billingham Anhydrite Formation present at Ulleskelf Mires which affects the character of the reflection event. The unevenness of the reflector may be due to variations in the residual thickness of Billingham Anhydrite gypsum.

On the southern side of the pond the seismic package interpreted as the top surface of the Brotherton Formation is prominent along the whole length of profile 01 (Figure 8.14). It is fractured and displaced downward by 4 ms at CMP 59, at a distance of 59 m from the first receiver station. The downthrown strata appear to have a hinge point around CMP 90. This depression feature does not correlate with the location of the rectangular pond; the southern edge of the pond is adjacent to the part of profile 01 between CMP 90 and CMP 110. Up to CMP 59 and beyond CMP 90, the reflection character is continuous and has a gentle dip down to the west, comparable with that displayed by profile 02 but without the rippled surface in the reflection event.

In the parallel profile 03 acquired across the pond, the strong reflection signal from the top of the Brotherton Formation is present with the same seismic character and comparable overall dip down to the west, but it has considerably more relief (Figure 8.15).

The reflection package from the top surface of the limestone has a pronounced depression, 40 m across with amplitude 5 ms, centred at CMP 60. Beyond CMP 100, the reflection event has a blocky appearance with discontinuities around CMPs 105, 135, 145 and 160. The position of the pond is located between CMP 85 and CMP 102, as shown by the zero values in the receiver statics solution. It does not coincide with any of the displacements imaged. The depression and discontinuities are interpreted as evidence of foundering, presumably due to the dissolution of deeper the Hayton Anhydrite Formation, but none of the structures imaged in profile 03 can be correlated with features observed in the parallel profiles 01 and 02.

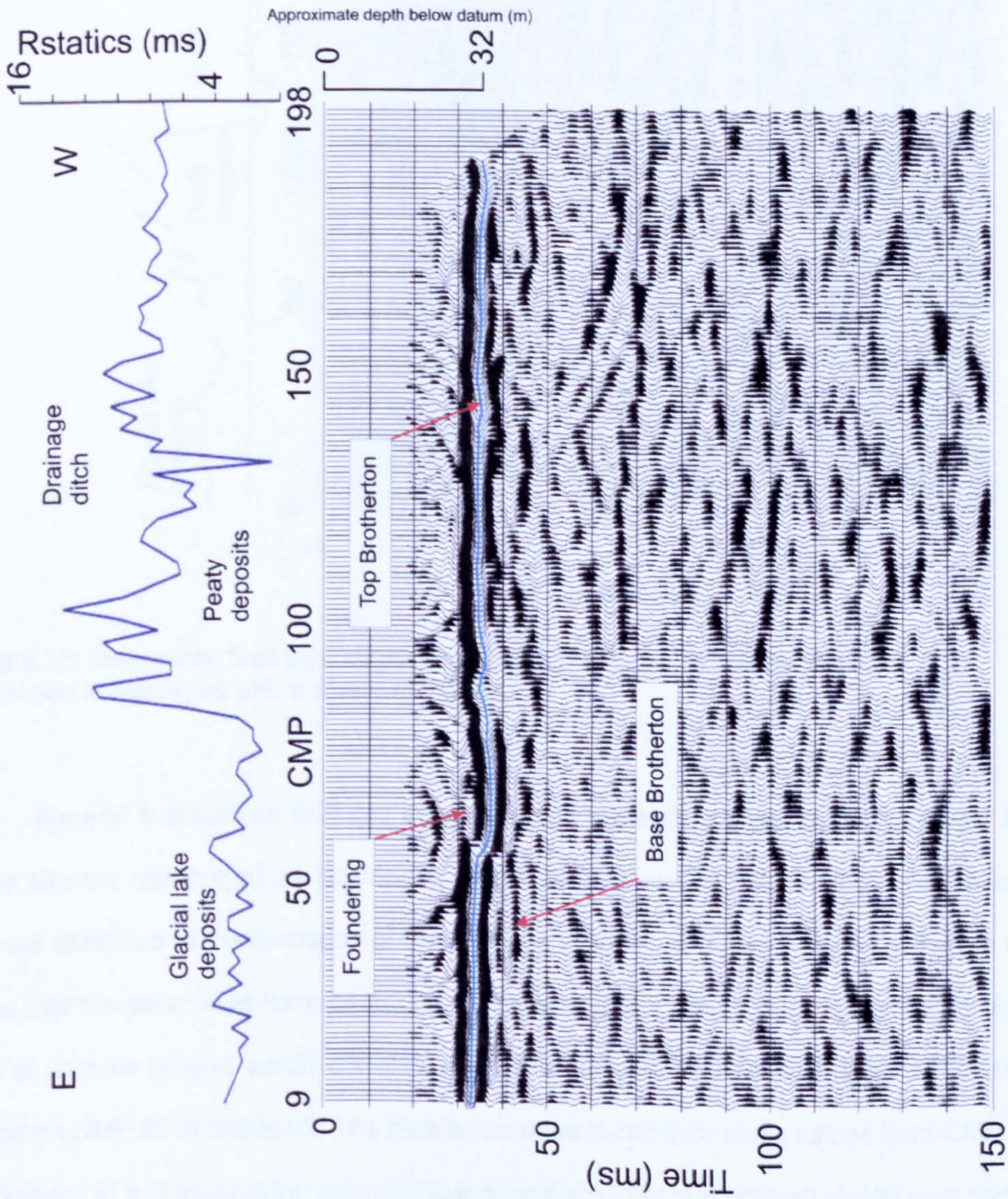

Figure 8.14: Interpreted final time migrated section of Ulleskelf Mires profile 01.
The section is displayed with a scalar multiplier.

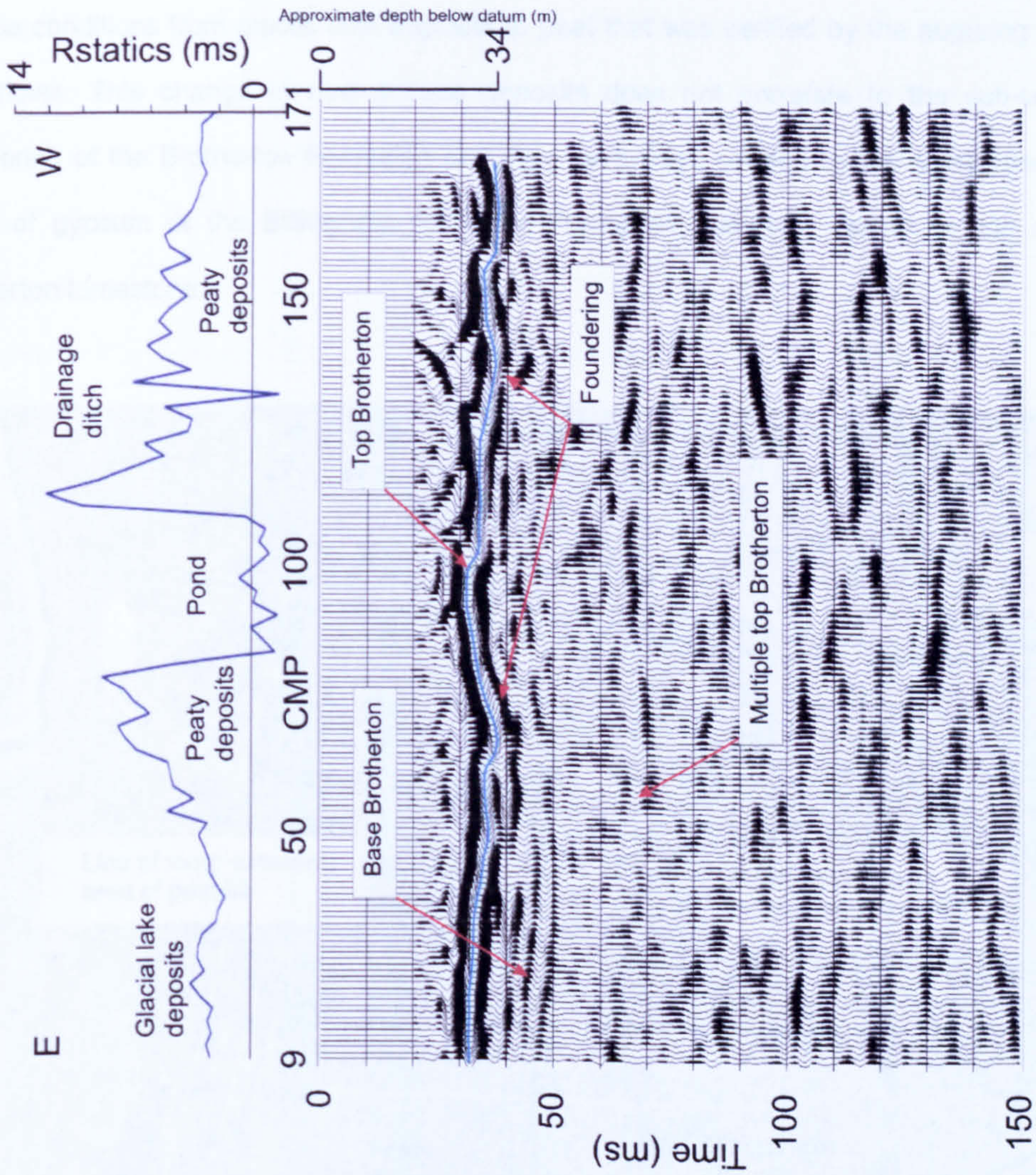

Figure 8.15: Interpreted final time migrated section of Ulleskelf Mires profile 03.
The section is displayed with a scalar multiplier.

Several sub-surface features imaged in the western profiles of the Ulleskelf Mires survey site are interpreted as foundering of the Brotherton Formation limestone. However, none are attributed to the formation of the rectangular pond. Aerial photography (Figure 8.16) proves that the pond must have been dug some time after 1974. It is located within a circular patch of smooth ground which correlates with the depression in the Brotherton Limestone centred on CMP 60 in profile 03. The steady increase in receiver static values from CMP 40 is an indication in a change in the near-surface conditions from fine grained glacial lake deposits to soft peaty conditions from which the pond was dug out. The peat probably filled in a depression formed at the surface by foundering of the sub-surface strata.

The receiver statics solutions for profiles 01, 02 and 03 pick out a change in near-surface conditions from glacial lake deposits to peat that was verified by the auguring of the shot holes. This change in near-surface deposits does not correlate to the sub-surface foundering of the Brotherton Formation and may have been caused by the dissolution of a patch of gypsum of the Bllingham Anhydrite Formation that once rested on top of the Brotherton Limestone.

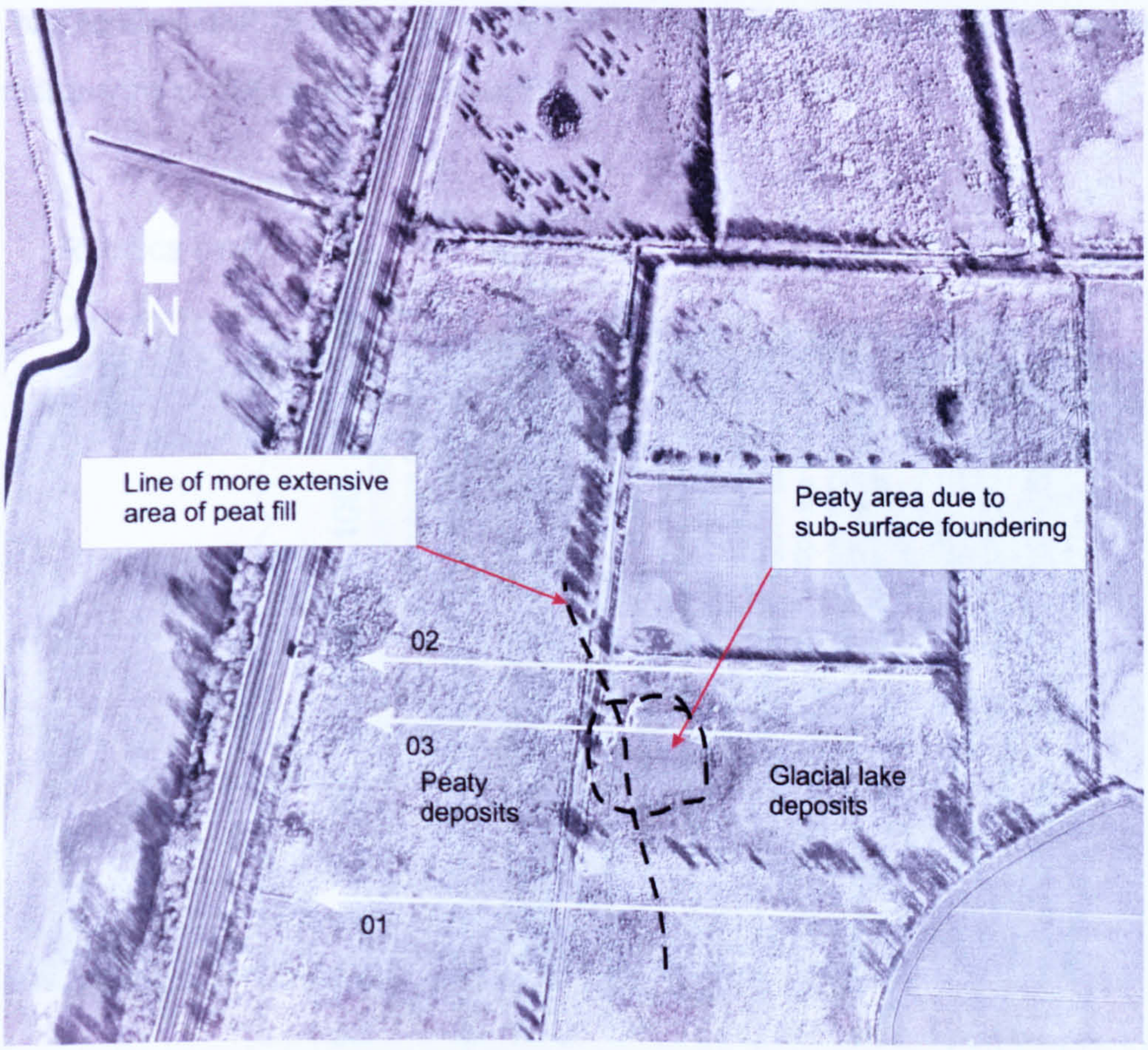

Figure 8.16: Aerial photograph taken in 1974 of the western half of Ulleskelf Mires.

8.4.2 Evidence for sub-surface gypsum

The character of the shallow reflection event on the time migrated stacked section of profile 04 (Figure 8.17) is more complicated than that on the western profiles at Ulleskelf Mires. It consists of a triplet of strong black positive amplitude loops. The uppermost black loop at 28 ms appears to coalesce with the second black loop between CMP 60 and CMP 100. It is preceded by a white loop interpreted as a side lobe resulting from bandpass filtering.

Near to Ulleskelf railway station (Figure 8.12) the British Gypsum Limited borehole BHP 74 (Figure 8.18) logged 5 m of gypsum sandwiched between two mudstone formations. This gypsum bed is interpreted as the Sherburn Anhydrite Formation. Up dip at borehole BHP 71 a thin 2 m bed of gypsum is present but resting on top of a limestone bed; this is the lower gypsum horizon, the Billingham Anhydrite Formation. The complete geological sequence spanning the mudstone, gypsum and limestone beds is observed in the deep Ulleskelf Nurseries borehole (Figure 2.11). Therefore, the Sherburn Anhydrite Formation thins out up dip from borehole BHP 74 towards borehole BHP 71. Further up dip, the Billingham Anhydrite Formation thins out before BHP boreholes 72 and 73.

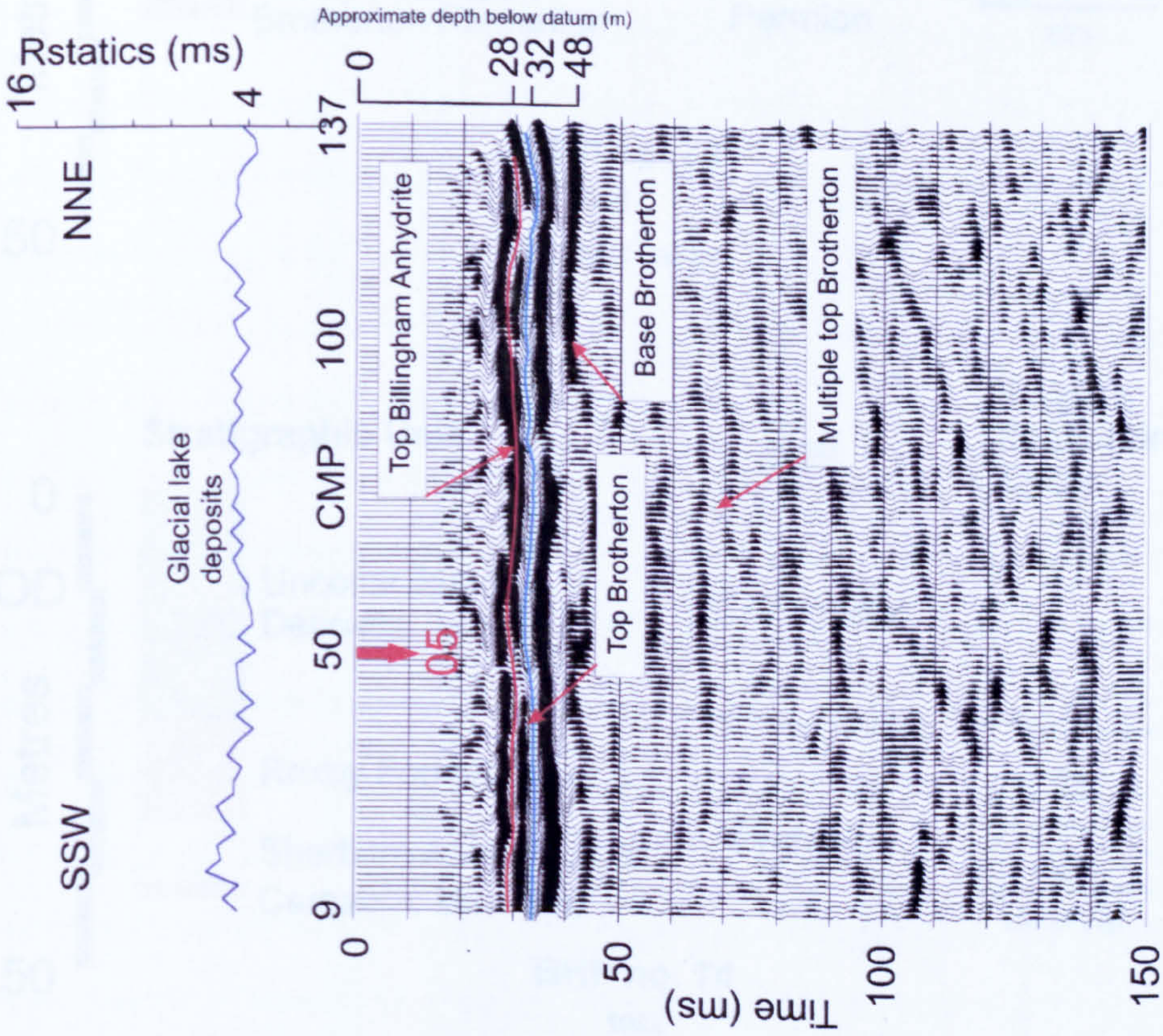

Figure 8.17: Interpreted final time migrated section of Ulleskelf Mires profile 04.
The section is displayed with a scalar multiplier.

The complex reflection package of profile 04 is interpreted as a thin bed of Billingham Anhydrite gypsum sitting on top the Brotherton Limestone. Borehole BHP 71 shows this geological sequence along strike from the Ulleskelf Mires survey site. The gypsum of the Billingham Anhydrite Formation may have sufficient mechanical integrity to give rise to a large contrast in acoustic impedance with the overlying Roxby Formation mudstones, resulting in a

strong reflection response. The signal from a geological interface with a positive reflection coefficient is typically a black-white-black seismic package. The Billingham gypsum bed is thin so the lower black leg from the Top Billingham reflection event may have been assimilated into the upper black leg of the reflection from the top of the Brotherton Limestone.

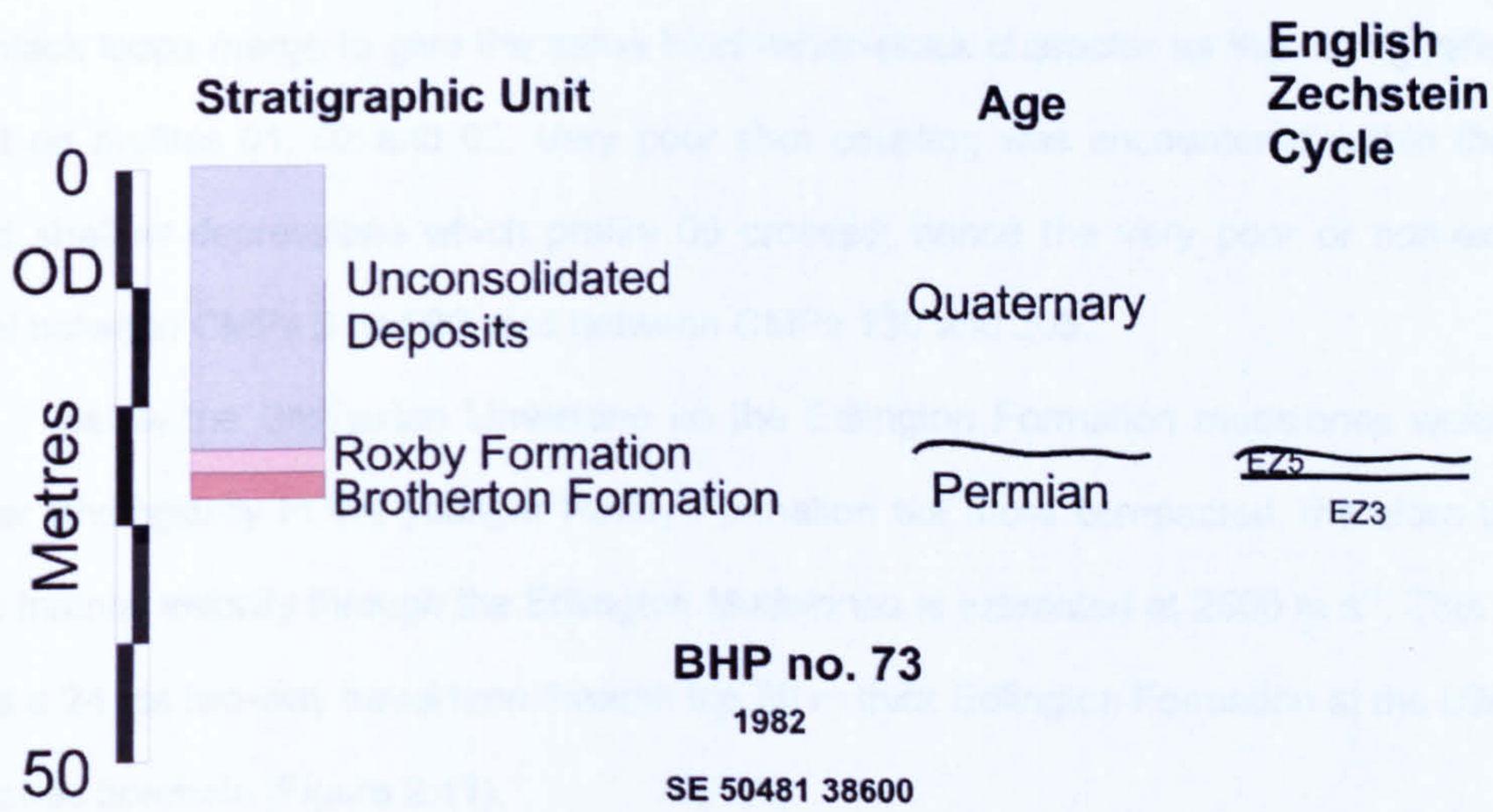

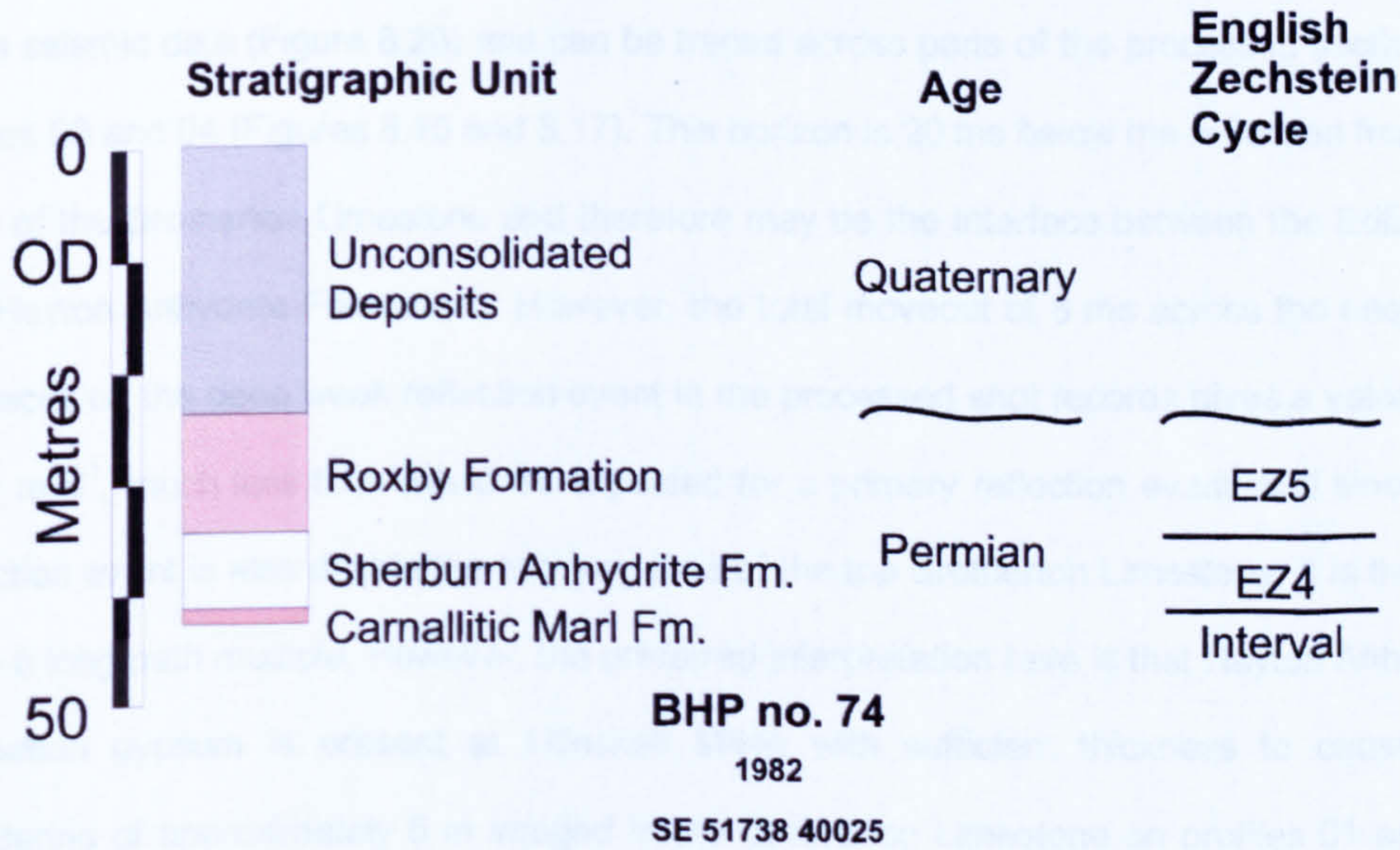

Figure 8.18: BHP 73 and 74 boreholes geological successions.

At the beginning of profile 04, the time difference of 4 ms between the first and second black legs is the approximate two-way time through the gypsum. This is equivalent to 7 m of gypsum assuming a P-wave interval velocity of 3500 m s^{-1} through the Billingham

Anhydrite Formation. The gypsum bed thickness is 5 m or less where the two upper black legs merge with each other.

The same triple black loop seismic reflection package is present at the intersection point of profile 04 (Figure 8.17) with the long profile 05 (Figure 8.19). At the extreme western end of profile 05 the Billingham Anhydrite Formation appears to thin out because the upper two black loops merge to give the same black-white-black character as the strong reflection event on profiles 01, 02 and 03. Very poor shot coupling was encountered within the two broad shallow depressions which profile 05 crossed; hence the very poor or non-existent signal between CMPs 9 and 80, and between CMPs 130 and 205.

Below the Brotherton Limestone lie the Edlington Formation mudstones which are similar lithologically to the younger Roxby Formation but more compacted, therefore the P-wave interval velocity through the Edlington Mudstones is estimated at 2500 m s^{-1}. This value yields a 24 ms two-way travel time through the 30 m thick Edlington Formation at the Ulleskelf Nurseries borehole (Figure 2.11).

Weak reflection events are present at 70 ms in some shot records from the Ulleskelf Mires seismic data (Figure 8.20) and can be traced across parts of the processed sections of profiles 03 and 04 (Figures 8.15 and 8.17). This horizon is 20 ms below the reflection from the base of the Brotherton Limestone and therefore may be the interface between the Edlington and Hayton Anhydrite Formations. However, the total moveout of 8 ms across the near and far traces on the deep weak reflection event in the processed shot records gives a velocity of 1720 m s^{-1}, much less than would be expected for a primary reflection event, and since this reflection event is also double the two-way time of the top Brotherton Limestone, it is thought to be a long-path multiple. However, the preferred interpretation here is that Hayton Anhydrite Formation gypsum is present at Ulleskelf Mires with sufficient thickness to cause the foundering of approximately 5 m imaged in the Brotherton Limestone on profiles 01 and 03 (Figures 8.14 and 8.15).

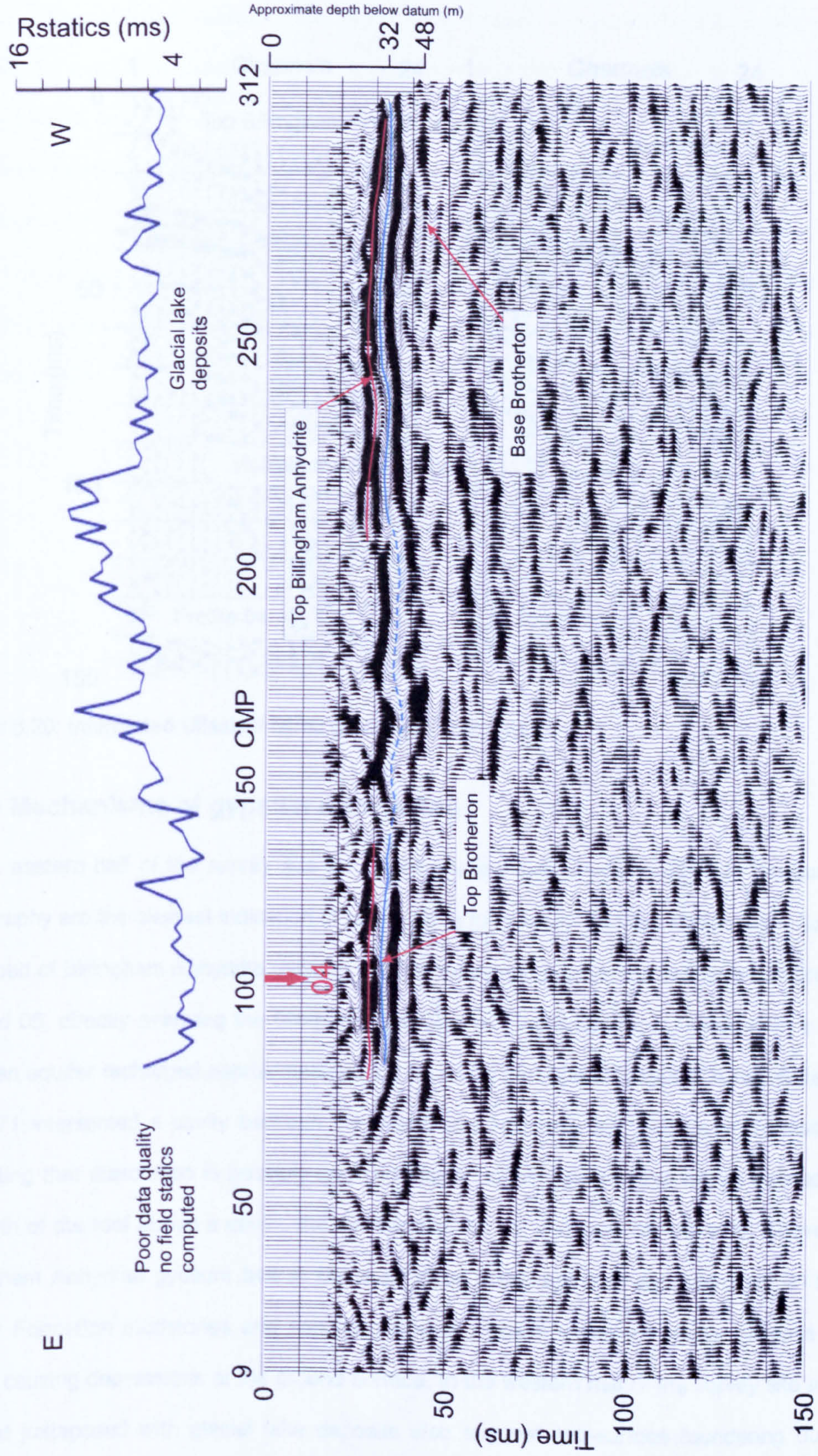

Figure 8.19: Interpreted final time migrated section of Ulleskelf Mires profile 05.
The section is displayed with a scalar multiplier.

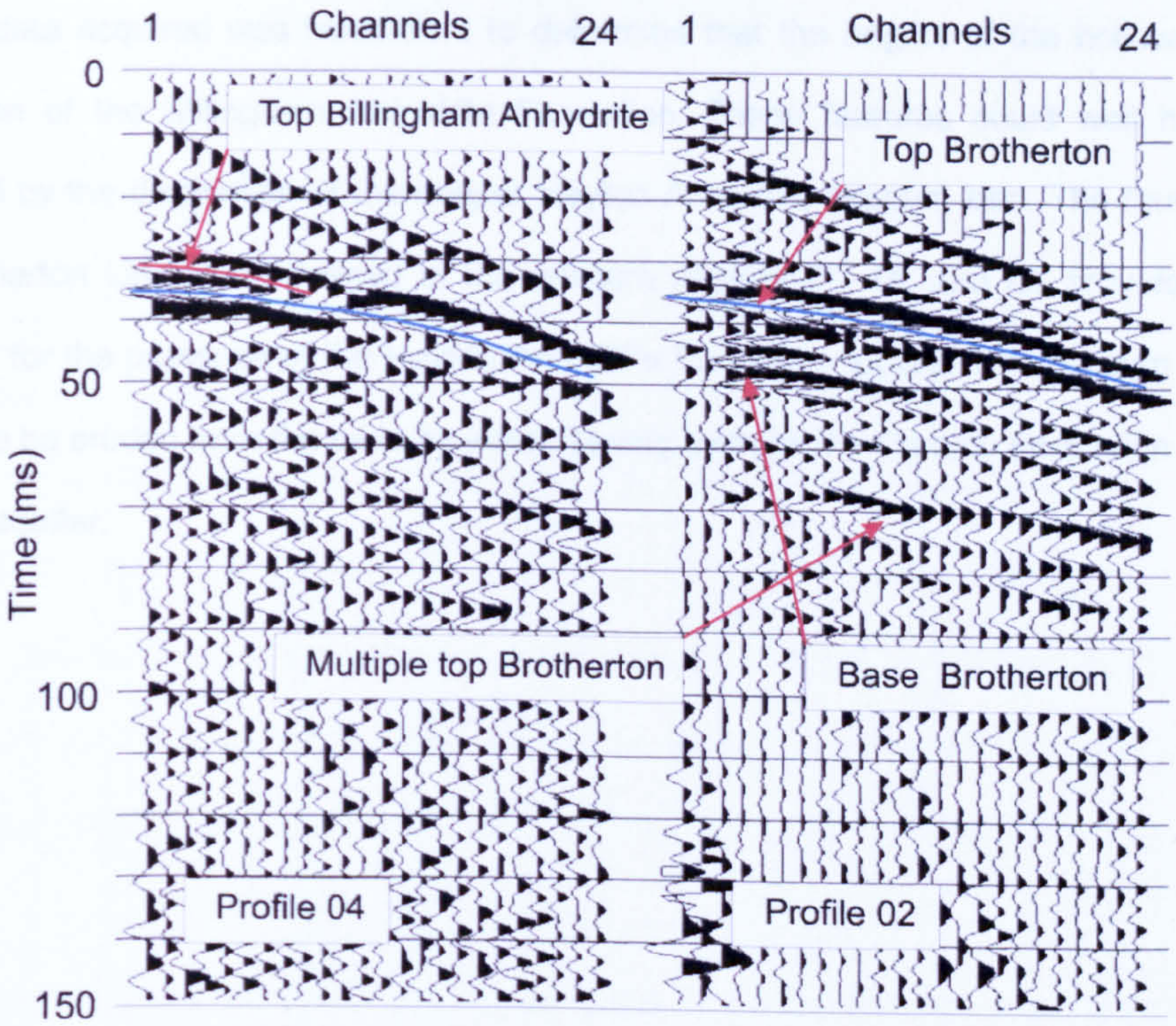

Figure 8.20: Interpreted Ulleskelf Mires processed shot records.

8.4.3 Mechanisms of gypsum dissolution

In the eastern half of the survey site the broad shallow sub-circular hollows in the surface topography are the clearest indication of sub-surface foundering. At this location a 5 m to 7 m thick bed of Billingham Anhydrite gypsum at 30 m below ground surface is imaged on profiles 04 and 05, directly overlying the Brotherton Limestone. The Brotherton Limestone is a local artesian aquifer recharged approximately 3 km up dip to the west of Ulleskelf Mires. Borehole BHP 71 intersected a cavity between the Billingham Anhydrite and Brotherton formations, indicating that dissolution is possibly ongoing locally. When gravitational forces exceed the strength of the roof above a cavity, the overlying strata will collapse into the void. Above the Billingham Anhydrite gypsum bed at Ulleskelf Mires, there are only approximately 25 m of Roxby Formation mudstones and soft glacial lake deposits which will easily collapse into voids, causing depressions at the ground surface. In the western half of the survey site areas of peat juxtaposed with glacial lake deposits also suggest sub-surface foundering due to Billingham Anhydrite that is now absent or very thin in profiles 01, 02 and 03.

Although broad shallow depressions were crossed by profile 05, the quality of the seismic data acquired was insufficient to determine that the origins of the hollows are due dissolution of the Billingham Anhydrite Formation. These features could well have been produced by the dissolution of the deeper Hayton Anhydrite gypsum bed. The foundering of the Brotherton Limestone imaged in the western profiles 01, 02 and 03 provides indirect evidence for the presence of the Hayton Anhydrite Formation locally. This gypsum formation is likely to be eroded from the base by water flowing through the Cadeby Formation limestone artesian aquifer.

9.0 Ure Bank

9.1 Site description

Ure Bank [SE 3164 7332] is 1.5 km north-east of the city centre of Ripon and is an area of gently undulating ground bordered to the west and north by the River Ure and an escarpment of Triassic Sherwood Sandstone to the east (Figure 9.1). Springs emanate from the base of the scarp slope, fed by water from the Sherwood Sandstone aquifer. Ure Bank is managed by Harrogate District Council and has a dual purpose. It is used as pastureland for sheep and cattle and as a local recreational area. There are several large rafts of concrete embedded in the ground surface across Ure Bank; these are the floors of former buildings in a WWII transit camp.

The course of the River Ure at this point is rapidly shifting and the river commonly floods the survey area during the winter months so the near-surface deposits are alluvial (Figure 2.14). Onsite is the River Ure Floodplain borehole which proves 33 m of sand and gravel deposits with a little silt and clay (Figure 9.2).

The River Ure Floodplain borehole proves that the unconsolidated deposits rest directly on top of an 8 m bed of gypsum, belonging to the Hayton Anhydrite Formation. Two cavities logged within Quaternary sands in the borehole may be voids that initially developed in the gypsum by dissolution processes and are now migrating to the surface. On the higher ground, above the escarpment, the Burtree Caravan Park borehole proved a 32 m thick bed of gypsum (Figure 2.15). Ure Bank is an active subsidence area. The 3 m diameter, 2 m deep hole by the access gate (Figure 9.1) was noted by Thompson et al. (1996). On the football field at the northern end of Ure Bank a freshly infilled 10 m diameter depression was found and a 1 m diameter shallow hollow appeared nearby during the period of this project. Several large hollows next to the dismantled railway line at the top of the escarpment are visible on aerial photographs (Figure 9.1). The cavities that generated these features must have been large to cause the collapse of the overlying bed of Sherwood Sandstone.

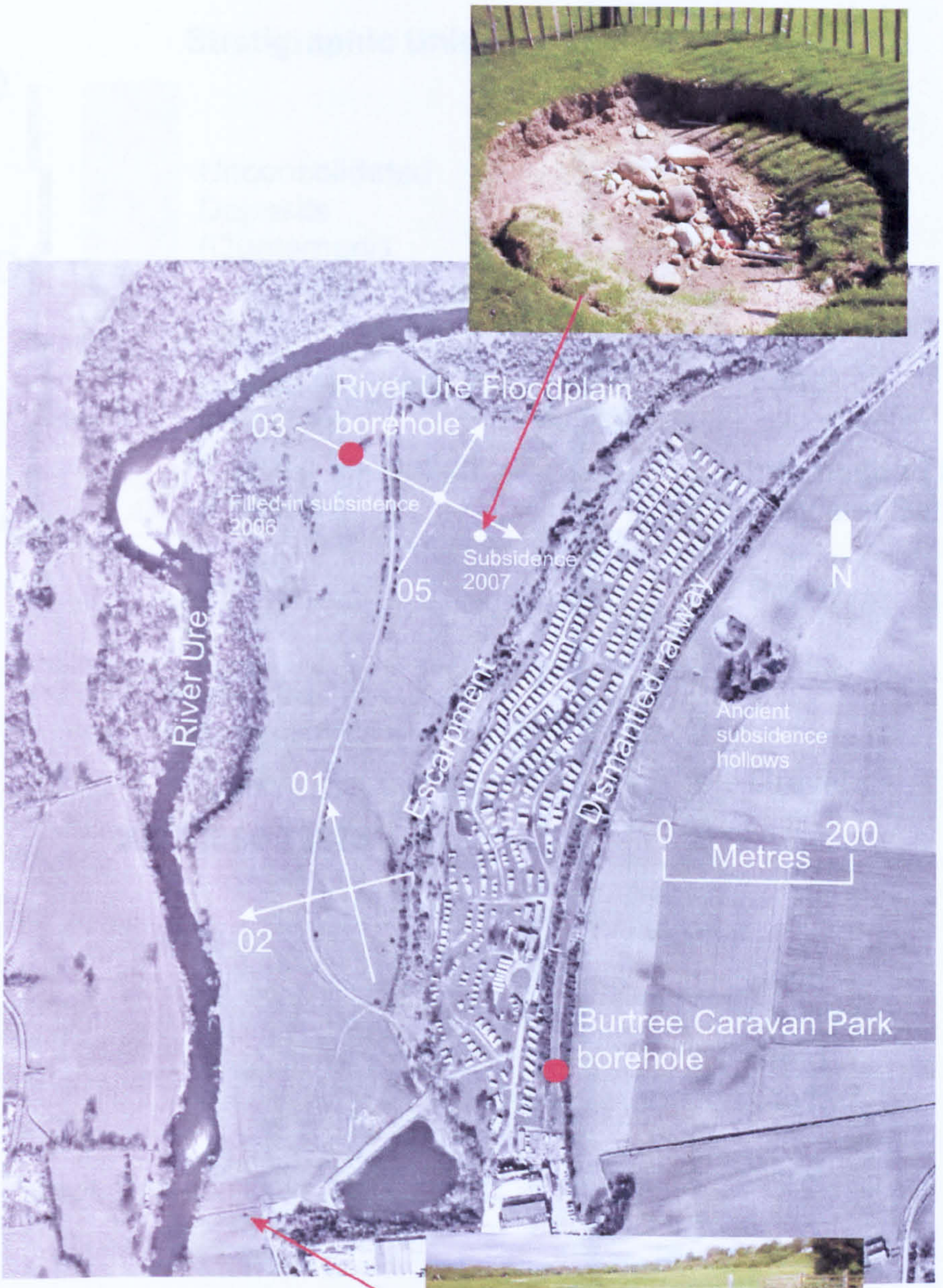

Figure 9.1: Aerial photograph taken in 1994 of the Ure Bank survey site.
Pictures showing two subsidence features on this very active site.

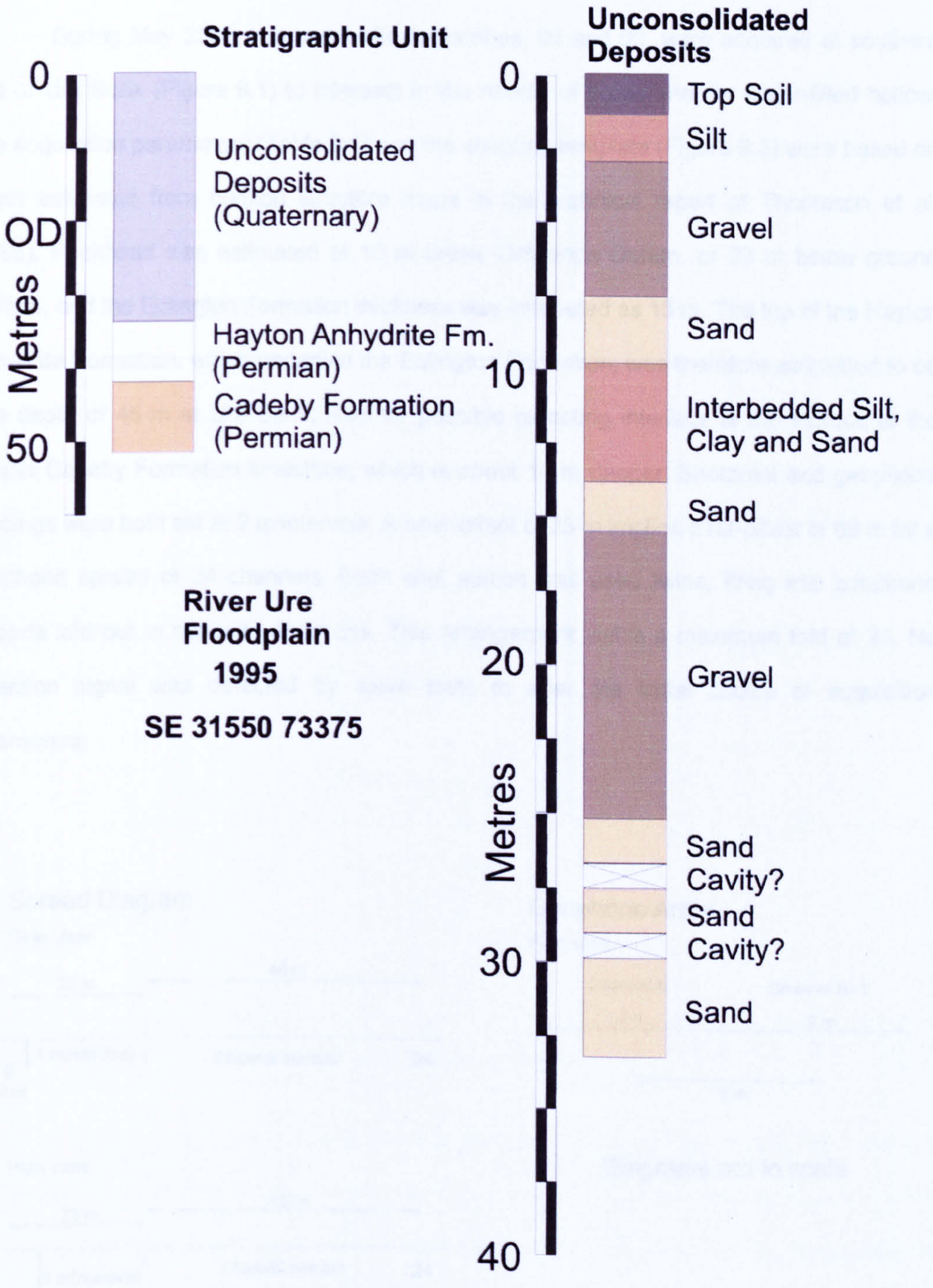

Figure 9.2: River Ure Floodplain borehole geological succession.
The unconsolidated deposits have been expanded to show the Quaternary layers.

9.2 Acquisition

During May 2006, two perpendicular profiles, 01 and 02, were acquired at southern end of Ure Bank (Figure 9.1) to intersect in the middle of broad shallow water-filled hollow. The acquisition parameters (Table 9.1) and the shooting template (Figure 9.3) were based on depth estimates from horizon structure maps in the technical report of Thompson et al. (1996). Rockhead was estimated at 10 m below Ordnance Datum, or 30 m below ground surface, and the Edlington Formation thickness was estimated as 15 m. The top of the Hayton Anhydrite Formation, which underlies the Edlington Formation, was therefore estimated to be at a depth of 45 m at Ure Bank. Another possible reflecting interface is top surface of the deeper Cadeby Formation limestone, which is about 10 m deeper. Shotpoint and geophone spacings were both set at 2 m intervals. A near-offset of 23 m implies a far-offset of 69 m for a geophone spread of 24 channels. Each shot station was used twice, firing into geophone spreads laid out in opposite directions. This arrangement yields a maximum fold of 24. No reflection signal was detected by wave tests to alter the initial choice of acquisition parameters.

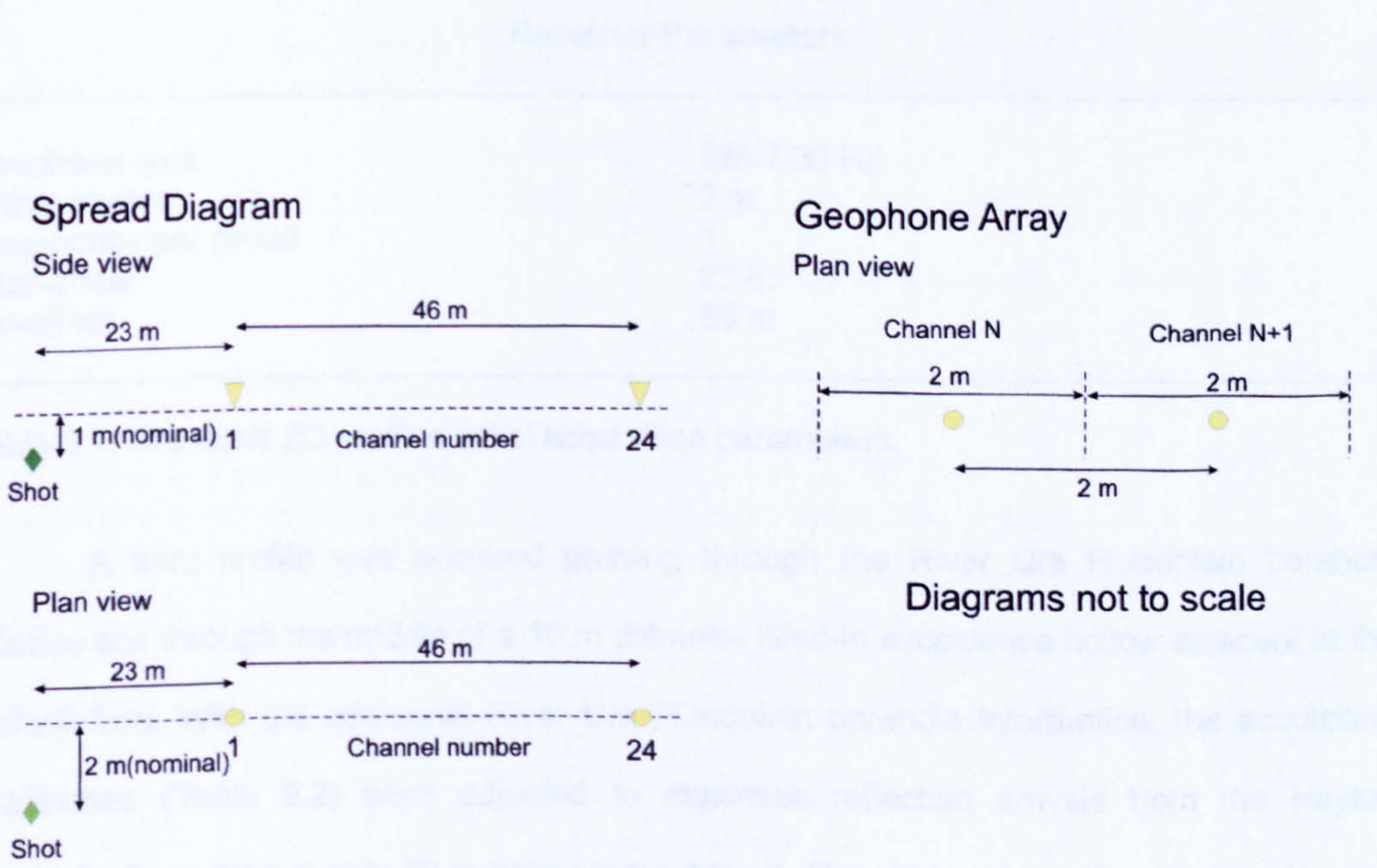

Figure 9.3: Ure Bank 2D profiles 01 and 02 shooting template.

Instrument Parameters	
Recording instrument	Geometrics SmartSeis S12
Format	SEG-2
Data channels	24
Pre A/D converter low-cut filter	10 Hz
Pre A/D converter high-cut filter	500 Hz
Sample interval	0.5 ms
Record length	512 ms
Delay	0 ms

Source Parameters	
Source type	Buffalo gun, 5 g black powder blanks
Shot interval	2 m
Shot depth	1 m
Shot in-line skid relative to geophones	1 m
Shot cross-line offset relative to geophones	2 m
Off-end shooting arrangement, forward and reverse shots to simulate symmetric split-spread.	
All shot holes tamped with water before firing.	

Receiver Parameters	
Geophone type	SM-7/30 Hz
Group interval	2 m
Geophones per group	1
Near-offset	23 m
Far-offset	69 m

Table 9.1: Ure Bank 2D profiles initial acquisition parameters.

A third profile was acquired passing through the River Ure Floodplain borehole location and through the middle of a 10 m diameter filled-in subsidence hollow adjacent to the football field. With the additional River Ure Floodplain borehole information, the acquisition parameters (Table 9.2) were adjusted to maximise reflection arrivals from the Hayton Anhydrite Formation at only 30 m below ground level. The shot and geophone intervals were kept the same at 2 m, but the geophone spread was altered to a symmetrical split-spread with only 12 active receivers to each side of the shot point and a short near-offset of 13m (Figure 9.4) to capture a shallow reflection whilst minimising the effects of ground roll, air-wave and refraction arrivals. Fold of coverage was therefore reduced to 12.

Profile 05 was acquired in 2007 perpendicular to profile 03 through the filled-in subsidence hollow with small adjustments to the acquisition parameters used on profile 03. The charge size was increased to 7 g yachting blanks, the shot point interval was increased to 4 m, reducing the fold of coverage to 6, and the shot holes were drilled to depths between 2 m and 2.5 m. Optical levelling measured the water table as 2.6 m deep at the filled-in subsidence hollow. It was not possible to drill the shot holes deeper than the water table because of a gravel bed.

Instrument Parameters	
Recording instrument	Geometrics SmartSeis S12
Format	SEG-2
Data channels	24
Pre A/D converter low-cut filter	10 Hz
Pre A/D converter high-cut filter	500 Hz
Sample interval	0.5 ms
Record length	512 ms
Delay	0 ms

Source Parameters	
Source type	Buffalo gun, 5 g black powder blanks
Shot interval	2 m
Shot depth	1 m
Shot in-line skid relative to geophones	1 m
Shot cross-line offset relative to geophones	2 m
Symmetrical split-spread shooting arrangement.	
All shot holes sprung with a dummy shot tamped with water before firing.	

Receiver Parameters	
Geophone type	SM-7/30 Hz
Group interval	2 m
Geophones per group	1
Near-offset	±13 m
Far-offset	±35 m

Table 9.2: Ure Bank 2D profile 03 acquisition parameters.

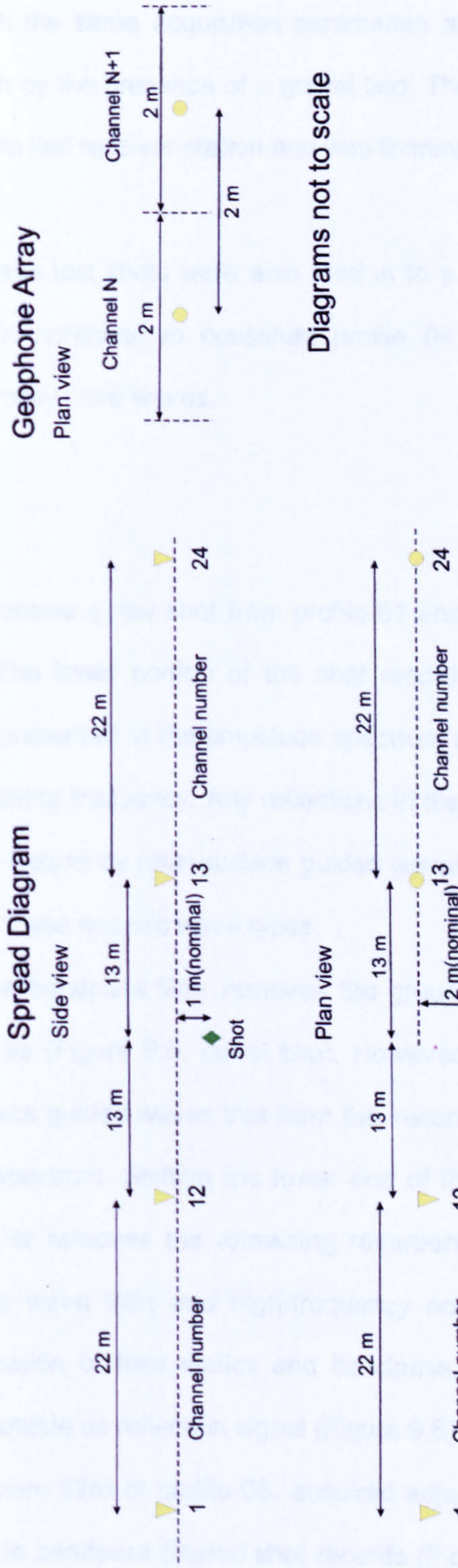

Figure 9.4: Ure Bank 2D profiles 03, 05 and 06 shooting template.

Profile 06 was acquired along part of the same line as profile 03, past the River Ure Floodplain borehole, with the same acquisition parameters as profile 05. Here, shot holes were limited to 1 m depth by the presence of a gravel bed. The total length of profile 06 was only 118 m from the first to last receiver station and was terminated close to the metalled road that bisects Ure Bank.

Several shear wave test shots were also fired in to a geophone spread laid next to the River Ure Floodplain borehole, to constitute profile 04. However, the records were swamped by very low-velocity Love waves.

9.3 Processing

Panel one in Figure 9.5 shows a raw shot from profile 01 and is typical of the seismic data collected at Ure Bank. The lower portion of the shot record is dominated by low-velocity dispersive ground roll, represented in the amplitude spectrum as a peak at 30 Hz which then rapidly decays with increasing frequency. Any reflections in the upper section of the raw shot record are hidden by low-frequency near-surface guided waves. A linear air-wave noise train is superimposed on all of these seismic wave types.

Applying a simple bandpass filter removes the ground roll signal and some of the near-surface guided waves (Figure 9.5, panel two). However, any reflection energy is still masked by the near-surface guided waves that form the secondary peak centred at 80 Hz in the raw shot amplitude spectrum. Shifting the lower end of the bandpass filter towards the high frequencies by 40 Hz removes the remaining reverberating guided wave signal, but leaves a strong air-wave wave train and high-frequency noise (Figure 9.5, panel three). Stacking after the application of field statics and bandpass filtering does not reveal any continuous events interpretable as reflection signal (Figure 9.6).

Only on the northern third of profile 05, acquired adjacent to the football field, were any reflections observed in bandpass filtered shot records (Figure 9.7). Because of the very limited extent of reflection signal found, only a stripped down processing sequence was applied to the seismic data collected at Ure Bank (Figure 9.8). The only sophisticated processing techniques applied were zero-phase spiking deconvolution and phase shift time

migration. Shot balancing was achieved simply with a 100 ms AGC sliding window. No residual statics were computed.

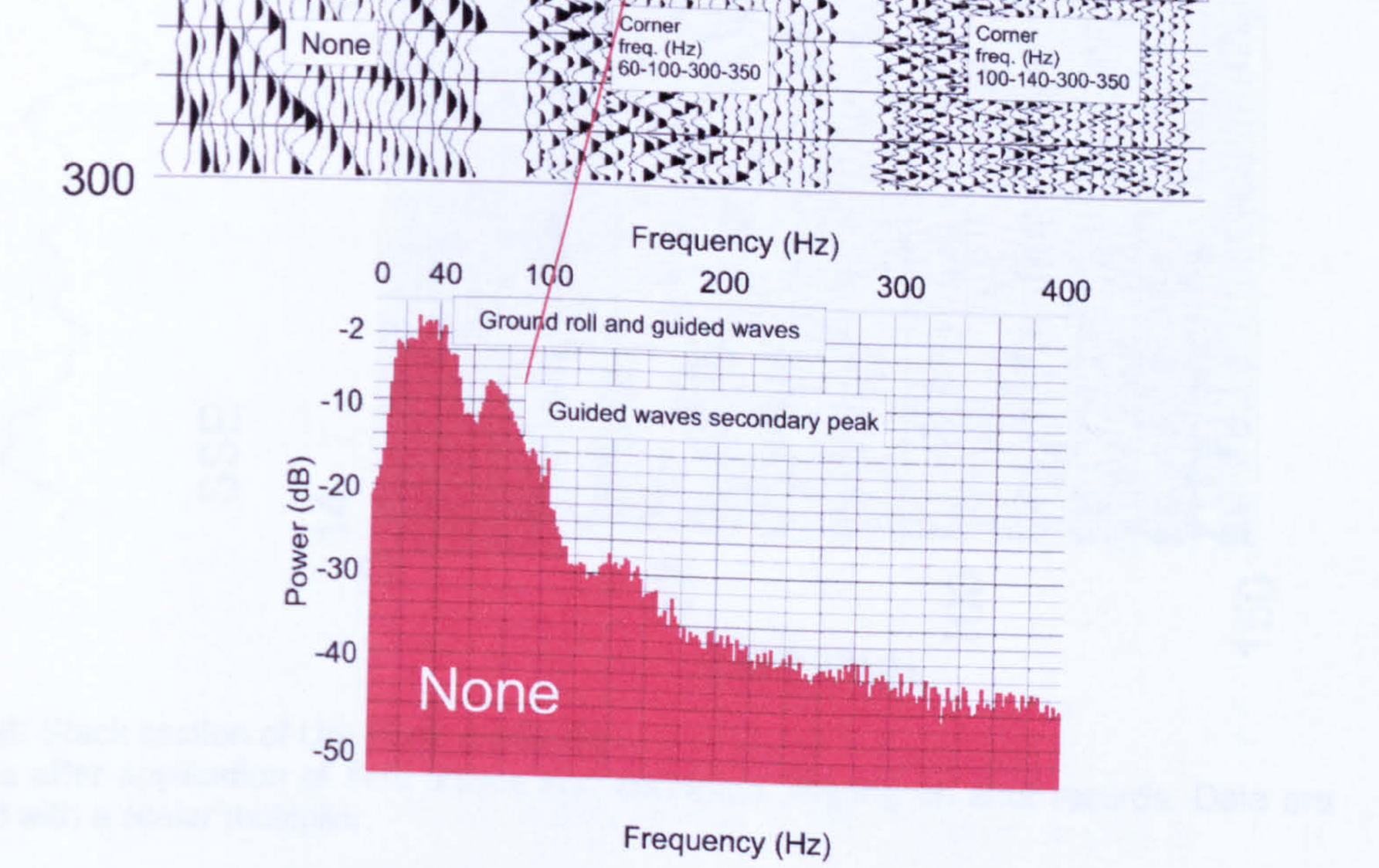

Figure 9.5: Typical shot record from Ure Bank profile 01.
The shot data are balanced with a 200 ms AGC window.

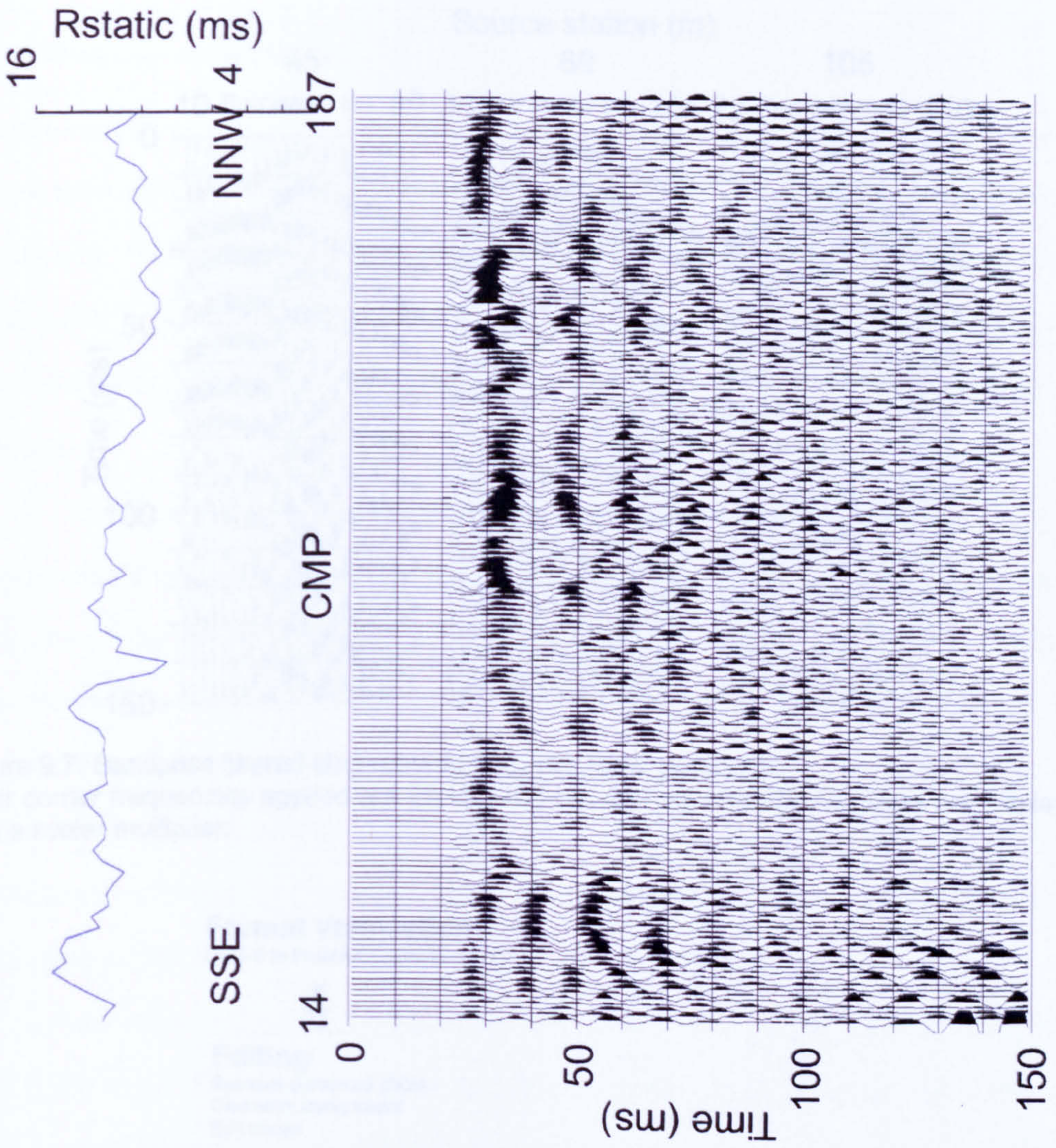

Figure 9.6: Stack section of Ure Bank profile 01.
Section is after application of field statics and bandpass filtering on shot records. Data are displayed with a scalar multiplier.

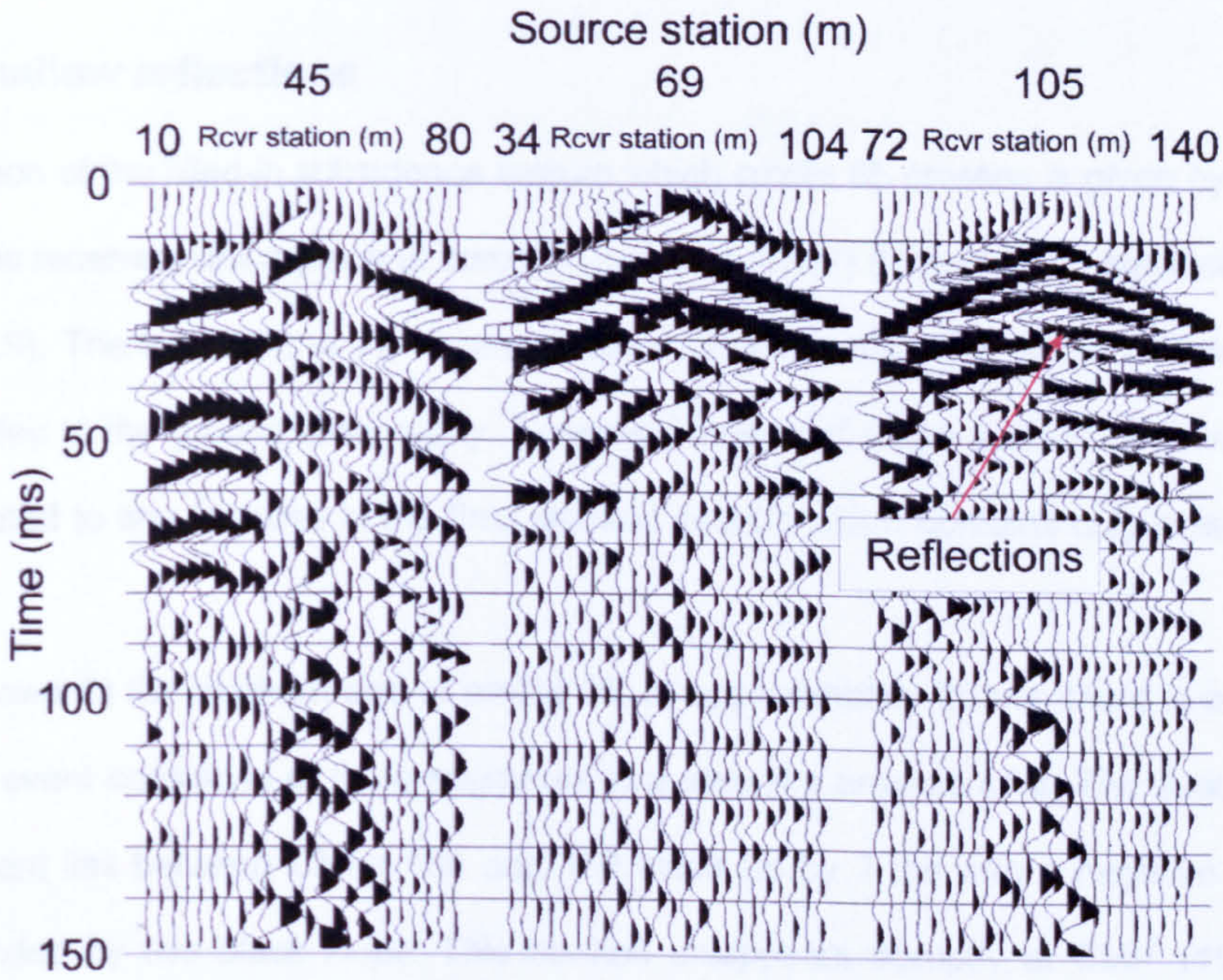

Figure 9.7: Bandpass filtered shot records from Ure Bank profile 05.
Filter corner frequencies applied are 60 Hz, 100 Hz, 330 Hz and 350 Hz. Data are displayed with a scalar multiplier.

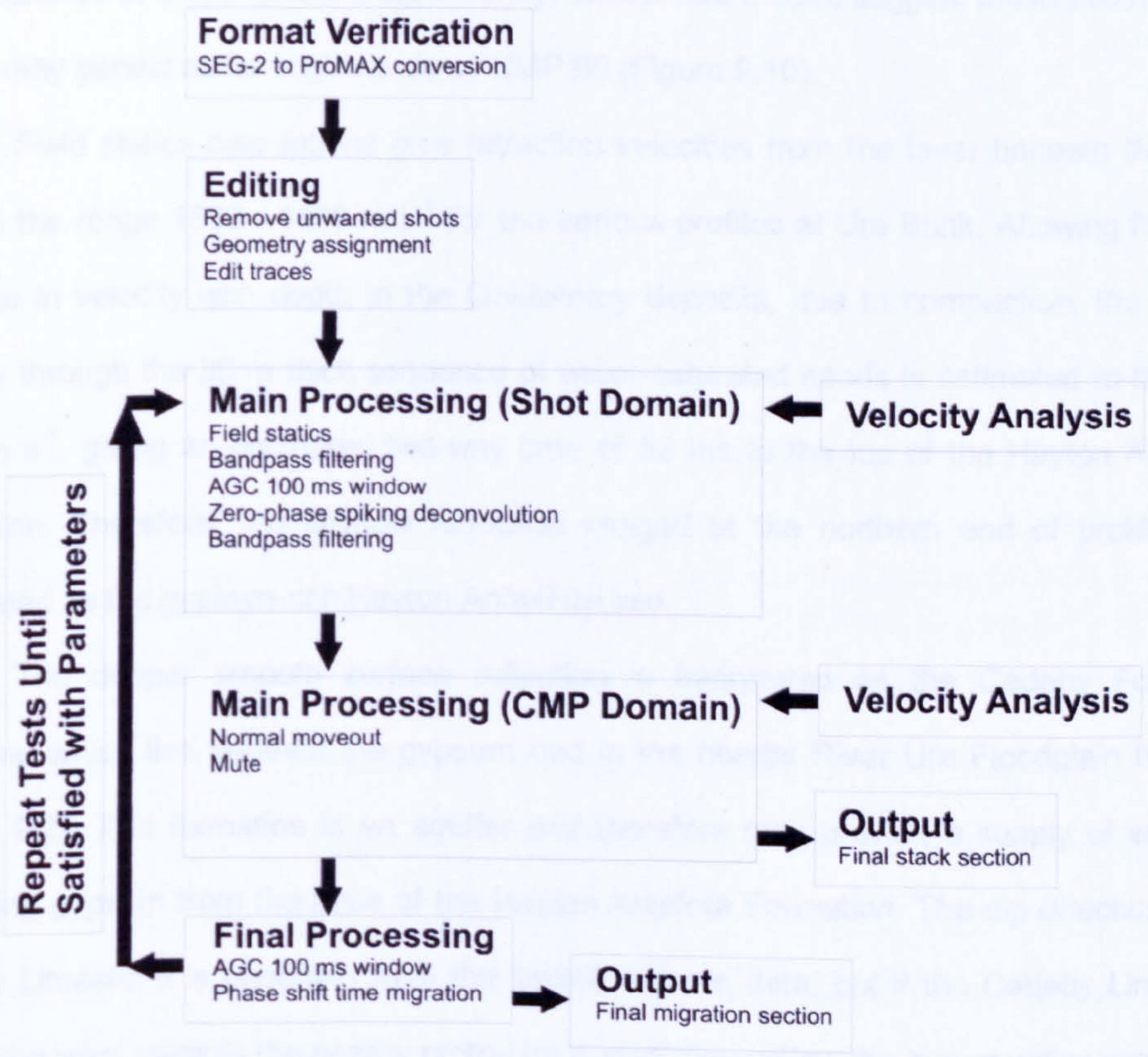

Figure 9.8: Ure Bank survey seismic data processing flow.

9.4 Interpretation

9.4.1 Shallow reflections

The position of the filled-in subsidence feature which profile 05 crosses is given by the sharp peak in the receiver statics graph at common midpoint (CMP) 94 in the final stack of profile 05 (Figure 9.9). The low point in the receiver statics near the start the profile coincides with a broad gulley in the ground topography. However, neither of these surface observations can be correlated to any features in the final stacked section which contains only noise at these locations.

Towards the northern end of profile 05, at approximately 30 ms, there is a disjointed reflection event consisting of three segments in a step-like arrangement. The middle section of this event lies between CMPs 135 and 150 steps up by 2 ms with a negative amplitude loop bounded by two black loops. This horizon disappears abruptly at CMP 115. Another more continuous but undulating weaker reflection event with a similar signal character is visible at 45 ms, and terminates around CMP 120. Time migration does not alter the characteristics of these horizons significantly, except that it does suggest these two reflection events may persist as far southwards as CMP 60 (Figure 9.10).

Field statics calculations give refraction velocities from the layer beneath the water table in the range 1500—1600 m s^{-1} for the various profiles at Ure Bank. Allowing for some increase in velocity with depth in the Quaternary deposits, due to compaction, the P-wave velocity through the 30 m thick sequence of water-saturated sands is estimated to be about 1800 m s^{-1}, giving an estimated two-way time of 33 ms to the top of the Hayton Anhydrite Formation. Therefore, the shallow reflection imaged at the northern end of profile 05 is interpreted as the gypsum-rich Hayton Anhydrite bed.

The deeper smooth surface reflection is interpreted as the Cadeby Formation limestone which lies beneath the gypsum bed in the nearby River Ure Floodplain borehole (Figure 9.2). This formation is an aquifer and therefore may provide a supply of water for dissolving gypsum from the base of the Hayton Anydrite Formation. The dip direction of the Cadeby Limestone is uncertain from the limited seismic data, but if the Cadeby Limestone dips to the west towards the nearby proto-Ure buried river valley, the buried valley may act as a sink for any dissolved gypsum. The Hayton Anhydrite gypsum is in direct contact with

highly permeable sand and gravel Quaternary deposits. Therefore, the variable nature of this surface shows that the Hayton Anhydrite Formation has likely been subject to dissolution processes at both the base and top surfaces of the gypsum bed.

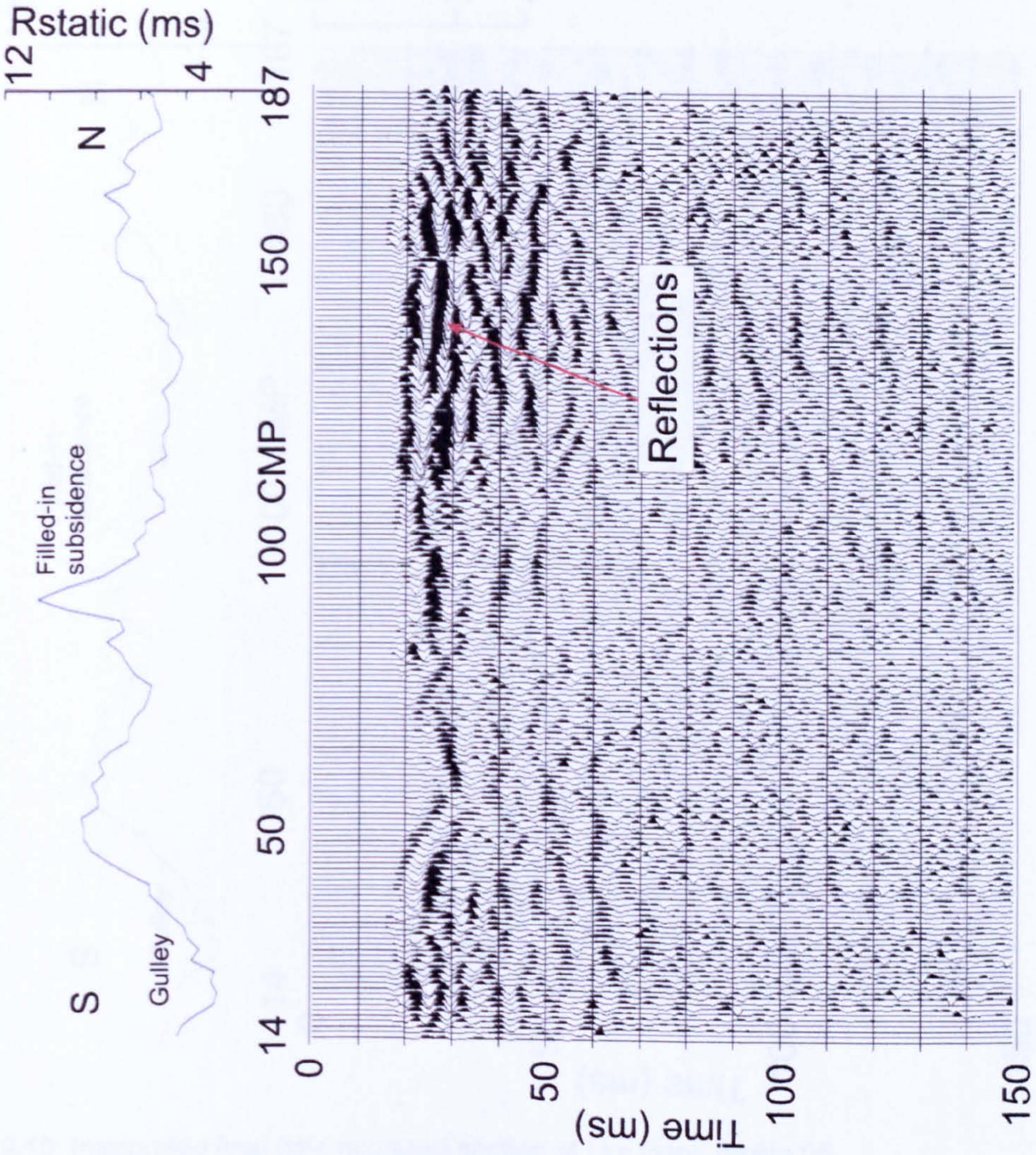

Figure 9.9: Final stack section of Ure Bank profile 05.
The distance between CMP traces is 1 m. The CMP numbering has been adjusted to represent the distance along the profile from the first receiver station. The section is displayed with a scalar multiplier.

Heavy infiltration by water of the Hayton Anhydrite gypsum bed will reduce the mechanical strength of the gypsum so that the P-wave interval velocity may be as low as 2000 m s^{-1} (e.g. Sheriff and Geldart, 1995). However, to produce a reflection event at Quaternary-Hayton Anhydrite interface at the northern end of profile 05 the gypsum must be compact and have a P-wave interval velocity greater than 2000 m s^{-1}.Therefore the time difference of 10 ms to 15 ms between the reflection events translates into the thickness of the

Hayton Anhydrite Formation being thicker at this location than the 8 m recorded in the River Ure Floodplain borehole.

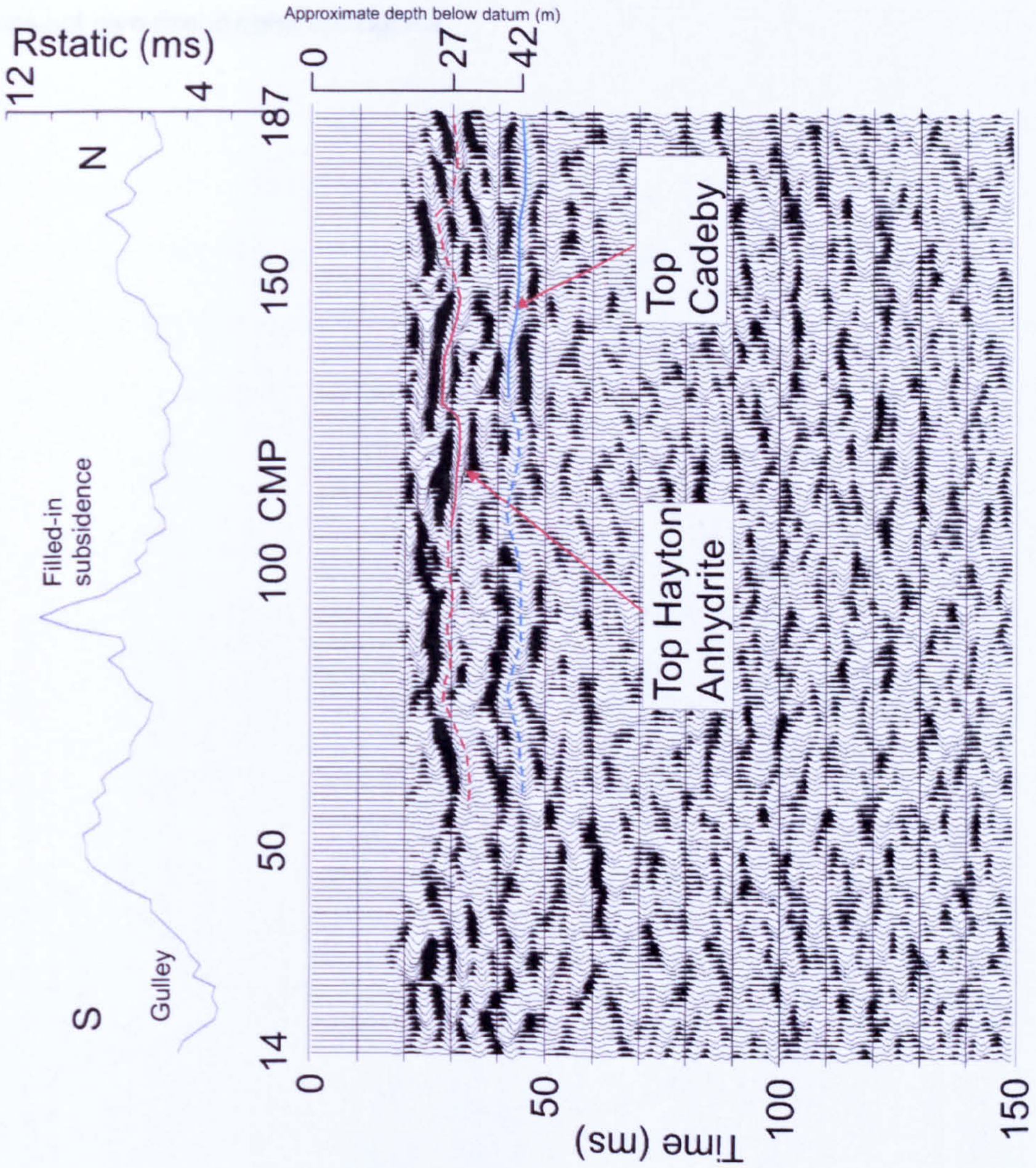

Figure 9.10: Interpreted final time migrated section of Ure Bank profile 05.
The section is displayed with a scalar multiplier.

At the southern end of profile 05, no coherent events are observed, just as for the other Ure Bank profiles. If the acoustic impedance contrast between the Quaternary deposits and the Hayton Anhydrite is not sufficient to produce an observable reflection, there might be expected to be a very strong acoustic impedance contrast between the Hayton Anhydrite and the Cadeby Limestone, giving rise to a strong reflection event. Bandpass filter tests show that no coherent reflection signals are observed in any frequency range on most of the profiles at Ure Bank (Figure 9.5). Possibly the seismic velocity is gradational through the Hayton

Anhydrite, such that the acoustic impedance contrasts at the top and base are both small. In addition, the Hayton Anhydrite bed may be extremely inhomogeneous in terms of water content and seismic velocity such that incident seismic energy is scattered in all directions and does not give rise to coherent signals.

10.0 Hutton Hill

10.1 Site description

The Hutton Hill survey site [SE 3288 7248] is located in a slight depression in the terrain in the higher ground surrounding Ripon, 2.5 km north-east of the city centre. Thompson et al. (1996) highlighted the hollow as a potential gypsum dissolution feature. The ground surface is at an elevation of approximately 45 m above Ordnance Datum (Figure 10.1), and the water table is at a depth of approximately 25 m.

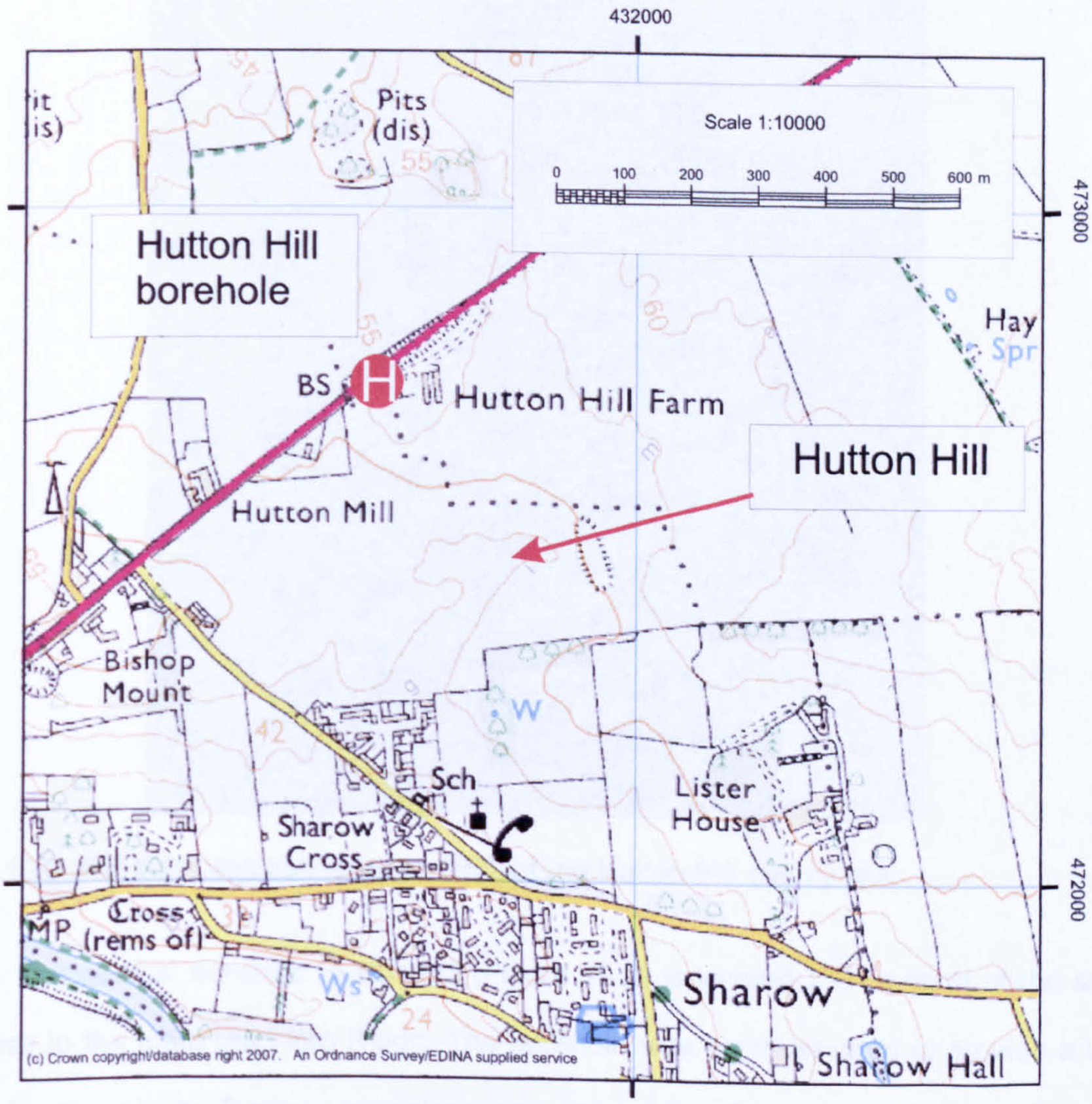

Figure 10.1: Ordnance Survey map of Hutton Hill.
Data supplied by Ordnance Survey/EDINA service © Crown Copyright Database 2007.

Only a single 2D seismic profile was acquired at Hutton Hill (Figure 10.2), crossing the shallow broad hollow in very open farm ground that was in stubble at the time of the survey. The topsoil has a red-brown soil colour hinting at the presence of the Triassic Sherwood Sandstone Group at rockhead (Figure 2.13). The central part of the target depression was waterlogged, even though the landowner had recently installed land drains to try to improve the soil drainage.

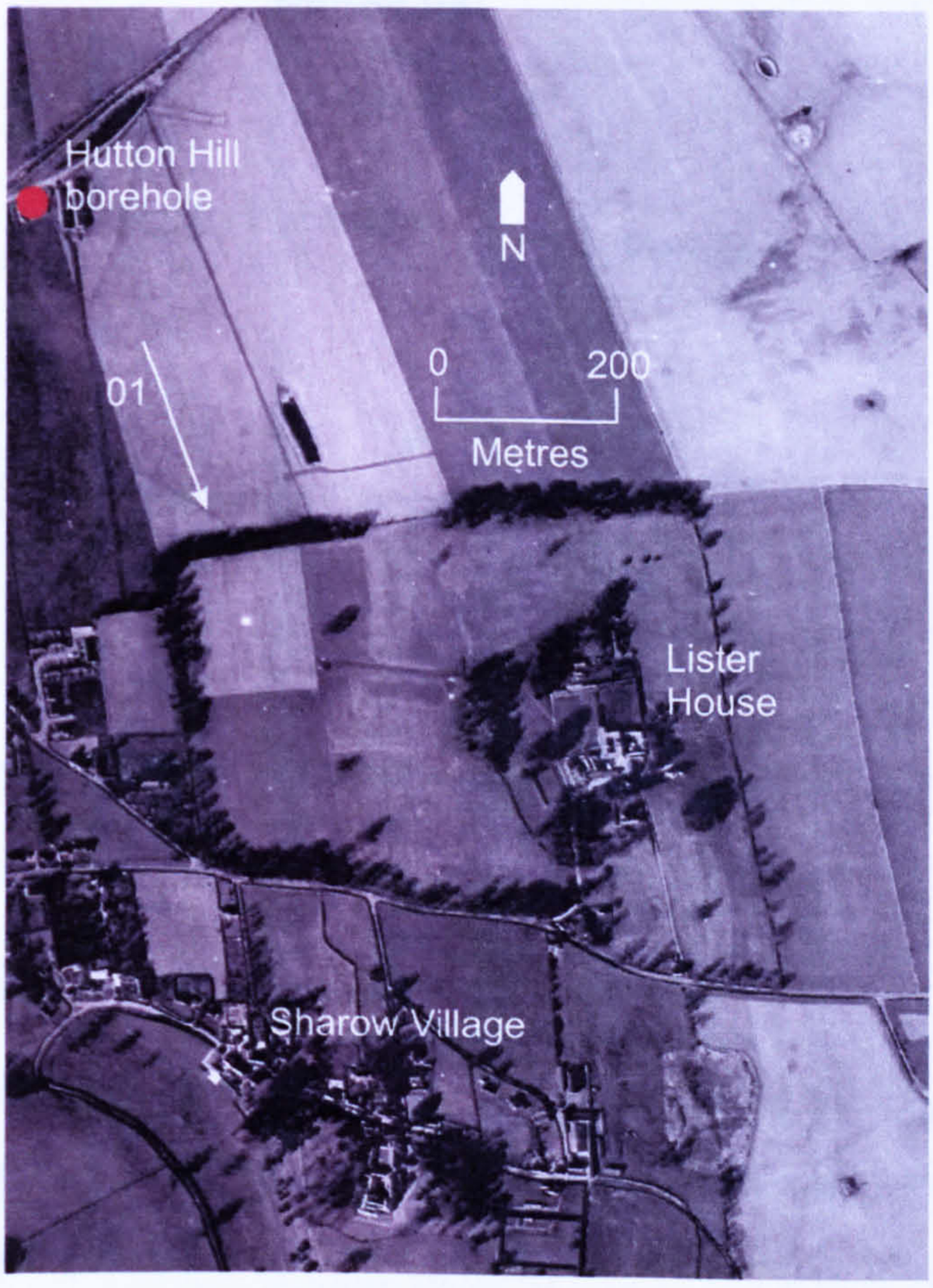

Figure 10.2: Aerial photograph taken in 1972 of the Hutton Hill survey site.

The nearest borehole Hutton Hill (Figure 10.3) is located 250 m north of the survey site close to the main road into Ripon. The borehole was commissioned to provide a water supply for the nearby farming operations and proved the Brotherton Formation limestone artesian aquifer at 75 m below the ground surface. No significant beds of gypsum are reported in the driller's log.

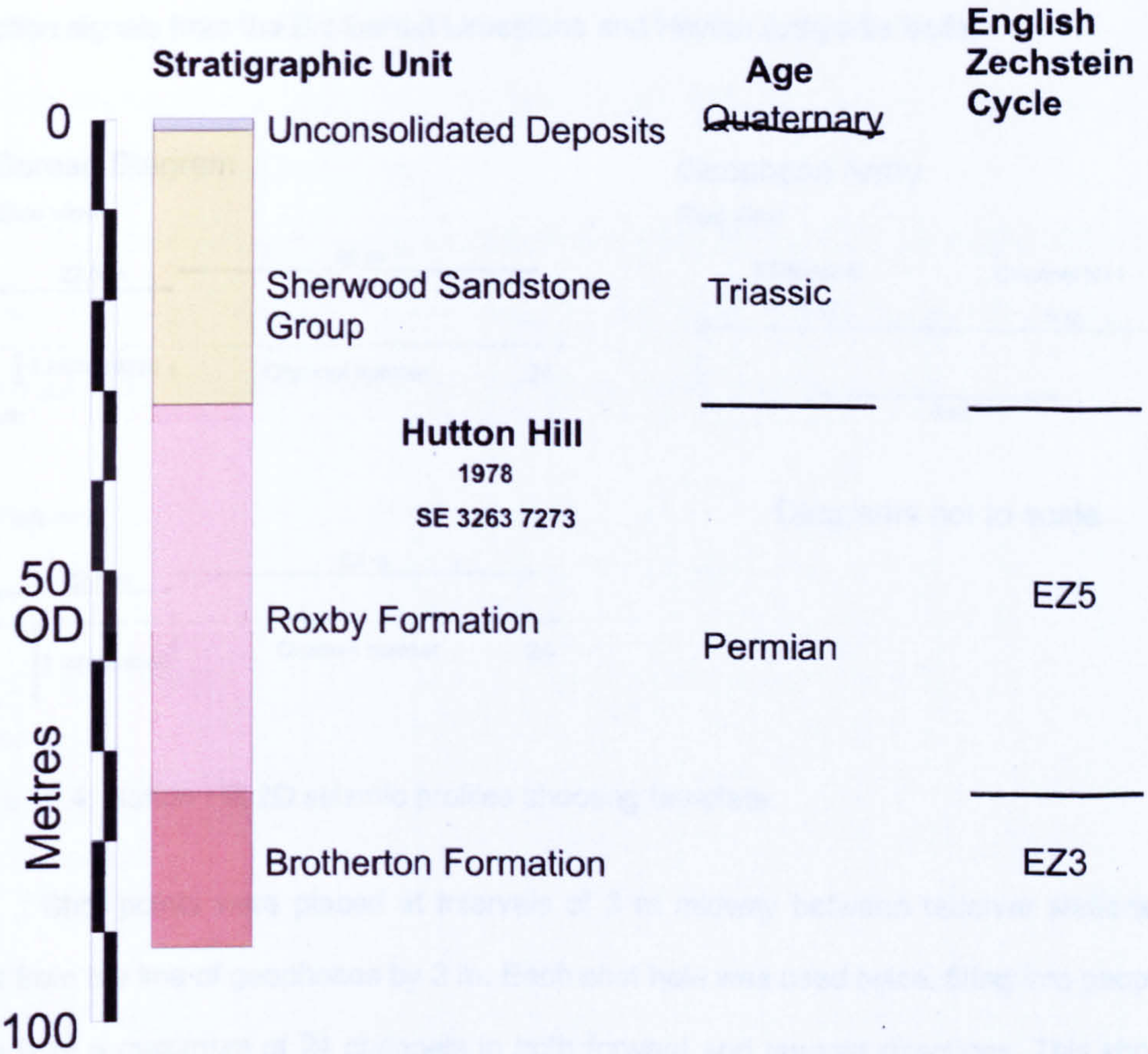

Figure 10.3: Hutton Hill borehole geological succession.

10.2 Acquisition and processing

From the log of the Hutton Hill borehole, it was anticipated that the first reflection event in the seismic data would be from the top of the limestone bed of the Brotherton Formation. Allowing for the difference in ground surface elevation between the borehole (56 m a.o.d.) and the seismic profile, it was estimated that the top of the Brotherton Limestone would be between 50 m and 60 m depth along the seismic profile. In the general geological succession of Ripon (Table 2.3), the Hayton Anhydrite Formation is below and separated from the Brotherton Limestone by the Edlington Formation mudstones. The Edlington-Hayton Anhydrite geological boundary, a potential reflecting interface, may be up to 100 m below ground surface at Hutton Hill. Therefore, the geophone station spacing was set to 3 m with a near offset of 22.5 m and

a far offset of 91.5 m for a 24-channel geophone spread (Figure 10.4) to adequately capture reflection signals from the Brotherton Limestone and Hayton Anhydrite beds.

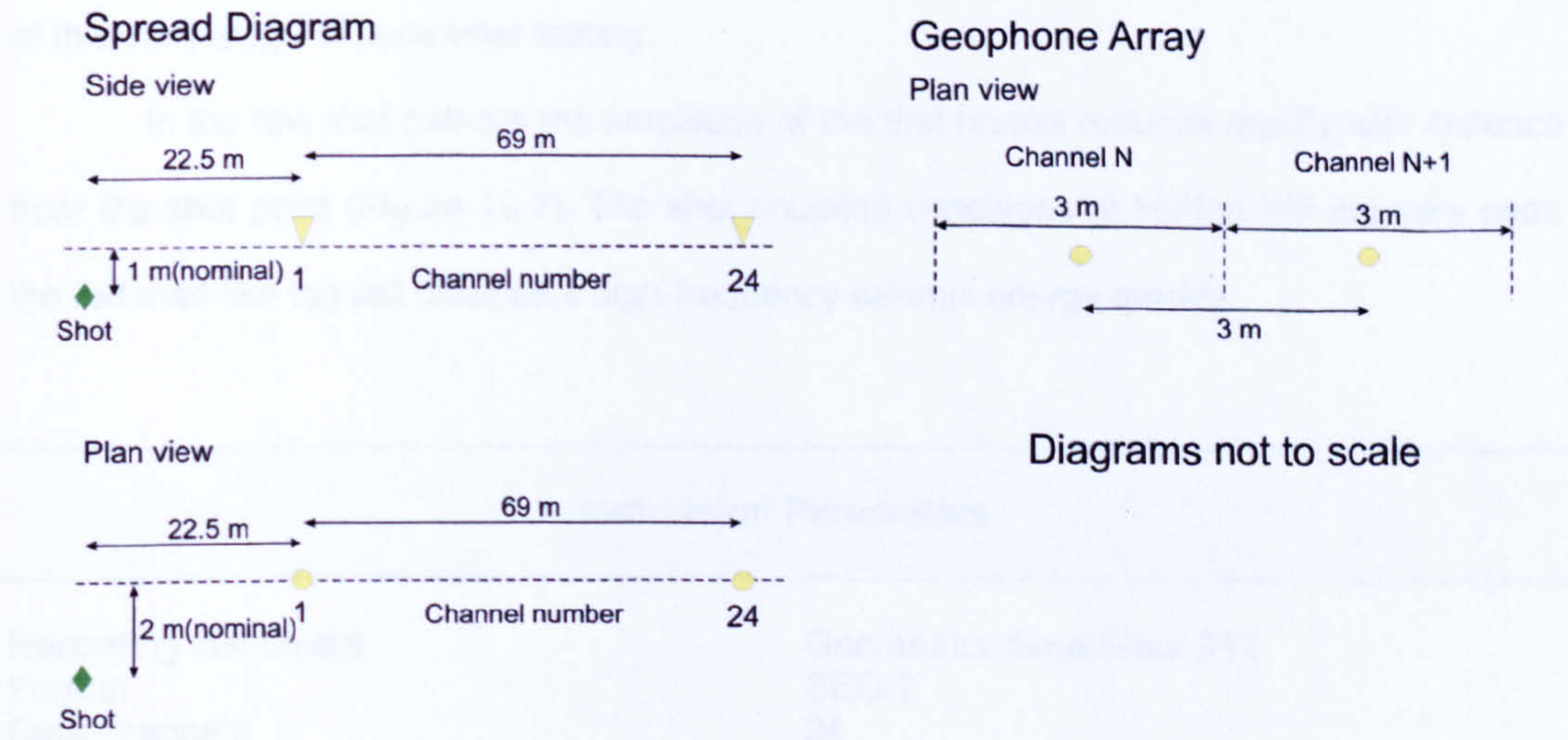

Figure 10.4: Hutton Hill 2D seismic profiles shooting template.

Shot points were placed at intervals of 3 m midway between receiver stations and offset from the line of geophones by 2 m. Each shot hole was used twice, firing into geophone spreads of a maximum of 24 channels in both forward and reverse directions. This shooting configuration satisfies the stack array criterion and yields a maximum fold of coverage of 24. No reflection signal was observed in wave tests to alter the acquisition parameters (Table 10.1) selected by considering the stratigraphy.

The first receiver station at the northern end of profile 01 was positioned by compass sightings on features such as field boundaries marked on the Ordnance Survey map. Manual compass readings have an accuracy of 1°, so to minimise errors sightings were taken on targets within 300 m over a wide spread bearings. The distance of the last receiver station, at the southern end of profile 01, from the hedge at the southern field boundary was measured along the bearing of the profile; and the distance was then measured between the intersection point with the hedge and a right-angled corner of the hedge.

The raw shots acquired at profile 01 Hutton Hill are dominated by large amplitude ground roll (Figure 10.5, upper panel). No hyperbolic reflection events are visible. Bandpass filtering removed the ground roll leaving linear high-frequency air-wave trains that overlap with the refraction arrivals on the near channels (Figure 10.5, lower panel). There are no coherent

reflection events present in the filtered shot gathers, but only high-frequency random noise. A stacked section after application of filtering and field statics shows no evidence of any reflection events (Figure 10.6). Digital processing of the Hutton Hill seismic data was aborted at this early stage of parameter testing.

In the raw shot gathers the amplitude of the first breaks reduces rapidly with distance from the shot point (Figure 10.7). The shot coupling conditions at Hutton Hill are very poor; the red marl-like top soil dissipates high-frequency seismic energy quickly.

Instrument Parameters	
Recording instrument	Geometrics SmartSeis S12
Format	SEG-2
Data channels	24
Pre A/D converter low-cut filter	10 Hz
Pre A/D converter high-cut filter	500 Hz
Sample interval	0.5 ms
Record length	512 ms
Delay	0 ms
Source Parameters	
Source type	Buffalo gun, 7 g black powder blanks
Shot interval	3 m
Shot depth	1 m
Shot in-line skid relative to geophones	1.5 m
Shot cross-line offset relative to geophones	2 m
Off-end shooting arrangement, forward and reverse shots to simulate symmetric split-spread.	
All shot holes tamped with water before firing.	
Receiver Parameters	
Geophone type	SM-7/30 Hz
Group interval	3 m
Geophones per group	1
Near-offset	22.5 m
Far-offset	91.5 m

Table 10.1: Hutton Hill 2D profiles acquisition parameters.

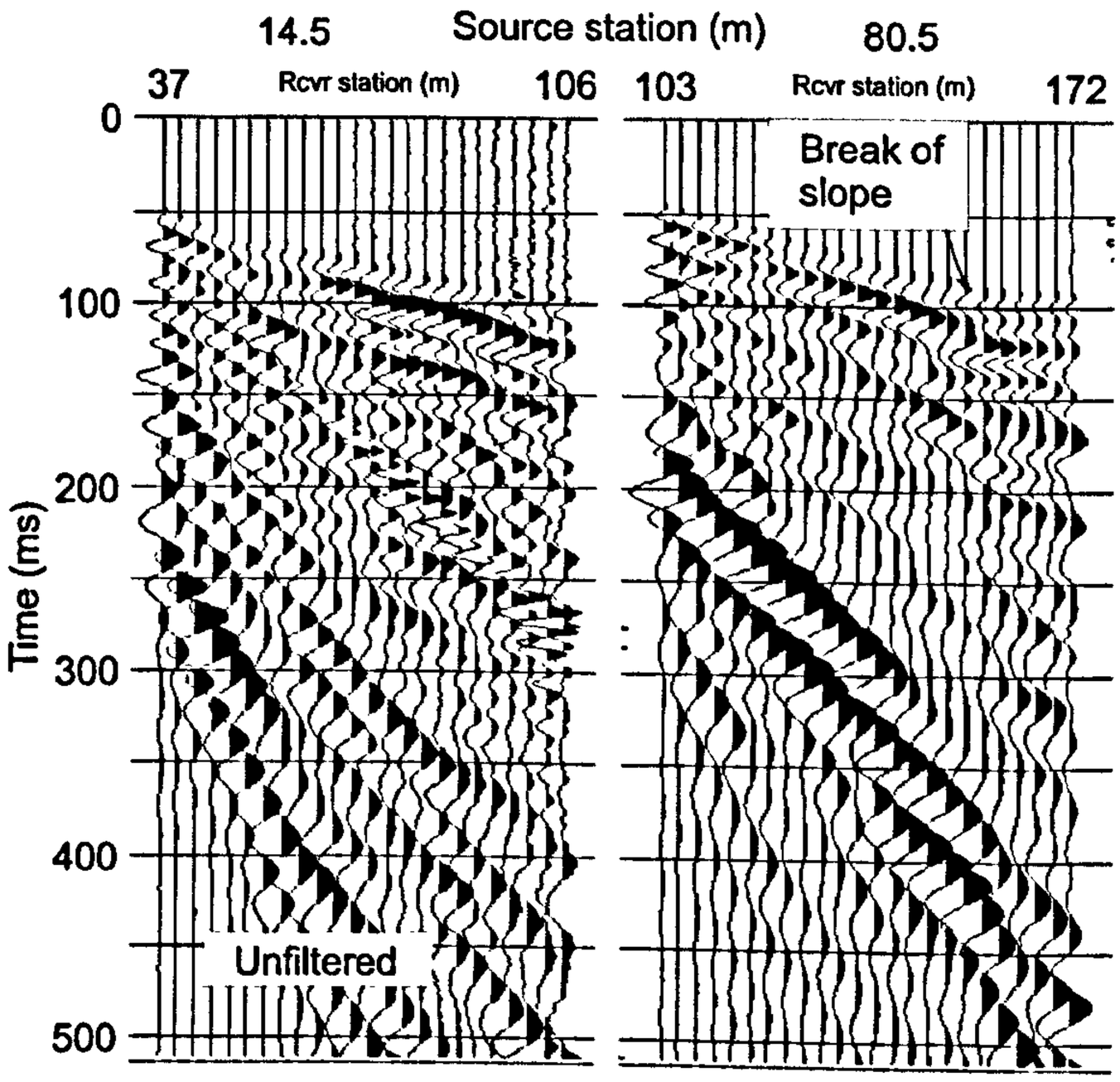

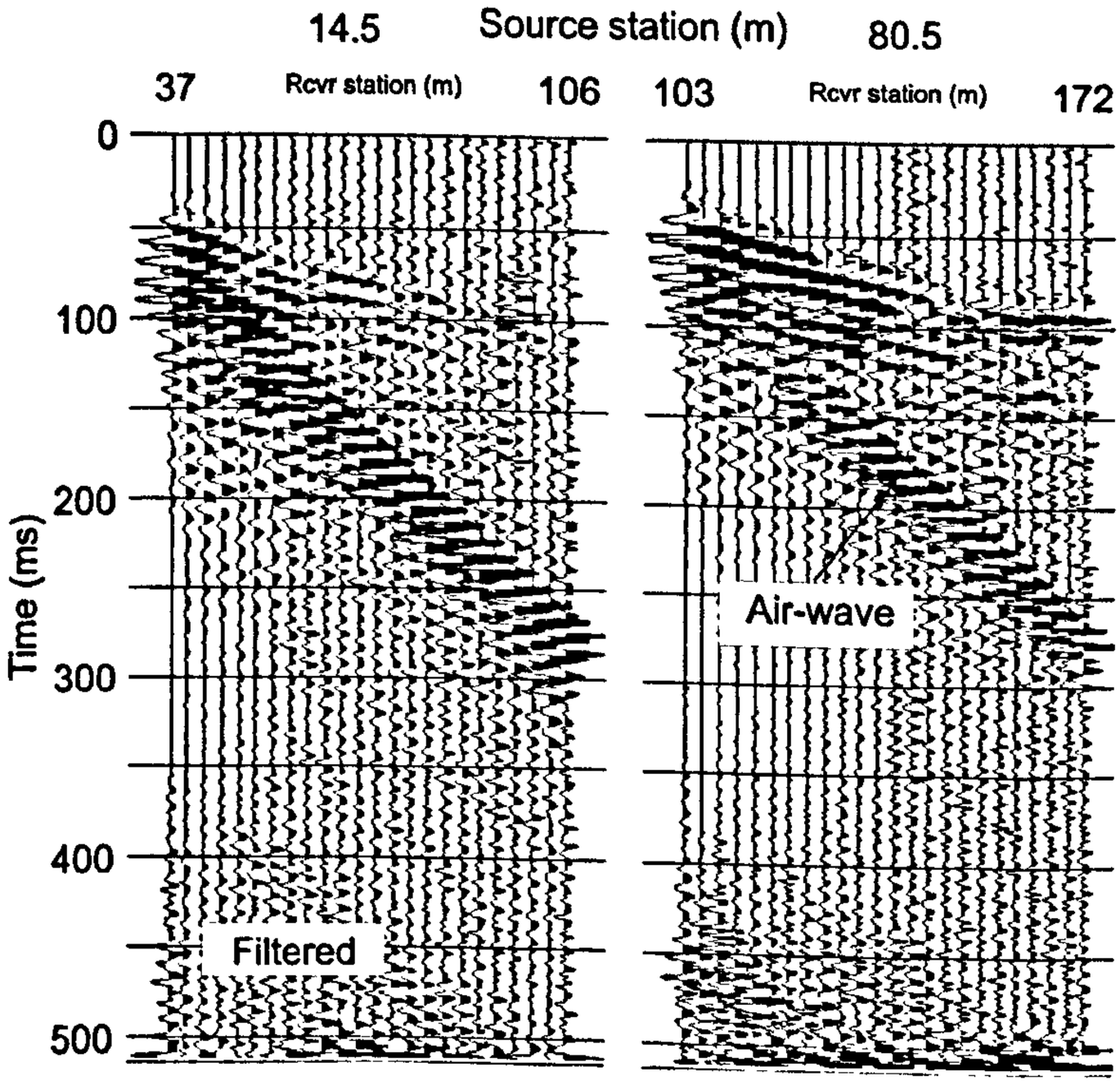

Figure 10.5: Raw and bandpass filtered Hutton Hill shot records.
Bandpass filter design applied with 60 Hz, 100 Hz, 330 Hz and 350 Hz corner frequencies.
The shots are displayed with a 200 ms AGC sliding window.

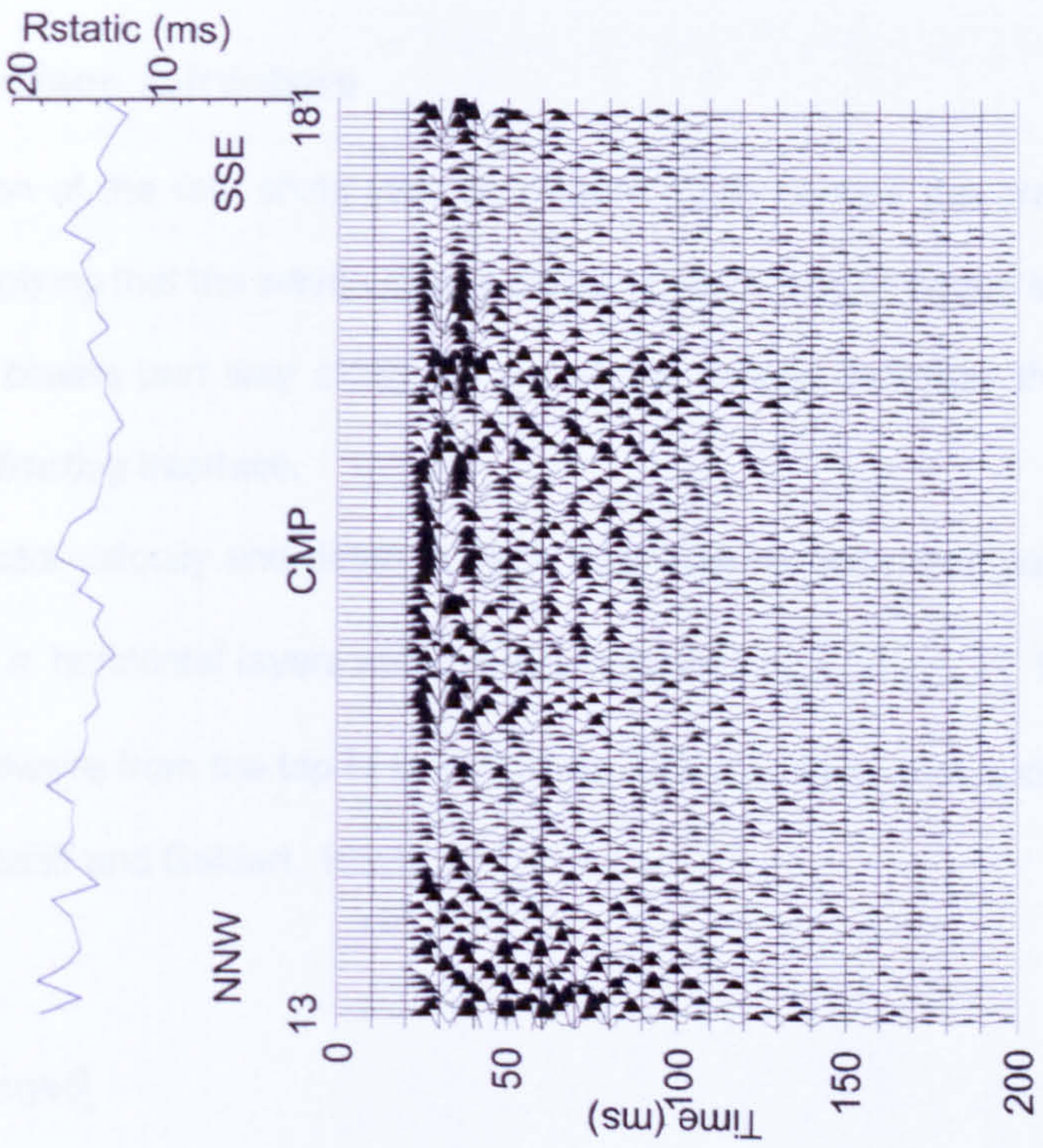

Figure 10.6: Stack section of Hutton Hill profile 01.
The distance between each trace is 1.5 m with the first CMP 13.25 m from the first receiver station. The section is displayed with a scalar multiplier.

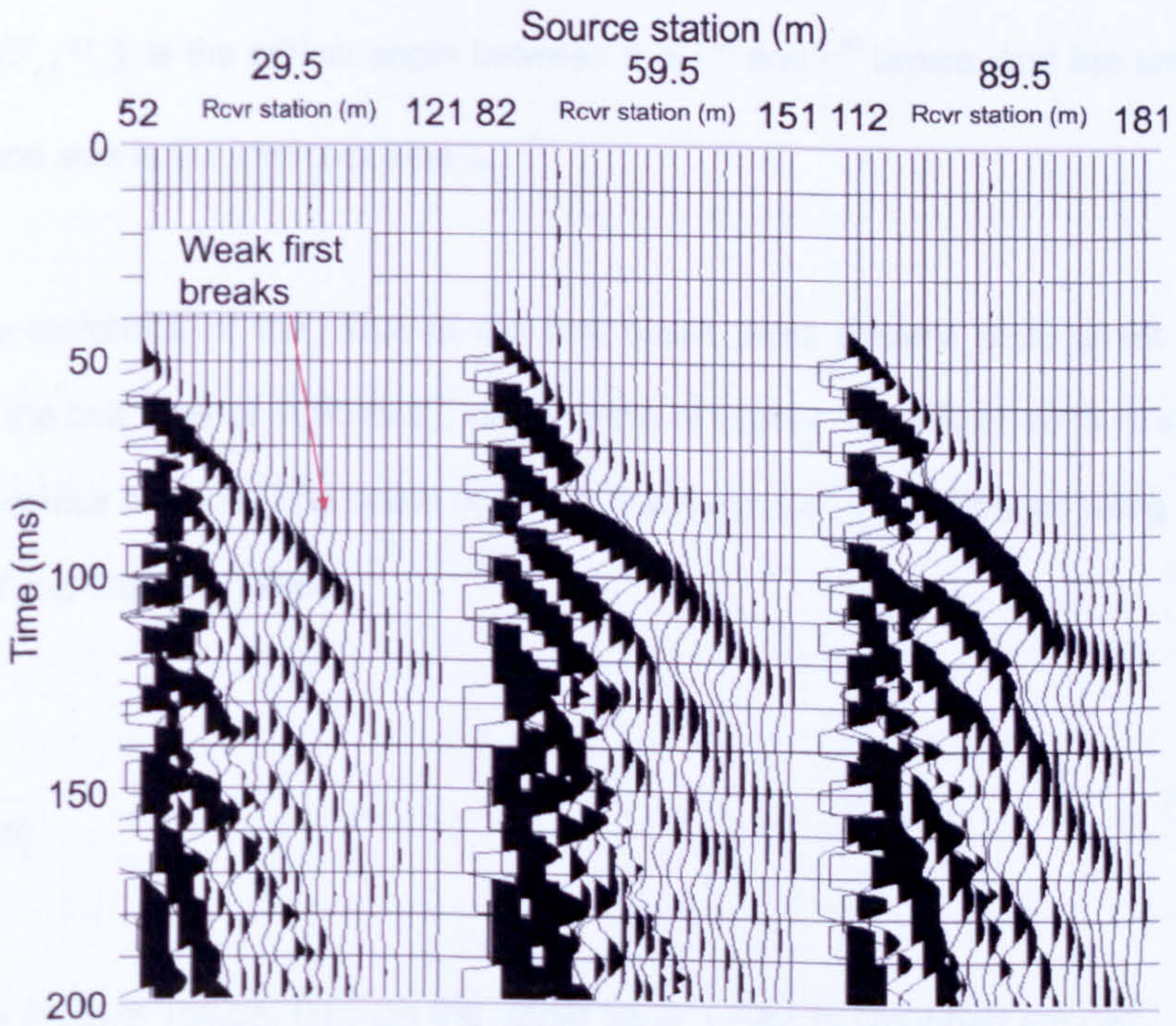

Figure 10.7: Raw shots from Hutton Hill.
The shots are displayed with a scalar multiplier.

10.3 Interpretation

10.3.1 Near surface refractors

A visual inspection of the raw shots records (Figure 10.5) reveals the gradient of the first breaks is high, implying that the wave velocity along the refracting interface is slow. A break in slope in the first breaks part way along the geophone spread indicates the existence of a second deeper refracting interface.

The refractor velocity and depth to each layer can be estimated using the intercept-time method. For n horizontal layers with P-wave velocities of $V_1, V_2 .... V_n$ the travel time for the refracted headwave from the top of the n^{th} layer, with a surface shot and receiver, can be written as (e.g. Sheriff and Geldart, 1995):

$$t = \frac{x}{V_n} + \sum_{i=1}^{n-1} \frac{2h_i}{V_i} \cos\theta_i \qquad (10.1)$$

where x is the distance between the shot and geophone, h_i is the thickness of the i^{th} layer, $\theta_i = \sin^{-1}(V_i/V_n)$ is the critical angle between the i^{th} and n^{th} layers, and the summation on the right hand side is the intercept time t_n.

The reciprocal of the slope of the first break picks (Figure 10.8) gives a refraction velocity for the first layer of 1060 m s^{-1}, close to the refraction velocity of 1075 m s^{-1} estimated by the plus-minus method. The depth h_1 of the first layer can be computed using the formula (e.g. Sheriff and Geldart, 1995):

$$h_1 = \frac{V_1 t_1}{2\cos\theta_1} \qquad (10.2)$$

The P-wave velocity through the upper layer, which is ploughed annually, is unknown since no geophones were deployed to measure the direct wave or uphole times. Assuming a P-wave velocity of 200 m s^{-1} and adjusting the intercept time upwards from 21 ms to 26 ms to

account for a shot depth of 1 m yields a depth of 3 m to the uppermost refraction layer. This refractor is interpreted as the top of the Triassic Sherwood Sandstone. The P-wave velocity may seem low for a sandstone, but the Sherwood Sandstone is commonly found to have high porosity and is dry at shallow depths. Furthermore, less than 2 m of unconsolidated Quaternary deposits were proved in the Hutton Hill borehole (Figure 10.3).

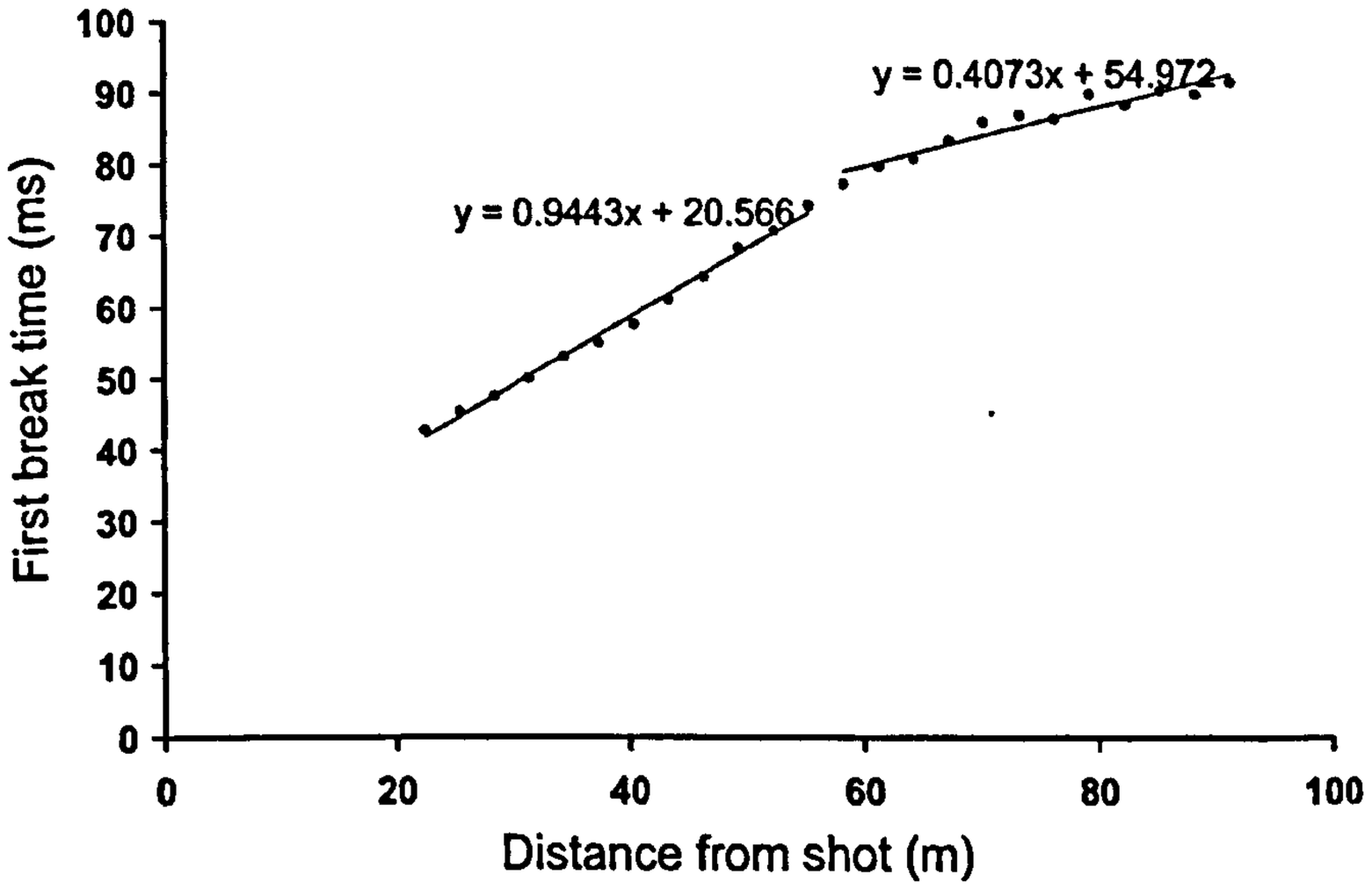

Figure 10.8: First break intercept-time graph.
First break picks from a record from a shot fired at station 86.5 m into a receiver spread at stations 109 m to 178 m.

Applying the calculated plus-minus field statics to the shot gathers is equivalent to projecting the shot and receiver stations down on to plough depth boundary. This process effectively strips out the near-surface effects of the unconsolidated deposits on the travel times. For the adjusted first breaks in (Figure 10.9) a refractor velocity of 2290 m s^{-1} for the lower layer was computed for the lower layer. This value is plausible for water-saturated sediments of the Sherwood Sandstone Group or of the Roxby Mudstones, so the top surface of the lower layer may either be the water table in the Permo-Triassic bedrock or the stratigraphic interface between the Roxby Mudstones and Sherwood Sandstone. The depth to the refractor obtained from the intercept time of 30 ms in Figure 10.9 is 18 m. Adding 3 m for the thickness of the plough soil gives a depth of 21 m for the lower layer.

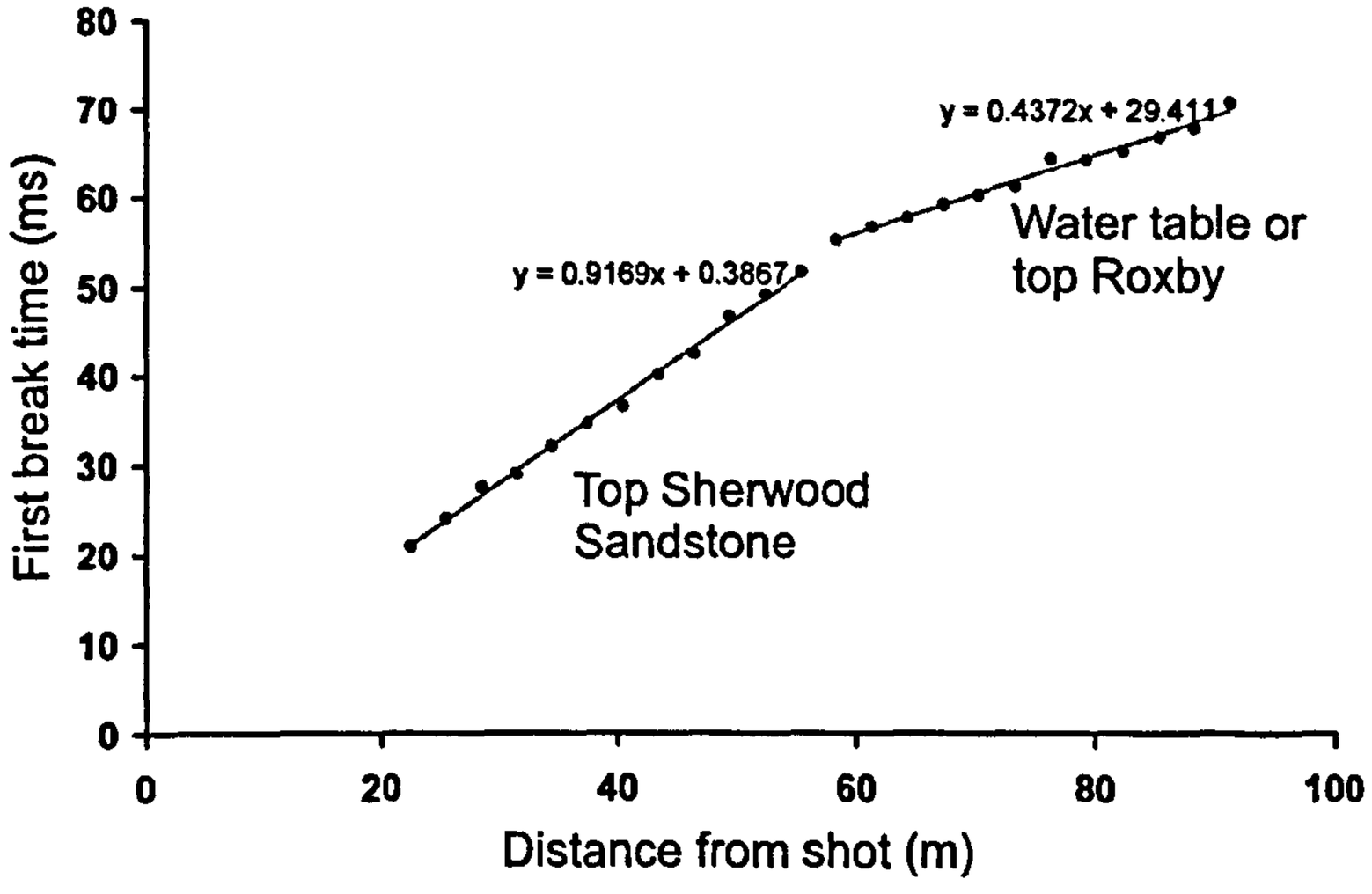

Figure 10.9: Adjusted first break intercept-time graph.

11.0 Sharow Hall

11.1 Site description

Pits shown on historical Ordnance Survey maps (Figure 11.1) at the western edge of Sharow village, approximately 1.5 km east-north-east of the city centre of Ripon, were first described in the scientific literature by Reverend Tute (1868). These depressions are now filled in. The most recent subsidence in the vicinity of the village was reported in February 1982 (Cooper and Waltham, 1999) approximately 100 m south-west of Tute's hollows. All of these subsidence features occur around Sharow Cross on the feather edge of the Triassic Sherwood Sandstone sub-crop (Figure 2.13).

The Sharow Hall survey site [SE 3332 7175] is in an area of peat fill in the superficial geology (Figure 11.2) on the eastern fringe of Sharow village (Figure 11.3). The peaty material may be the accumulation of organic matter in an ancient surface depression caused by sub-surface gypsum dissolution.

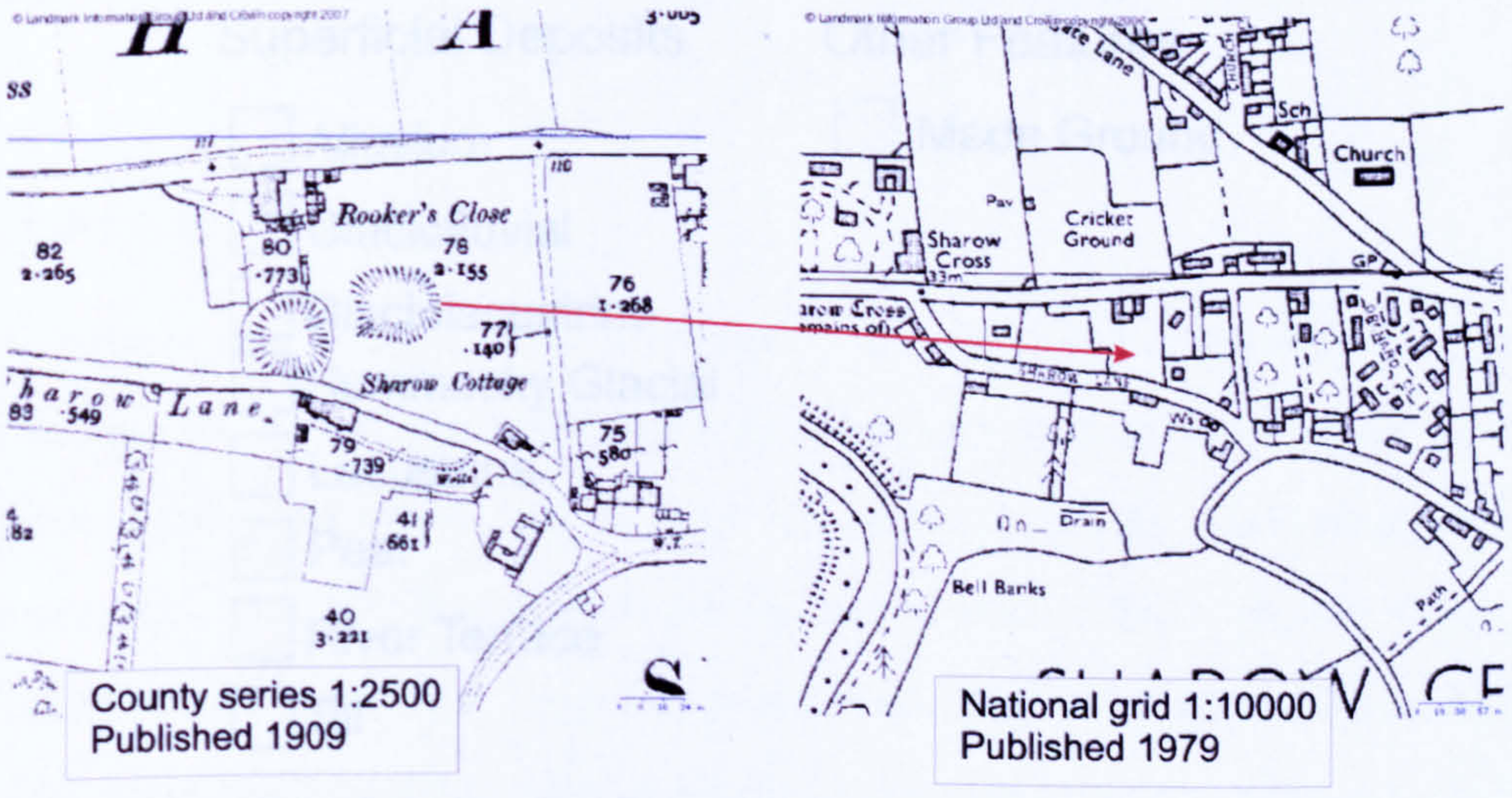

Figure 11.1: Historical Ordnance Survey maps of Sharow Cross.
Data supplied by Ordnance Survey/EDINA service © Crown Copyright and land Information Group Ltd. Database 2007.

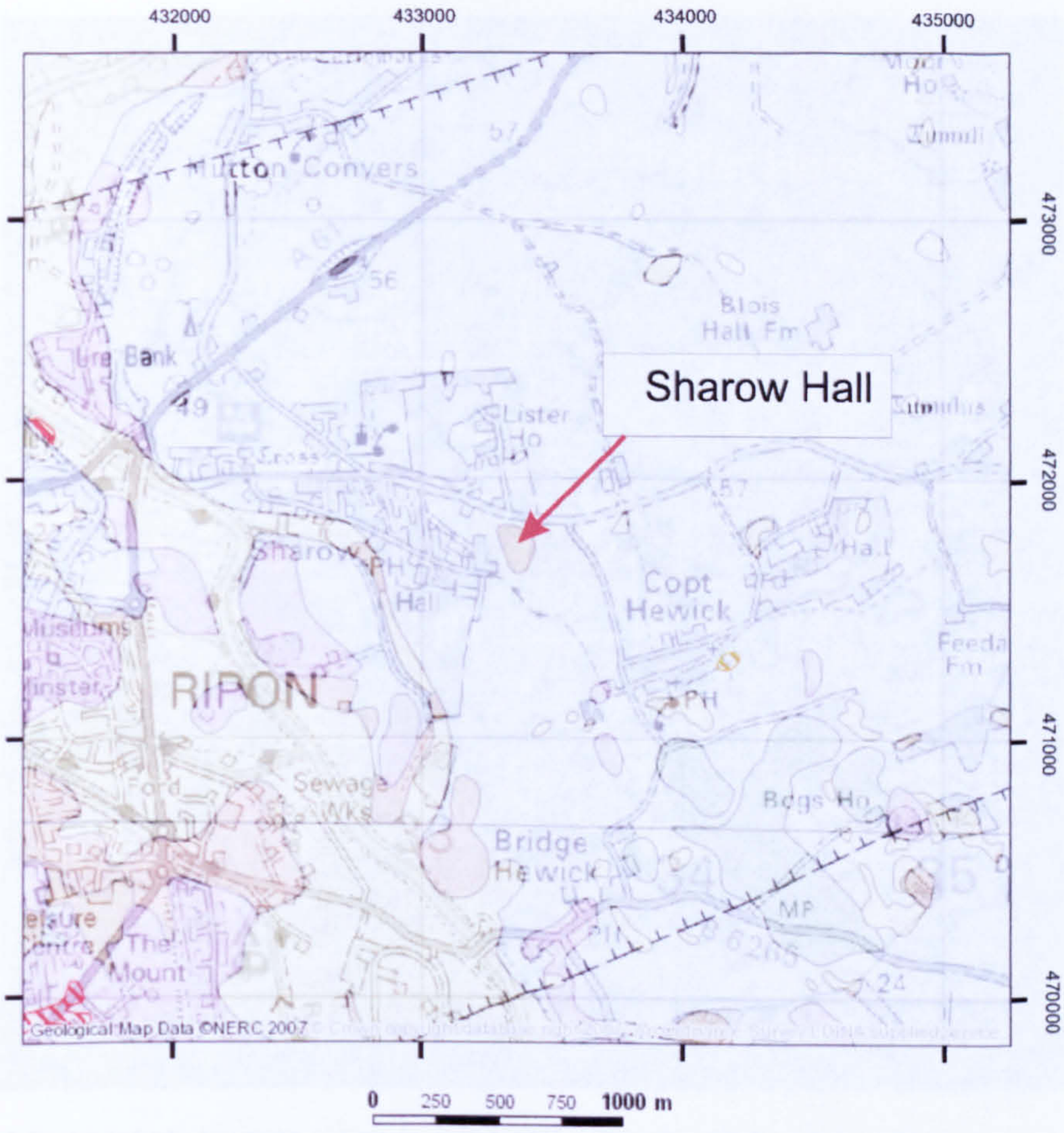

Superficial Deposits

- Alluvium
- Glaciofluvial
- Glaciolacustrine
- Hummocky Glacial
- Lacustrine
- Peat
- River Terrace
- Till

Other Features

- Made Ground

Figure 11.2: Superficial deposits at the Sharow Hall survey site.
Data supplied by Ordnance Survey/EDINA service © Crown Copyright Database 2007.

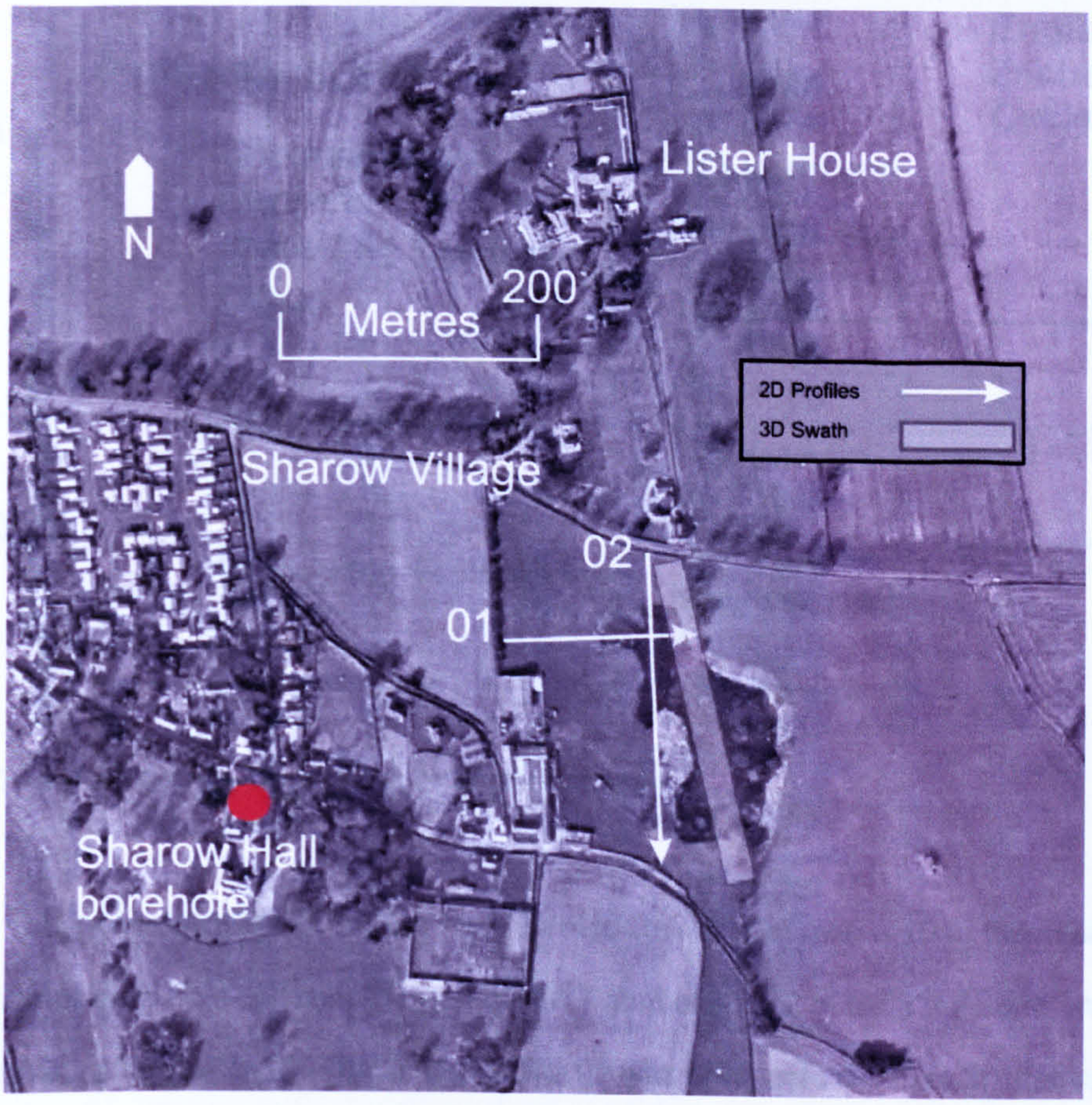

Figure 11.3: Aerial photograph taken in 1994 of the Sharow Hall survey site.

11.2 Acquisition

The nearest borehole, 400 m to the south-west of the survey site at the main buildings of Sharow Hall (Figure 11.4), was sunk to provide a water supply to the farm from the Brotherton Limestone aquifer, intersected at 41 m below ground level. Only thin bands of gypsiferous material within the Roxby Formation mudstones are reported in the drilling log. Below the Brotherton Limestone in the general geological succession at Ripon (Table 2.3) lie mudstones the Edlington Formation, which in turn overlie the Hayton Anhydrite Formation gypsum bed. The top surface of the Hayton Anhydrite is estimated at between 50 m and 60 m below the ground surface at Sharow Hall. The Burtree Caravan Park borehole (Figure 2.15) proves that large thicknesses of the Hayton Anhydrite Formation exist locally.

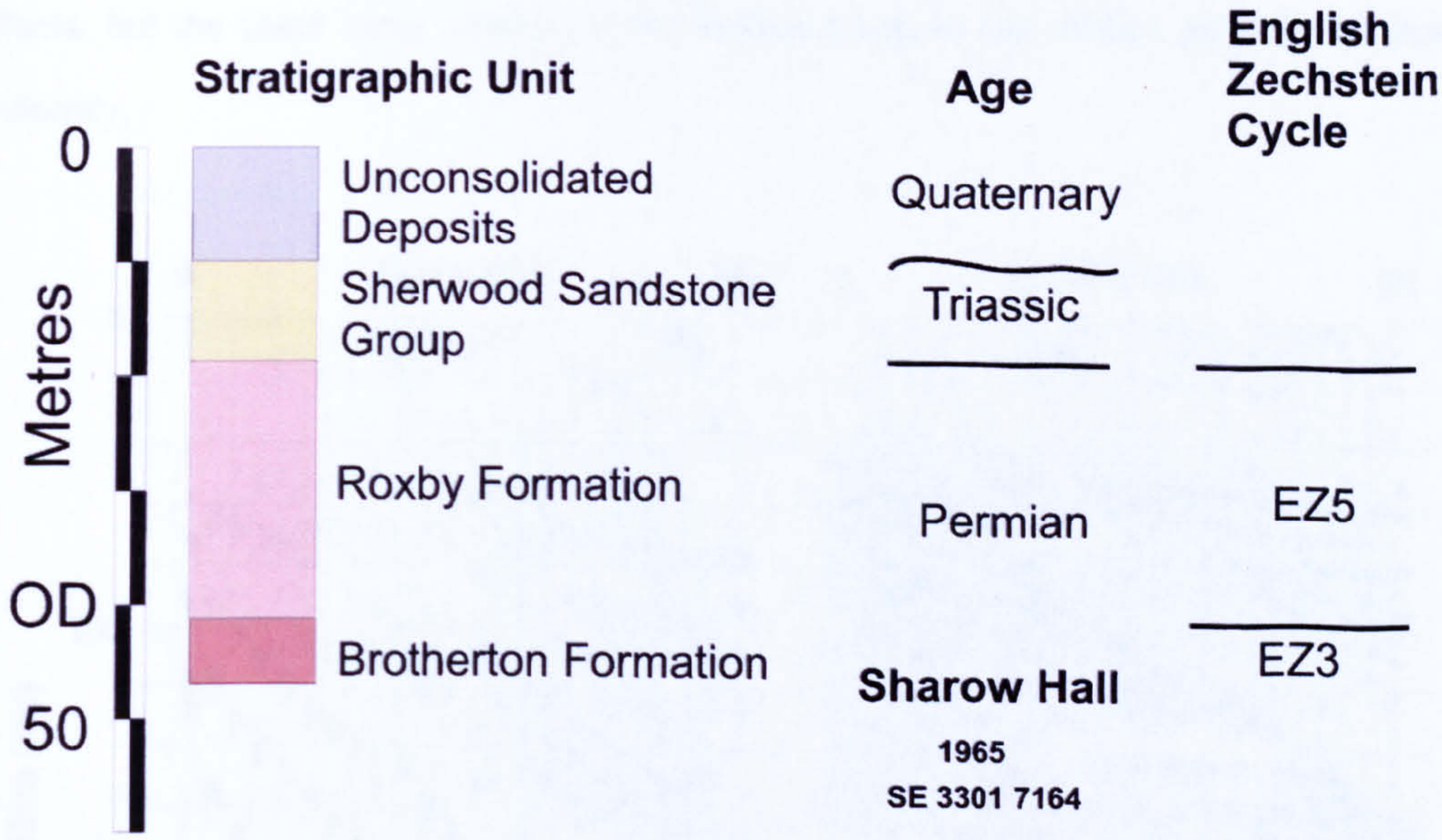

Figure 11.4: Sharow Hall borehole geological succession.

Two perpendicular 2D profiles were located to intersect over a 10 m diameter boggy area in the pasture field adjacent to Sharow Hall Farmhouse just outside the north end of the pond enclosure (Figure 11.3). The longer profile 02 was orientated north-south starting at the Dishforth Road hedge boundary running parallel to the western enclosure fence line. The start of the profile crosses an area of made ground, which provided poor shooting conditions, prior to the boggy ground where the two profiles intersected in an area of sticky grey clay. Good shooting conditions continued in the middle section of the profile, but became increasingly dry and sandy towards the end of profile. The shorter profile 01 was acquired eastwards down slope towards the boggy area with a drop in elevation of 6.10 m measured by optical levelling.

Based on the borehole data, an off-end geophone spread of 24 channels with a geophone spacing of 2 m, near-offset 23 m and far-offset 69 m was selected to record any reflection events from the Brotherton and Hayton Anhydrite formations. These parameters were confirmed by wave tests which, after bandpass filtering, showed a reflection event beyond the linear air-wave noise train (Figure 11.5). Shot holes were drilled at intervals of 4 m placed midway between receiver stations and offset from the line of geophones by 2 m. Each shot hole was used twice; firing in to geophone spreads in forward and reverse directions to simulate a 48-channel split-spread arrangement (Figure 11.6, Table 11.1). These parameters

gave a maximum fold of coverage of 12. All the traces in each CMP gather do have different offsets, but the stack array criterion is not fulfilled because the offsets are not distributed uniformly.

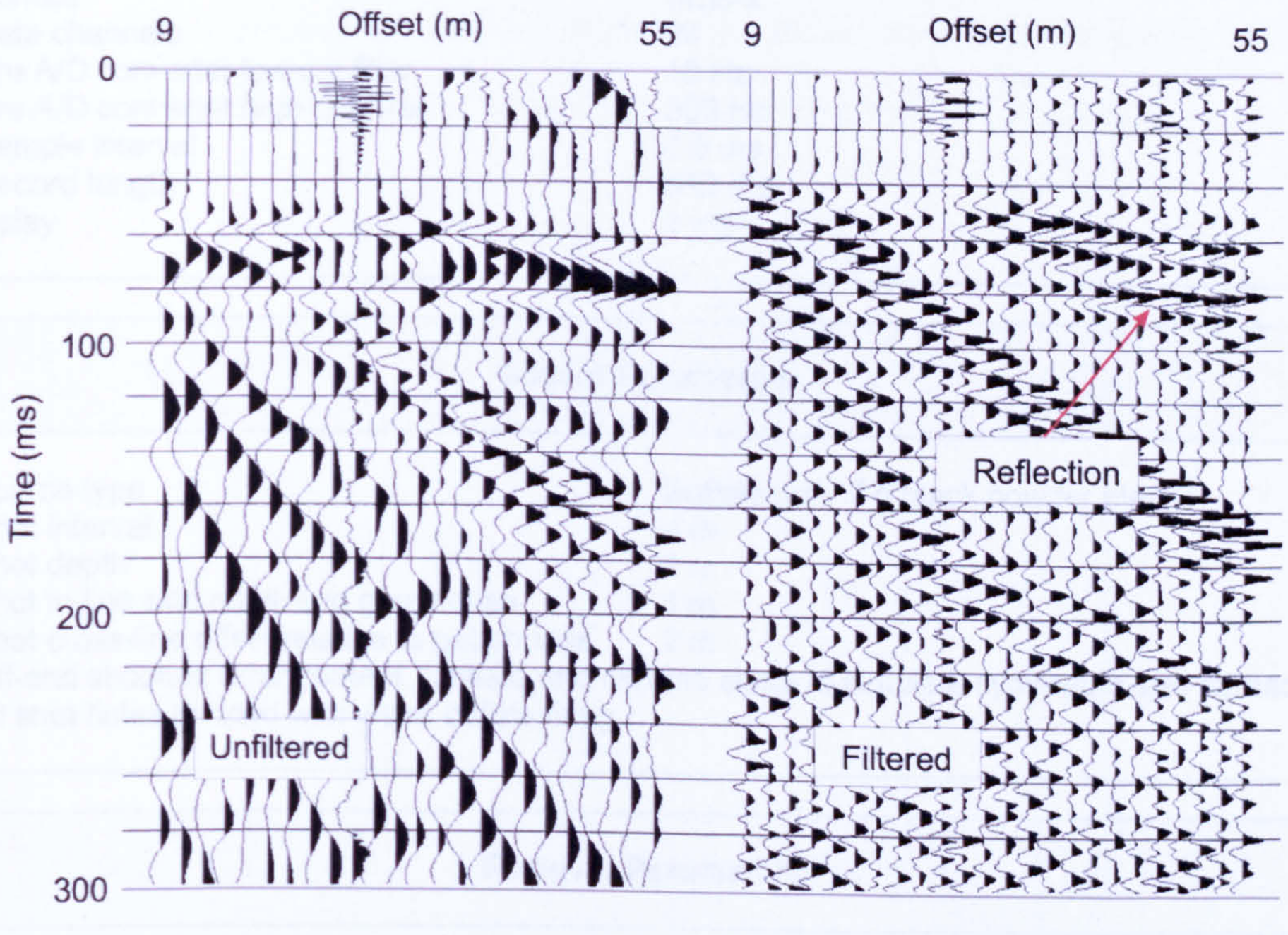

Figure 11.5: Sharow Hall wave test shot record.
The bandpass filter applied had corner frequencies of 60 Hz, 100 Hz, 330 Hz and 350 Hz.
The data are displayed with a 100 ms AGC window.

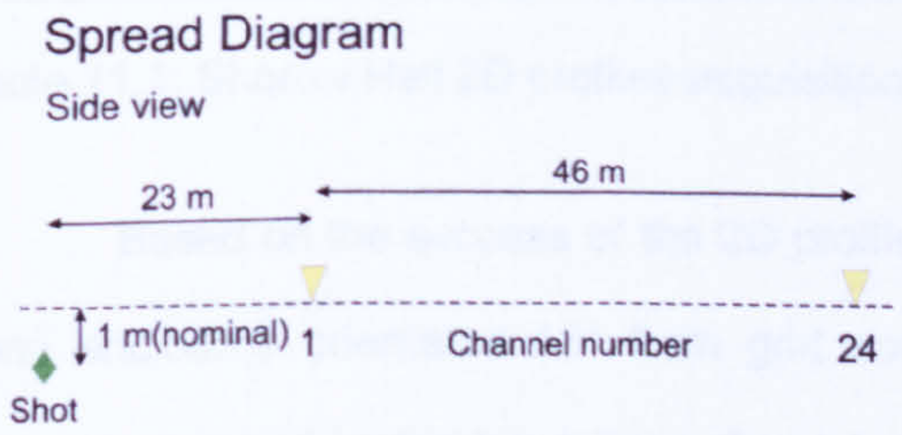

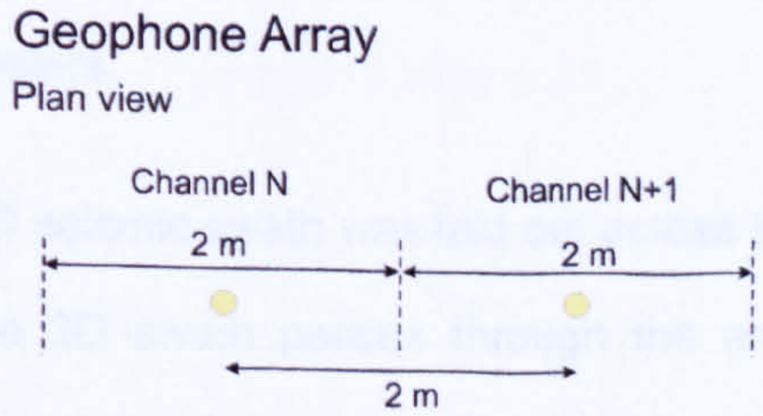

Figure 11.6: Sharow Hall 2D seismic profiles shooting template.

Instrument Parameters

Recording instrument	Geometrics SmartSeis S12
Format	SEG-2
Data channels	24
Pre A/D converter low-cut filter	10 Hz
Pre A/D converter high-cut filter	500 Hz
Sample interval	0.5 ms
Record length	512 ms
Delay	0 ms

Source Parameters

Source type	Buffalo gun, 7 g black powder blanks
Shot interval	4 m
Shot depth	1 m
Shot in-line skid relative to geophones	1 m
Shot cross-line offset relative to geophones	2 m

Off-end shooting arrangement, forward and reverse shots to simulate symmetric split-spread.
All shot holes tamped with water before firing.

Receiver Parameters

Geophone type	SM-7/30 Hz
Group interval	2 m
Geophones per group	1
Near-offset	23 m
Far-offset	69 m

Table 11.1: Sharow Hall 2D profiles acquisition parameters.

Based on the success of the 2D profiles, a 3D seismic swath was laid out across the pond enclosure orientated 13° from grid north. The 3D swath passes through the area formerly occupied by the two kidney-shaped ponds indicated in the enclosure on the modern Ordnance Survey map (Figure 11.7). The area where the ponds were located is now very boggy ground with tall weeds interspersed with clearer grassy zones. Only a narrow swath consisting of eight lines of sub-surface coverage spaced 2 m apart could be sandwiched between the large apron of rubble and the boundary fencing visible in the aerial photography as a grey lozenge (Figure 11.3). Three lines of shot stations were placed 8 m apart in the cross-line direction and at 4 m intervals in the in-line direction. Four lines of receiver stations

were placed 4 m apart in the in-line and cross-line directions with the two outer lines of receiver stations offset by 2 m from the two outside lines of shot stations. For each line of sub-surface coverage, each shot point was used once firing in to a symmetrical split-spread geophone arrangement (Figure 11.8, Table 11.2). A near-offset of 26 m and a geophone spacing of 4 m gave a similar range of offsets to the 2D profiles. These parameters fulfilled the stack array criterion and gave 12-fold coverage for CMPs on a 2 m by 2 m grid.

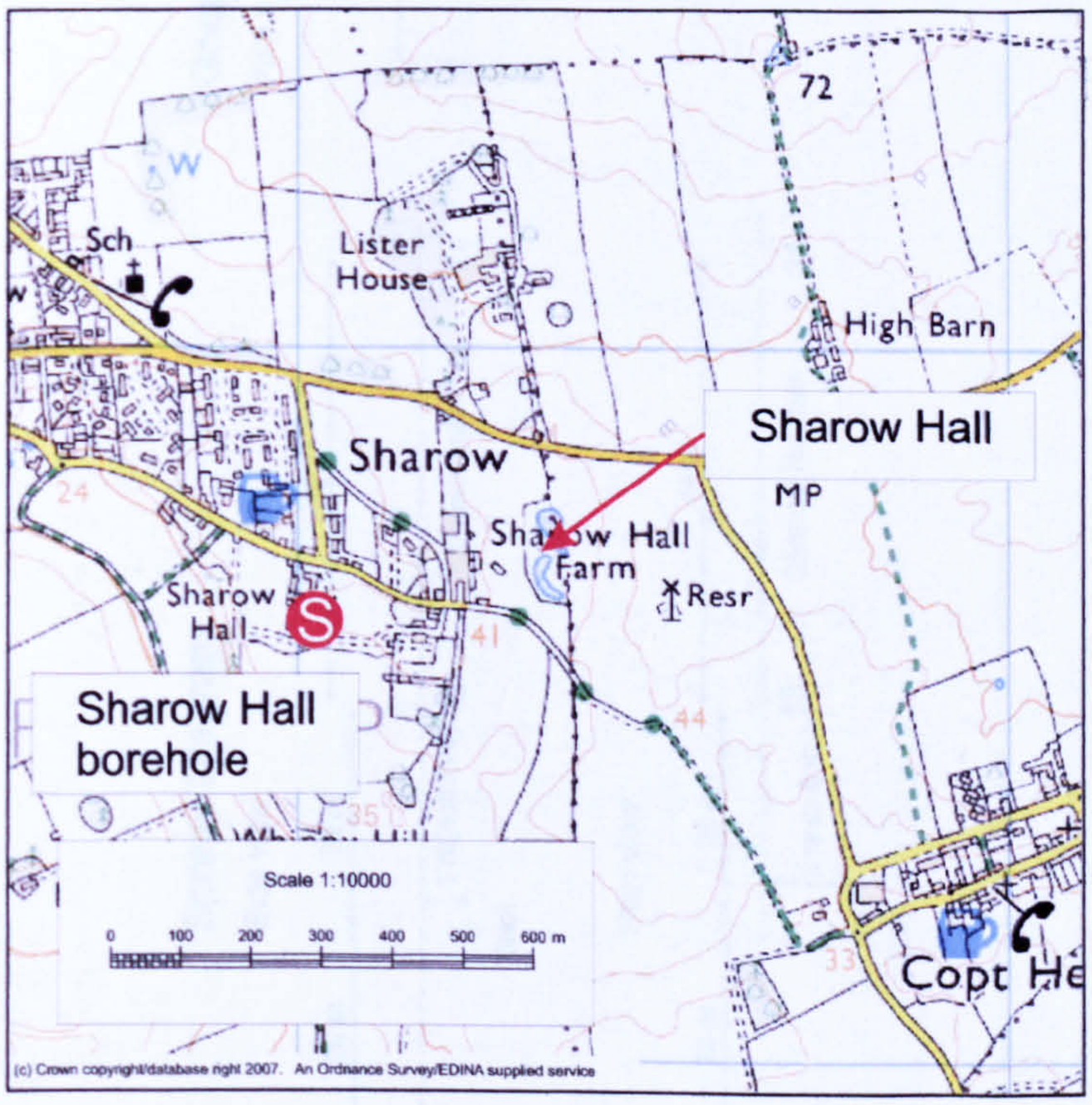

Figure 11.7: Ordnance Survey map of Sharow Hall.
Data supplied by Ordnance Survey/EDINA service © Crown Copyright Database 2007.

11.3 Processing

The processing parameters were tested on Sharow Hall profile 02 which crosses over a variety of shot coupling conditions. The raw shot records are dominated by low-frequency near-surface guided waves (Figure 11.9). With bandpass filtering, deconvolution and field statics applied, clear reflection events between 50 ms and 80 ms could be seen on all the shot records. In Figure 11.9, there is a clear loss of high-frequency reflection energy on the shot record from areas of poorer shot coupling conditions.

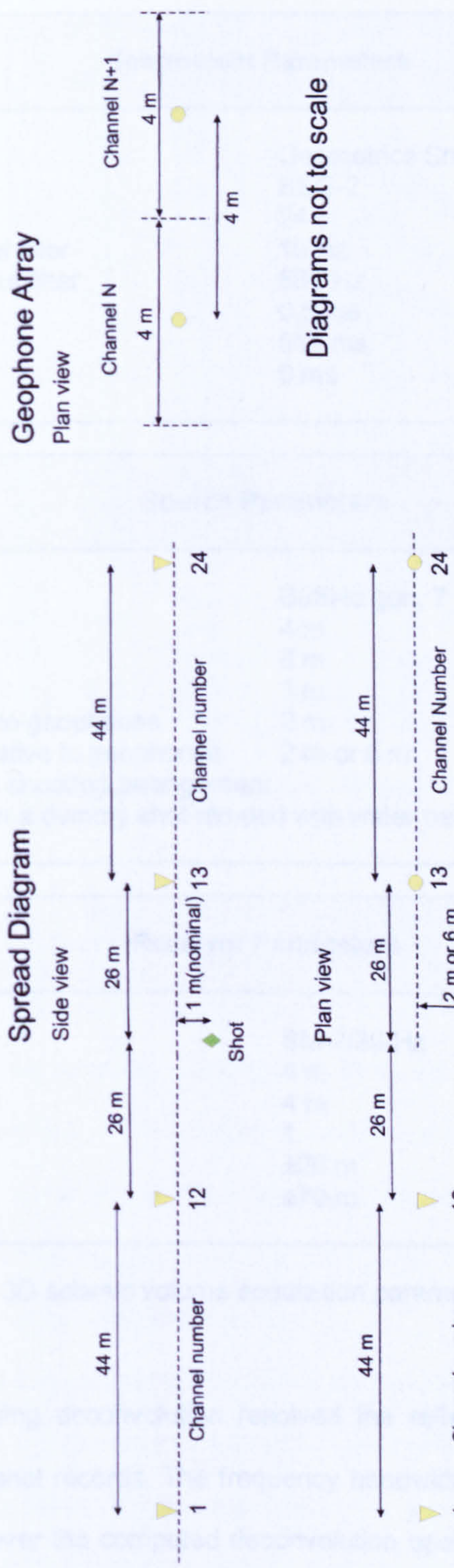

Figure 11.8: Sharow Hall 3D seismic volume shooting template.

Instrument Parameters	
Recording instrument	Geometrics SmartSeis S12
Format	SEG-2
Data channels	24
Pre A/D converter low-cut filter	10 Hz
Pre A/D converter high-cut filter	500 Hz
Sample interval	0.5 ms
Record length	512 ms
Delay	0 ms

Source Parameters	
Source type	Buffalo gun, 7 g black powder blanks
Shot in-line interval	4 m
Shot cross-line interval	8 m
Shot depth	1 m
Shot in-line skid relative to geophones	2 m
Shot cross-line offset relative to geophones	2 m or 6 m
Symmetrical split-spread shooting arrangement.	
All shot holes sprung with a dummy shot tamped with water before firing.	

Receiver Parameters	
Geophone type	SM-7/30 Hz
Group in-line interval	4 m
Group cross-line interval	4 m
Geophones per group	1
Near-offset	±26 m
Far-offset	±70 m

Table 11.2: Sharow Hall 3D seismic volume acquisition parameters.

Zero-phase spiking deconvolution resolved the reflection energy into two distinct events in both the test shot records. The frequency bandwidth of the data is comparable in both shot records; however the computed deconvolution operator has shaped the reflection events differently. In the moderate shot coupling conditions each reflection event is represented only by a single black positive amplitude loop preceded by a negative side lobe, whereas in good shot coupling conditions reflections have a black-white-black signature. The prominent linear air-wave noise train is removed efficiently by surgical muting.

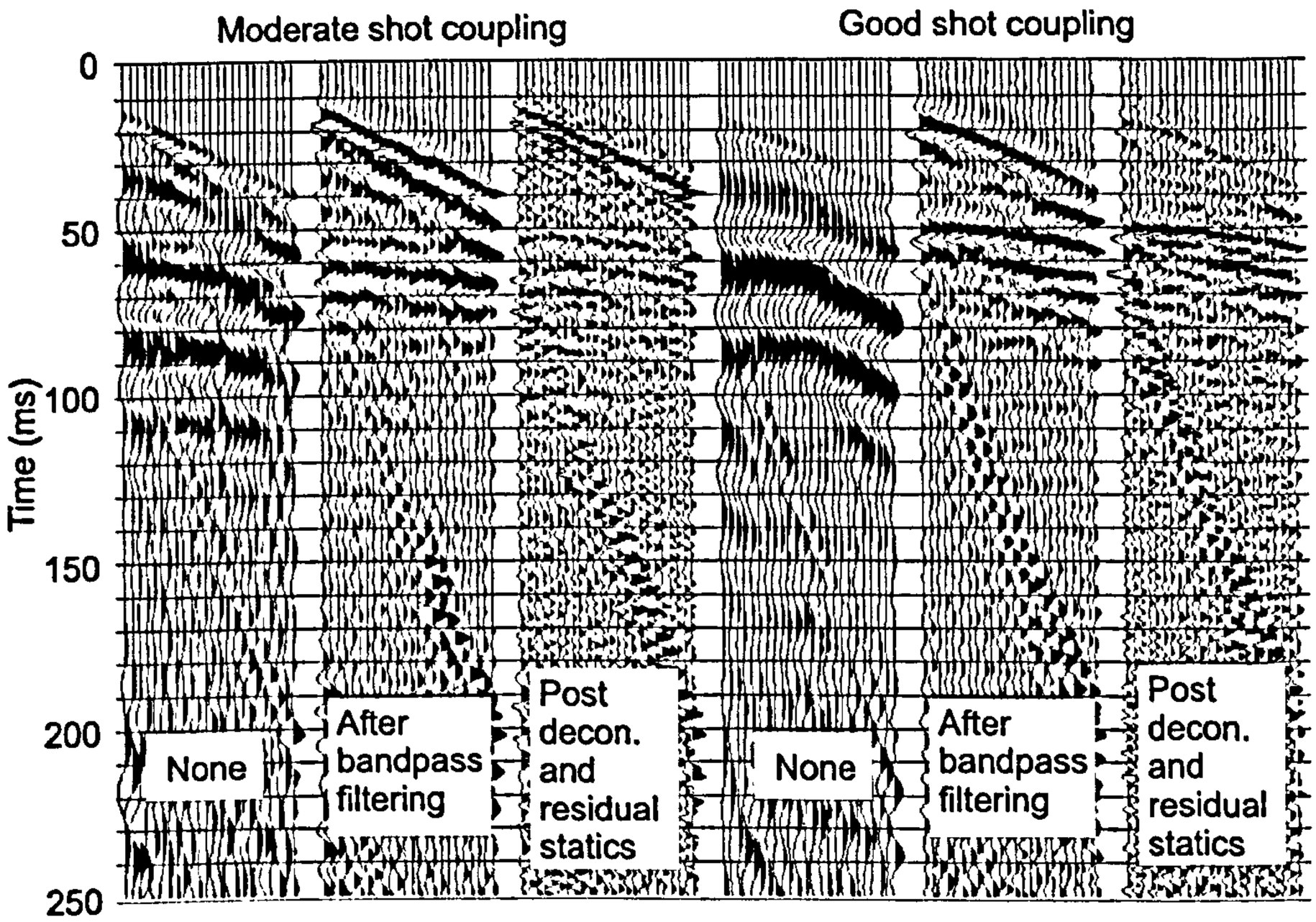

Figure 11.9: Shot coupling comparison on data from Sharow Hall 2D profile 02. Data are displayed with a 200 ms AGC window before being cropped.

Field statics were calculated using the plus-minus method with surface-consistent residual statics removing localised high-frequency jitter. Shots were balanced with a gain function dependent on the stacking velocity and time, followed by a statistical surface-consistent amplitude correction for each individual shot and receiver station. *F-x* deconvolution was used to remove any remaining discrete strong noise in the lower parts of the seismic data to prevent phase shift time migration from moving such noise into the region where reflection events reside in the stack section.

The initial stacking velocity field was based on the geology of the nearby Sharow Hall borehole and applied across the complete length of the profile. As the sub-surface reflection events became better resolved at various points in the processing sequence, the stacking velocity field was refined by interactive velocity analysis at several equidistant CMP points along the length of the profile. Once the final processing sequence was established (Figure 11.10) it was also applied to Sharow Hall profile 01 to ensure a site-consistent approach.

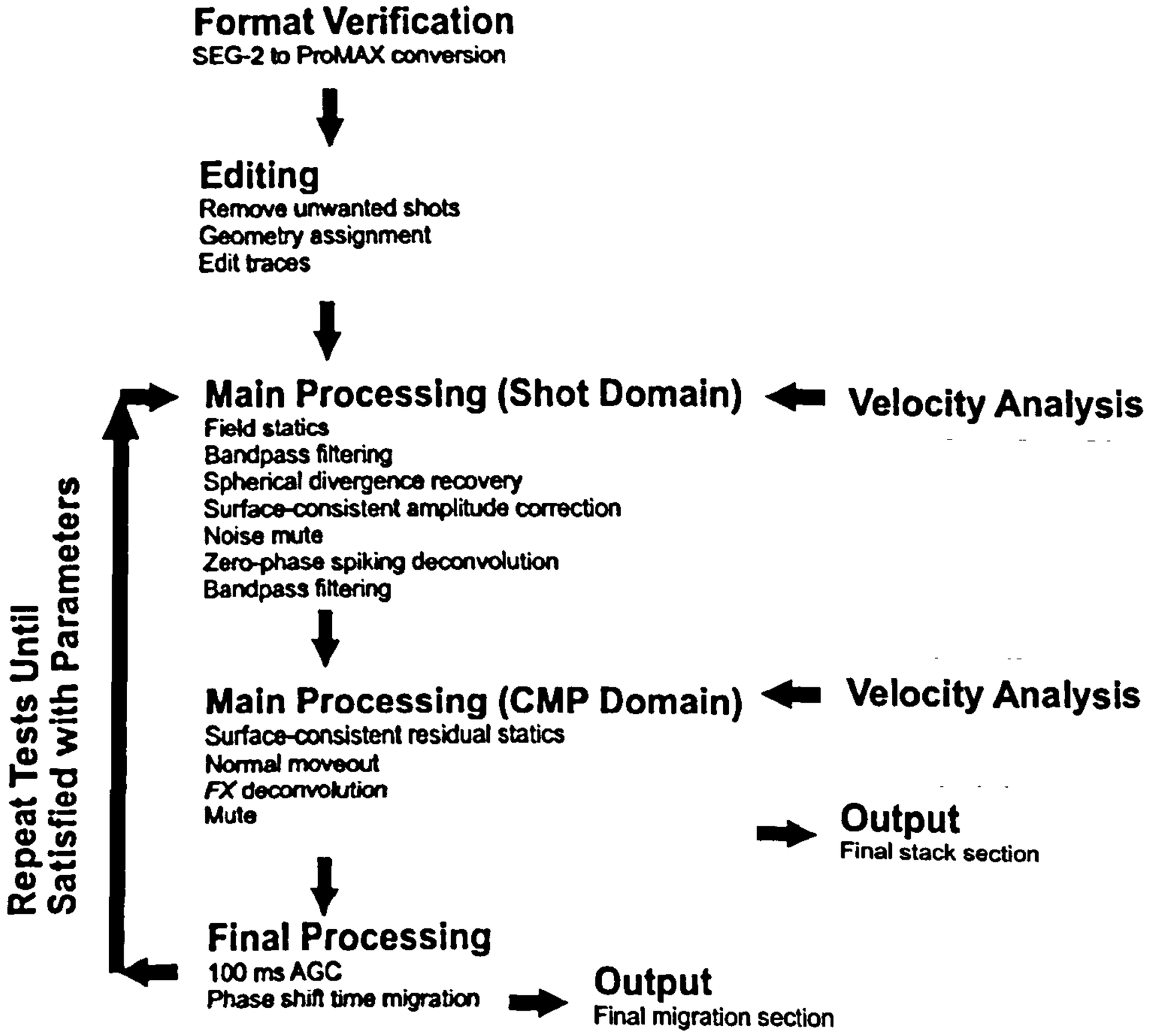

Figure 11.10: Sharow Hall survey seismic data processing flow.

11.4 Interpretation

11.4.1 Sub-surface geology

The shallowest reflection event is present around 50 ms in the time migrated stack section of profile 02 (Figure 11.11), with a gentle dip down to the north. Only between CMPs 130 and 150 in the region of good shot coupling is the lower black leg visible of the black-white-black reflection signature from a positive acoustic impedance geological boundary. Elsewhere the lower black leg is coincident with the upper black leg of a deeper seismic reflection package. Preceding the strong black loop at 50 ms is a white loop with a leading intermittent weaker black loop; these earlier loops are side lobe effects from bandpass filtering.

From the strata proved in the Sharow Hall borehole, this reflection event probably arises from the interface between the soft mudstones of the Roxby Formation and the hard limestone of the Brotherton Formation. Assuming an interval velocity of 2000 m s^{-1} through

the overlying Quaternary unconsolidated deposits, Sherwood Sandstone Group and Roxby Formation, the estimated depth to the limestone is 50 m below the shallow refractor reference datum. At the Sharow Hall borehole the Roxby-Brotherton interface is recorded at 41 m depth, and since the Sharow Hall survey site is down dip from the borehole according to the regional trend (Figure 11.12), the estimated depth of 50 m for the reflection event is consistent with the interpretation that it comes from the top surface of the Brotherton Limestone.

The Sharow Hall borehole does not cut through the total thickness of the Brotherton Limestone artesian aquifer. Boreholes in and around Ripon prove that the thickness and lithology of the Brotherton Limestone is very consistent as it wedges out gradually eastwards. Approximately along strike from Sharow, the thickness of the Brotherton Limestone is recorded as 10 m at the Ripon Parks cliff section (Figure 11.13) and in the Burtree Caravan Park borehole (Figure 2.15). Therefore, at the Sharow survey site the Brotherton Limestone is estimated to be 10 m thick.

Minor deviations of no more than 2 ms in amplitude are present in the top surface of the Brotherton Limestone. Ripon lies at the western fringe of the depositional extent of the Billingham Anhydrite Formation (Figure 2.4). Thin beds of this gypsum-rich formation are recorded in boreholes to the east of Ripon. Therefore, the localised undulations could be small patches of Billingham Anhydrite Formation gypsum lying on top of the Brotherton Limestone. It is possible that borehole chippings from a thin bed of gypsum sitting on top of limestone may be misinterpreted as limestone.

In the general geological succession at Ripon (Table 2.3) below the hard compact Brotherton Formation are the soft mudstones of the Edlington Formation. A reflection response would be expected at this interface, with opposite polarity to the reflection from the top surface of the limestone. For 10 m of limestone, the time difference between the reflections from the top and bottom of the limestone is 5 ms assuming a P-wave interval velocity of 4000 m s^{-1}. However, no distinct reflection from the base of the Brotherton Limestone is visible in the time migrated section of profile 02.

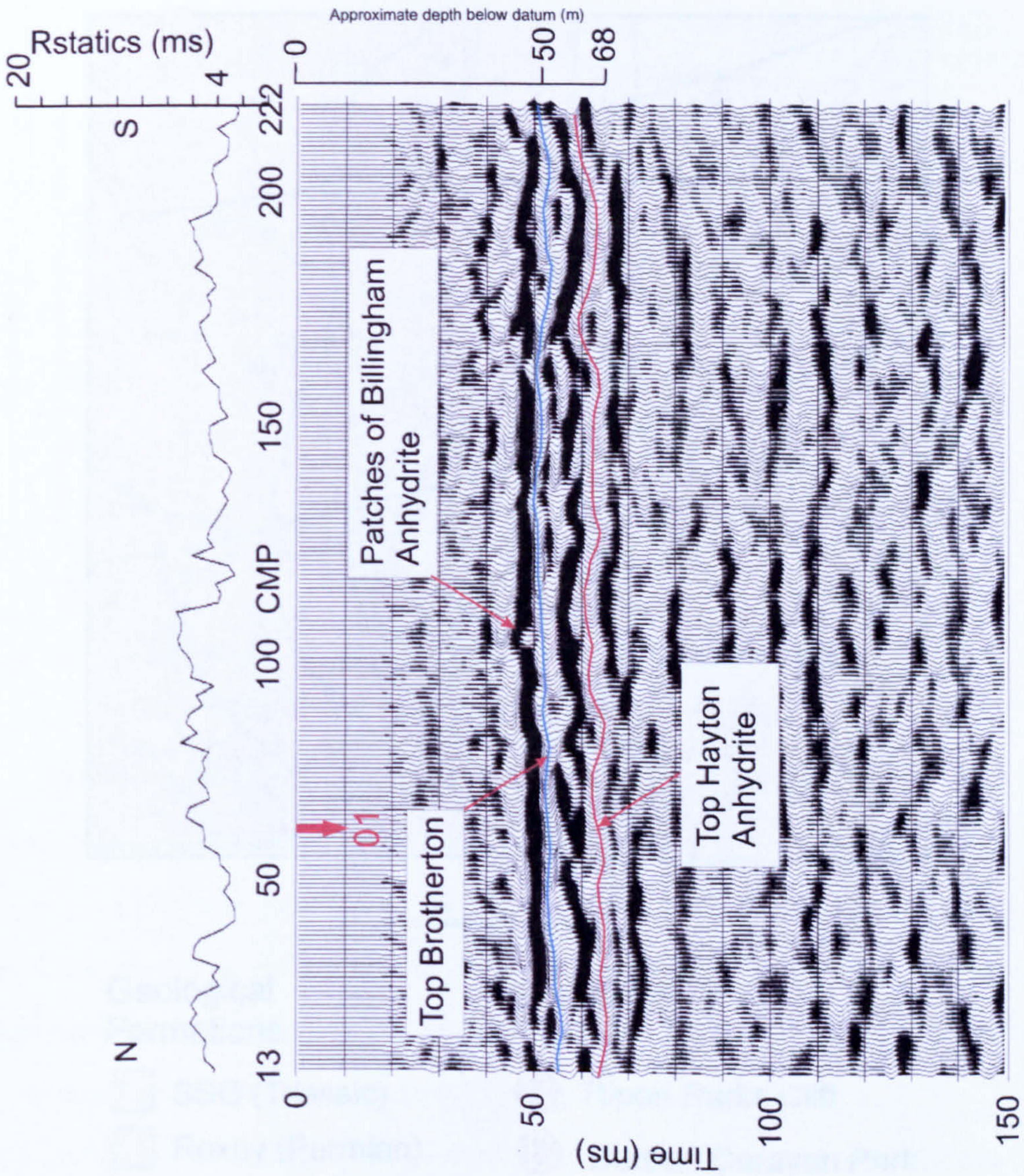

Figure 11.11: Interpreted final time migrated section of Sharow Hall profile 02.
The distance between CMP traces for all Sharow Hall Fen 2D profiles is 1 m. The CMP numbering has been adjusted to represent the distance along the profile from the first receiver station. The section is displayed with a scalar multiplier.

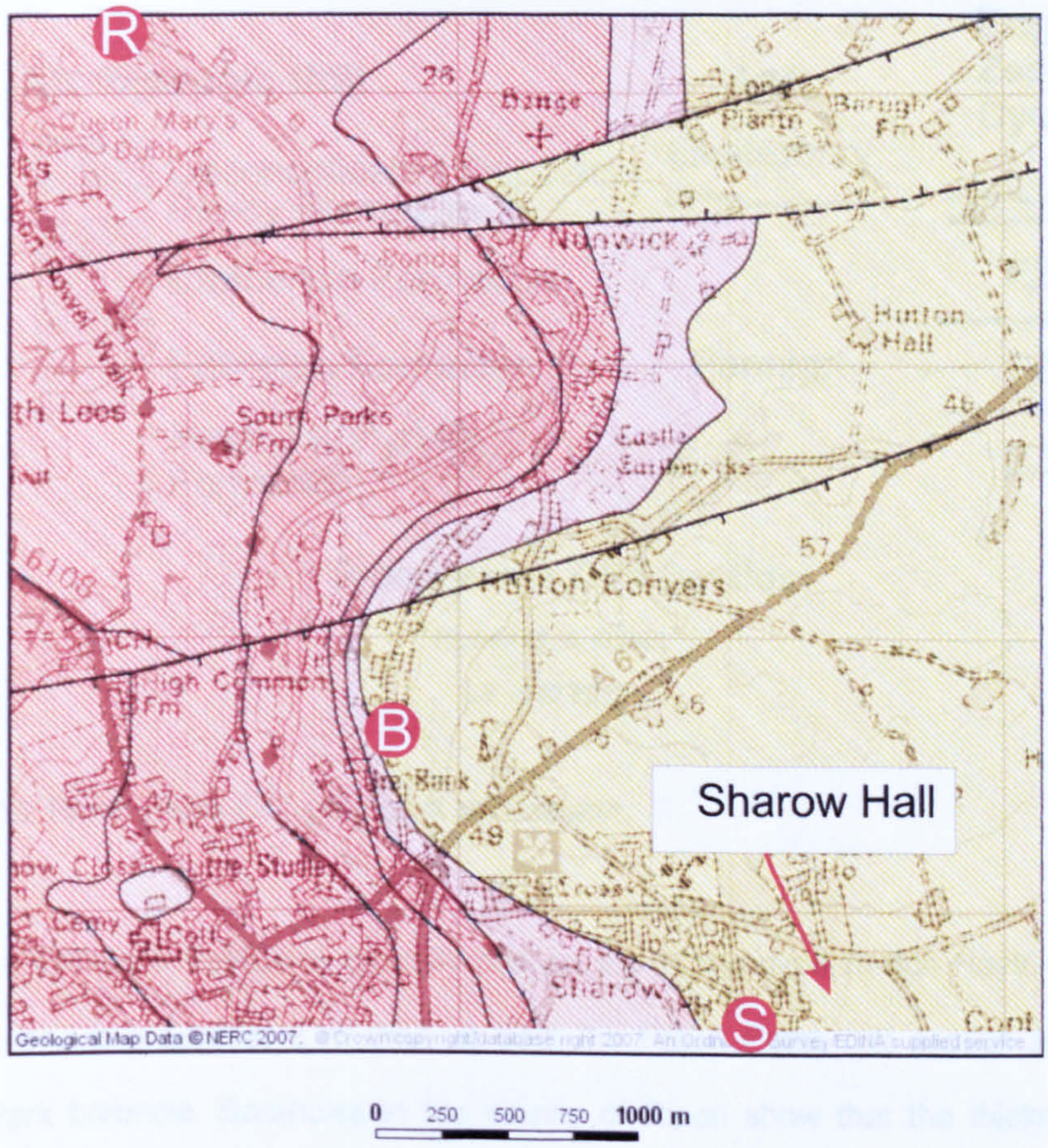

Figure 11.12: Solid geology beneath the Sharow Hall survey site.
Data supplied by Ordnance Survey/EDINA service © Crown Copyright Database 2007.

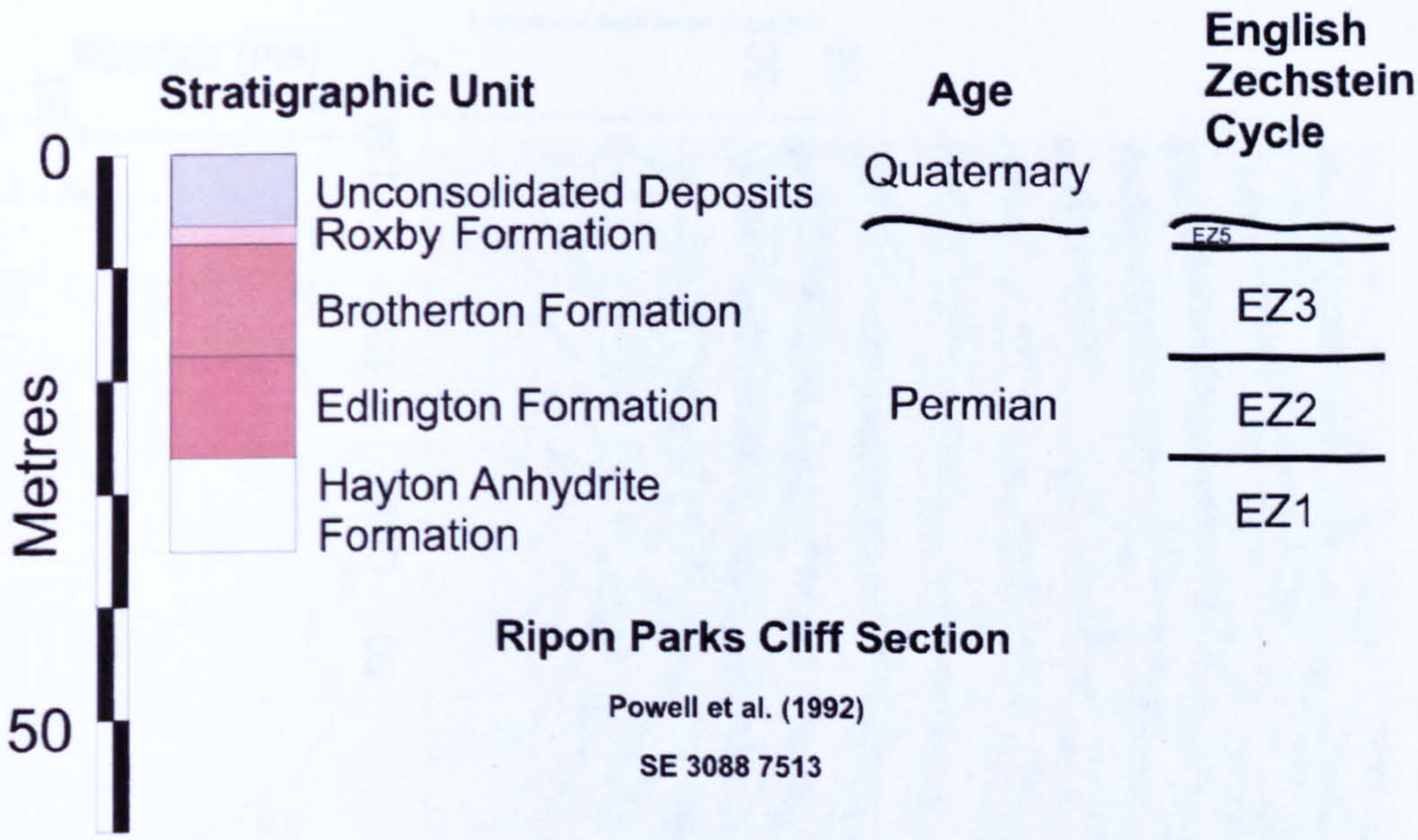

Figure 11.13: Ripon Parks Cliff geological succession.

The Edlington Formation typically rest on top of the gypsum-rich Hayton Anhydrite Formation, and is logged at 8 m thick at both the Ripon Parks cliff section and Burtree Caravan Park borehole. Boreholes in the vicinity of Ripon show that the thickness of the Edlington Mudstones is not consistent laterally. If there are 8 m of Edlington Mudstones present below the Sharow survey site with a P-wave interval velocity of 2500 m s^{-1}, the two-way travel time through the mudstones would be 6 ms.

Along the full length of profile 02 is another strong black positive loop with a central peak that varies over the range 55–62 ms. The time difference between these two reflection events, which both appear to correspond to interfaces with positive reflection coefficients, is equal to the estimated thicknesses of the Brotherton Limestone and Edlington Mudstones. The lower reflection event has a convoluted shape and is interpreted as the top of the Hayton Anhydrite Formation. The thickness of the gypsum bed is not determined from the seismic data.

The seismic data quality along the perpendicular 2D profile 01 (Figure 11.14) is poor compared to profile 02. Half of the shots acquired were in poor shot coupling conditions on dry sandy rising ground, or made ground, resulting in lower frequency content and loss of detail.

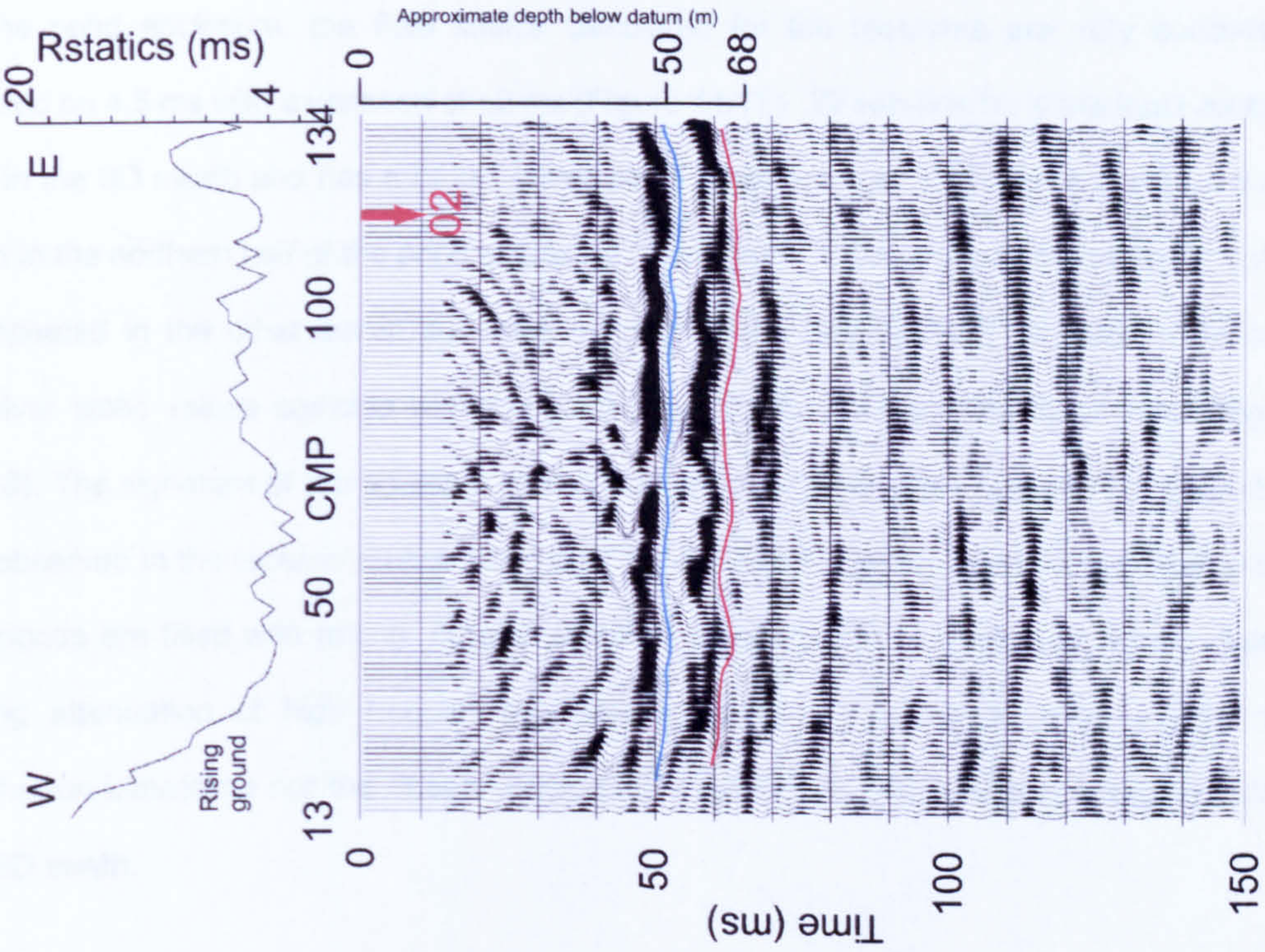

Figure 11.14: Interpreted final time migrated section of Sharow Hall profile 01.

11.4.2 3D Swath

Typically the raw shots records acquired for the narrow Sharow 3D swath are dominated by low-velocity ground roll and low-frequency guided wave reverberations sub-parallel to the first breaks (Figure 11.15). Bandpass filtering designed to remove the ground roll and guided waves reveals reflectivity on the shot close by the northern fence line of the pond enclosure (Figure 11.16, upper panel) and also from shots inside the enclosure towards the southern end of the profile. On the shot record from the middle of the profile, the reflection event is not so well defined. This was unexpected since the ground within the enclosure was water logged where there used to be two ponds.

Increasing the corner frequencies at the low-cut side of the bandpass filter by 40 Hz removed almost all the reflection energy from the shot records (Figure 11.16, lower panel). Higher frequency reflection signal can be recovered in shots acquired at the beginning and end of the 3D swath, but is completely overwhelmed by noise in shots fired in the middle of the 3D swath.

For the Sharow Hall 2D profile 02, aligned north-south just outside the western edge of the pond enclosure, the field statics calculated for the receivers are very consistent, centred on 4.5 ms with a variation of ±2 ms (Figure 11.17). 3D sub-line 01 is the most easterly line in the 3D swath and has a broad envelope of large receiver field statics across a 90 m span in the northern half of the pond enclosure. This hump in the shape of the receiver statics is repeated in the other seven sub-lines making up the Sharow Hall 3D swath. The high receiver static values coincide with the position of the now filled-in northern pond (Figure 11.18). The signature of the southern kidney-shaped pond, also not visible on the ground, is not observed in the receiver statics since only 3D sub-line 08 skims past it. It is probable that the ponds are filled with rotting, organic material, aerated with biogenic gas, which causes strong attenuation of high frequencies seismic waves. As a consequence, neither the Brotherton Limestone nor the deeper Hayton Anhydrite Formation could be mapped across the 3D swath.

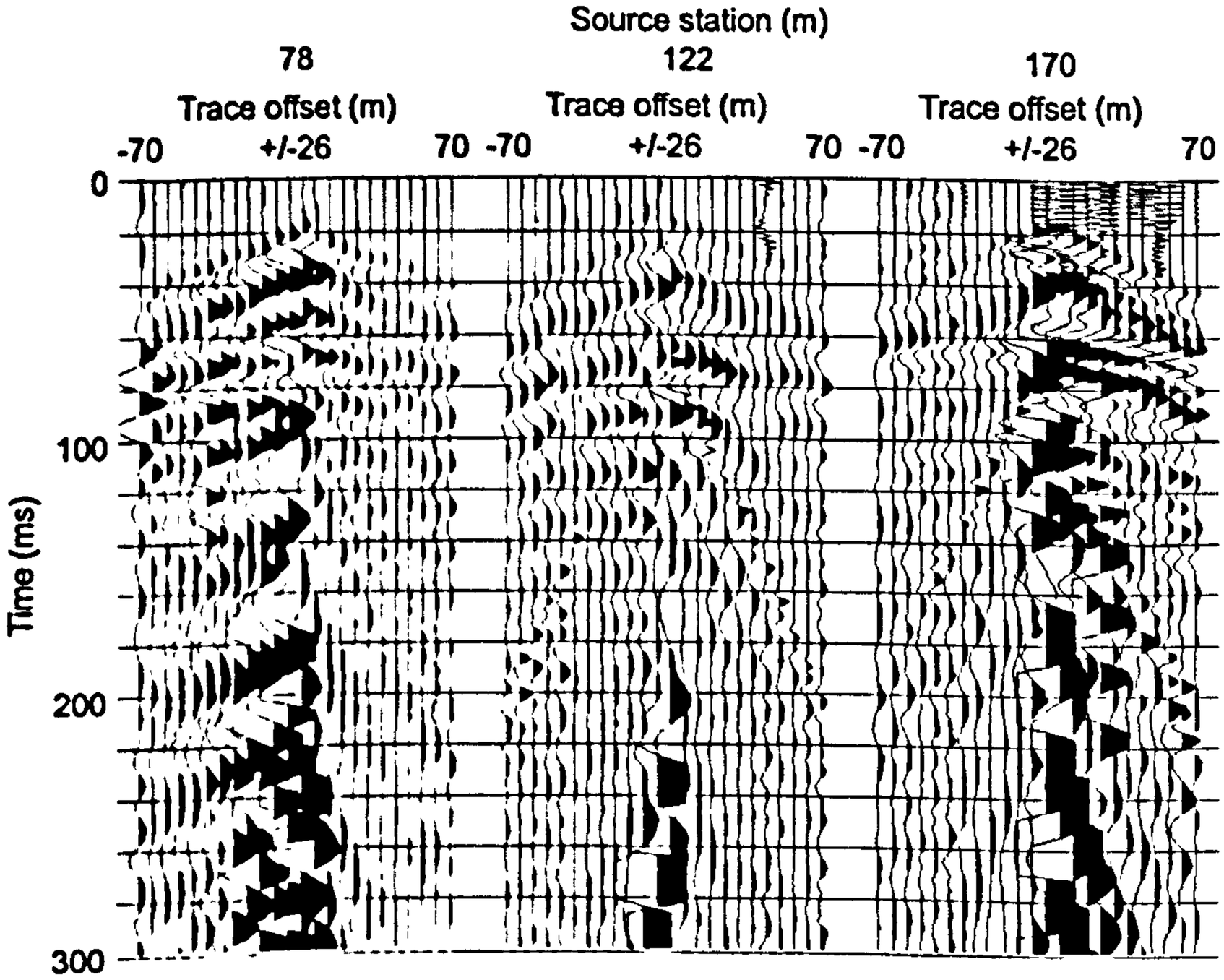

Figure 11.15: Raw shots from Sharow Hall 3D sub-line profile 01.
Data are displayed with a scalar multiplier.

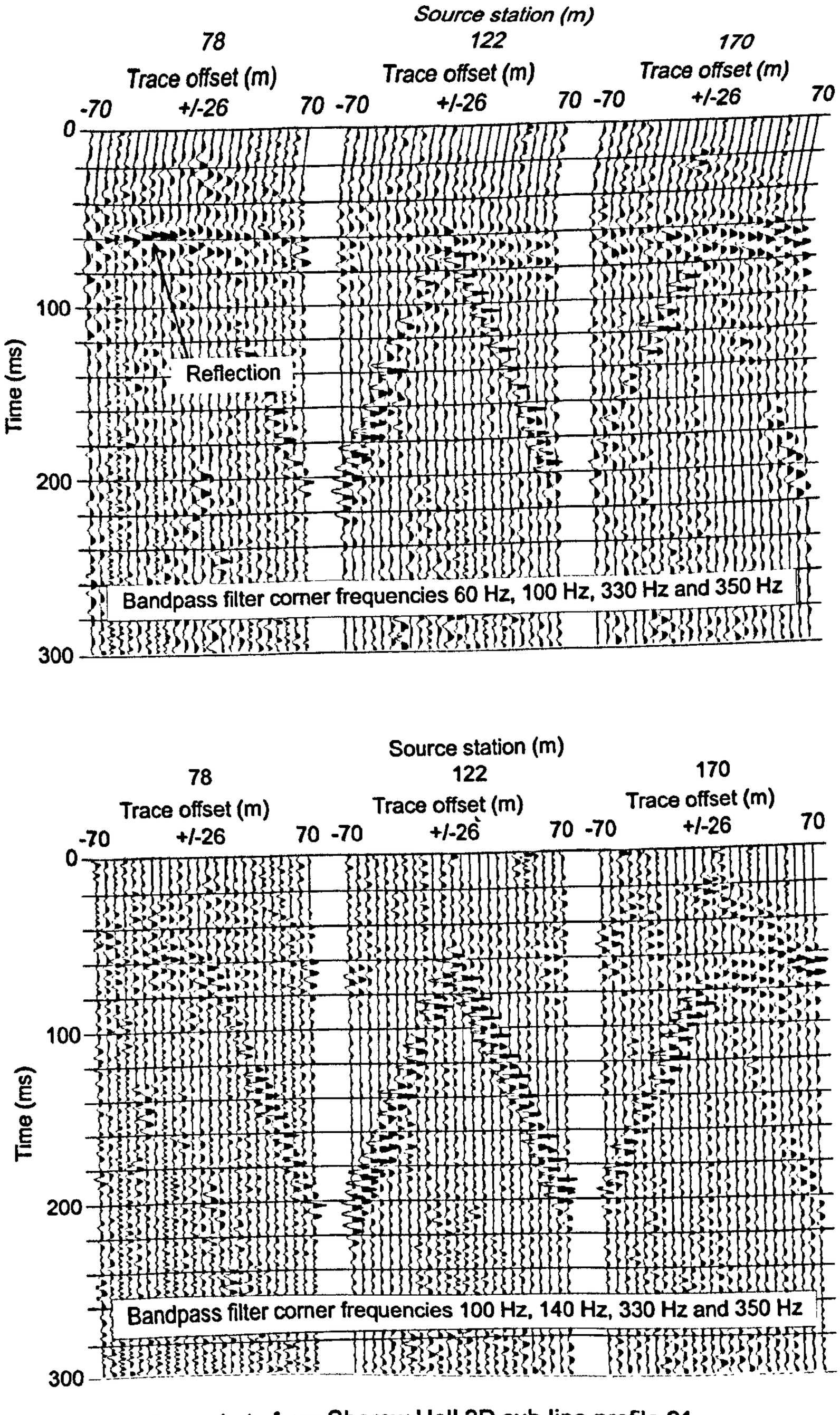

Figure 11.16: Filtered raw shots from Sharow Hall 3D sub-line profile 01.
Data are displayed with a 200 ms AGC window.

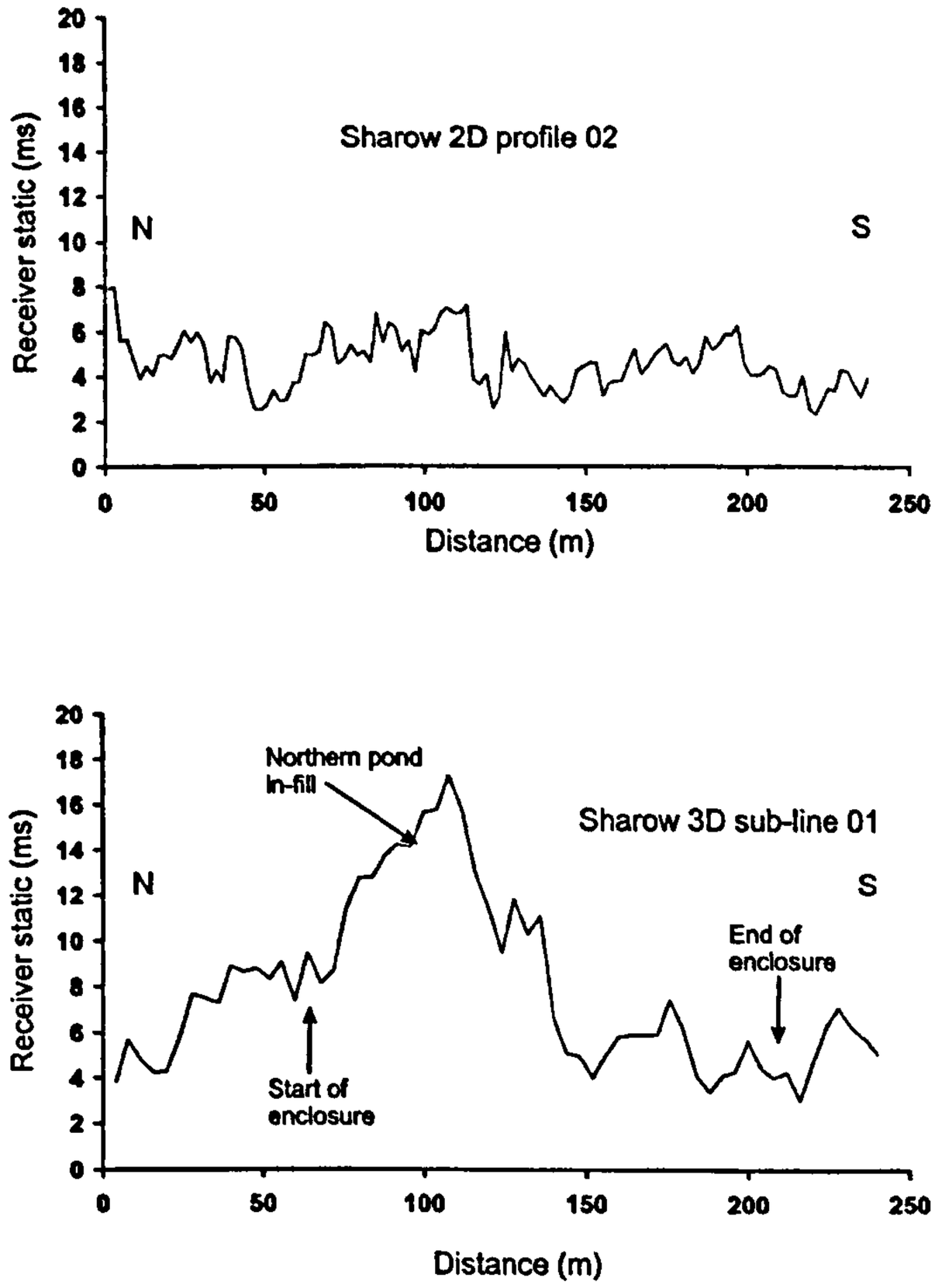

Figure 11.17: Comparison of 2D and 3D receiver statics solution.

11.4.3 Foundering

The rugose surface interpreted in Sharow Hall 2D profile 02 (Figure 11.11) as the top of the Hayton Anhydrite Formation may be due to the expansion of the crystal lattice as water infiltration transforms the anhydrite mineral into gypsum. Such folding structures are observed at the Ripon Parks cliff section (Figure 11.19) and the volume expansion is likely to have been absorbed by the overlying plastic Edlington Mudstones.

No major foundering of the sub-surface geology is imaged in the Sharow Hall 2D profile 02. A review of the historical Ordnance Survey maps and aerial photographs over the Sharow Hall survey area (Figure 11.20) did not reveal any natural features that can be possibly attributed to sub-surface gypsum dissolution, and suggest that the ponds were dug

out as an ornamental feature in the early to mid 1960s. Although this inference could not be confirmed by the current landowner or by the seismic data because of the extremely poor quality of the raw 3D swath field shot records; the condition of the sub-surface geology below the pond enclosure could not be ascertained.

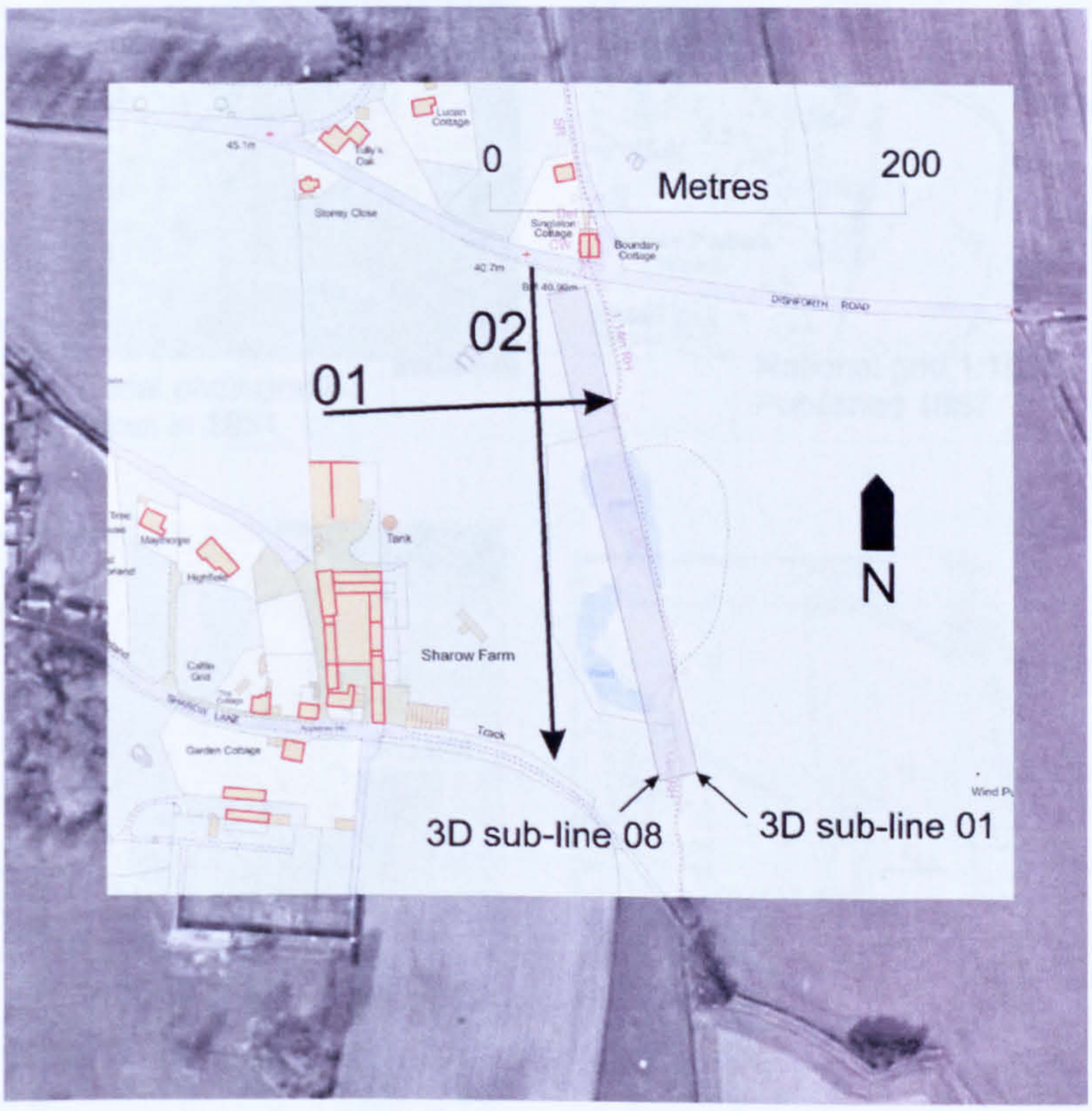

Figure 11.18: Ordnance Survey map overlaid on 1994 aerial photograph of Sharow Hall.

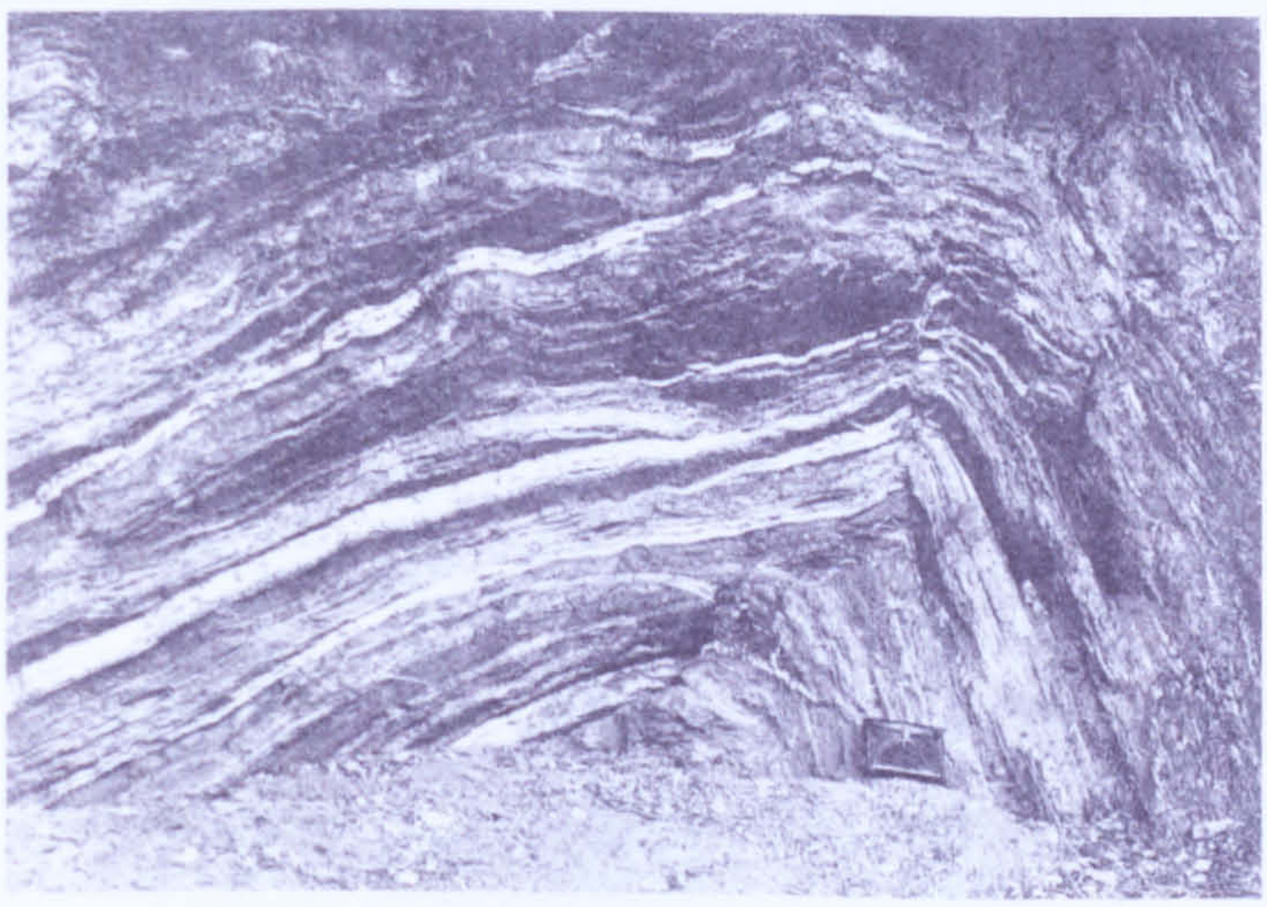

Figure 11.19: Contorted bedding at Ripon Parks.
Photograph from Cooper and Burgess (1993).

Aerial photograph
taken in 1951

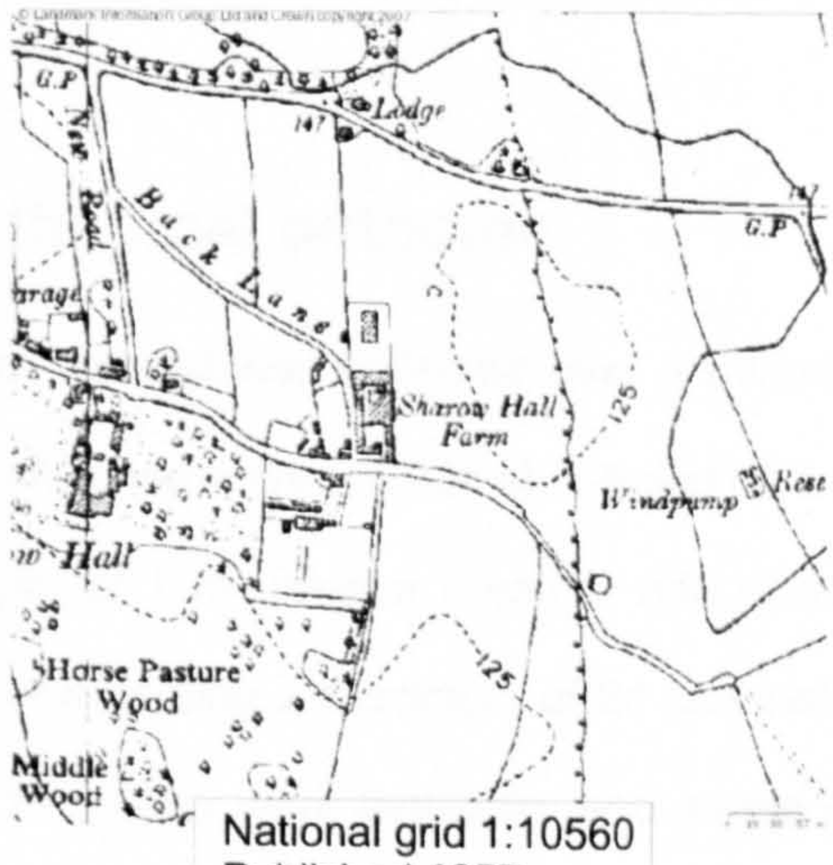

National grid 1:10560
Published 1957

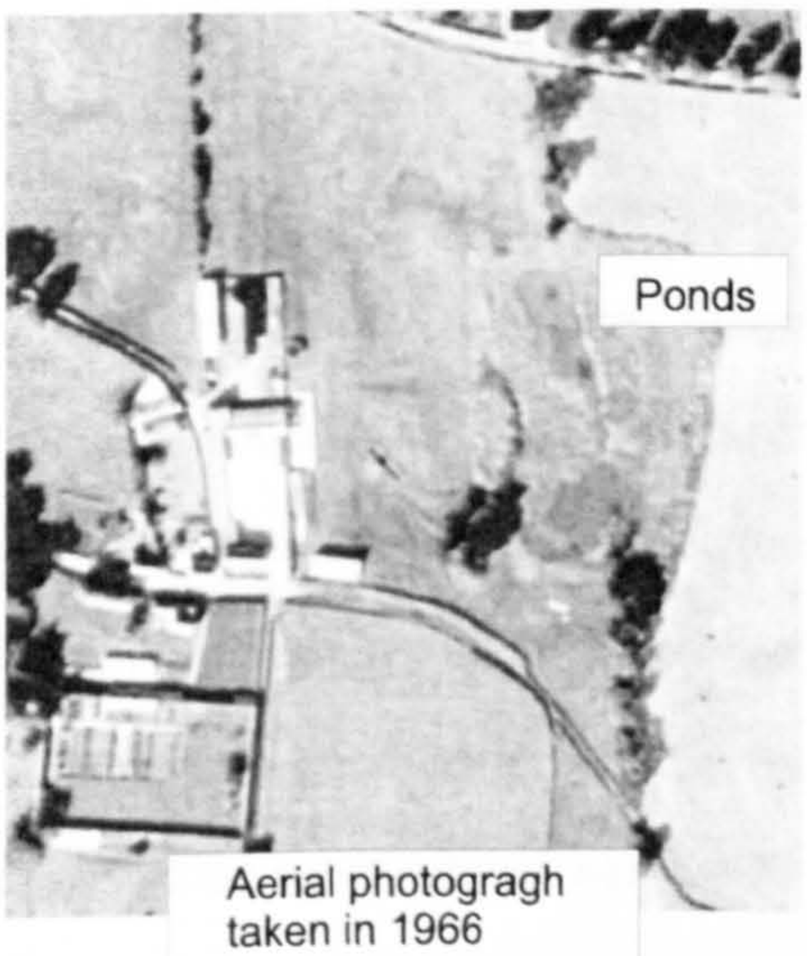

Aerial photogragh
taken in 1966

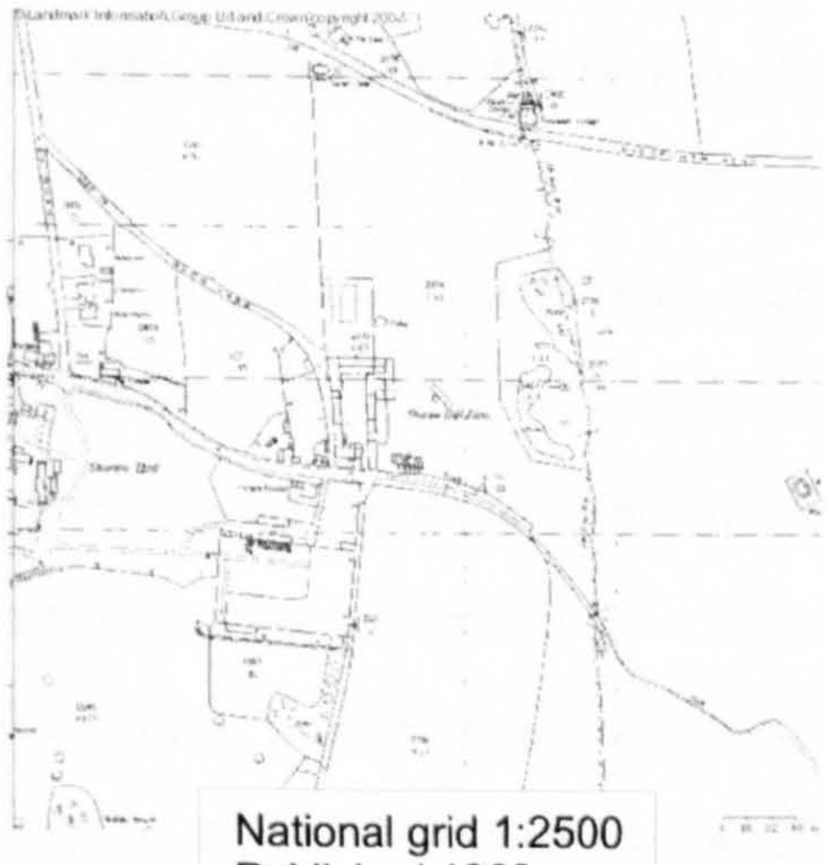

National grid 1:2500
Published 1968

Figure 11.20: Sharow Hall historic Ordnance Survey maps and aerial photographs.
Data supplied by Ordnance Survey/EDINA service © Crown Copyright and Land Information Group Ltd. Database 2007.

12.0 Discussion and conclusions

12.1 Suggestions on improving the final outcome

The 3D seismic volume acquired at Hell Kettles dataset was collected over a period of 14 days with a crew of 3—4 persons. In total 1512 shots were fired in 384 shot-holes on a grid of 16 lines of 24 holes drilled manually to a depth of 1 m using a hammer and stake. The SmartSeis S12 seismograph was only capable of recording a maximum of 24 channels, only SENSOR SM-7 geophones of 30 Hz resonant frequency were available, and all the source and receiver positioning was carried out with tape measures.

With these limited acquisition resources, the final 3D seismic volume, processed with post-stack time migration, revealed a series of depressions within the Seaham Formation limestone (Figure 5.49) that have been interpreted as due to dissolution of the deeper gypsiferous Hartlepool Anhydrite Formation. These detailed metre-scale sub-surface geological structures are imaged at depths of approximately 50 m below ground surface. However, only one reflection event was resolved, the interface between the soft mudstones of the Roxby Formation and the hard compact Seaham Formation limestone.

Very little improvement in the final interpretable product from the Hell Kettles 3D dataset could be achieved with alternative processing. If more resources were available, the key to improvement in data quality lies in revised acquisition parameters.

Hand auguring revealed that the shallow depression (Figure 5.3), the target feature of the Hell Kettles 3D survey, consisted of fine black organic material interpreted as sediment laid down at the bottom of a shallow pond. At this location trial shots were fired below the water table. After processing, the top of the gypsum-rich Hartlepool Anhydrite Formation can be observed (Figure 5.16). Therefore, it is anticipated that an order of magnitude improvement in the quality of the Hell Kettles 3D dataset could be achieved by firing shots below the water table to resolve details of the condition of the Hartlepool Anhydrite gypsum bed.

The advantages of placing the shot below the water table have been known for many decades. However, trial deep shots at Hell Kettles (Figure 5.17) show that placing the charge

below the water table does not significantly reduce the generation of the guided waves. A proportion of the seismic energy radiating outwards from the shot is still trapped between the free surface and the water table. Shots detonated below the water table will also generate a source ghost from the underside of the water table. The notch frequency f is given by the equation (e.g. Evans, 1997):

$$f = \frac{nV}{2d} \qquad (12.1)$$

where V is the P-wave velocity of the propagation medium, d is the depth below the water table and n is a positive integer. For a shot located 1 m below the water table with a typical P-wave velocity of 1800 m s^{-1} through water-saturated unconsolidated material, the first notch frequency would be 900 Hz. Only when the depth of shooting is 3 m or more below the water table will the source ghost impinge on the quality of the raw seismic data.

Outside a small area centred on the shallow depression, the near-surface strata comprise fluvial deposits. A drilling rig was hired (Figure 12.1) to drill a series of shot holes below the water along a line through the shallow depressions in which small dynamite charges were to be fired. The results were to be compared with the shots fired using the buffalo gun at the normal depth of 1 m. However, the shot holes drilled by the rig immediately collapsed inwards when the drill bit was withdrawn. Therefore, at this site any shot holes drilled below the water table would have to be drilled using casing.

The scaling law (Equation 5.5) states that *larger charges increase the amplitude and* duration of the wavelet. However, this law is only valid when comparing charges of the same composition and when the zones of chemical change and anelastic response around the shot scale in proportion to charge size. It is anticipated that the frequency bandwidth, and therefore the temporal resolution, for smaller dynamite charges will be comparable to that of 5—7 g of black powder. Higher amplitude noise may be generated by dynamite shots, but deeper reflection events such as from the top of the Ford Formation limestone and from the Coal Measures may be imaged if the shots are small charges of dynamite.

The Hell Kettles 3D acquisition layout was simple, with the shots fired into receiver spreads parallel to the lines of shot holes. This layout meant that raw 3D seismic data only had a very narrow distribution range of azimuths, leaving linear striations in the 3D statics picture (Figure 4.35). These striations are known as seam statics (Cox, 1995). The top of the gypsum-rich Hartlepool Anhydrite Formation across the Hell Kettles 3D survey area is likely to be rugose in nature with water infiltration following exhumation causing dissolution and volumetric expansion due to conversion of anhydrite to gypsum. To image this complex surface optimally, a full and evenly distributed range of offsets and azimuths are required. These requirements can be achieved with the latest models of portable engineering seismographs which have the capability to record up to 1024 channels simultaneously. They also have 24-bit recording capability, giving a theoretical dynamic range of 138 dB that potentially allows weak reflections to be recorded.

Figure 12.1: Large mechanical rig for drilling shot holes.

Buker et al. (1998) acquired such an intensive 3D shallow seismic survey covering a sub-surface area of 324 m x 398 m with a CMP bin size of 1.5 m x 1.5 m. Each bin had a nominal fold of 40 populated with a full range of azimuths. The effort required a crew of 5—7

persons over 85 days to fire 12000 shots using a buffalo gun into a 240-channel recording system.

Tests show that no improvement was made in the final time migrated interpretable section (Figure 5.12) when using tight 1-m diameter circular arrays of 6 geophones in place of single geophones. This observation is not in agreement with Meekes et al.(1990), but is the preferred set-up in coal exploration Ziolkowski and Lerwill (1979) and with current trends in the hydrocarbon exploration industry (Baeten and van der Heijden, 2008).

The geophones of 30Hz natural resonant frequency provide a flat amplitude response up to 300 Hz. Employing geophones of 100 Hz resonant frequency would suppress low frequencies more, and so would attenuate the ground roll and near-surface guided waves. However, Yilmaz (2001) shows that for optimum temporal resolution both low and high frequencies are required in signal bandwidth, so the 30 Hz geophones are an equally good choice provided that their spurious resonances are above the signal bandwidth and provided that the dynamic range of the recording system is not exceeded. These geophones will let through much of the low-frequency shot generated noise, but the low-frequency part of the primary reflection signal will also be preserved, and the unwanted seismic waves may be filtered out during processing. Burying the geophones only a few centimetres below the ground surface can reduce environmental noise significantly (Bland, 2002). The quality of the stacked section in shallow seismic reflection profiling is very sensitive to the level of environmental or cultural background noise within the raw seismic data. The first break picks used in the shot and receiver field static solution must be within ±1 ms of the time break to image small geological features properly (Figure 5.26), so the data must be acquired in calm weather conditions. The signal to noise ratio can also be improved by increasing the fold of coverage by using small geophone station spacing.

Tests show that even when the acquisition parameters are chosen to fulfil the stack array criterion, the ground roll is not significantly reduced (Figures 5.24 and 5.25). However, the stack array criterion results in an even distribution of offsets in the common midpoint domain and gives extra control for the interactive velocity analysis (Knapp, 1986); therefore it is recommended that the criterion should be obeyed wherever possible.

With the suggested changes to the acquisition parameters, the improved quality of raw seismic data will translate into simpler processing routes with more open filters, broader signal bandwidth and fewer computer-generated artefacts that may be construed as geological events. First break picks and interactive velocity analysis will be more accurate, leading to increased confidence in the field statics solution and final time-migrated datasets. It is anticipated that small voids and conduits will generate diffraction events in the final stacked sections. The common-diffraction point section (D-section) (Landa and Keydar, 1998) is an unusual process that may be used to highlight the position of sub-subsurface more accurately than standard processing routes.

Prior to acquisition, an onsite borehole that is accurately cored with a wireline logging tolls run would add considerable geological value to any near-surface investigation. With the elastic parameters of each horizon well constrained, for a particular frequency bandwidth the patterns in the shot, CMP and stack domains from water-filled conduits of various diameters within the Hartlepool Anhydrite Formation could be modelled, and hence compared to the real data as an aid for the interpretation of sub-surface voids. Forward modelling would also enable the acquisition parameters to be fine-tuned for the target horizons. Based on the wireling logging data and synthetic seismograms produced from them, shaping filters could be designed to convert the wavelet in the processed seismic data to zero-phase, and would improve resolution as well as enabling accurate positioning of each horizon below the ground surface.

At the Parkside survey site, the shooting conditions were excellent and resulted in the imaging of several reflecting horizons. These included two intra-Quaternary events and the top of the Ford Formation limestone aquifer at a depth of approximately 80 m below ground surface. Even so, the depth of penetration and the temporal resolution of the Parkside data could be improved by applying the recommendations described above, as would also be the case at Ulleskelf Mires.

Outside the pond enclosure at Sharow Hall, improvement in the raw seismic data quality is likely by applying the methods as described for the Hell Kettles survey site. However, within the ponds are thought to be man-made and can be delineated by the high values of source and receiver statics (Figure 11.17). Here the shot holes must be placed

beneath the disturbed ground. Additionally, this area is exceedingly boggy so the use of marsh geophones is recommended to improve the geophone ground coupling.

The Hutton Hill survey area is estimated to be at 25 m above the water table with the top of the Sherwood Sandstone Group approximately 3 m below ground surface. Goulty (1983) showed that shots fired in the dry Sherwood Sandstone Group (formally the Bunter Sandstone) are very poor. Therefore, better results might be achieved at Hutton Hill by detonating dynamite charges in the loose soil just above the Sherwood Sandstone Group.

At Neasham Fen the peaty ground conditions cause areas within the fen to be water-logged, but where the peat is dry beneath the tree cover all useful seismic data is lost. Shallow corings across the fen show that very fine clays are only 4 m below ground surface (Bartley et al., 1976). This fine-grained material provides the best shooting medium (Bredewout and Goulty, 1986) and so the shots should be placed here.

Across the majority of the Ure Bank survey area, the condition of the gypsiferous Hayton Anhydrite Formation is interpreted to be heavily hydrated so that the acoustic impedance contrast with the overlying water-saturated alluvial deposits is weak. Even with the recommended acquisition parameters proposed for Hell Kettles, the seismic method will not image any reflections from this bed, except in isolated areas such as that found at the northern end of profile 05 (Figure 9.10).

12.2 Suggestions for improving the standard acquisition

The standard firing procedure was to raise the firing pin a few decimetres above the blank shotgun cartridge percussion cap and dropping the pin on the observer's command. The source field statics show variations in the trigger timing of the shots of the order of a few milliseconds, and occasionally of larger magnitude (Figure 4.16). In the worst case, the profiles acquired at the Ulleskelf Mires exhibited variable trigger delays of up to ~15 ms (Figure 12.2). These were caused by mud being lodged in the firing pin guide-hole, and also due to the trigger sensitivity in the seismograph software being set wrongly for the shooting conditions.

Ideally an electronic pulse at time zero, called the time break would be recorded on a dedicated channel which all the first breaks could be referenced to. A simpler scheme to

minimise trigger delays is to place the firing pin directly on top of the percussion cap and tap it lightly with a hammer (pers. comm. D. Skinner). The trigger line is connected to the head of the hammer and the body of the buffalo gun so that the trigger input is shorted at the instant the hammer taps the firing pin.

In wet ground conditions or during rain, very high-frequency electrical cross-feed is commonly observed on the raw seismic data (Figure 3.12). This can usually be filtered out during processing without any significant damage to the primary reflection signal. However, when the cross-feed overrides the first breaks then it is necessary for the shot to be re-acquired. The cross-feed can be usually mitigated by placing the geophone take-outs on insulating material such as small wooden stakes. It is also possible to buy geophones and cables with waterproof take-outs.

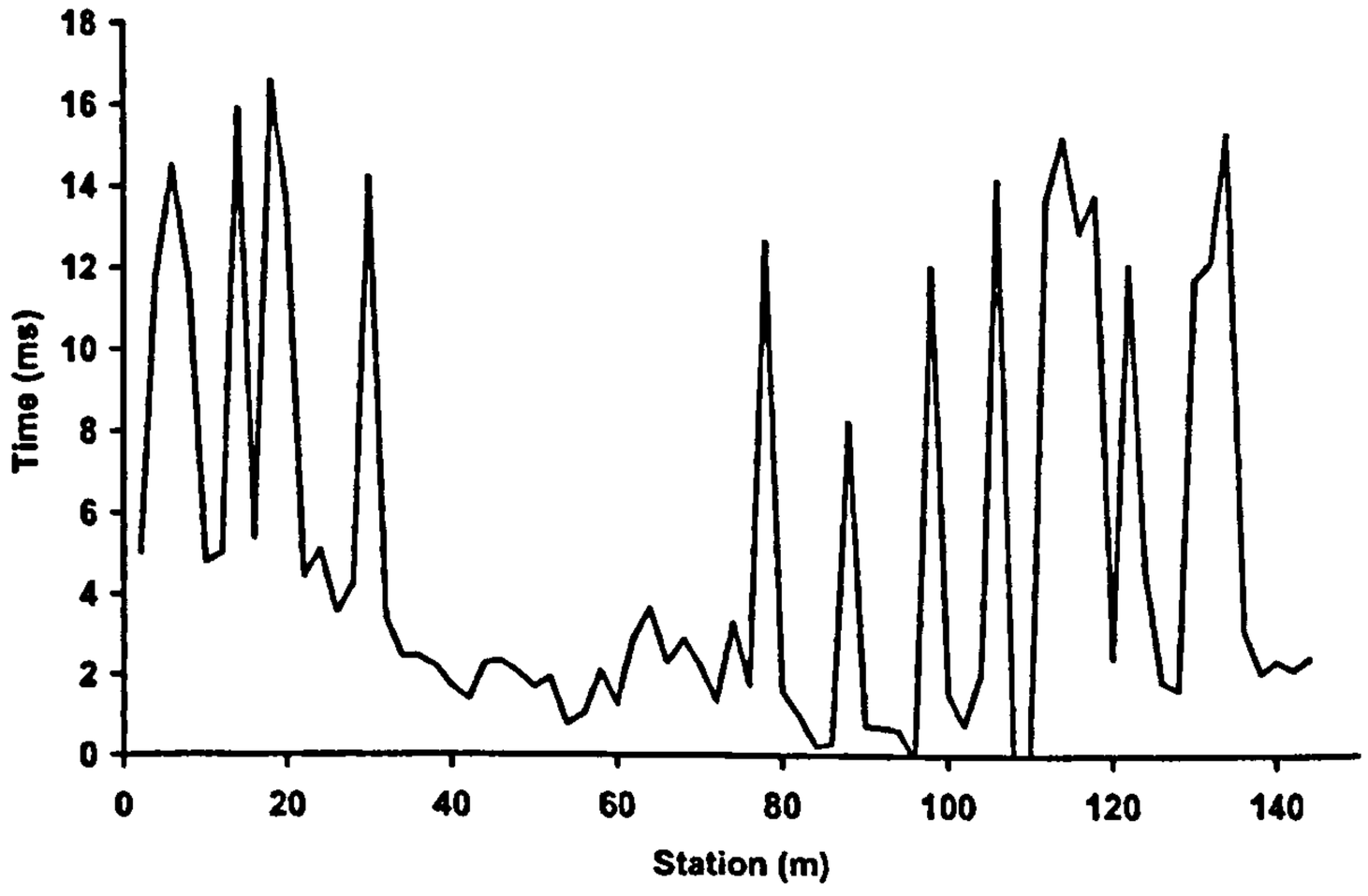

Figure 12.2: Extreme variable source statics along Ulleskelf Mires profile 03.

12.3 Novelty, uses and further research

Comparison of the built-in 2D profile and the 3D sub-line at the Hell Kettles survey area (Figure 5.48) show the increased resolution gained by 3D seismic technology. The impact of 3D seismic acquisition in delineating hydrocarbon reserves has undoubtedly been beneficial (Nestvold, 1992), and potentially could have the same impact in the delineation of shallow geology, as demonstrated by the metre-scale geological structures imaged at depths of 50 m by the Hell Kettles and Parkside 3D seismic volumes (Figure 5.42 and 6.18). The Hell Kettles survey is the first shallow seismic reflection 3D volume from the United Kingdom to be published in the scientific literature (Sargent and Goulty, 2009).

2D seismic profiles are capable of detecting the pillars in gypsum mines at depths of 60 m (Kourkafas and Goulty, 1996). Al-Rawahy and Goulty (1995) used 2D seismic profiles to monitor the changes in seismic velocity above longwall panels being mined in the Selby coalfield. Using the improved resolution of 3D seismic methods, it would be feasible to monitor the condition of mine workings over time.

High-amplitude low-frequency reverberations sub-parallel to the first breaks are typically prominent in shallow seismic reflection raw data (Figure 5.13). These guided waves usually exhibit two dominant frequencies and mask the reflection signal completely. Firing shots just below the water table does not remove or even significantly suppress the high-energy near-surface guided waves (Figure 5.17). So guided waves provide the most challenging processing obstacle. For shallow shots, they are always observed in the raw seismic data unless the water table is very close to the ground surface. Spitzer et al. (2001) showed that the guided-wave signal can be partially suppressed by processing a scheme using a combination of linear and hyperbolic $\tau - p$ domains. Potentially, the Kuhenen-Loève transformation can be used to discriminate between the primary reflection signal and guided waves (Bitri and Grandjean, 2004). However, for maximum impact the design of the $\tau - p$ and Kuhenen-Loève parameters would have to be tailored for every individual shot since the character of the guided waves changes rapidly with the near-surface conditions. The guided-wave reverberations are easily, but crudely, removed from the seismic record by simple bandpass filtering, reducing the bandwidth to approximately 100Hz to 330Hz, or 1.5 octaves. Further research is required to develop a processing technique for removing the

reverberations efficiently without destroying the primary reflection signal. Such a technique would significantly broaden the signal bandwidth, thereby increasing the temporal resolution and hence enabling improved geological interpretation of the seismic data.

S-waves have a velocity that is 70% less than that of P-waves, and therefore have a higher temporal resolution capability for a given frequency bandwidth. A combination of S and P-wave data can allow for the measurement of a Poisson's ratio of the sub-surface geology and can indicate seismic anisotropy (Desios et al., 1999). Pugin et al (2006) used P-waves to map gas plumes to see if they correlate to bedrock fractures located by S-wave sections. However, there is a paucity of shallow seismic S-wave studies because S-wave reflections are commonly masked by dispersive Love waves. Love waves are surface waves, the S-wave equivalent of Rayleigh waves, and are generated when a low-velocity layer overlies a half-space such as unconsolidated materials above a shallow water table. Further research is required to develop a processing technique for removing the Love waves without destroying the primary reflection signals.

12.4 Comments on gypsum dissolution in the survey areas

Three conditions must exist for the gypsum dissolution process to proceed (Martinez et al., 1998). Firstly, there must be a water supply which is unsaturated with respect to calcium sulphate ions. Secondly, there must be energy to drive the water through the system, and thirdly there must be an outlet for the water carrying the dissolved solids.

Three limestone formations underlie Darlington, dipping towards the east-south-east, the Seaham, Ford and Raisby formations. The Hurworth Place borehole (Figure 2.8) shows that the Billingham Anhydrite and Hartlepool Anhydrite gypsum beds rest directly on the Seaham and Ford formations. These formations are artesian aquifers, and the development of the Ford Formation limestone aquifer as a water supply in the 1970s showed that the groundwater flow is from north-west to the south-east, in the same direction as the geological dip (Cairney, 1972). Therefore, energy is available for the flow of water through the limestone to carry away any dissolved gypsum solids from the base of the gypsum formations. Boreholes monitored in the South Darlington area (Lamont-Black et al., 2002) proved that the water in the Ford Formation limestone is under-saturated with respect to gypsum and that

water is flowing through this unit, so there must be an outlet. Thus all conditions required for gypsum dissolution to proceed are present beneath Darlington. Gypsum scoured away from the base of the Hartlepool Anhydrite Formation by water flowing through the underlying Ford Formation is a possible cause of the foundering imaged at the Hell Kettles survey site (Figure 5.49).

Dissolution of gypsum at the Ulleskelf Mires survey site, as evidenced by profile 05 (Figure 8.19), probably occurs by a similar mechanism. Here the Brotherton Formation limestone aquifer dips down towards the north-east, and is imaged underlying a thin bed of Billingham Anhydrite Formation which disappears over an area coinciding with a broad shallow depression at the ground surface. An additional piece of information supporting this mechanism is provided by the recording of a 1-m high cavity is recorded in a nearby borehole (Figure 8.13).

The gypsum-rich Hayton Anhydrite Formation at Sharow Hall is overlain by the Permian Roxby, Brotherton and Edlington formations. The Hayton Anhydrite bed exhibits a rugose surface with a few undulations having horizontal dimensions of about 10 m (Figure 11.11). The gypsum bed is protected from the Brotherton Limestone aquifer by approximately 10 m of Edlington Formation mudstones. However, over a long period of time water will percolate down through the leaky Edlington Formation aquitard and alter the anhydrite mineral into gypsum, resulting in expansion of the crystal lattice and creating the rugged surface.

The top surface of the Hartlepool Anhydrite Formation also exhibits a convoluted surface on the southernmost Hell Kettles profiles (Figures 5.29, 5.32, 5.33, 5.36 and 5.41). At this site, water is probably percolating down from the Seaham Formation through the Edlington Formation mudstones to alter the calcium sulphate crystal structure. The water flow is likely to be very sluggish and so the water will become saturated with calcium sulphate ions dissolved out of gypsum bands in the Edlington Formation, so that no significant quantities of gypsum will be removed from the top surface of the Hartlepool Anhydrite gypsum bed.

At the southern end of Parkside profile 04 (Figure 6.11), the top surface of the Hartlepool Anhydrite Formation is also very rugose. The rough surface is interpreted as the result of volumetric expansion in the conversion of anhydrite to gypsum by infiltration of water

percolating down through the Quaternary deposits. This meteoric water will be under-saturated with respect to gypsum. Although the rough surface could have been caused by dissolution as the glaciers retreated at the end of the Quaternary Devensian stage, it seems more likely that the dissolution has mostly occurred underground, beneath Quaternary deposits, because the gypsum would only have been exposed at the ground surface for a relatively brief period of time.

Ure Bank is a special case where gypsum in the Hayton Anhydrite Formation is being vigorously dissolved at the top and the base of the formation by flowing water that is under-saturated with respect to calcium sulphate ions.

12.5 A wider geographical view of karstic subsidence

This project has concentrated on three locations in north-east England, Darlington, Ripon and Church Fenton that are known to underlain by thick Permian gypsum beds. Other evaporite deposits of different geological ages are to be found in the United Kingdom which could potentially be dissolved by flowing groundwater, and hence cause ground subsidence (Figure 12.3).

Triassic gypsum outcrops over a wider extent than Permian gypsum, but the effects are much less severe since the Triassic gypsum is inter-bedded within weakly permeable mudstones (Cooper et al., 2001).

The other highly soluble evaporite deposits present in UK Permo-Triassic strata are halites. The Permian salts are centred on Whitby, but are deeply buried and therefore pose no subsidence risk. Four areas of Triassic salt deposits have been extensively worked Cheshire, Staffordshire, Lancashire and Worcestershire. Old style salt extraction by brine pumping operations caused widespread and catastrophic subsidence in the Cheshire salt field around Northwich and Middlewich (Cooper, 2001). With modern salt mining techniques, the saline groundwater levels have returned to their natural state, brine springs have re-established and natural karstification and subsidence may occur (Cooper et al., 2001). Similarly, the three other smaller salt fields have also suffered subsidence induced by salt extraction), and may be liable to such instances in the future.

Limestones are significantly stronger than evaporates and also have a dissolution rate that is 100—200 times less. Carbonate sinkholes are classified into six main types: solution, collapse, caprock, dropout, suffosion and buried (Waltham et al., 2005), and extensive rectilinear cave systems often develop in carbonate deposits. Limestone deposits are widely distributed throughout the United Kingdom (Figure 12.3) and have a large age span from Cambro-Ordovician through to Jurassic. Most of the limestone areas are in rural settings and therefore only pose a limited geo-hazard.

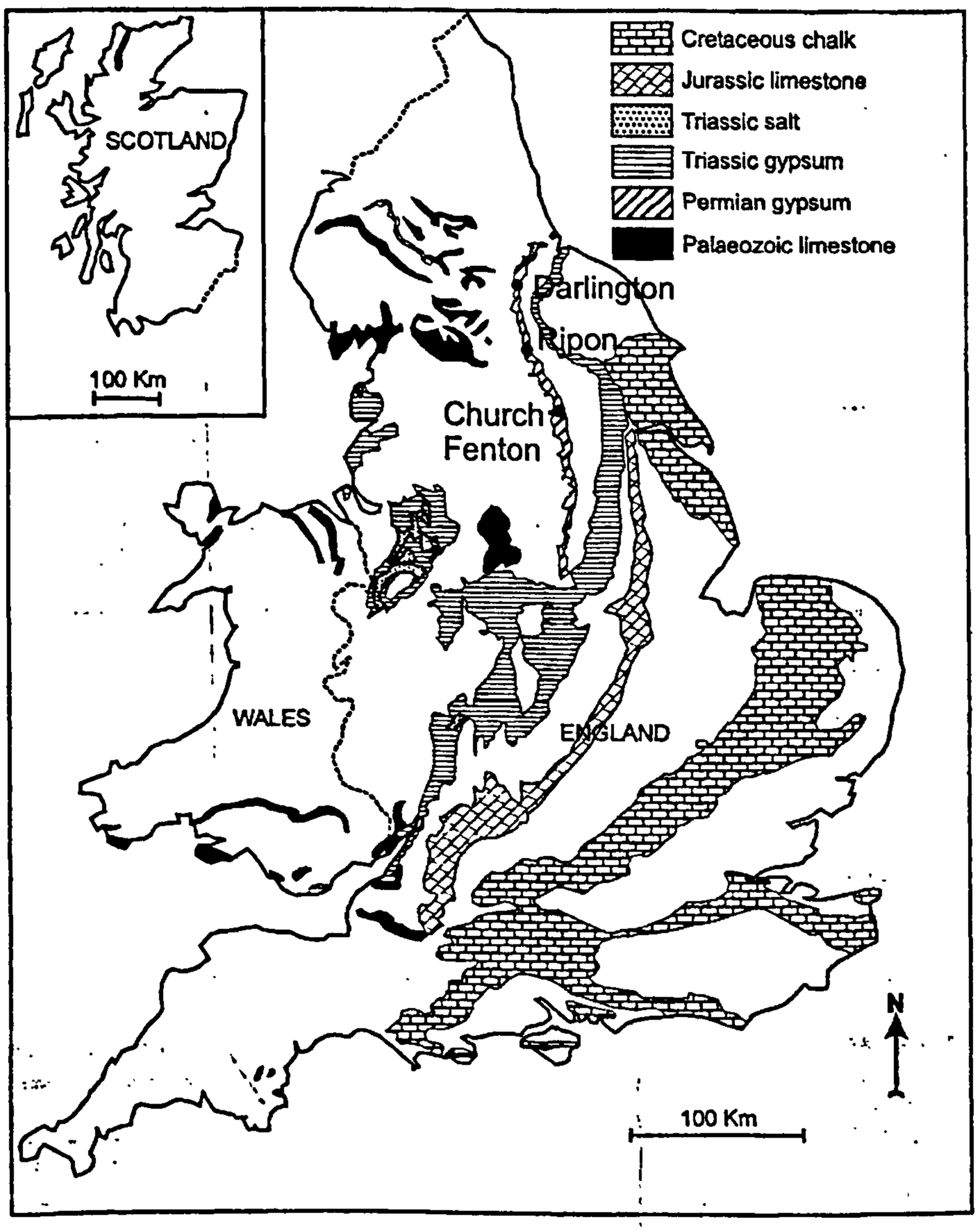

Figure 12.3: Outcrop distribution of rocks prone to karst across the United Kingdom. Map modified from Cooper et al. (2001).

Chalk underlies large swaths of southern and eastern England and is a very important water aquifer in these regions. Chalk has low mechanical strength compared to dense, compact limestones and so consequently sinkholes of any size are rare, but where they do exist, variable chalk-clay ratios often filling in the depression cause problems in civil engineering projects (Culshaw and Waltham, 1987). The main geo-hazard in chalk areas is due to ancient unmapped mine workings.

Waltham et al. (2005) described a number of case studies in the United Kingdom over gypsum and chalk karsts. Elsewhere, the micro-gravity geophysical method has been employed successfully to investigate near-surface cavities at less than 10 m depth in the United Kingdom associated with halite (Branston and Styles, 2003), limestones (Styles et al., 2005) and chalk beds (Reynolds, 2004). The shallow seismic reflection method, in particular in 3D mode, has only rarely been used to study these geological problems in the United Kingdom.

As a worldwide phenomenon, large areas of the Earth's surface are underlain by evaporitic basins (Figure 12.4). The largest of these basins is the Late Cambrian Eastern Siberian Basin, which covers 1.5 million km^2 (Warren, 1999). The European Permian Zechstein basin laps on to north-east England and is the third largest ancient salt deposit after the Middle Jurassic Gulf of Mexico basin. Modern evaporitic environments are very small In comparison with the ancient salt basins (Figure 12.5).

Limestone is one of the most common sedimentary rocks. One eighth of the continental landmass has an outcrop of carbonate rocks (Table 12.1). Almost every country in world has the potential for the development of limestone karst (Figure 12.6).

The formation of sinkholes In Kansas and Oklahoma, USA are well documented, but the rate of development has increased with of oil and gas exploration since 1940. The recent sinkholes are all centred at sites of salt-water disposal wells. Leakage from some of these wells into Permian Hutchinson Salt, of 76 m average thickness, has caused localised dissolution of the salt deposits with subsequent ground subsidence (Steeples et al., 1986). In particular, the Macksville sinkhole (Figure 7.15) is similar in size and shape to Neasham Fen.

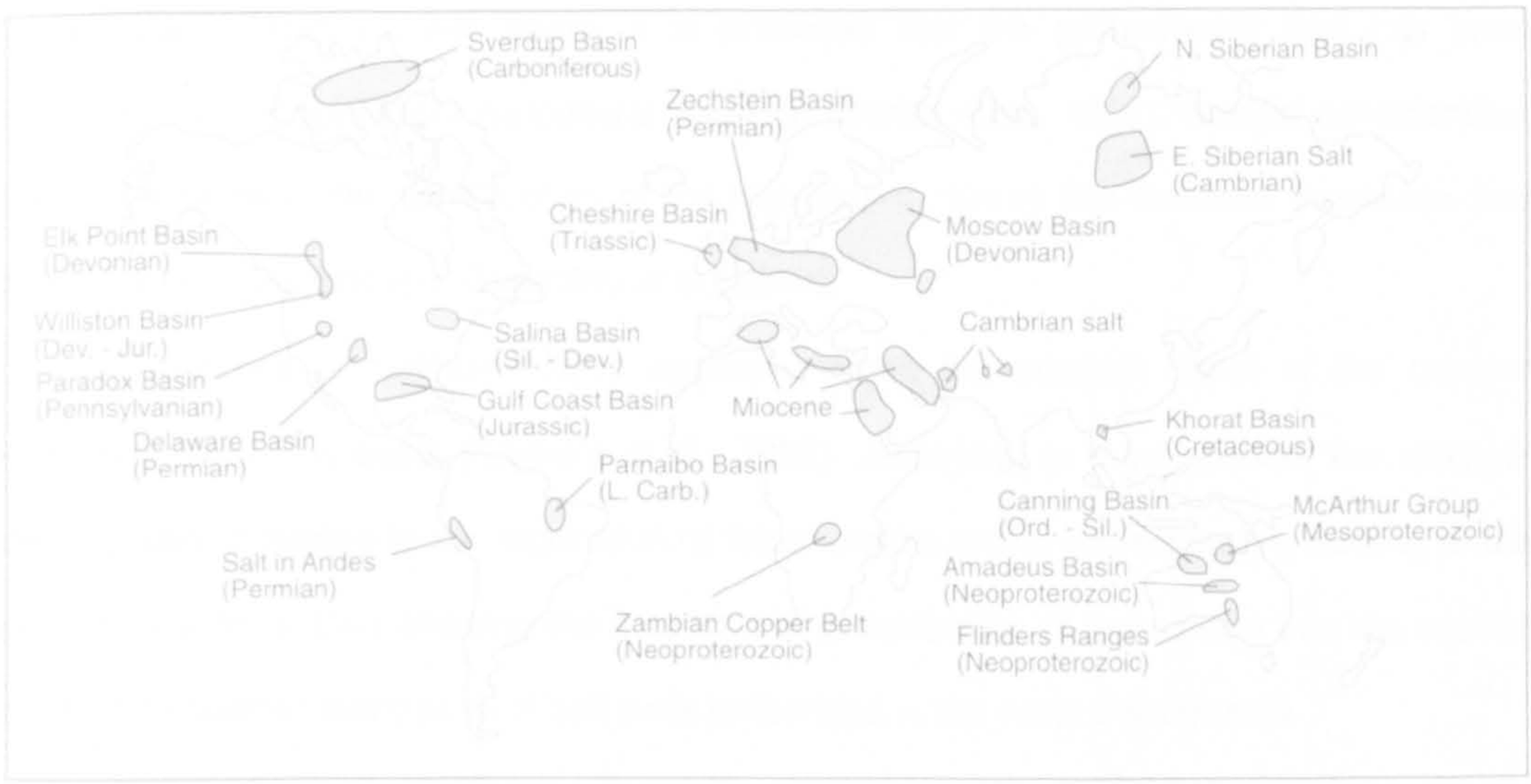

Figure 12.4: Major basinwide evaporite deposits.
From Warren (1999). Basins are not drawn to exact scale.

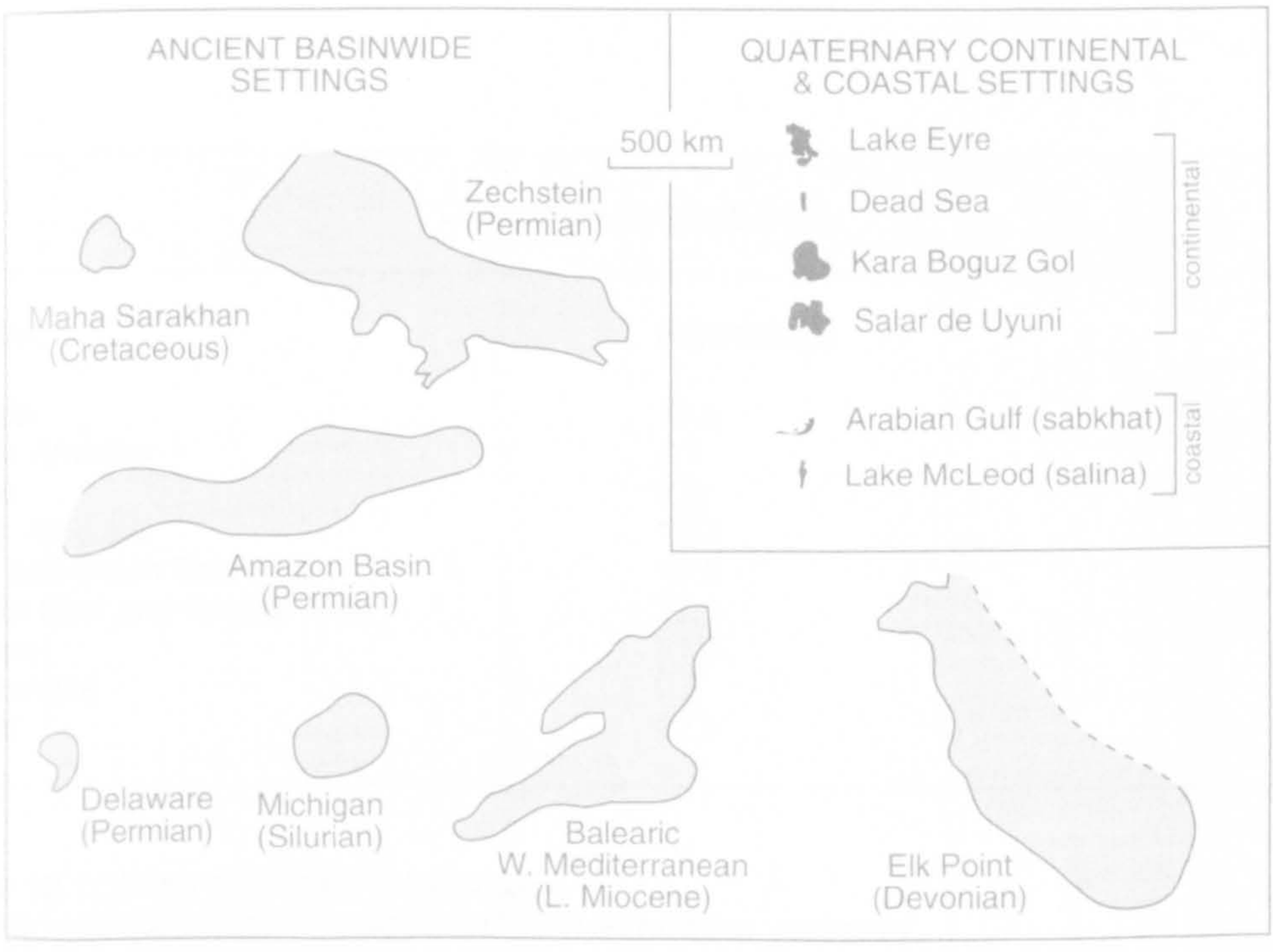

Figure 12.5: Comparison of aerial extent of Quaternary and ancient evaporite deposits.
From Warren (1999).

Induced sinkholes have been formed by dissolution of the Permo-Triassic gypsum beds around Zaragoza, NE Spain. It is proposed that the groundwater flow has been increased by leakages from agricultural irrigation (Benito et al., 1995). Special consideration had to be taken in the construction of the high-speed railway link between Barcelona and Madrid over this landscape (Guerrerro et al., 2004).

Hundreds of sinkholes have appeared along the western coast of the modern evaporite Dead Sea coast (Ezersky et al., 2006). According to most studies, the sinkhole development is related to the regression of the shoreline with a corresponding sinking of the groundwater level, thus allowing the incursion of groundwater of low salinity into the coastal area which washes away pods of salt pods embedded in the coastal sediments.

It has been shown by many studies that both the ancient and modern evaporite deposits are potentially a geo-hazard, either naturally or induced, where the salt deposits are shallow enough to become in contact with water flows that are under-saturated with respect to the salt type present.

Carbonate Outcrop Area

Region	Percentage
Russia	16.1
South America	2.1
Africa	9.2
North America	18.3
East and South East Asia	10.8
Middle East and Central Asia	23.0
Europe	21.8
Australasia	6.2
World	12.5

Table 12.1: World carbonate outcrop area.
Data downloaded from www.sges.auckland.ac.nz/sges_research/.

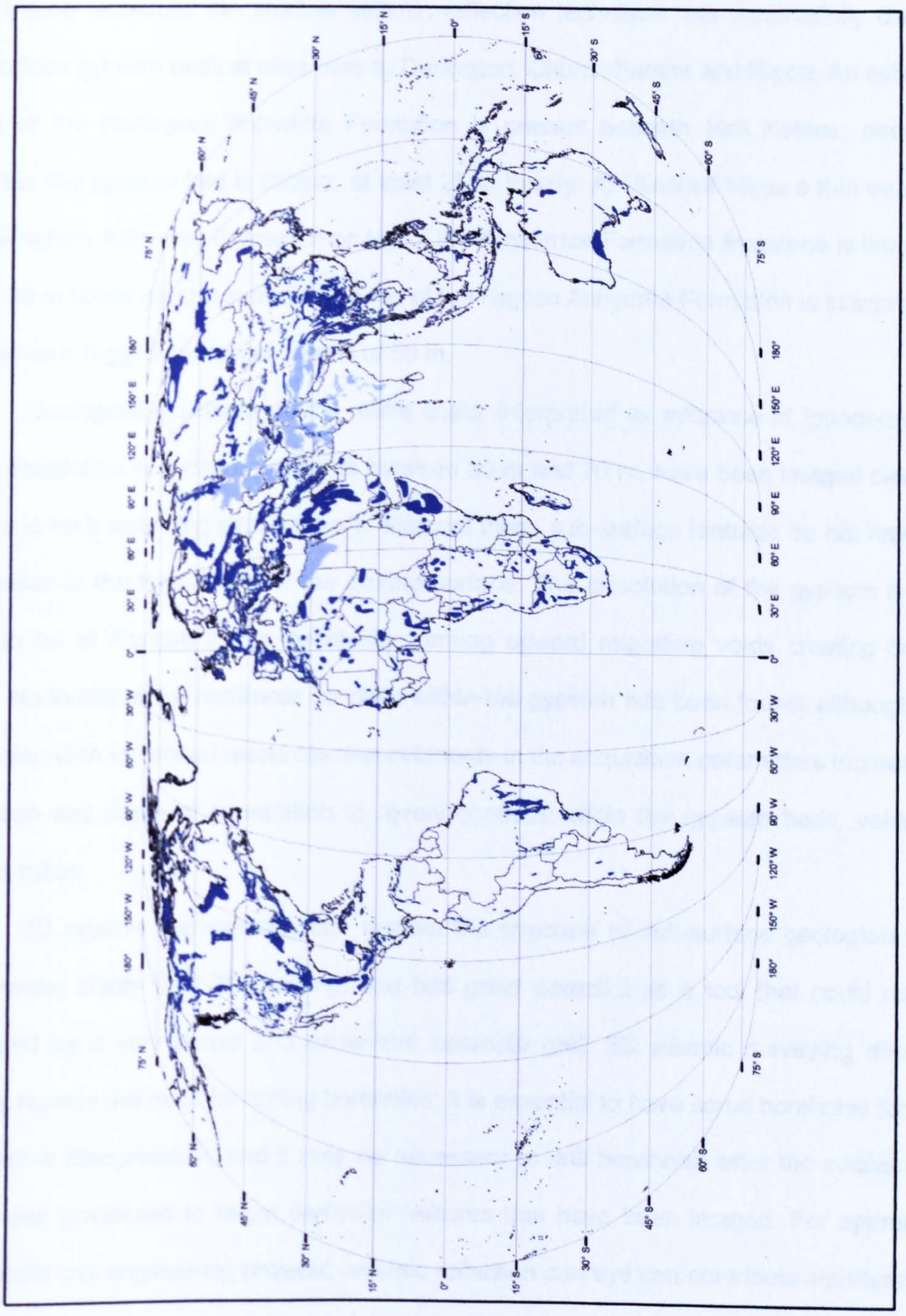

Figure 12.6: World distribution of potential carbonate karst.
Download from www.sges.auckland.ac.nz/sges_research/karst.shtm. Used in Ford and Williams (2005). The dark blue areas are the main areas of limestone outcrop. The light blue areas are where carbonate rocks are abundant, but discontinuous or impure.

12.6 Conclusions

With limited resources the shallow seismic reflection technique has successfully detected sub-surface gypsum beds at sites near to Darlington, Church Fenton and Ripon. An estimated 15 m of the Hartlepool Anhydrite Formation is present beneath Hell Kettles; nearby at Parkside this gypsum bed is thicker, at least 25 m locally. At Ulleskelf Mires a thin veneer of the Billingham Anhydrite Formation on top of the Brotherton Formation limestone is imaged at about 30 m below ground surface. The top of the Hayton Anhydrite Formation is interpreted at Sharow as a rugged surface at depths of 50 m.

Geological structures on the metre scale, interpreted as evidence of foundering due to the dissolution of gypsum at depths between 30 m and 70 m, have been imaged clearly in limestone beds overlying gypsum beds. Many of these sub-surface features do not have any expression in the topography at the ground surface. The dissolution of the gypsum is most likely to be at discrete points eventually forming upward migrating voids creating breccia tubes. No evidence for rectilinear conduits within the gypsum has been found, although they may exist. With increased resources improvements in the acquisition parameters increase the resolution and depth of penetration to reveal conduits within the gypsum beds, voids and breccia tubes.

3D seismic methodology can resolve the structure of sub-surface geological detail with greater clarity than 2D profiling, and has great potential as a tool that could only be replicated by a very dense and expensive borehole grid. 3D seismic surveying does not entirely replace the need for drilling boreholes: it is essential to have some boreholes for tying the seismic interpretation, and it may be necessary to drill boreholes after the seismic data have been processed to target particular features that have been imaged. For appropriate large-scale civil engineering projects, seismic reflection surveys can contribute significantly to the evaluation of subsidence hazards in site investigation.

13.0 References

Al-Rawahy, S.Y.S. and Goulty, N.R. 1995. Effect of mining subsidence on seismic velocity monitored by a repeated reflection profile. *Geophysical Prospecting* **43**, 177-193.

Anderton, R., Bridges, P.H., Leeder, M.R. and Sellwood, B.W. 1983. *A Dynamic Stratigraphy of the British Isles: A Study in Crustal Evolution,* 3rd edn. George, Allen and Unwin, London, UK.

Anstey, N. 1986. Whatever happened to ground roll? *The Leading Edge* **5**(3), 40-45.

Baeten, G. and van der Heijden, H. 2008. Improving S/N for high frequencies. *The Leading Edge* **27**, 144-153.

Baker, G.S., Steeples, D.W. and Drake, M. 1998. Muting the noise cone in near-surface reflection data: An example from southeastern Kansas. *Geophysics* **63**, 1332-1338.

Baker, G.S., Schmeissner, C. and Steeples, D.W. 1999. Seismic reflections from depths of less than two meters. *Geophysical Research Letters* **26**, 279-282.

Bartley, D.D., Chambers C. and Hart-Jones B. 1976. The vegetational history of parts of south and east Durham. *New Phytology* **77**, 437-468.

Benson, A.K. 1995. Applications of ground penetrating radar in assessing some geological hazards: examples of groundwater contamination, faults, cavities. *Journal of Applied Geophysics* **33**, 177-193.

Benito, G., Pérez del Campo, P., Gutiérrez-Elorza, M. and Sancho, C. 1995. Natural and human-induced sinkholes in gypsum terrain and associated environmental prolems in NE Spain. *Environmental Geology* **25**, 156-164.

Birk, S., Liedl, R., Sauter, M. and Tuetsch, G. 2005. Simulation of the development of gypsum maze caves. *Environmental Geology* **48**, 296-306.

Bitri, A. and Grandjean, G. 2004. Suppression of guided waves using the Karhunen-Loève transform. *First Break* **22**(5), 45-47.

Bland, H.C. and Gallard, V. 2002. Avoiding wind noise: How helpful is geophone-burying? *CSEG Geophysics* Canadian Society of Exploration Geophysicists, Calgary (available at: www.cseg.ca/conferences/2002/2002abstracts/Bland_HC_Avoiding_wind_noise_ACQ-1.pdf).

Brabham, P.J., McDonald, R.J. and McCarroll, D. 1999. The use of shallow seismic techniques to characterize sub-surface Quaternary deposits: the example of Porth Neigwl (Hells Mouth Bay), Gwynedd, N. Wales. *Quarterly Journal of Engineering Geology* **32**, 119-137.

Branham, K.L. and Steeples, D.W. 1988, Cavity detection using high-resolution seismic reflection methods. *Mining Engineering* **40**, 115-119.

Branston, M.W. and Styles, P. 2003. The application of time-lapse microgravity for the investigation and monitoring of subsidence at Northwich, Cheshire. *Quarterly Journal of Engineering Geology and Hydrogeology* **36**, 231-244.

Bredewout, J.W. and Goulty, N.R. 1986. Some shallow seismic reflections. *First Break* **4**(12), 15-23.

Brown, A.R. 2004. *Interpretation of Three-Dimensional Seismic Data,* 6th edn. American Association of Petroleum Geologists and Society of Exploration Geophysicists, Tulsa, USA.

Bruno, F. and Marillier, F. 2000. Test of high-resolution seismic reflection and other geophysical techniques on the Boup Landslide in the Swiss Alps. *Surveys in Geophysics* **21**, 333-348.

Büker, F., Green, A.G. and Horstmeyer, H. 1998. Shallow 3-D seismic reflection surveying: Data acquisition and preliminary processing strategies. *Geophysics* **63**, 1434-1450.

Cairney, T. 1972. Hydrological investigation of the magnesian Limestone of south-east Durham, England. *Journal of Hydrology*, **16**, 323-340.

Canales, L. 1984. Random noise reduction. 54th Annual International Meeting, Society of Exploration Geophysicists, Expanded Abstracts, 525.

Cardarelli, E., Di Filippo, G. and Tuccinardi, E. 2006. Electrical resistivity tomography to detect buried cavities in Rome: a case study. *Near Surface Geophysics* **4**, 387-394.

Chamberlain, A.T., Sellers, W., Procter, C. and Coard, R. 2000. Cave detection in limestone using ground penetrating radar. *Journal of Archaeological Science* **27**, 957-964.

Chun, J.H. and Jacewitz C.A. 1981. Fundamentals of frequency domain migration. *Geophysics* **46**, 717-733.

Cooper, A.H. 1986. Subsidence and foundering of strata caused by the dissolution of Permian gypsum in the Ripon and Bedale areas, North Yorkshire. *In:* Harwood, G.M and Smith D.B. (eds). *The English Zechstein and related topics.* Geological Society Special Publication No. 22, London, U.K., 127-139.

Cooper, A.H. 1989. Airbourne multispectral scanning of subsidence caused by Permian gypsum dissolution at Ripon, North Yorkshire. *Quarterly Journal of Engineering Geology* **22**, 219-229.

Cooper, A.H. and Burgess, I.C. 1993. *The geology of the country around Harrogate.* British Geological Survey Memoir, Sheet 62.

Cooper, A.H. 1995. Subsidence hazards due to the dissolution of Permian gypsum in England: investigation and remediation. *In:* Beck, F.B. (ed.) *Karst Geohazards: Engineering and Environmental Problems in Karst Terrain.* Proceedings of the 5th multidisciplinary conference on sinkholes and the engineering and environmental impacts of karst, Gatlinburg, Tennessee, 2-5 April 1995. A.A.Balkema, Rotterdam, Netherlands, 23-29.

Cooper, A.H. and Waltham, A.C. 1999. Subsidence caused by gypsum dissolution at Ripon, North Yorkshire. *Quarterly Journal of Engineering Geology* **32**, 305-310.

Cooper, A.H. 2001. Natural and induced halite karst geohazards in Great Britain. *In:* Beck, F.B. and Herring, J.G. (eds.) *Geotechnical and Environmental Applications of Karst Geology and Hydrology.* Swets and Zeitlinger, Lisse, Netherlands, 119-124.

Cooper, A.H., Farrant, A.R., Adlam, K.A.M. and Walsby, J.C. 2001. The development of a national Geographic Information System (GIS) for British karst geohazards and risk assessment. *In:* Beck, F.B. and Herring, J.G. (eds.) *Geotechnical and Environmental Applications of Karst Geology and Hydrology.* Swets and Zeitlinger, Lisse, Netherlands, 125-130.

Cox, M. 1999. *Static corrections for seismic reflection surveys, 1st edn.* Society of Exploration Geophysicists, Tulsa, USA.

Culshaw, M.G. and Waltham, A.C. 1987. Natural and artificial cavities as ground engineering hazards. *Quarterly Journal of Engineering Geology* **20**, 139-150.

Daniels, J. 1988. Locating caves, tunnels and mines. *The Leading Edge* **7**(3), 32-52.

De Franco, R. 2005. Multi-refractor imaging with stacked refraction convolution section. *Geophysical Prospecting* **53**, 335-348.

Debgelia, N., Bitri, A. and Thierry, P. 2006. Karst investigations using microgravity and MASW; Application to Orleans, France. *Near Surface Geophysics* **4**, 215-226.

Demanet, D., Renardy, F., Vannestse, K., Jongmans, D., Camelbeeck, T. and Meghraoui, M. 2001. The use of geophysical prospecting for imaging active faults in the Roer Graben, Belgium. *Geophysics* **66**, 78-89.

Desios, A., McCann, C., Astin, T.R., McCann, D.M., and Fenning, P. 1999. Seismic imaging of the shallow subsurface: shear-wave case histories. *Geophysical Prospecting* **47**, 565-591.

Dunkin, J.W. and Levin, F.K. 1973. Effect of normal moveout on a seismic pulse. *Geophysics* **38**, 635-642.

Edwards, W., Mitchell, G.H. and Whitehead, T.H. 1950. *The geology of the district north and east of Leeds.* British Geological Survey Memoir, Sheet 70.

Evison, F.F. 1952. The inadequacy of the standard seismic techniques for shallow surveying. *Geophysics* **17**, 867-875.

Evans, B.J. 1997. *A Handbook for Seismic Data Acquisition in Exploration, Geophysical monograph series: No. 7.* Society of Exploration Geophysicists, Tulsa, USA.

Ezersky, M., Bruner, I., Keydar, S., Trachtman, P. and Rybakov, M. 2006. Integrated study of the sinkhole development site on the western shores of the Dead Sea using geophysical methods. *Near Surface Geophysics* **4**, 335-343.

Fairbairn, C., Holt, J.M. and Padget, N.J. 1986. Case histories of the use of the surface seismic method in the UK, coal mining industry. *In:* Buchanan, D.J. and Jackson, L.J. (eds.) *Coal Geophysics. Geophysics reprint series No. 6.* Society of Exploration Geophysicists, Tulsa, USA.

Ford, D.C. and Williams, P.F. 2005. *Karst hydrogeology and geomorphology,* 1st edn. Wiley, New York, USA.

Fourie, C.J.S.and Odgers, A.T.R. 1995. Spreadsheet interpretation of seismic refraction data. *Computers and Geosciences* **21**, 273-277.

Francese, R., Giudici M., Schmitt D.R. and Zaja, A. 2005. Mapping the geometry of an aquifer system with a high-resolution reflection seismic profile. *Geophysical Prospecting* **53**, 817-828.

Grandjean, G., Senechal, G., Bitri, A. and Daban, J.-B. 2002. Détection de carrières souterraines par sismique haute résolution à Annet-sur-Marne (France). *Comptes Rendus Geoscience,* **334**, 441-447.

Gordon, J. 2002. An examination of the natural constraints on the origins and development of Darlington. *Unpublished Ph.D thesis, University of Durham.*

Goulty, N.R. 1983. Seismic surveying over Bunter Sandstone. *First Break* **1**(7), 17-23.

Goulty, N.R. and Brabham, P.J. 1984. Seismic refraction profiling in opencast coal exploration. *First Break* **2**(5), 26-34.

Guerrerro, J., Gutiérrez, F. and Lucha, P. 2004. Paleosubsidence and active subsidence due to evaporite dissolution in the Zaragoza area (Huerva River valley, NE Spain): processes, spatial distribution and protection measures for transport routes. *Enigineering Geology* **72**, 309-329.

Hagedoorn, J.G. 1959. The plus-minus method of interpreting seismic refraction sections. *Geophysical Prospecting* **7**, 158-182.

Hanshaw, B.B. and Bredeheoft, J.D. 1968. On the maintenance of anomalous fluid pressures. Source layering at depth. *Geological Society of America Bulletin* **79**, 1107-1122.

Hardie, L.A. 1967. The gypsum-anhydrite equilibrium at one atmosphere pressure. *American Mineralogist* **52**, 171-199.

Harris,C. and Ross, N. 2007. Pingos and pingo scars. *In:* Elias, S. A. (ed). *Encyclopedia of Quaternary Science, volume 3.* Elsevier, Amsterdam, Netherlands, 2200-2207.

Hatton, L., Worthington, M.H. and Makin, J. 1986. *Seismic data processing: Theory and* practice, 1st edn. Blackwell Scientific Publications, Oxford, UK.

Hobbs, N.B. 1986. Mire morphology and the properties and behaviour of some British and foreign peats. *Quarterly Journal of Engineering Geology* **19**, 7-80.

Hunter, J.A., Pullan, S.E., Burns, R.A., Gagne, R.M. and Good, R.L. 1984. Shallow seismic reflection mapping of the overburden-bedrock interface with the engineering seismograph – Some simple techniques. *Geophysics* **49**, 1381-1385.

Ismail, A. and Anderson, N. 2007. Near-surface characterization of a geotechnical site in the north-east Missouri using shear-wave velocity measurements. *Near Surface Geophysics* **5**, 331-338.

James, A.N., Cooper, A.H. and Holliday, D.W. 1981. Solution of the gypsum cliff (Permian Middle Marl) by the River Ure at Ripon Parks, North Yorkshire. *Proceedings of the Yorkshire Geological Society*, **43**, 433-450.

Jowett, E.C., Cathles III, L.M. and Davis, B.W. 1993. Predicting depths of gypsum dehydration in evaporitic sedimentary basins. *American Association of Petroleum Geologists Bulletin* **77**, 402-413.

Kallweit, R.S. and Wood, L.C. 1982. The limits of resolution of zero-phase wavelets. *Geophysics* **47**, 1035-1046.

Kourkafas, P. and Goulty, N.R. 1996. Seismic reflection imaging of gypsum mine workings at Sherburn-in-Elmet, Yorkshire, England. *European Journal of Environmental Engineering Geophysics* **1**, 53-63.

Klimchouk, A.B. 2000a. Dissolution and conversions of gypsum and anhydrite. *In:* Klimchouk, A.B., Ford, D.C., Palmer, A.N. and Dreybrodt W. (eds). *Speleogenesis: Evolution of Karst Aquifers.* International Union of Speleology, Huntsville, USA, 160-167.

Klimchouk, A.B. 2000b. Speleogenesis of the great gypsum mazes in the Western Ukraine. *In:* Klimchouk, A.B., Ford, D.C., Palmer, A.N. and Dreybrodt W. (eds). *Speleogenesis: Evolution of Karst Aquifers.* International Union of Speleology, Huntsville, USA, 261-273.

Klimchouk, A.B. 2000c. Speleogenesis in gypsum. *In:* Klimchouk, A.B., Ford, D.C., Palmer, A.N. and Dreybrodt W. (eds). *Speleogenesis: Evolution of Karst Aquifers.* International Union of Speleology, Huntsville, USA, 431-442.

Knapp, R.W. 1986. Using half-integer source offset with split spread CDP seismic data. *The Leading Edge* **4**(10), 66-69, 108.

Knapp, R.W. and Steeples, D.W. 1986. High-resolution common-depth-point reflection profiling: Field acquisition parameter design. *Geophysics* **51**, 283-294.

Lambrecht, J.L. and Miller, R.D. 2006. Catastrophic sinkhole formation in Kansas: A case study. *The Leading Edge* **25**, 342-347.

Lamont-Black, J., Younger, P.L., Forth, R.A., Cooper, A.H, and Bonniface, J.P. 2002, A decision-logic framework for investigating subsidence problems potentially attributable to gypsum karstification. *Engineering Geology* **65**, 205-215.

Lamont-Black, J., Baker, A., Younger, P.L. and Cooper, A.H. 2005 Utilising seasonal variations in hydrogeo-chemistry and excitation-emission fluorescence to develop a conceptual groundwater flow model with implications for subsidence hazards: an example from C. Durham, UK. *Environmental Geology* **48**, 320-335.

Landa, E. and Keydar, S. 1998. Seismic monitoring of diffraction images for detection of local heterogeneities. *Geophysics* **63**, 1093-1100.

Lanz, E., Pugin, A., Green, A.G. and Horstmeyer, H. 1996. Results of 2 and 3-D high-resolution seismic reflection surveying of surficial sediments. *Geophysical Research Letters* **23**, 491-494.

Lindsey, J.P. 1989. The Fresnel zone and its interpretive significance. *The Leading Edge* **8**(10), 33-39.

MacDonald, G.J.F. 1953. Anhydrite-gypsum equilibrium relations. *American Journal of Science* **251**, 884-898.

Martinez, J.D., Kenneth, J.S. and Neal, J.T. 1998. Sinkholes in evaporite rocks. *American Scientist* **86**, 39-52.

Mayne, W.H. 1962. Common-reflection-point horizontal data stacking techniques. *Geophysics* **27**, 927-938.

McCann, D.M., Baria, R., Jackson, P.D., Culshaw, M.G., Green, A.S.P., Suddaby, D.L., and Hallam, J.R. 1982. *The use of geophysical methods in the detection of natural cavities, mineshafts and anomalous ground conditions.*, Report of the Engineering Geology Unit, Institute of Geological Sciences, No. 82/5.

McCann, D.M., Jackson, P.D. and Culshaw, M.G. 1987. The use of geophysical surveying methods in the detection of natural cavities and mineshafts. *Quarterly Journal of Engineering Geology* **20**, 59-73.

Meekes, J.A.C., Scheffers B.C. and Ridder, J. 1990. Optimization of high-resolution seismic reflection parameters for hydrogeological investigations in the Netherlands. *First Break* **8**, 263-270.

Miller, R.D., Pullan, S.E., Waldner, J.S. and Haeni, F.P. 1986. Field comparison of shallow seismic sources. *Geophysics* **51**, 2067-2092.

Miller, R.D., Pullan, S.E., Steeples, D.W. and Hunter, J.A. 1994. Field comparison of shallow P-wave seismic sources near Houston, Texas. *Geophysics* **59**, 1713-1728.

Miller, R.D., Xia, J., Park, C.B. and Ivanov, J. 1999. Multichannel analysis of surface waves to map bedrock. *The Leading Edge* **18**, 1392-1396.

Morse, P.F. and Hildebrandt, G.F. 1989. Ground-roll suppression by the stack array. *Geophysics* **54**, 290-301.

Mossop, G.D. and Shearman, D.J. 1973. Origins of secondary gypsum rocks. *Transactions of the Institute of Mining and Metallurgy* **82**, B147-B154.

Nestvold, E.O. 1992. 3-D seismic: Is the promise fulfilled? *The Leading Edge* **11**, 12-19.

Ostroff, A.G. and Metler, A.V. 1966. Solubility of calcuim sulphate dihydrate in the system NaCl-$MgCl_2$-H_2O from 28° to 70°C. *Journal of Chemical and Engineering Data* **11**, 346-350.

Palmer, D. 1981. An introduction to the generalized reciprocal method of seismic refraction interpretation. *Geophysics* **46**, 1508-1518.

Palmer, D.2001. Imaging refractors with the convolution section. *Geophysics* **66**, 1582-1589.

Palmer, D. 2006. Refraction traveltime and amplitude corrections for very near-surface inhomogeneties. *Geophysical Prospecting* **54**, 589-604.

Park, C.B., Miller, R.D., and Xia, J. 1999. Multichannel analysis of surface waves. *Geophysics* **64**, 800-808.

Patterson, D.A., Davey, J.C., Cooper, A.H., and Ferris, J.K. 1995. The investigation of dissolution subsidence incorporating microgravity geophysics at Ripon, Yorkshire. *Quarterly Journal of Engineering Geology and Hydrogeology* **28**, 83-94.

Perry, E.C. and Lefticariu, L. 2004. The gypsum/anhydrite transition: A source of water during diagnesis? *Geochimica et Cosmochimica acta* **68**, A174.

Peet, W.E. 1960. A shock wave theory for the generation of the seismic signal around a spherical shot hole. *Geophysical Prospecting* **17**, 509-533.

Piwakowski, B., Watelet, J-M. and, Moreaux, D. 1997. High-resolution seismic prospecting of old gypsum mines—evaluation of detection possibilities. *European Journal of Environmental and Engineering Geophysics,* **2**, 109-120.

Powell, J.H., Cooper, A.H. and Benfield, A.C. 1992. *The geology of the country around Thirsk.* British Geological Survey Memoir, Sheet 52.

Pugin, A. J. M., Sargent, S.L., and Hunt, L. 2006. SH and P-wave seismic reflection using landstreamers to map shallow features and porosity characteristics in Illinois. *Proceedings of the Symposium on the Application of Geophysics to Environmental and Engineering Problems,, 2-6 April 2006, Seattle, Washington*, 1094-1109.

Pullan, S.E. 1990. Recommended standard for seismic (/radar) data files in the personal comport environment. *Geophysics* **55**, 1260-1271.

Pullan, S.E. and MacAulay, H.A. 1987. An in-hole shogun source for engineering seismic surveys. *Geophysics* **52**, 985-996.

Reynolds, J.M. 2004. Environmental geophysics investigations in urban areas. *First Break* **22**, 63-69.

Ronen, J. and Claerbout, J.F. 1985. Surface-consistent residual statics estimation by stack-power maximization. *Geophysics* **50**, 2759-2767.

Roth, M., Holliger, K. and Green, A.G. 1998. Guided waves in near-surface seismic surveys. *Geophysical Research Letters* **25**, 1071-1074.

Rybakov, M., Goldshmidt, V., Fleischer, L. and Rotsteain, Y. 2001. Cave detection and 4-D monitoring: A microgravity case history near the Dead Sea. *The Leading Edge* **20**, 896-900.

Ryder, P.F. and Cooper, A.H. 1993. A cave system in Permian gypsum at Houtsay Quarry, Newbiggin, Cumbria, England. *Cave Science* **30**, 23-28.

Santos, F.A.M. and Afonso, A.R.A. 2005. Detection and 2D modelling of cavities using pole-dipole array. *Environmental Geology* **48**, 108-116.

Sargent, C. and Goulty, N.R. 2009. Seismic reflection survey for investigation of gypsum dissolution and subsidence at Hell Kettles, Darlington, UK (In press). *Quarterly Journal of Engineering Geology and Hydrogeology*.

Sharpe, J. 1940. The production of elastic waves by explosion pressures. I. Theory and empirical field observations. *Geophysics* **4**, 144-154.

Sheriff, R.E. and Geldart, L.P. 1995. *Exploration Seismology*, 2nd edn. Cambridge University Press, Cambridge, UK.

Siahkoohi, H.R. and West, G.F. 1998. 3-D seismic imaging of complex structures in glacial deposits. *Geophysics* **63**, 1041-1052.

Smith, D.B., Harwood, G.M., Pattison, J. and Pettigrew, T. 1986. A revised nomenclature for Upper Permian strata in eastern England. *In:* Harwood, G.M. and Smith D.B. (eds). *The English Zechstein and related topics.* Geological Society Special Publication No. 22, London, UK, 9-17.

Smith, D.B. 1989. The late Permian paleogeography of north-east England. *Proceedings of the Yorkshire Geological Society* **47**, 285-312.

Smith, D.G. and Jol, H.M. 1995. Ground penetrating radar: antenna frequencies and maximum probable depths of penetration in Quaternary sediments. *Journal of Applied Geophysics* **33**, 93-100.

Spitzer, R., Nitsche, F.O. and Green, A.G. 2001. Reducing source-generated noise in shallow seismic data using linear and hyperbolic $\tau - p$ transformations. *Geophysics* **66**, 1612-1621.

Spitzer, R., Green, A.G., and Nitsche, F.O. 2001. Minimizing field operations in shallow 3-D seismic reflection surveying. *Geophysics* **66**, 1761-1773.

Steeples, D.W., Knapp, R.W. and McElwee, C.D. 1986. Seismic reflection investigations of sinkholes beneath Interstate Highway 70 in Kansas. *Geophysics* **51**, 295-301.

Steeples, D.W., Miller, R.D. and Black, R.A. 1990. Static corrections from shallow-reflection surveys. *Geophysics* **55**, 769-775.

Stone, D.G. 1994. *Designing seismic surveys in two and three dimensions*. Society of Exploration Geophysicists, Tulsa, USA.

Styles, P., McGrath, R., Thomas, E. and Cassidy, N.J. 2005. The use of microgravity for cavity characterization in karstic terrains. *Quarterly Journal of Engineering Geology and Hydrogeology* **38**, 155-169.

Sweeney, M., Turner, P. and Vaughan, D. 1987. The marl slate: model for the precipitation of calcite, dolomite and sulphides in a newly-formed anoxic sea. *Sedimentology* **34**, 31-48.

Taner, M.T., Koehler, F. and Alhilali , K.A. 1974. Estimation and correction of near-surface time anomalies. *Geophysics* **41**, 441-463.

Taner, M.T. and Koehler, F. 1981. Surface consistent corrections. *Geophysics* **46**, 17-22.

Thompson, A., Hine, P.D., Greig, J.R. and Peach, D.W. 1996. *Assessment of subsidence arising from gypsum dissolution,* Technical Report for the Department of the Environment, Symonds Group Ltd, East Grinstead, UK.

Tronicke, J., Villamor, P. and Green, A.G. Detailed shallow geometry and vertical displacement estimates of the Maleme Fault Zone, New Zealand, using 2D and 3D georadar. *Near Surface Geophysics* **4**, 155-162.

Tute, Rev. J.S. 1868. On certain natural pits in the neighbourhood of Ripon. *Geological Magazine* **5**, 178-9.

Van der Veen, M. and Green A.G. 1998. Land streamer for shallow seismic data acquisition: Evaluation of gimbal-mounted geophones. *Geophysics* **63**, 1408-1413.

Van der Veen, M., Spitzer, R., Green A.G. and Wild P. 2001. Design and application of a towed land-streamer system for cost-effective 2D and pseudo-3D shallow seismic data acquisition. *Geophysics* **66**, 482-500.

Van Schoor, M. 2002. Detection of sinkholes using 2D electrical resistivity imaging. *Journal of Applied Geophysics* **50**, 393-399.

Waltham, A.C., Simms, M.J., Farrant, A.R. and Goldie, H.S. 1997. *Karst and caves of Great Britain*, 1st edn. Chapman and Hall, London, UK.

Waltham, A.C., Bell, F.G. and Culshaw, M.G. 2005. *Sinkholes and subsidence,* 1st edn. Springer, Berlin, Germany.

Warren, J.K. 1999. *Evaporites: their evolution and economics,* 1st edn. Blackwell Science, Oxford, UK.

White, R.E. 1980. Partial coherence matching of synthetic seismograms with seismic traces. *Geophysical Prospecting* **28**, 333-358.

Yilmaz, Ö. 2001. *Seismic data analysis, volume 1*, 2nd edn. Society of Exploration Geophysicists, Tulsa, USA.

Ziolkowski, A. 1984. *Deconvolution,* 1st edn. International Human Resources Development Corporation, Boston, USA.

Ziolkowski, A. and Lerwill, W.E. 1979. A simple approach to high resolution seismic profiling for coal. *Geophysical Prospecting* **27**, 360-393.

Ziolkowski, A., Lerwill W.E., March D.W. and Peardon, L.G. 1980. Wavelet deconvolution using a source scaling law. *Geophysical Prospecting* **28**, 872-901.